# Mohiddin Lone

# CHAPTER INDEX

## Results 36

# FIGURE INDEX

# TABLE INDEX

# 1. INTRODUCTION

## 1.1 The importance and nature of synapses

The nervous system is a highly complex organ composed of numerous neuronal circuits which form the cellular basis of animal behavior. Different types of neurons that build up these neuronal circuits carry out distinct functions. Sensory neurons perceive the information, inter-neurons integrate and process this information which is then passed on to muscles and glandular cells through motor and neurosecretory neurons causing a behavioural output. The neuronal contacts at which information is passed on to other cells are characterised by synapses, highly complex cell junctional specialisation designed for this task (Sherrington, 1906). Some cells communicate via electrical synapses where action potentials simply travel from one cell to the next through specialised channels, called gap junctions. Most cells, however, communicate via chemical synapses where chemicals, called neurotransmitters, are used to transmit the signal from one cell to the next (Albright et al., 2000). Action potentials at the axon terminal trigger the opening of voltage gated $Ca^{2+}$ channels. $Ca^{2+}$ influx modifies certain presynaptic molecules which cause neurotransmitter-filled vesicles to fuse with the cell membrane and release neurotransmitter molecules into the synaptic cleft. The neurotransmitter diffuses across the cleft and binds to receptors on the post-synaptic cell. The activated receptors translate the message back to the electrical signal. Depending on the kind of membrane channels opened, the transmission can be excitatory or inhibitory. Synapses do not merely transduce signals by converting an electrical signal into chemical information and back again but they represent the sites of key regulators of information flow, signal modulation and filtration in neuronal networks which is prerequisite for neural circuits to function appropriately in the mature brain and an essential feature underlying phenomena like learning and memory.

This complex task of synapses requires many molecular players and, consequently, a significant number of gene products and transmitters localised at the synapse have been described so far (Albright et al., 2000; Goda and Davis, 2003; Prokop, 1999; Waites et al., 2005). These synaptic components comprise molecules involved in synaptic architecture (e.g. cell adhesion molecules, molecules involved in localisation and assembly of synaptic

elements), molecules conferring the electrical properties to cell membranes (e.g. voltage gated ion channels), releasable transmitters and neuropeptides, proteins involved in transmitter metabolism, components required for regulation of the synaptic vesicle cycle, metabotropic and ionotropic receptors for transmitters and neuropeptides, and components involved in signalling and second messenger pathways. Many of these components are specific to or enriched at synapses and can therefore be used as marker molecules for the visualisation of synapses (FIG. 1).

## 1.2 Mechanisms underlying the formation of synaptic contacts

Given their crucial regulatory role in neuronal circuit function, we need to understand how synaptic contacts can be established reliably and reproducibly during development. The aim of my work was to uncover mechanisms controlling the development of synaptic cell junctions. The first step of the formation of functional neuronal circuits is coordinated growth and differentiation of neurons. Thus, neurons establish dendrites and axons which have to grow and navigate to find their targets and establish cell contacts with other neurons, muscles and glandular cells. Synapse formation occurs at these contacts and is the ultimate step in wiring a nervous system. Synaptogenesis comprises the establishment and maintenance of neuronal cell contacts, the process of defining these areas as synaptic compartments, the shaping and and size determination of these compartments, and the localisation and assembly of synaptic components at these sites. A number of molecules or molecule classes have been shown to be involved in the formation of synaptic contacts. For example, at vertebrate synapses cell adhesion molecules like N-cadherins and neurexins and scaffolding molecules Bassoon and Piccolo are highly concentrated at presynaptic terminals associated with presynaptic plasma membrane or particularly with the active zone and in close opposition to this is the postsynaptic electron dense region reffered to as postsynaptic density (PSD) harboring proteins like membrane-associated guanylate kinases (MAGUKs) with clustering function of acetylcholine receptors, They are composed of a number of modular domains involved in protein-protein interactions, such as PDZ repeats (first discovered in **P**SD95/SAP90, **D**lg, and **Z**O1), src homology 3 (SH3) domain, a HOOK domain, and a guanylate kinase-like (GUK) domain. The MAGUKs potentially scaffold proteins; bind to and localise receptors, link the

cytoskeleton and signaling proteins, neuroligins and other membrane spanning proteins that bind to similar complexes on presynaptic side

One strategy to uncover further mechanisms underlying the formation of synaptic contacts is to capitalise on the advantages of simple invertebrate genetic model organisms where the involved molecules can be identified in an unbiased way and which provide techniques their analyses *in situ*, i.e. in the whole organism, demonstrating the relevance of discovered mechanisms. The model organsism most commonly used are *C. elegans* or *Drosophila melanogaster* (Jin, 2002). My project followed this strategy and focused on the genetic model organism *Drosophila melanogaster*. The first step was to finalise an unbiased genetic screen for mutations affecting the formation of synaptic contacts, then identify the genes associated with these mutations, determine their normal function and, in parallel, carry out translational work by investigating whether orthologous genes exist in vertebrates.

## 1.3 The choice of *Drosophila* as a model system

### *1.3.1. General possibilities of Drosophila as a model system*

*Drosophila* as a model system can offer efficient experimental strategies and tools. First of all, flies are easy and cheap to keep in large numbers and have a short generation time of 10 days (FlyMove, ; Weigmann et al., 2003). The genome of *D. melanogaster* has been entirely sequenced (Adams et al., 2000). Thousands of fly stocks carrying identified mutations, transgenes and/or chromosomal aberrations are available, and thousands of P-element-insertions are being made with the goal of having insertions in every open reading frame (ORF) readily available to the fly community (DrosDel, ; FlyBase, 1999). Extensive databases containing up-to-date information on all known genes of *Drosophila* and related species are online accessible (FlyBase, 1999; Matthews et al., 2005). The development of *Drosophila* in general is well documented (Bate and Martínez-Arias, 1993; Campos-Ortega and Hartenstein, 1997). The morphology and behaviour of *Drosophila* has been extremely well described, providing a valuable foundation from which to launch new studies of gene function and nervous system development. Efficient genetics can be applied such as easy generation of double and triple mutations and a variety of genetic

tricks, allowing the analysis of complex genetic networks and the unravelling of functional interactions between genes (e.g. )(Entchev et al., 2000; Fly-Pushing). *Drosophila* serves an excellent model to discover new genes, and its relatively easy laboratory maintenance combined with sophisticated genetic tools allows large-scale, high throughput forward genetic screens (St Johnston, 2002). Such screens are arguably the best method available for discovering surprising new facets of biological phenomena, since few preconceptions about the underlying mechanisms are required. In these screens, randomly mutagenised flies are selected based on irregularities in any process that interests a researcher. This approach has been used successfully by neuroscientists to identify genes that play a role in diverse developmental processes such as different aspects of axonal growth (Kolodziej et al., 1995; Martin et al., 1995; Seeger et al., 1993; Vactor et al., 1993). Individual genes, mechanisms, and processes (often first) described in *Drosophila* have repeatedly been shown to be highly conserved, validating this model's usefulness as a tool for understanding different developmental processes. Indeed, about 61% of known human disease genes have a recognizable match in the genetic code of fruit flies, and 50% of fly protein sequences have mammalian analogues. A further powerful experimental tool in *D. melanogaster* is the Gal4/UAS system for targeted gene expression (Brand and Perrimon, 1993; Duffy, 2002). It allows the expression of genes in defined cells or tissues, manipulating gene expression levels in whole animals or single identified cells, expressing genes ectopically or manipulating gene activity via RNA interference, activated or dominant negative constructs. A wide range of cellular markers and antibodies is readily available and can be used to complement genetic approaches, visualising a broad number of proteins to analyse the development of nervous systems (e.g.) (Landgraf et al., 2003). Furthermore, transgenic fly strains carrying gene constructs can be generated relatively easy, making the fly an ideal test tube for *in situ* and *in vivo* assays.

Taking all these possibilities together, *Drosophila* enables us to do genetic screens to discover new genes and unravel the functions of genes which are otherwise difficult to explore in other systems (Featherstone and Broadie, 2000).

### *1.3.2. The idea of P-elements and mutant screens*

I addressed the problem of synapse formation in Drosophila making use of a genetic strategy developed more than 15 years ago (Bellen et al., 1989; Bier et al., 1989), so-called P-element mediated mutagenesis. Before the advent of this strategy, mainly DNA-damaging agents, such as chemical mutagens or X-rays, have been used to induce mutations in forward genetics studies. Chemical mutagenesis offers the advantages of a relatively high mutation rate and broad target range. Since its introduction in 1968, ethyl methanesulphonate (EMS) has been the most commonly used chemical mutagen in *Drosophila*. EMS is an alkylating agent that produces primarily G/C to A/T transitions. G/C base pairs are potential targets for EMS mutagenesis, and therefore the probability of inducing a mutation in a specific gene is closely related to the size of the gene. Previous forward genetic screens using chemical mutagens, for fly NMJ mutants have successfully identified important synaptogenesis proteins (Aberle et al., 2002; Parnas et al., 2001). These screens are effective but require subsequent laborious mapping to identify the mutant gene. This limits the ability to perform genome-scale analyses. So a versatile genetic method for identifying and cloning *Drosophila* genes affecting many recognisable phenotypes is the P-insertion screen. In this kind of screen mutant strains are constructed in which the insertion of a single P transposable element has caused a new mutation. This strategy has greatly simplified the genetic and molecular analysis of mutations, since the P insertion allows rapid mapping, complementation testing and cloning of the affected gene (Searles et al., 1982)

The most efficient approach to P element mutagenesis utilises an immobile copy of the transposase gene combined with one or more mobile, but non-autonomous, P elements to serve as "ammunition". The *P{ry$^{+}$Δ2-3}99B* element is an example of an immobile transposase source that has been widely used for P mutagenesis (Robertson et al., 1988). Its transposase gene lacks the 2-3 intron, thus precluding the production of any 66 kD protein, which functions as a repressor of transposition (Gloor et al., 1993; Handler et al., 1993; Misra et al., 1993; Rio et al., 1986). This element cannot transpose due to a deletion of one of its termini. Injecting a P element into *P{ry$^{+}$Δ2-3}99B* embryos or a cross with the transposase source coming from one parent and the “ammunition” elements from the

other yields progeny in whose germ cells mutagenesis occurs. The transposase source is then eliminated by segregation in the next generation to stabilise any mutations obtained.

A general strategy is to use an artificially constructed ammunition element (Cooley et al., 1988) that carries a bacterial origin of replication, antibiotic resistant gene and marker gene, usually the *white* (*w*+) or *rosy* (*ry*+) eye-colour genes, is included so that integration and excision can be followed phenotypically. Additional sequences can be included to provide other features. This requires a large screen, but any mutation obtained is easy to isolate.

P-elements insert at random, but their distribution is not uniform. There is a strong preference for euchromatin and the 5' untranslated regions of genes (FIG. 3.13). They also tend to insert adjacent to other P-elements and have a slight preference for target sequences resembling GGCCAGAC. Precise insertional hotspots have been seen in several genes, suggesting that there are additional specificities not yet characterized (O'Hare and Rubin, 1983).

Taken together, the P-element mutagenesis offers more advantages over chemical mutagens for forward genetic screens and, most importantly, P-element insertions in most of the ORFs are available and their number is steadily increasing. For these reasons, the search for P element insertion mutations engages much of the effort of *Drosophila* workers regardless of their particular biological focus.

A

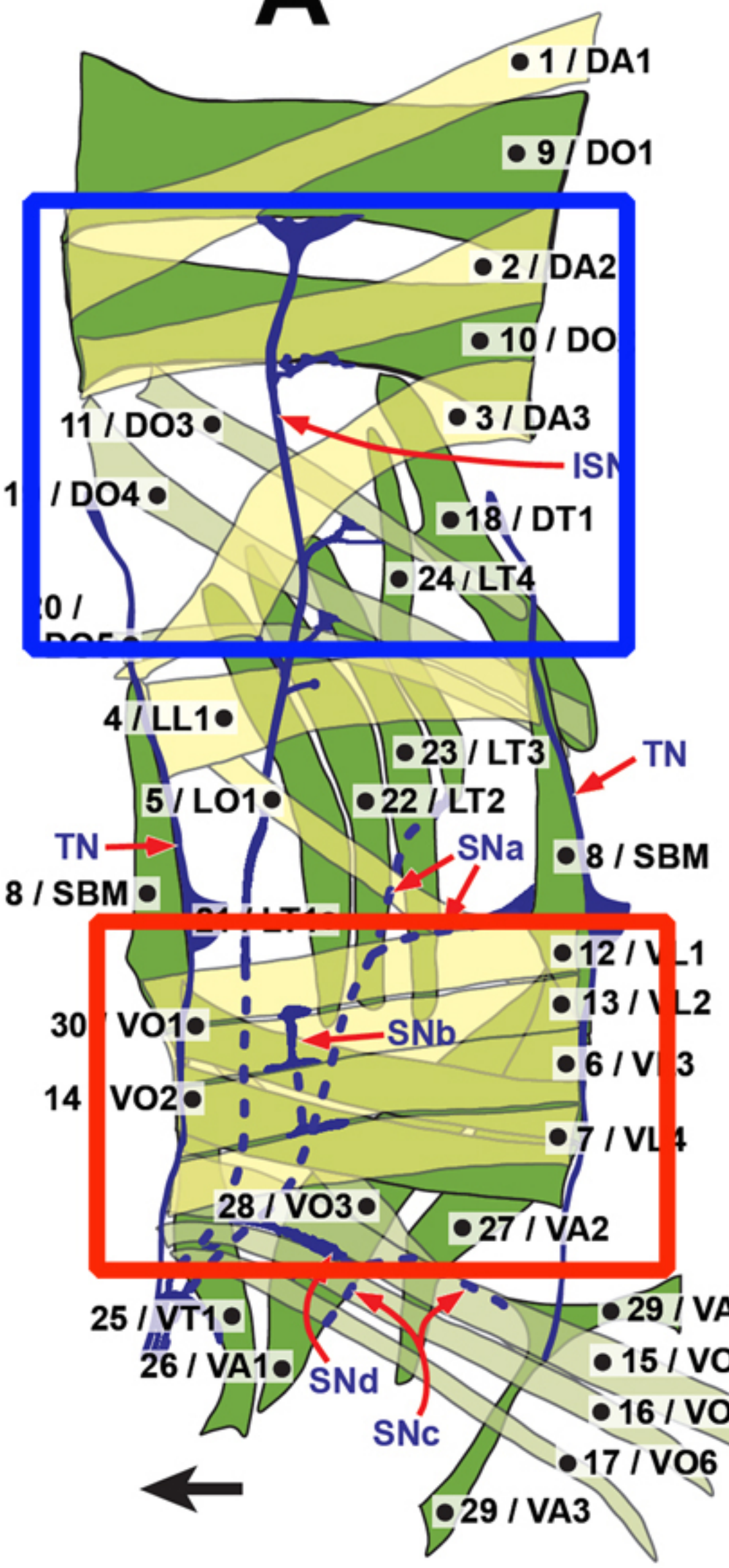
1 / DA1
9 / DO1
2 / DA2
10 / DO
11 / DO3
3 / DA3
ISN
/ DO4
18 / DT1
24 / LT4
4 / LL1
23 / LT3
TN
5 / LO1
22 / LT2
TN
SNa
8 / SBM
8 / SBM
12 / VL1
13 / VL2
30 / VO1
SNb
6 / VL3
14 / VO2
7 / VL4
28 / VO3
27 / VA2
25 / VT1
29 / VA3
26 / VA1
SNd
15 / VO4
SNc
16 / VO5
17 / VO6
29 / VA3

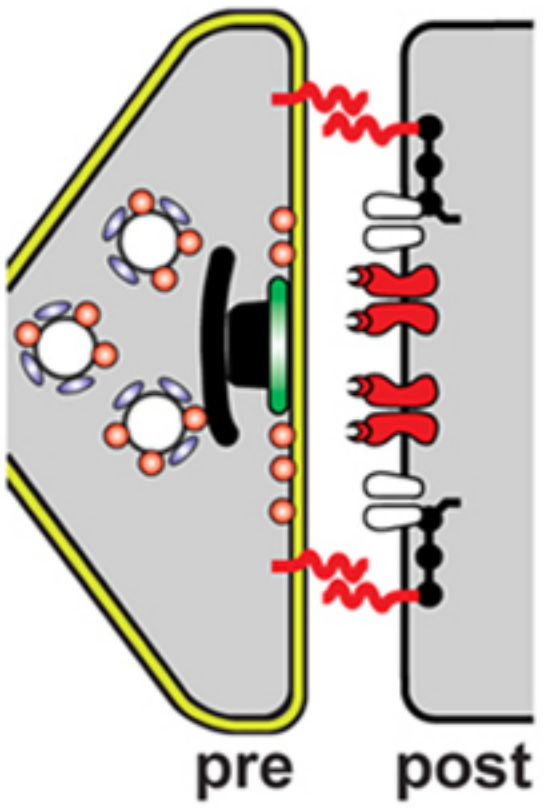
pre
post

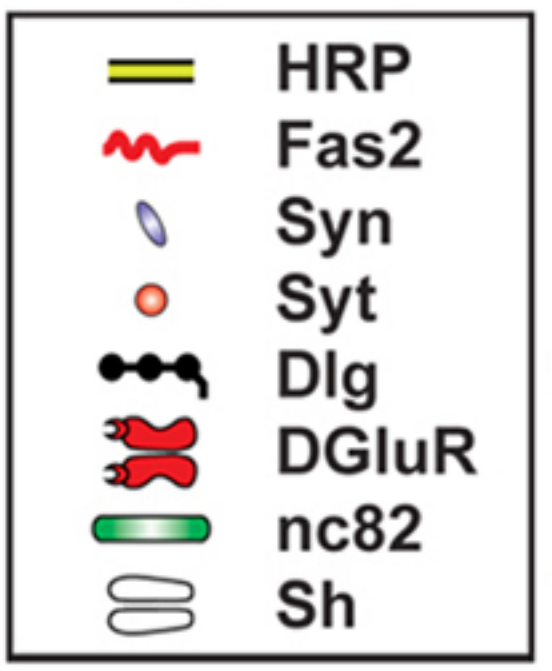
HRP
Fas2
Syn
Syt
Dlg
DGluR
nc82
Sh

B

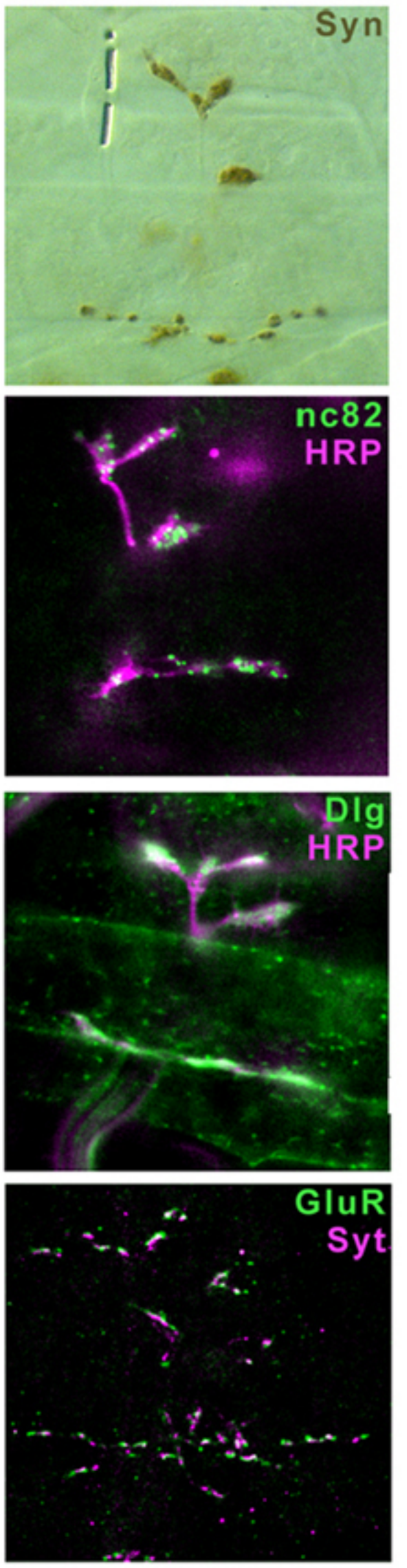
Syn
nc82
HRP
Dlg
HRP
GluR
Syt

**Fig. 2.1 Localisation of NMJs, their visualisation and characterisation with different markers.**

**(A) Neuromusculature of *Drosophila* embryonic and larval abdomibal hemisegment: Each hemisegment is comprised of about 30 individual muscles which are labeled green or yellow. All these muscles are named (in black), according to their position in the hemisegment. Each muscle is innervated by at least one individually identified motoneuron forming highly stereotypic and reproducible muscle specific branches called NMJs. Dorsal muscles are innervated by the intersegmental nerve (ISN) and ventral muscles by the segmental nerve (SN). These NMJs on the dorsal and the ventral muscles are easily accessible and thus well studied in *Drosophila*. Their reproducible and specific shape serves as a good read out for genetic screens. I mainly focused on ventral muscle NMJs (highlighted in red box) during my screen and dorsal muscle NMJs (highlighted in blue box) were analysed in only highly interesting candidates. (B) I used a pellet of different markers to spot mutant phenotypes like anti-Horseradish peroxidase (HRP) which labels neuronal surfaces, anti-Discs large (Dlg) labels preferentially postsynaptic cytoskeletal structures, anti-Synapsin (Syn) labels presynaptic vesicle pools and (nc82) labels presynpatic active zones.**

**Other synaptic markers including Anti-Synaptotagmin (Syt) which labels presynaptic vesicle pools and synaptic membranes, anti-Glutamate receptor (GluR) which labels postsynaptic ionotropic transmitter receptors, and anti-Shaker (Sh) postsynaptic voltage gated potassium channels were not used for my studies.**

### *1.3.3. Why looking at the embryonic NMJ?*

The focus of my work lies on mechanisms underlying the development of synaptic compartments, and I have capitalised on a P-element mutagenesis screen to this purpose. The cellular model used for my studies was the Drosophila neuromuscular junction (NMJ), the best characterised synaptic contact in *Drosophila* or even in general (Keshishian et al., 1996; Prokop and Meinertzhagen, 2006). The development of the *Drosophila* nervous system has been thoroughly investigated and its morphology extensely studied. The NMJ of *Drosophila* embryos serve as a potent model for work on synapse formation for various reasons. In the *Drosophila* embryo a stereotypical pattern of 30 somatic muscles forms per abdominal hemisegment, and each muscle is individually identifiable by its characteristic shape and position (Bate and Martínez-Arias, 1993). *Drosophila* muscles are single polynucleated fibres and much of their development is well studied (Baylies et al., 1998).. Each muscle is innervated by at least one individually identified motoneuron, of which most can be assigned to a particular neural lineage (Landgraf et al., 1997). Many of these motorneurons are amenable to specific genetic manipulation (Landgraf et al., 2003; Sanchez-Soriano and Prokop, 2005). These motorneurons display muscle-specific terminals which take on precise and reproducible shapes and sizes with reproducible numbers of varicosities, called boutons (Johansen et al., 1989). Therefore, NMJ morphology is highly stereotyped (FIG. 2.1), and it is possible to identify a particular NMJ based solely on nerve entry point, branch pattern, and the number and type of presynaptic boutons (Gramates and Budnik, 1999). Because of this relative simplicity and stereotyped reproducibility from animal to animal, it is possible to recognise and quantify subtle defects in NMJ morphology, serving as a strong readout for genetic and experimental work. Any quantitative or qualitative aberrations from the norm reflect gene functions relevant to NMJ development or plasticity. Such analyses benefit from the fact that NMJs are easily accessible and can be monitored with single cell resolution. Individual identifiable *Drosophila* synapses are reliably accessible throughout development to a wide variety of cell biology techniques, including electron microscopy,

immuno-histochemistry, patch-clamp electrophysiology, and quantifiable fluorescent optical imaging (Budnik and Gramates, 1999).

Embryonic and larval NMJs possess and utilise most of the same processes and molecules important for development and plasticity at other synapses (Jin, 2002). Like other arthropods, *Drosophila* NMJs utilise glutamate as a transmitter (Jan and Jan, 1976; Johansen et al., 1989), and they display several aspects of synaptic plasticity and glutamate receptor regulation similar to those demonstrated in mammalian central neurons (Koh et al., 2000; Tejedor et al., 1997; Zhong et al., 1992). Indeed, some genes, mechanisms or processes (first) described at *Drosophila* NMJs have been shown to be highly conserved, validating this model's usefulness as a tool for understanding synaptic development and function in 'higher' organisms.

### *1.3.4. Some insights into the development of the Drosophila NMJ*

After motorneuronal growth cones reach their target muscles, cell-cell contacts have to be established, at which synapses can form. Initially, growth cones of *Drosophila* motorneurons enlarge upon target muscle contact (pre-varicous stage) to break down subsequently and refine into branches with varicosities ('boutons') that characterises a morphologically mature NMJ (Rheuben et al., 1999). Early association between the growth cone and muscle fiber appears to be stabilised by focal contacts with an intervening layer of basal lamina, or projections from intra-membranous proteins (Rheuben et al., 1999; Suzuki et al., 2000). During this process, individual filopodia seem to contain sufficient 'decision-making power' to initiate or refuse synaptogenesis (Rose and Chiba, 1999). Although the development of normal numbers of functional presynaptic structures appears to proceed independently of postsynaptic input, and this was shown in *myoblast city* (*mbc*) or *mef2* mutant embryos, in which muscle size is severely reduced or their differentiation impaired (Prokop et al., 1996). Under these conditions, motorneuronal terminals are partly not attached to muscles, but display nevertheless boutons with presynaptic structures. This observation suggests that the gross presynaptic morphology may be pre-determined, at least during embryogenesis. However, proper orientation and localisation of active zones, requires differentiated postsynaptic muscles and close apposition of pre and postsynaptic membranes (Prokop, 1999; Prokop et al., 1996). The

most prominent presynaptic structure visible in boutons, is the 'T-bar' around which vesicles cluster (Prokop, 1999), also referred to as presynaptic active zones (Zhai and Bellen, 2004). The T-bars could be required either for vesicle clustering or recycling, or represent molecules involved in synaptic release machinery or the aggregation of that machinery (Atwood et al., 1993; Prokop, 1999; Prokop and Meinertzhagen, 2006). Only few components of active zones have been identified so far, such as the calcium channel subunit cocophony ánd the adaptor molecule Bruchpilot/nc82 (Kawasaki et al., 2004; Sigrist, 2006). The number of T-bars per bouton increase as boutons enlarge.

Postsynaptic glutamate receptors of *Drosophila* muscles DGluR cluster in response to presynaptic innervation, as a function of their motorneuronal electrical activity (Broadie and Bate, 1993a; Saitoe et al., 1997) and their glutamate content (Broadie and Bate, 1993a; Broadie and Bate, 1993b; Featherstone and Broadie, 2000). However, disruption or complete elimination of vesicle exocytosis by mutation of synaptic vesicle fusion proteins (syntaxin, synaptobrevin, Dunc-13) or neural expression of tetanus toxin, does not prevent formation of normal glutamate receptor fields (Aravamudan et al., 1999; Broadie et al., 1995; Sweeney et al., 1995). Within the muscle, two components have been implicated in DGluR clustering, *Discs-large* (DLG) and Coracle. Dlg is the *Drosophila* PSD-95 orthologue and is highly enriched at *Drosophila* NMJs. Dlg has been shown to be responsible for the clustering of some components of the postsynaptic apparatus (e.g., Shaker potassium channels, FasII) (Tejedor et al., 1997; Thomas et al., 1997; Zito et al., 1997), and does so in a CaMKII phosphorylation-dependent manner (Koh et al., 1999). Only recently, it has been shown to be required for the clustering of B-type DluRs (Chen and Featherstone, 2005). In contrast, coracle is responsible for the clustering of A-type DluRs (Chen et al., 2005). DGluRs begin clustering within minutes of initial motor neuron contact, and later on muscle initiates the expression of new functional receptors and makes it 20 fold by the end of embryogenesis, whereas in non-innervated postsynaptic muscles, neither glutamate receptors nor *Dlg* cluster at synapses (Chen and Featherstone, 2005). Glutamate receptors and *Dlg* might cluster in response to parallel signals from the presynaptic neuron, after which *Dlg* regulates subunit composition by stabilising (probably indirectly) receptors that contain the *GluRIIB* subunit. Also at glutamatergic synapses of vertebrates, membrane-associated guanylate kinases (MAGUKs, such as Dlg)

are thought to localise postsynaptic molecules, including glutamate receptors (Gomperts, 1996).

As soon as the postsynaptic machinery is in place, a normal NMJ assumes physiological functionality, suggesting that postsynaptic development is the time-limiting process during wild type development. Thus, a functional (but immature) NMJ exists within less than an hour of initial contact between growth cone and muscle (Broadie et al., 1993). However, these NMJs continue to mature during late embryogenesis and continue growing at larval stages. Morphological maturation of the embryonic NMJ involves presynaptic branching, and the addition and enlargement of presynaptic varicosities. During larval development, the NMJ continues to expand together with the muscle, the surface area of which reaches approximately 100 times the embryonic size at the end of larval life. The most dramatic morphological change in the postsynaptic muscle is the elaboration of 'subsynaptic reticulum' (SSR). It may serve to concentrate and/or isolate postsynaptic molecules, increase postsynaptic area, or structurally stabilize the presynaptic terminal. *Dlg* mutants fail to develop normal elaborate SSR, and overexpression of *Dlg* (either pre or postsynaptically) results in an increase in SSR (Budnik et al., 1996). Branch length, morphology, and/or bouton number can be altered by genetically modifying motorneuronal electrical excitability (by altering ion channel function; )(Budnik et al., 1990), cell adhesion (e.g. mutations of fasciclin1; )(Zhong and Shanley, 1995), or signal transduction (e.g. genetic disruption of the cAMP cascade or CaMKII activity; )(Wang et al., 1994; Zhong et al., 1992)(; further examples listed in supplementary material of;)(Prokop and Meinertzhagen, 2006). Interestingly, nerve terminal morphology also expands in response to overexpression of certain GluRIIA postsynaptic glutamate receptor subunits (Sigrist et al., 2002), which are known to be regulated by activity during embryogenesis. This suggests that presynaptic electrical activity could first be communicated to postsynaptic muscles to regulate receptors, and receptor levels in turn control presynaptic growth via a retrograde signal. However, this pre- to postsynaptic relationship becomes more complicated through homeostatic regulation: in mutants with reduced numbers of presynaptic boutons, overall synaptic transmission remains unaltered due to a compensatory increase in the size and number of active zones per bouton (Stewart et al., 1996). Also at hypomorphic *fasciclinII* mutant

NMJs, which are severely reduced in size at larval stages, neurotransmitter release is quantitatively normal (Schuster et al., 1996). Similarly, genetically decreasing postsynaptic glutamate receptor conductance results in a compensatory increase in neurotransmitter release (Davis et al., 1998; Davis and Goodman, 1998; Petersen et al., 1997). Thus, postsynaptic glutamate receptor number, presynaptic morphology, and active zone function all appear to play important roles in maintaining the NMJ capability to induce proper muscle depolarization at different developmental stages. The molecular mechanisms underlying homeostatic regulation are so far unknown.

However, a number of retrograde signals have been described, although they have not yet been implicated in homeostatic control. Thus, the BMP Gbb is released from muscles and required for NMJ size regulation (McCabe et al., 2003). Restoration of Gbb in the nervous system of *gbb* mutant larvae can rescue neurotransmitter release to wild-type levels while not restoring normal synaptic size (McCabe et al., 2003) but postsynaptic restoration rescues size**.** Accordingly, the BMP receptor Wishful thinking (Wit) is necessary for the homeostatic regulation of neurotransmitter release (Aberle et al., 2002). It may be that the involvement of BMP signalling in this process is independent of, but complementary to, its role in regulating synaptic structural growth. The BMP signalling cascade enhances NMJ growth, as revealed by respective mutant phenotypes (McCabe et al., 2004). However, overexpression of any of its components fails to induce NMJ growth beyond wildtype levels. A negative control mechanism seems to be in place, and this was recently suggested to be represented by the E3 ubiquitin-ligase activity of Highwire (Hiw). Hiw ubiquitinates the Smad complex subunit Medea (Med; )(McCabe et al., 2004) and as such seems to trigger its degradation and to prevent overstimulation of the Gbb pathway.

In summary, the timeline of NMJ formation in *Drosophila* is relatively well understood. Genetics has identified far more than 100 genes important for larval growth regulation (supplement) (Prokop and Meinertzhagen, 2006), but genes involved in *de novo* NMJ formation, i.e. in target recognition, adhesion, size regulation and synapse assembly, are still vastly unknown. My task was therefore, to identify new gene functions involved in the *de novo* formation of NMJs in the *Drosophila* embryo.

## 1.4. Work leading on to this project

The basis for this thesis was a collection of 2460 lethal or semi-lethal mutations induced via random insertions of transposable P-elements (PlacW) on the third chromosome of *Drosophila* and collected in the Szeged Stock Centre in Hungary (Salzberg et al., 1997). To identify genes involved in the process of synaptic contact formation, this collection was screened in a stepwise procedure. Initially, late mutant embryos from this stock collection were analysed for potential neuromuscular junction (NMJ) defects in Cahir O'Kane's laboratory in Cambridge (unpublished). The first criterion used to select mutations of interest was to select for mutant embryos displaying paralysis or impaired movement. Since paralysis or sluggishness may be due to defects in the musculature, the selected candidates were analysed with the muscle marker myosin and discarded, if defects in the muscle pattern were observed. A second potential cause for impaired movement is incomplete axonal growth, i.e. failure of motorneurons to reach their target muscles. Therefore, embryos from the selected mutant fly stocks were stained with anti-Fasciclin2 to check basic nerve pattern defects. Again, stocks with nerve pattern defects were discarded. The remaining collection of mutant lines was analysed further at the molecular and morphological level, as outlined in the following. The molecular mapping of P-element insertions was attempted using plasmid rescue strategies (Hamilton et al., 1991) and inverse PCR strategies (Dalby et al., 1995; Sentry and Kaiser, 1994) followed by *in silico* analyses mapping the obtained genomic sequences onto the fully sequenced *Drosophila* genome (Spradling et al., 1999; Spradling et al., 1995)(Appendix 6.5). The potential mapping positions obtained by this approach were checked via preliminary genetic complementation tests using deletions available for the respectively predicted genomic areas. In parallel to this molecular genetic strategy, morphological studies were carried out on NMJs of mutant embryos using different presynaptic markers, such as Cysteine string protein (Csp) and Synaptotagmin (Syt). These analyses were rather preliminary analyses monitoring maximally 5 embryos per mutant fly stock.

A number of mutations were discarded on the basis of the molecular genetic analysis (e.g. identified transcription factors or genes with known functions at the NMJ) and phenotypic analyses. Out of the remaining fly stocks, 14 mutations appeared to display interesting NMJ phenoptypes.

## 1.5. Objectives of this work and summary of outcome

My analyses started at this stage of the screen. The aim was to analyse the pre-selected 14 mutant strains in greater detail for morphological NMJ defects, pinpoint the affected gene loci and investigate mechanistic details of their function. My aim was to identify proteins directly involved in the structural development of NMJs, i.e. mediating signalling or assembly processes at the synaptic contact or representing structural components of NMJs.

From my phenotypic analyses I could confirm morphological NMJ defects for 8 mutant strains which were of sufficient severity to allow follow-up investigation. Out of these 8 mutant lines 6 could be assigned to candidate gene loci using complementation analyses. 3 of these lines could be studied in greater detail at the genetic and cell biological level. For reasons given below, most work was eventually focussed on the gene *CG4699* (later named *waharan*) towards the end of this project. My genetic, molecular biological, cell biological, biochemical and *in silico* analyses strongly suggest that *waharan* is a ubiquitin binding protein which seems to be important for the targeting of ubiquitinated proteins to the proteasome and/or nucleus.

# 2. MATERIALS AND METHODS

## 2.1 Fly genetics and cell biology

### *2.1.1. Stock maintenance*

Fly stocks were maintained and raised on standard cornmeal-yeast-agar medium vials. Stock collection was maintained at 18°C and changed to fresh vials every 4-5 weeks. For experiments stocks were mostly raised at 25°C and transferred every 2 weeks to fresh vials.

### *2.1.2 Fly Stocks*

Following Fly stocks were used and generated in the context of this study. All the mutant stocks used are embryonic lethal and were kept over TM3,Kr-Gal4,Uas-GFP balancer.

**Table 2.1**: *Fly stocks used in the context of this thesis*

| **Mutant strains** | **Source** | **Refrence** |
|---|---|---|
| 1107-02/TM3,Kr-Gal4,Uas-GFP | Cahir '0' Kane | |
| 0094-13/TM3,Kr-Gal4,Uas-GFP | Cahir '0' Kane | |
| 242-41/TM3,Kr-Gal4,Uas-GFP | Cahir '0' Kane | |
| 0151-02/TM3,Kr-Gal4,Uas-GFP | Cahir '0' Kane | |
| 0287-07/TM6BTb | Cahir '0' Kane | |
| 0066-40/TM3,Kr-Gal4,Uas-GFP | Cahir '0' Kane | |
| 0010-12/ TM3,Kr-Gal4,Uas-GFP | Cahir '0' Kane | |
| 1227-10/TM3,Kr-Gal4,Uas-GFP | Cahir '0' Kane | |
| 0237-13/TM3,Kr-Gal4,Uas-GFP | Cahir '0' Kane | |
| 0327-08/TM3,Kr-Gal4,Uas-GFP | Cahir '0' Kane | |
| 0339-03/TM3,Kr-Gal4,Uas-GFP | Cahir '0' Kane | |
| 0804-14/TM3,Kr-Gal4,Uas-GFP | Cahir '0' Kane | |
| 0885-13/TM3,Kr-Gal4,Uas-GFP | Cahir '0' Kane | |
| 0985-13/TM3,Kr-Gal4,Uas-GFP | Cahir '0' Kane | |
| **P-insertions** | | |
| w1118;PBac{WH}MED19f07123/TM3,Kr-Gal4,Uas-GFP | Bloomington | BL-19047 |
| w1118; P{GT1}eIF4AIIIGT-000230 | Bloomington | BL-20978, eIF4 |
| y1 w67c23; P{EPgy2}eIF4AIIIEY14207/TM3, Sb1 Ser | Bloomington | BL-20914, eIF4 |
| w1118; PBac{WH}CG5567f05921/TM6B, Tb | Bloomington | BL-18918 |
| y1 w67c23; P{SUPor-P}CG5577KG00497 ry506 | Bloomington | BL-13674 |
| y1 w67c23; P{EPgy2}CG5577EY08509 | Bloomington | BL-20027 |
| P{GT1}taraBG01673/TM3,Kr-Gal4,Uas-GFP | Cahir '0' Kane | |
| P{lacW}8B7,cpo[12]/TM3,Kr-Gal4,Uas-GFP | Cahir '0' Kane | |
| P{lacW}l(3)06536j2E5/TM3,Kr-Gal4,Uas-GFP | Cahir '0' Kane | |
| P{lacW}casj1C2/TM3,Kr-Gal4,Uas-GFP | Cahir '0' Kane | |
| Rec 1107-02/TM3,Kr-Gal4,Uas-GFP | Generated | |
| **Deficiencies and mutations** | | |
| Df(3L)W10, ru1 h1 Sbsbd-2/TM6B, Tb1 | Bloomington | |
| w- ; Df (3R)116/TM3Ser | Palacios | (Plaacios et al, 2004) |

| | | |
|---|---|---|
| eIF4AIII19 red1 e4/TM3,Kr-Gal4,Uas-GFP | Palacios | (Plaacios et al, 2004) |
| Df(3R)CA3/TM3,Kr-Gal4,Uas-GFP | Cahir '0' Kane | |
| Dr72/TM3,Kr-Gal4,Uas-GFP | Cahir '0' Kane | |
| Df (3R) 3450/TM3,Kr-Gal4,Uas-GFP | Cahir '0' Kane | |
| Df (3L) BK10/TM3,Kr-Gal4,Uas-GFP | Cahir '0' Kane | |
| shot[sf20]/Cyo,Kr::GFP | Prokop | (Prokop et al, 1998b) |
| yDlgPG100/FM7,Kr-Gal4,Uas-GFP | U. Thomas | |
| w-; hiwND8 ; CyoGFP/Sco | Cahir '0' Kane | |
| Df (3L) XS-533/ TM3,Kr-Gal4,Uas-GFP | Cahir '0' Kane | |
| Df (3R) 3450/ TM3,Kr-Gal4,Uas-GFP | Cahir '0' Kane | |
| Df (3L) ED4710/ TM3,Kr-Gal4,Uas-GFP | Drosdel | |
| **Recombinants generated** | | |
| Recomninant 1107-02 (*1107-02$^{75A}$*) | Generated | |
| Recombinant wah :: Hb9-Gal4 | Generated | |
| **UAS-stocks** | | |
| Uas-EGFP-Dlg[S97] | U.Thomas | |
| yw;p[Uas-tkv-9Wt]/TM6Tb | Hilary, Ashe | |
| Uas-CD8GFP; TM3Sb/TM6Tb | Prokop | |
| w;If/cyo; UasProtDTS5 | M.Baron | |
| Uas-HA-wah | Generated | 6 stocks mappig in progress. |
| Uas-wah | Generated | 8 stocks mapping in progress. |
| **GAL-4 Llines** | | |
| f/Cyo ; eve-Gal4[RN2-E] | Prokop | |
| Vg-Gal4/TM6B | M. Baron | |
| TubGal4/TM3,Kr-Gal4,Uas-GFP | Prokop | |
| ftz-Gal4/TM3Sb | Stefan Thor | (Thor et al, 1999) |
| Sca-Gal4 | Prokop | |
| MS1096-Gal4 | Dr. Fesion | |
| Hb9-Gal4/TM3,Kr-Gal4,Uas-GFP | Stefan Thor | (Thor et al, 1999) |
| 24B-Gal4 | Prokop | |
| dpp-Gal4 | M. Baron | |
| +;OK6-Gal4;UAS-mCD8 | Prokop | |
| Elav-Gal4 | Prokop | (Lin and Goodman, 1994; Luo et al, 1994) |
| Ptc-Gal4 | M. Baron | |
| Mj9-Gal4/Fm7; syn$^{97}$ | Prpkop | (Joiner and Griffith, 2000) |
| **RNAi Stocks** | | |
| 4699-R3/TM3Sb | Cahir '0' Kane | |

### *2.1.3 Virgin collection and genetic crosses*

For genetic crosses virgin female flies were collected. Stocks for virgin collection were always kept at 25°C, all eclosed females were collected every 4-5 hours to ensure that they had not mated yet, and kept in separate vials.
To set up a cross the virgins were crossed to males of a particular genotype and allowed to mate for couple of days to get enough larvae before transferring to new vials.

### *2.1.4 Embryo collection*

To collect embryos, flies were placed in plates containing apple juice with 2% Agar on which yeast powder was sprinkled to boost egg laying. To ensure that most embryos of one batch are synchronised in their development, flies were allowed to lay eggs for 2-3 hours. The egg lays were allowed to get to the required embryonic stage at 25°C, or 29°C. The eggs were subsequently de-chorionised with 7.5% commercial bleach (sodium hypochloride) for about two minutes followed by a thorough wash with dH2O. The embryos were then ready for dissections.

### *2.1.5 Balancing the mutant stocks over green-balancer*

Our screen required the unambiguous identification of homozygous mutant embryos. Therefore all mutant stocks were rebalanced using *GFP*-tagged balancer (*TM3Sb,Kr-Gal4,UAS-GFP*) chromosome. In *Kr-GAL4/UAS-GFP* green balancers, *GFP* activity can be reliably scored at late germ band extension (stage 9) and at various stages subsequently. Absence of green fluorescence allowed the unambiguous selection of homozygous embryos and/or larvae. All the stocks were then checked for the absence of TM3Sb adults. No TM3Sb adults were found, suggesting all the mutant lines carry recessive lethal mutations. Subsequently the exact lethal stage was determined for each mutant.

### *2.1.6 Whole mount embryo preparation for in-situ hybridisation or antibody staining*

Embryos were dechorionised as described above (2.1.4). They were fixed in a solution of 50% heptane, 4% formaldehyde in PBS (fresh) for 25' with constant mild shaking. (PBS: 130mM NaCl, 7mM Na2HPO4, 3mM NaH2PO4). ~500µl of the PBS, formaldehyde mix was removed (lower of the two immiscible phases) and an equal volume of methanol, was added. The cap was rigorously vortexed for 30s. About 750µl of the lower layer was removed and an equal volume of methanol was added again. The cap was vortexed again for 30s. Embryos were washed twice with Methanol for 15min each time and with constant mild rocking. They were stored at -20°C or directly used for in-situ hybridization and/or immuno-histochemistry.

### *2.1.7 Dissection of embryos and larvae*

In order to visualize the CNS and peripheral nerve pattern and synapses of the embryos by antibody staining living embryos were dissected prior to fixation. Mutants and controls were dissected and processed together on the same slide to ensure identical treatment throughout all analytical steps.

#### *2.1.7.1 Dissection of early stage embryos (modified from Patel, 1994)*

These dissections were carried out on specially prepared microscope coverslips (22x22mm). These cover-slips were dipped and turned around in poly-lysine to ensure these are clean and let to dry for about 30 minutes. Silicone sealant was then placed along

the edges of the coverslips. A small square of double stick tape was stuck on to the cover slip inside the silicon ring. This cover-slip was fixed with a drop of oil to a microscope slide. Using blunt forceps, 10-12 pre-selected, dechorionised embryos were positioned as dorsal up on the double stick tape. The sealed space was then filled with Broadie and Bate medium (B&B; Broadie, 2000). The embryos were taken out by introducing a pulled out pointed glass needle (Appendix 7.7.3) at flat angle into the posterior end until the tip reaches the anterior pole and the specimen. The embryos now out of vitelline membrane were carefully lifted up inside the liquid, and moved to an area of clean glass and gently pushed against it, orienting their anterior to the top. The embryos stick to the surface. Using the same needle the embryos were dissected flat, cutting along the dorsal midline and unfolding down the body walls against the glass surface. A needle with broken off tip connected to a rubber tube with mouth piece was used to remove the gut in order to expose the underlying CNS by applying gentle blows (avoiding bubbles). The dissected embryos were then fixed by exchanging the preparation buffer with fixative solution (Appendix 7.6). Exchange of the solutions was always carried out carefully without letting the meniscus of the liquid touch the embryos. Embryos were fixed with fixative solution described above for 40 minutes to one hour at room temperature. The specimens were then washed three times ten minutes with PBT followed by one hour incubation in PBT at room temperature. All procedure fixation, washing steps and the following antibody staining were carried out in a humid chamber.

*2.1.7.2 Dissection of stage 17 embryos (modified from Broadie, 2000; Prokop et al., 1996; Rohrbough et al., 1999)*

A prerequisite for identification of NMJ defects is the formation of neuromusculature, which normally occurs at 22-24 hours after egg laying (AEL) at 25°C. The morphological maturity is evaluated by the presence of typical late stage 17 characteristics such as clear segmentation, mouthhook development, condensation of the CNS, malphigian tubules formation, and visible trachea.
As the cuticle forms, at late stage 16/early stage 17 embryos lose their ability to stick to a clean glass surface. So, it becomes necessary to perform vivisection. To this end, Histoacryl glue is used to attach the specimen to the surface. The glue is applied through a broken off glass capillary, gently blowing into the attached flexible rubber tubing. The glue polymerises upon contact with the buffer. For dissections a drop of about 150µl B&B medium was applied in the middle of the Sylgard coated coverslip (Appendix 7.7.2) which was previously fixed with a drop of oil to a microscope slide. With blunt forceps about 10 to 30 preselected stage 17/L1 dechorionised embryos were transferred into B&B drop. The embryos were attached to the sylgard by their anterior end then holding the posterior pole with the glue, stretched slightly before attaching them to the sylgard surface. The embryos were then cut open using sharpened tungsten wires (Appendix 7.7.1). The gut was then removed by sucking it up with a pulled-up broken glass capillary. The cut embryos were then opened-up, holding the edge of the body well with the minimum glue, stretched slightly before being attached to the sylgard surface. The dissected embryos were then fixed by exchanging the preparation buffer with fixative solution (Appendix 7.6). Preperations were fixed for 40 minutes to one hour at room temperature then washed three times ten minutes with PBT followed by one hour

incubation in PBT at room temperature. All procedures fixation, washing steps and the following antibody staining were carried out in a humid chamber.

*2.1.7.3 Dissection of stage 17 CNS*

These dissections were again carried out on sylgard coated coverslips. Here the anterior end of the embryos was glued and attached to sylgard surface and then holding the posterior end of the embryo with forceps and carefully pulled apart. This procedure leaves the CNS attached to the sylgard. These dissected brains were then fixed by exchanging the preparation buffer with fixative (Appendix 7.6). Preperations were fixed for 40 minutes to one hour at room temperature then washed three times ten minutes with PBT followed by one hour incubation in PBT at room temperature. All procedure of fixation, washing steps and the following antibody staining were carried out in a humid chamber.

*2.1.7.4. Dissection of third instar larvae (modified from Ranjan et al., 1998)*

Late third instar larvae which tend to climb were placed one in each of about ten drops of B&B medium along the periphery inside a Petri dish coated with a thin layer of sylgard resin. The larvae, dorsal up were pinned down anteriorly with tungsten wire pins then holding the posterior tip with the forceps stretching it well before pinning it down posteriorly. Larvae were then cut along the dorsal midline using micro scissors. With forceps the body walls were stretched out and pinned at the edges. After removing the viscera with forceps, the segmentally repeated larval body wall muscle pattern and the innervating nerve fibers are clearly visible. Following one hour fixation, the filleted larvae were washed briefly with PBT, un-pined and transferred to PBT containing Eppendorf tube.
Mutant larvae and wildtype controls were processed in the same Eppendorf tube. In order to be able to differentiate the two, mutant larvae were cut at the anterior end removing the mouth hooks using microscissors. Mouth hooks and spiracles were removed from wildtype controls only prior to mounting. In the eppendorf tube the dissected larvae were washed with PBT three times 15 minutes, antibody staining was carried out in the same eppendorf tube.

### *2.1.8 Antibody staining of the dissected animals*

After washing the PBT was removed and the primary antibody of appropriate dilution (Table 2.2) was added to dissected specimens. The preparations were incubated in primary antibody overnight at 4°C, or 3 hours at room temperature. Afterwards, the preparations were washed with PBT three times for 15 minutes each. The preparations were then incubated in secondary antibody (coupled with fluorescent dye, Biotin) of appropriate dilution for 2 to 3 hours at room temperature. The secondary antibody was then washed off with PBT three times 15 minutes each. At this stage the preparations were treated differently for fluorescence (see chapter 2.1.8.1) and Biotin (see chapter 2.1.8.2). For double or triple immune-stainings, preparations were sequentially incubated

with different primary antibodies, with three PBT washing steps of 15 minutes in-between these incubations. Finally, preparations were again washed, and incubated with respective secondary antibodies for about 3 hours at room temperature.

*2.1.8.1 Fluorescence staining*

After secondary antibody incubation and PBT washes, the preparations were briefly rinsed with PBT before mounting them in Vectashield fluorescent mounting media (Vector Laboratories Burlingame, USA) in order to be visualized and scaaned in fluorescent microscopes. The flat preparations and brain dissections were mounted differently (see chapter 2.1.9)

*2.1.8.2 Biotin Staining*

DAB (Diaminobenzidine) staining was done when the secondary antibody used was Biotin-conjugated resulting in a brown colour reaction upon staining. The AB complex (from the Vector ABC Elite kit-Vector laboratories) was prepared by adding 3µl each of solution A and B to 300µl of PBT and left shaking for 20 minutes. The two components form a complex of Biotin and Streptavidin which is coupled to horseradish peroxidase, this amplifies the signal. The AB complex was then added to preparations and incubated at room temperature for 20 minutes after which the AB complex was washed with PBT 2 to 3 times. Subsequently, DAB solution with freshly added hydrogen peroxide (final concentration of 0.1%) was added to the preparation. The reaction was allowed to take place for 2 to 3 minutes then stopped by washing with PBT couple of times before mounting.

### *2.1.9 Mounting of preparations*

Flat preparations of early stage embryos were embedded on the same coverslips on which they were dissected after removing the silicon ring and the double stick tape from the coverslip. Stage 17 flat preparations were carefully cut off the preparation slide using a razor blade splinter (held between a pair of forceps) and transferred to a clean microscope slide. Mouth hooks and the glue was carefully removed from stage 17 brains which were transferred to a new slide and arranged in to a row for easy and convenient analysis and documentation. Flat preparations of third instar larvae were transferred to a new clean microscope slide. For embedding a small drop of 70% glycerol or Vectashield fluorescent mounting medium (Vector Laboratories; only if labeling with fluorescent antibodies) was used. The cover-slips were sealed with commercial nail polish.

### *2.1.10 Synaptic markers*

I mainly used three synaptic marker proteins: (1) Anti-Synapsin, for labelling of presynaptic vesicle pool (Klagges et al, 1996), and analysis of vesicle accumulation and distribution. Synapsin is a very precise presynaptic marker and was used also to look at the shape and sizes of synaptic boutons/terminals. Anti-Syn stainings was detected with DAB staining or Cy3-fluorescent antibody. (2) Bruchpilot (nc82) antiserum detects active

zones and reveals the presence and number of presynaptic densities. The nc82-stainings were usually carried out with Cy3-fluorescent secondary antibodies and co-labelled with anti-HRP coupled to FITC. (3) Dlg, is a membrane associated protein preferentially on the postsynaptic side, responsible for clustering of ion channels and cell adhesion molecules. Anti-Dlg has the potential to reveal disturbances of the postsynaptic cytoskeletal organisation. Anti-Dlg-stainings were usually detected with fluorescent secondary antibodies. Other markers used are listed in (Table 2.2)

### *2.1.11 List of Primary and secondary antibodies used during this studies*

These antibodies were always diluted in PBT. Primary antibodies were azidated (0.1% azide) to prevent bacterial contaminations and were used many times.

**Table 2.2**: Antibodies used for this study

| **Primary antibody** | **Animal source** | **Dilution** | **Source** |
|---|---|---|---|
| FITC conjugated anti Horse raddish peroxidase (HRP) | Rabbit | 1 in 200 | Jackson Immuno Research Laboratories |
| Anti- FasciclinII (FasII) | Mouse | 1:10 | DHSB |
| Anti-Discs large (DLG) | Mouse | 1:10 | DHSB |
| Anti-Synapsin (Syn) | Mouse | 1:10 | DHSB |
| Anti-CD8 | Rat | 1:10 | Caltech laboratories. |
| Anti-GFP | Rabbit | 1:10 | Caltech laboratories. |
| Anti-synaptotagmin (Syt) | Rabbit | 1:10000 | |
| Anti-Bruchpilot (nc82) | Mouse | 1:10 | Eric Buckner |
| Anti-polyubiquitin (FK2) | Mouse | 1:50 | Martin Baron |
| Anti-castor | Mouse | 1:10 | Dr. Joachim Urban |
| Anti-evenskipped (eve) | Mouse | 1:10 | Dr. Joachim Urban |
| **Secondary antibody** | **Animal source** | **Dilution** | **Source** |
| Biotinylated: anti-mouse and rabbit | Goat | 1:200 | Jackson Immuno-research Laboratories |
| FITC, TRITC and Cy5 conjugated anti-rabit, mouse and rat | Goat | 1:200 | Jackson Immuno-research Laboratories. |

### *2.1.12 Analysis of embryos and documentation*

The analysis of preparations was carried out on an Axioplan microscope mainly using Normaski optics. Preparations labelled with fluorescent dyes were documented with a Leica TCS confocal microscope or Zeiss Axiophot microscope. The digital pictures were analysed using Leica Scanware and/or using Adobe Photoshop 5.1-7.0 software (Adobe Systems, Mountain View, CA). Non fluorescent images were digitally recorded with a CCD video camera (Sony 3 CCD color video camera). For clarity, different focal planes were combined into one picture using Adobe Photoshop 5.1-7.0, ratios synapse length to muscle length (synaptic span), boutons and active zones were measured on scanned or

recorded images using several functions within the Photoshop and NIH Image software (http://rsb.info.nih.gov/nih-image/). Students t-test was used to check the significance of deviationm, calculations were done using Microsoft Excel programme. Values ($P<0.005$) is considered significant.

### *2.1.13 Measurement of different parameters of synaptic phenotype*

Using the markers discussed above, different types of phenotypes can theoretically be expected: (a) Changes of the characteristic terminal shapes, (b) increase or decrease in length of NMJ with respect to muscle length, (c) changes in size and number of boutons, (d) changes in size and number of active zones, (e) changes of the characteristic spacing of boutons or active zones.
To detect potential phenotypes, the following measurements were carried out:

1. Ratio of NMJ to muscle length [%] (anti-Syn, anti-HRP, or anti-Dlg).
2. Counting numbers of boutons (anti-Syn, anti-HRP, or anti-Dlg).
3. Counting numbers of active zones (nc82, together with HRP).
4. Measuring bouton sizes by taking the longest diameter in arbitrary angle [µm].

Significance of data was tested with standard statistics procedures (t-test).

### *2.1.14 In- situ hybridisation of whole mount embryos*

*General procedures and precautions:*

Due to the environmental abundance of RNAses, RNA in-situ hybridisations were done with special precautions. A specific set of pipettes was reserved for RNA. Stuffed, RNAse free pipette tips were used. If possible procedures were done under in a sterile bench. All solutions were made RNAse free using DEPC and autoclaved.
*RNAse inactivation using DEPC (diethylpyrocarbonate):*
DEPC was added to solutions to inactivate RNAses. Solutions with DEPC were incubated over night under the hood and constant stirring with a magnetic stirrer. On the next day the solutions were autoclaved to inactivate the DEPC. Solutions were only opened under the hood.

*In-situ hybridisation:*

Whole embryos in methanol prepared as described above (2.1.6) were used for *in-situ* hybridisation. They were washed with PBT 3 times for 2´. Subsequently they were washed twice in PBT/Hyb. solution for 5'.

*Hybridisation:*
Embryos were prehybridised in 1ml Hyb.soln. complemented with 10µl sonicated salmon sperm DNA (10mg/ml) at 55°C for about 80´. The mixture was removed and the denatured (100°C) anti-wah probes (Appendix 6.1) were added. Incubation was done over

night with low stringency at 45°C. To obtain satisfactory results washing steps had to be optimised and were finally done extensively for about 2-3h.

*Washing:*
All washing steps were done extensively and at stringent 65°C. After hybridisation embryos were washed in Hyb.soln. for 30´ and twice in Hyb.soln./PBT (1:1) for 30´each. Subsequently they were washed 5x in PBT for 20´ and finally washed in PBT at room temperature for 10´.

*Staining:*
Embryos are incubated in PBT/anti-Dig-Ab coupled to Alkaline phosphatase 1:1000 (Roche) plus Roche Western blotting reagent (10x) to prevent background for 80´. After incubation they were washed five times in PBT for 10´ each. Subsequently they were washed in AP buffer twice for 5´each.

### *2.1.15 Determination of the insertion chromosomes of transgenic flies*

Transgenic fly lines generated were obtained as G0 adults and the independent p-insertions were mapped. To determine the insertion chromosomes of transformants, male flies with coloured eyes were crossed to double balancer flies w-*;If/CyO;MKRS/TM6b*;+. F1-virgins with coloured eyes carrying the balancer chromosomes CyO;TM6b were selected and crossed with white eyed males carrying *If; MKRS*. F2 flies were analysed upon occurrence of red eye colour in combination with balancers. For example an insertion on the second chromosome was identified when w-;red/*CyO;MKRS/TM6b* occurred whilst insertions on the third chromosome were identified by the occurrence of flies with coloured eyes carrying a balancer combination w-;*If/CyO*;red/*TM6b*.

## 2.2 Molecular Biology

### *2.2.1 Sterilisation of solutions and glassware*

Media, solutions and buffers were autoclaved at 2 bar, 120°C for about 20 minutes. Glassware was sterilised at 1 bar, dry heat (90°C) for 48 hours.

### *2.2.2 E.coli culture*

Frozen bacterial strains (*E.coli* DH5-α, BL21) were thawed and left on ice for 10 minutes. 200ml aliquots were plated on to 25ml of LB-agar plates with appropriate antibiotic and grown at 37°C overnight. Single colonies were picked up and 5ml liquid culture inoculated. The inoculated culture was grown in media containing 100µg/ml Ampicillin (sigma) or 170 µg/ml Chloromphenicol (sigma) overnight at 37°C, 300rpm. For long term storage of *E.coli*, 150µl of overnight culture was added to 750µl of glycerol, mixed well and votexed, frozen in liquid nitrogen and stored at -80°C.

### *2.2.3 DNA quantification. and purification*

Quantification of dsDNA in solution was carried out using UV spectrophotometer. Optical absorption at 260nm and 280nm was used to quantify nucleic acids, and the ratio between these two measurements gives the idea of quality. Ideally A260/A280 should be in the range of 1.8-2.0. Alternatively, the concentration of PCR-products and plasmid DNA was assessed by agarose gel electrophoresis by comparing the band intensity with that of DNA standards of known concentration run in parallel.

### *2.2.4 Optical density (OD) of Bacterial cultures*

Bacterial growth was measured at a wavelength of 600nm in 2ml disposable plastic cuvettes, using the original, sterile medium as reference. Bacteria are still in a logarithmic growth phase when an $OD_{600}$ of 0.7-0.8 is measured.

### *2.2.5 Preperation of Competent cells*

Chemocompetent cells from Invitrogen (DH5α) were used for most of the experiments. But for some transformations, competent cells prepared in our lab were chosen. Escherichia coli DH5a cells from a glycerol stock were plated on a LB plate without antibiotics and grown over night. 2ml LB-Broth (+0,02M $MgSO_4$ + 0,01M KCl) were inoculated with a single fresh colony from the Plate and incubated over night at 37ºC with vigorous shaking. In a 300ml Erlenmeyer (conical flask), 100ml LB–Broth (+0,02M $MgSO_4$ + 0,01M KCl) were inoculated with 1 ml of the overnight culture and grown at 37ºC with shaking untill an $OD_{600}$ of approx. 0.3 – 0.55 was reached. The Erlenmeyer flask was transferred to ice and kept there for 10 min gently shaking it now and again. Cells were centrifuged for 10 min at ~6000 rpm in pre-cooled centrifuge at 4ºC. The medium was decanted and the pellet was carefully resuspended in 50 ml TFB-I buffer without generating bubbles. Cells were centrifuged again as before. The pellet was

resuspended in 4ml TFB-II, and 100µl aliquots were distributed into precooled 1,5 ml eppendorf tubes (precooled on a mixture of dry ice and acetone under a fume Hood). Cells were stored at -70ºC. All reagents and buffers are listed in the (Appendix 7.3)

*2.2.5.1 Determination of cell transformation competence:*

One frozen 100µl aliquot of our competent cells (DH5a) was transformed with 0.1ng of laboratory routinely used plasmid (e.g. pUC18) following a standard transformation protocol. After incubation of the heat shocked cells, 900µl of LB medium was added and they were incubated at 37°C for 1h with vigorous shaking. After this incubation period, 10µl, 20µl, 50µl and 100µl respectively were plated out on standard LB-plates with antibiotics.
Colonies were grown over night and counted the next day. The number of colonies per 1ml was extrapolated, for example: if 10 µl produced 16 colonies; I can estimate 1600 colonies/1ml. Following this rule the average number of colonies per ml were determined by counting the colonies on all plates. The average number was divided by the starting amount of the plasmid ($1x10^{-4}$ µg). The resulting number indicates the cells competence which in general reached from $1x10^{6}$ to $1x10^{7}$.

### *2.2.6 Transformation of E.coli competent cells*

Electrocompetent cells: Frozen competent cells were thawed and left on ice for ten minutes. One to 5µl of the DNA sample (<100ng) to be transformed were cooled on ice. After adding the DNA, the cell suspension was transferred to a pre-cooled quartz cuvette. The cuvette was placed in the electroporation chamber of a pulse apparatus (EasyjecT, Prima, EQUIBIO, Peqlab, Labotec, Wiesbaden) and the electrical impulse was triggered off (capacity 25µF, resistance factor 200, voltage 2,5kV). Strait after the electroporation, 200µl of preheated (37°C) standard liquid LB medium were added. The transformation was then transferred to a clean safe lock Eppendorf tube and left shaking at 37°C and 300rpm for 40minutes, After this time the cells were plated out on LB-agar plates with selective antibiotics and kept overnight at 37°C.
Chemocompetent cells: Frozen aliquots of 50µl of competent cells were slowly thawed and kept on ice for about 5 minutes. Two to 6µl of ligation reaction or 1-50 ng of circular plasmid was added to competent cells and left on ice for 30 minutes. The cells were given a heat shock at 42°C for 2 minnutes and left to recover on ice for another 2 monutes. 500µl of SOC was then added to the cells and kept at 37°C for 1 hour with gentle shaking. Finally 50µl and 200µl volumes were plated on dry plates with appropriate anti-biotic and left at 37°C overnight.

### *2.2.7 Processing of DGRC clones*:

The cDNA clones from DGRC are shipped as Whatman FTA discs. The clones (cDNA in POT2) obtained as discs have chemicals attached to it to facilitate the lysis of these clones and allow the DNA to stick. This chemical has to be washed off before transformation so these clones were briefly washed in 50µl of 1X TE buffer by pipetting it up and down quickly twice. The tubes with the disc were kept on ice for half an hour.

Meanwhile frozen competent cells were thawed and used for transformation. The only difference from normal procedure (2.2.6) is that the heat shock is given at 37°C for 2 minutes instead of 42°C.

### *2.2.8 Miniprep Plasmid DNA purification*

QIAprepSpin miniprep DNA purification (QIAGEN) was used to perform all plasmid DNA isolations and purifications, following manufacturer's recommendations. Plasmid DNA elution was carried out with either 50µl of EB as recommended and stored at -20°C, or preferably with 50µl water if the DNA was to be subsequently used for digestions. This modification was introduced to keep low salt concentrations, as higher concentration could interfere with the restriction enzymes activities

### *2.2.9 Restriction enzyme digestion*

Restriction enzyme digestions were carried out using the recommended conditions from the enzyme supplier (Roche or NEB). In general, less than 1µg of plasmid DNA or the PCR fragment was digested in 50µl volume reaction using 5µl of the buffer and 1µl of the enzyme. Double digestions were carried out simultaneously in a buffer compatible with both enzymes. If a suitable buffer was not available, double digestion reactions were carried out sequentially, with a purification step in between to allow optimal buffers to be used. The digestion was incubated at 37°C for 2 hours.

### *2.2.10 Dephosphorylation of linearised DNA*

To prevent digested/linearised vectors from re-annealing and re-ligating without insert, I used Calf intestine alkaline phosphatase (CIAP) (Roche) to remove their 5'-phosphates. Immediately after restriction enzyme digestion, 1µl of CIAP was added to the tube and incubated for I hour at 37°C. After this time, the DNA was either cleaned using PCR cleaning Kit (Qiagen) or extracted and purified from agarose gel using Gel extraction Kit (Qiagen).

### *2.2.11 Generation of Primers*

Primers were designed manually, using software, Vector NTI Suite 7.1 for Macintosh (Invitrogen) or open source freeware PerlPrimer v.1.1.10 (http://perlprimer.sourceforge.net/). They were analysed for primer dimer occurrence, secondary structures and melting temperature (Tm) using the same programes.
At least a G or C nucleotide was at the 3´end of the primer to ensure a tight binding of the oligo at this crucial point. Stability of primer dimers or secondary structures (ΔG values) were kept at > -3.0 kcal/mol when possible. To prevent the occurrence of primer dimers, self-annealing and complementarities at 3'ends was avoided. Sequencing primers were mostly 16-20bp long with relatively low Tm (~50°C). If primers were designed to introduce restriction sites or other non annealing sequences the Tm of the template-specific parts of the primer was generally >/= 60°C. When restriction sites were added, they were confirmed using NEBcutter V2.0 (http://tools.neb.com/NEBcutter2/index.php).

7-8 random bases were always added at the 5´end of an inserted restriction site to facilitate the cutting with restriction endonucleases. Primer sequences were verified using alignment programs and uniqueness was checked using Vector NTI or lalign (http://www.ch.embnet.org/software/LALIGN_form.html). If tags were included in the primers the translation was tested using the sequence utilities of BCM Search Launcher (http://www.searchlauncher.bcm.tmc.edu ). Primers were ordered from BioSpring, Frankfurt, Germany (http://www.biospring.de) or MWG-Biotech, Germany (http://www.mwg-biotech.com). Primers were diluted to 100µM and stored at -20°C. Working aliquots with 20µM were used for PCR. Each individual primer is listed in the (Appendix 7.9).

### *2.2.12 Polymerase Chain Reaction*

A thermal reactor PCR machine (Biometra) was used for all PCR reactions. A standard program consisting of following cycling parameters was used:

| | |
|---|---|
| 1. 95°C | 45 seconds |
| 2. 95°C | 45 seconds: Denaturing |
| 3. Primer $T^m$ | 45 seconds: Annealing |
| 4. 72°C | 2 minutes/kb of PCR target Extension |
| | step 2-4 30 cycles |
| 5. 72°C | 10 minutes. |
| 6. 4°C | hold. |

The annealing temperature varied depending on the melting temperature of the primers.

Standard conditions for 50µl reaction are as follows:

| | |
|---|---|
| 10X buffer+$Mg^{2+}$ | 5µl |
| dNTPs (2mM each NTP) | 6µl |
| Plasmid DNA template (100ng/µl) | 1µl (100ng) |
| Primer1 (20pm/µl) | 1µl |
| Primer2 (20pm/µl) | 1µl |
| Native or cloned *pfu* polymerase (2.5U/µl ) | 1µl |
| Deionised water up to a volume of | 50µl |

#### *2.2.12.1 Single Colony PCR*

To test ligation success and presence of specific inserts in a DNA construct, single colony PCR was performed. Colonies transformed from a ligation on a LB-plate were picked using a sterile pipette tip or tooth pick. They were first streaked out on a subdivided and numbered LB plate and then dissolved in 30µl or 50µl of PCR master mix (for 30µl reaction see below):

0.1-0.2µl taq polymerase (Bioline)
3µl 10x PCR buffer (Bioline)
1µl $Mg^{2+}$(50mM); 1,5µl dNTPs (2mM)

1µl primer A (20ng/µl)
1µl primer B (20ng/µl)

Primers were chosen such that the presence and orientation of inserts could be determined. Samples were subsequently subjected to PCR using the following protocol:

1: 10min 92°C to crack the bacterial cell walls
2: 2min 92°C to denature DNA
3: 45sec 50-55°C to anneal the primers
4: 45sec- 2min 72°C to elongate
5: steps [2-4] were cycled 40 times
6: 8min 72°C fill up
7: 4°C until used

5µl of the yielded PCR products were analysed on standard 0.7-2.0% agarose gels depending on the size of the predicted amplicon. Positive colonies were identified and could be picked from the plates on which they were streaked out prior to the PCR. Generally 2-4 positive colonies were cultured and plasmid DNA was obtained by standard mini/midi prep procedures.

### *2.2.13 Agarose gel electrophoresis*

Agarose gels were made with 0.70-1.5% agarose in 1X TAE buffer. Ethidium bromide (0.5µg/ml) was added to the gel to bind the DNA, and allow the detection of bands on an UV transilluminator. Loading dye (6X) was added to each sample. The gels were run at 90V, and the sizes of DNA run on gels was calculated by comparing with the distance migrated by DNA fragments of known length. Different standard molecular weight DNA markers (Appendix 7.10)

### *2.2.14 Extraction of DNA from agarose gel*

To recover the DNA from gel, DNA was run on 1% agarose gel, using a sterile scalpel blade, an agarose gel slice containing the DNA band was carefully excised under UV illuminator. The DNA was purified using a QIAquick gel extraction kit (Qiagen) according to the manufacturer's instructions.

### *2.2.15 Ligation of DNA molecules*

Linearised and dephosphorylated vector and cut insert were purified and typically 100ng of linearised vector DNA was ligated with 1-3 molar ratio of insert DNA. Vector and insert were mixed in 30µl volume with 3µl of ligation buffer and I µl of T4 DNA ligase (Roche). The sample was laft at 4°C overnight. Alternatively Rapid ligation kit (Roche) was used for fast ligations. In here about 150 ng of linearised vector DNA was ligated with 1-3 molar ratio of insert DNA. The two were mixed required volume of DNA dilution buffer, 10µl DNA ligation buffer, Iµl of T4 DNA ligase in a final volume of 20µl.

The mixture was incubated at 25°C for 5 minutes and 1/10$^{th}$ of the ligate used for the transformation.

### *2.2.16 Ethanol precipitation of DNA*

In some processes, following enzymatic reactions DNA fragments or plasmids were cleaned using ethanol precipitation. To this end 1/10 Vol of sodium acetate (pH 4.5) and 2.5vol % of ice cold Ethanol or 0.75vol % room temperature isopropanol were added to the aqueous DNA solution. The solution was mixed thoroughly by inverting it several times and incubated on ice for 10-30´. Depending on the size of the DNA fragments it was subsequently centrifuged between 10´- 30´ at maximum speed in a standard tabletop centrifuge. For large DNA fragments the centrifugation times were reduced to 5´ - 15´ to facilitate subsequent re-dissolving. The supernatant was carefully discarded and the pellet was resuspended in and washed with 500µl ice cold 70% Ethanol. The sample was centrifuged again for 5´- 10´minutes and as much as possible of the supernatant was carefully removed. The pellet was carefully dried for 10-30´ at RT or in a Speedvac centrifuge. Traces of ethanol were tolerated. The DNA was resuspended in appropriate amounts of dd$H_2O$, TE or EB buffer depending on the downstream applications.

### *2.2.17 Sequencing*

The componenets of sequencing reaction are as follows:
BigDye$^{TM}$ Terminator cycle sequencing kit (Perkin Elmer) 3µl
5XReaction buffer 2µl
Template DNA 300-500ng
Primer 4pmols
deionised water to a volume of 20µl.

The cycling parameters used for sequencing are as follows:

| | | |
|---|---|---|
| Denaturing (initial) | 96°C | 2 minutes |
| Denaturing | 96°C | 40 seconds |
| Annealing | 50°C | 15 seconds |
| Extension | 60°C | 4 minutes. |
| | 30 cycles | |

4°C hold.

The DNA was ethanol precipitated as follows:
To 20µl reaction tube was added
2µl of 125mM EDTA (pH 8.0) (removes chromophore)
2µl of 3M Sodium acetate (pH 4.5)
50µl of 96% ethanol
The mixture was centrifuged at 14000rpm for 30 minutes

The precipitate was washed with 250ml of 70% ethanol.

The pellet was then dried by leaving it at 90°C for 2 minutes.

The precipitated DNA was given to Manchester University sequencing service (to sequence on Applied Biosystems automated sequencer). Sequence analysis was carried out using Chromas version 2.3 and aligned with known sequences using William Pearson's *lalign* program.

### *2.2.18 Generation of digoxygenin (DIG) labelled DNA probe*

The longest exon (number 8) was used to create about 925bp long DNA probe. cDNA clone *LP09056* described (Chapter 3.5.6) was used as template, using primers P1 and P2 (Appendix 6.1), a Dig-labelled DNA probe was synthesized by PCR and confirmed by Gel electrophoresis.

### *2.2.19 Generation of Digoxygenin (DIG) labelled RNA probe*

To synthesize RNA probe, *LP09056* covering 2/3$^{rd}$ of the C-terminal of the gene in POT2 vector was used as template. To synthesise about 3440bp antisense probe the vector was digested with with Bgl1 at 824bp of *LP09056* using T7 promotor of TOPO vector. All subsequent steps were carried out under highly sterile conditions. All reagents were DEPC treated to avoid RNAse contamination.

#### *2.2.19.1 Labelling of probes*

3µg of linearised template DNA was precipitated with 1/10 volumes of 2M NaCl (DEPC) and 2.5 volumes of 100% Ethanol, incubated on -20°C for 10´and spun down for 45´at full speed. The supernatant was removed carefully and the DNA pellet was washed with 500µl of 70% Ethanol (diluted with DEPC treated distilled water). The sample was centrifuged for another 10´ at 4°C with full speed. The supernatant was removed and the pellet was carefully dried using a speedvac. The DNA pellet was resuspended in 20ul DEPC treated water and dissolved carefully. The linearization success and the concentration was checked on a standard agarose gel. The DIG RNA Labelling Kit (T7) from Roche was used to obtain Dig labelled RNA by in-vitro transcription. The reaction mix was made as follows: 14ul of clean DNA template, 2ul 10x transcription buffer, 2ul NTP (Dig) labelling mixture plus 2ul T7 polymerase. Everything was mixed well, collected at the bottom of the tube by briefly centrifuging it down and incubated at 37°C for 2h. To remove the template DNA 2ul of RNAse free DNAseI was added and the incubation was prolonged for 15´. The reaction was stopped by adding 2ul of 0,2M EDTA solution.

#### *2.2.19.2 Precipitation of the RNA probe*

2,5ul 4M LiCl and 70ul 100% Ethanol were added to the Dig labelled RNA (see above) and incubated for at least 30´at -20°C and spun down for 60´at 4°C at full speed. The supernatant was removed and the RNA pellet was washed with 70% Ethanol (diluted with DEPC-dH20) and spun for another 10´ at 4°C at full speed. The supernatant was removed and the pellet was carefully dried until all Ethanol was evaporated. The RNA probe was finally dissolved in 30ul of DEPC treated water and used or stored at -20°C.

### *2.2.20 Dot blot to asses the labelling success of digoxygenin labelled DNA probes*

1µl of Dig labelled probes in three different dilutions (1:1, 1:10 and 1:100) were dropped on a Nylon membrane and dried. 7 dilutions of a labelled control probe were pipetted on the same membrane. Positions and concentrations were indicated using a pencil. The membrane was transferred into a plastic Petri dish and incubated for 10´in a blocking solution. After 10´ anti-Dig-Fab- antibody (1:7500) was added and gently swirled for 15´. The antibody/blocking solution was disposed off and the membrane was washed 2x 5´with P1 buffer. The washing buffer was discarded. 10ml of AP-buffer were added into the plastic dish and 66µl NBT and 33µl BCIP were added to develop the precipitation. The staining progress was monitored and as sufficient staining intensities were achieved the nylon membrane was washed with tap water and dried. Probe staining intensities were compared with the control probe dilutions.

### *2.2.21 RNA gel electrophoresis*

The presence of RNA probes was tested on an RNAfree agarose gel. RNA electrophoresis under denaturing conditions in 2.2M formaldehyde was performed according to Maniatis et al., (1982) using the MOPS buffer system. RNA under these conditions is fully denatured and migrates according to the $\log_{10}$ of its molecular weight.
An RNA agarose gel was prepared by melting the required amount of agarose in distilled water, cooling to approximately 60°C (hand hot) and adding 40% formaldehyde and 10 x MOPS buffer (Appendix 7.3) to give 2.2M formaldehyde and 1 x MOPS, respectively. Ethidium bromide was added to visualise RNA. The gel was run in 1x MOPS, 2,2M formaldehyde. RNA samples were prepared by adding 5µl of RNA to 15µl of RNA denaturing buffer (Appendix 7.3). Immediately prior to loading the samples were heated to 65°C for 10min to denature them and transferred to ice for 2min. 2µl of sterile loading buffer was added and the probes were run at 5V/cm. RNA concentrations were compared with standard probes.

## 2.3 Protein Expression and purification

### *2.3.1 GST fusion products*

*2.3.1.1 Cloning of GST fusion constructs.*

To generate fusion constructs Different primers were engineered (Chapter 2.2.11) with restriction enzymes EcoR1 site in the sense primer and Xho1 in the anti-sense primer (Appendix 7.9). The restriction sites were introduced in order to make the peptides compatible to be subcloned in to GST-fusion vector pGEX-4T1. Peptides were PCR amplified from the cDNA templates (Chapter 3.5.6), cleaned and digested with EcoR1 and Xho1. Digested PCR products were ligated directionally to corresponding EcoR1 and Xho1 digested and de-phosphorylated 4.9 kb, bacterial expression vector, pGEX-4T1. Ligated products were Transformed in to expression strains, BL21. After the successful transformation the bacteria were cultured overnight and next morning DNA was extracted from the bacterial cells, digested with EcoRI and XhoI, ran on agarose gel to confirm the successful insertion. Finally the DNA was sequenced using T7 and PM001 primers (Appendix 7.9).

*2.3.1.2 Test expression of GST fusion products*

To test the expression of the fusion constructs, 5ml of overnight culture was grown at 37°C using LB broth (with 50mg/liter Ampicillin). Next day overnight culture was added to fresh LB (Amp.) at 1:20 ratio and grown till O.D reached 1.0 at fixed wavelength A 600.
Expression of fusion proteins was then induced by adding isopropyl-B-D-thiogalactoside (IPTG) to a final concentration of 0.1mM. The cells were allowed to grow for further 3 hours at 37°C., a control un-induced (no IPTG) tube was grown in parallel. After 3 hours I ml of cells was taken form each sample and spun down at 3000rpm (sigma) for 10 minutes. Pellet was re-suspended in 200µl lysis solution (10ml bug buster, 40µl of 10mg/µl each DNAse and RNAse, 2mg lysozyme and a mini protease inhibitor tablet) and left shaking for 20 minutes. The mixture was again spun at 14000rpm for 10 minutes. Both the supernatant and pellet were then boiled with reducing solution (mercaptoethanol+sample buffer) and 30µl loaded on gel.

*2.3.1.3 Large scale expression of GST-fusion products*

50ml culture of cells was grown overnight at 37°C using LB broth (with 50mg/l Ampicillin). Next morning this culture was added to 450ml of fresh LB (Amp.) and grown till O.D reached 1.0 at fixed wavelength $A_{600}$.
Expression of fusion products was induced by adding IPTG to a final concentration of 0.1mM and incubated at 37°C or 30°C for 2 and 4 hours respectively. The cells were spun down at 5K (JA10) for 10 minutes and the pellet stored at -20 overnight at this stage.

*2.3.1.4 Purification of GST-fusion products*

Next day cells were thawed and re-suspended in 10ml of lysis solution (50ml bug buster, 200µl of 10mg/µl each DNAse and RNAse, 10mg lysozyme and one protease inhibitor tablet) and left shaking for about 20 minutes at room temperature. The lysate was then transferred to small cylinders and spun at 18K (sigma) for 10 minutes. The supernatant was mixed well with pre-prepared Glutathione-sepharose 4 flow, and left shaking at room temperature for about 40 minutes. The mixture was then poured back in to the column. Flow-through from the column was collected and the column was washed with 5-10 volumes of PBS, the wash fraction was also collected separately and finally the fusion-protein was eluted with 7.5ml reduced glutathione (15mg of glutathione, 0.5ml 1M tris in 10ml milipore water, PH=8), separate 1ml elution fractions were collected and all these elution fractions together with flow-through and wash fractions were boiled with reducing solution (mercaptoethanol+sample buffer) and 30µl loaded on gel to verify size and purification procedure.

***2.3.2 His-tag constructs***

*2.3.2.1 Cloning of His-tag fusion constructs*

To generate fusion constructs Different primers were engineered with restriction enzymes BamH1 site in the sense primer and EcoR1 in the anti-sense primer (Appendix 7.9). The restriction sites were introduced in order to make the peptides compatible to be subcloned in to His-tag-fusion vectors pHis or pHisTrx2. Peptides were PCR amplified from the cDNA templates (Chapter 3.5.6), cleaned and digested with BamH1 and EcoR1. Digested PCR products were ligated directionally to corresponding BamH1 and EcoR1 digested and de-phosphorylated, bacterial expression vector, pHis or pHisTrx2. Ligated products were Transformed in to expression strains, BL21. After the successful transformation the bacteria were cultured overnight and next morning DNA was extracted from the bacterial cells, digested with EcoRI and XhoI, ran on agarose gel to confirm the successful insertion. Finally the DNA was sequenced using T7 primers.

*2.3.2.2 Test expression of His-tag fusion products*

To test the expression of the fusion constructs, 5ml of overnight culture was grown at 37°C using LB broth (with 50mg/liter Ampicillin). Next morning overnight culture was added to fresh LB (Amp.) at 1:20 ratio and grown till O.D reached 1.0 at fixed wavelength A 600.
Expression of fusion products was then induced by adding isopropyl-B-D-thiogalactoside (IPTG) to a final concentration of 0.1mM. The cells were allowed to grow for further 3 hours at 37°C., a control un-induced (no IPTG) tube was run in parallel. After 3 hours I ml of cells was taken form each sample and spun down at 3000rpm (sigma) for 10 minutes. Pellet was re-suspended in 200µl binding buffer (Appendix 7.5) and sonicated. The mixture was again spun at 14000rpm for 10 minutes. Both the supernatant and pellet were then boiled with reducing solution (mercaptoethanol+sample buffer) and 30µl loaded on gel to verify size and purification procedure.

*2.3.2.3 Large scale expression of His-tag fusion products*

50ml culture of cells was grown overnight at 37°C using LB broth (with 50mg/l Ampicillin). Next morning this culture was added to 450ml of fresh LB (Amp.) and grown till O.D reached 1.0 at fixed wavelength A 600.
Expression of fusion products was induced by adding IPTG to a final concentration of 0.1mM and incubated at 37°C or 30°C for 2 and 4 hours respectively. Alternatively auto-induction was performed overnight by inoculating the 5ml bacterial culture grown over day into 450ml of fresh LB (Amp) with all these reagents (Appendix 7.5). The cells were spun down at 18K (JA10) for 20 minutes and the pellet stored at -20 overnight at this stage.

*2.3.2.4 Purification of His-tag fusion products*

Next day cells were thawed, re-suspended in 15ml of binding buffer(Appendix 7.5) and sonicated The cell lysate was then transferred to small cylinders and spun at 18K (JA10) for 20 minutes. The supernatant was loaded on pre-charged His-Bind resin column (Amersham Bioscience), after equilibrating it with 5 volumes of 1x-binding buffer. After loading the protein ,flow-through from the column was collected and the column was washed with 5 volumes of 1x-binding buffer, at least 30 volumes of 1x-wash buffer, the wash fraction was also collected separately and finally the fusion-protein was eluted with 7.5ml reduced glutathione (15mg of glutathione, 0.5ml 1M tris in 10ml milipore water, PH=8), separate 1ml elution fractions were collected and all these elution fractions together with flow through and wash fractions were boiled with reducing solution (mercaptoethanol+sample buffer) and 30µl loaded on gel to verify size and purification procedure.

***2.3.3 Protein refolding***

To recover the native recombinant protein, refolding protocol was employed 5 times against 5 litres of dialysis solution at 4ºC, as:

**Table 2.3:** Protein refolding protocol

| Day | Urea | 2-mercaptoethanol | Tris HCL | pH |
|---|---|---|---|---|
| 1 | 4M | 1mM | 20mM | 8.5 |
| 2 | 2M | 1mM | 20mM | 8.5 |
| 3 | 1M | 1mM | 20mM | 8.5 |
| 4 | - | - | 20mM | 8.5 |
| 5 | - | - | 5Mm | 7.4 |

***2.3.4 Thrombin digestion***

Small samples dissolved in thrombin cleavage buffer were used for test thrombin digestion. An aliquot of 2 µl thrombin (0.1 U/µl, Roche) was added to 100µl elution fraction in the presence of 2.8µl of 2.5 mM $CaCl_2$. These test digestions were performed (2 hr intervals, 2-10hr and overnight).

### *2.3.5 SDS-Polyacrylamide gel electrophoresis (PAGE)*

SDS-PAGE is a standard method for separation of proteins according to their molecular weight (Sambrook et al., 2001). The proteins are first denatured with DTT (Dithiothreitol) and SDS (Sodium dodecyl sulfate), which cause disruption of the intra- and intermolecular disulfide-, hydrogen- and hydrophobic bonds, respectively. The proteins lose their native structure and are masked by a surplus of negative charges. Hence, in an electrical field, the separation of the molecules in mixture within the gel mainly occurs according to their molecular weight.

Proteins were separated on 15% (w/v) SDS polyacrylamide gels. After assembling the electrophoresis apparatus, the resolution gel (lower gel, see Appendix 7.3) mixture was carefully poured between the glass plates (10x7 cm) separated by two spacers of 0.75mm thickness, then a layer of 100% ethanol was applied to the top surface of the gel to ensure there are no air bubbles in the gel while it polymerises and left to set for 30 minutes. After removing the ethanol, a 4% (w/v).SDS polyacrylamide staking gel (upper gel, see Appendix 7.3) was poured over the lower gel, a 10 lane comb was inserted into the upper gel and was allowed to set for 30 minutes.

The gel plates were placed in an upright position within the electrophoresis apparatus after removing the comb and washing the lanes with double distilled water. The protein samples containing 1x SDS sample buffer and the molecular weight markers were heated in a heating block for 5 minutes, centrifuged briefly and loaded on the gel and electrophoresed in 1X SDS running buffer at 150V for 70 minutes, by then the gel front reaches the bottom of the gel.

Following electrophoresis the glass plates were gently prised apart and the gel removed to a bath of Comassie blue stain at room temperature and left shaking for about 30 minutes. The stained gel was then immersed in destaining solution to remove excess/non-specific stain to a degree that the efficiency of the separation of the protein extraction could be assessed.

**Table 2.4:** SDS-Polyacrylamide gel recipes

| Composition | Lower gel mixture (µl) | Upper gel mixture (µl) |
|---|---|---|
| Distilled water | 1250 | 1575 |
| Lower gel buffer* | 1250 | - |
| Upper gel buffer* | - | 625 |
| 0.05% (w/v) Acrylamide | 2500 | 300 |
| 10% Ammonium persulphate | 25 | 25 |
| 0.05% (v/v) TEMED | 2.5 | 7.5 |

Note*: Lower gel buffer,0.375M Tris-HCl (pH8.8); Upper gel buffer, 0.125M Tris-HCl (pH6.8)

# 3. RESULTS

## 3.1 Morphological analysis of homozygous mutant fly strains

### *3.1.1 Strategy for the morphological analysis of mutant embryos*

To identify genes required for the proper formation of NMJs, I analysed the 14 mutant stocks preselected by the group of Cahir O'Kane to be potentially involved in embryonic NMJ formation. Since the phenotypical analyses carried out so far were rather superficial, thorough second analyses had to be carried out. To this end, mutant embryos were selected using green balancer chromosomes (Halfon et al., 2002) and manually dissected at late embryonic stage 17 or early first larval instar (Material and Methods 2.1.7). At late embryonic stage 17, NMJs are fully differentiated and display a reproducible morphology (Broadie et al., 1993). Owing to the difficulty of late embryonic dissection techniques, numbers of embryos analysed per mutant line were restricted to about 10-15 homozygous animals, in parallel to 5-6 wild type animals. In such preparations, NMJs are found in reproducible, precise and invariant patterns in each hemisegment of the embryo (FIG. 2.1), facilitating the comparison between wildtype and mutant morphology. Several features of these NMJs were analysed, as explained in the following.

Late embryonic NMJs display varicosities of about 1 μm diameter (called boutons; FIG. 2.1). Boutons can be visualised with antibody stainings against presynaptic proteins, such as Synapsin (Syn) and Synaptotagmin (Syt), or the postsynaptic proteins Disc large, or glutamate receptors. Within boutons, active zones can be visualized with antisera like nc82/Bruchpilot. The whole motorneuronal surface can be labelled and visualised with antibodies specific to the cell adhesion molecule FasciclinII, or with anti-Horseradish Peroxidase antibodies, which recognise an epitope presented by a membraneous glycosylated protein found exclusively on the surface of all neuronal cells and male reproductive tissue (Fabini et al., 2001).

Capitalising on these markers, different kinds of qualitative and quantitative changes in NMJ development were assessed by visualising and measuring different parameters and features of the mutant terminals to uncover structural and/or growth

defects (Materials and Methods 2.1.13). Using anti-Synapsin (Klagges et al., 1996) or anti-HRP (Jan and Jan, 1982), the ratio of terminal length to muscle length (synaptic span), bouton number and size was determined to assess potential increase or decrease in synaptic growth. The use of anti-Synapsin indicated in addition the absence or presence of presynaptic vesicle pools. The anti-Bruchpilot (nc82; )(Wagh et al., 2006) antiserum was used to screen for absence or qualitative/quantitative changes of active zones or, in combination with anti-HRP, for changes in the number of synapses per bouton. Anti-Dlg (Guan et al., 1996) was used to analyse disturbances of the postsynaptic cytoskeletal organisation. Significance of data was tested with standard statistics procedures (Materials and Methods 2.1.12).

### *3.1.2. NMJ phenotypes of homozygous mutant embryos*

Applying the strategies discussed in chapter 3.1.1., detailed light microscopic analyses of all the 14 mutant lines were carried out at late embryonic/early larval stages. The most prominent phenotypes found are changes in size of motorneuronal terminals, enlarged or increased numbers of boutons, altered amounts or arrangements of active zones. Details are given in (FIGs. 3.2-3.8), and only the most important findings are described here. All of the mutant stocks except *0242-41* and *1107-02* showed no qualitative defects like loss or accumulation or mis-localisation of synaptic markers reflecting that the integrity of synaptic contacts is intact and there are no structural changes present in these mutant synapses. All these phenotypes reflect quantitative defects, either an increase or decrease in synaptic growth of the mutant terminals. Mutant line *1107-02* has got bigger or fused boutons and nc82 reveals enlarged almost continuous active zones (most likely due to their fusion), demonstrating that the mutation causes structural aberrations. The mutant line *0242-41* which displays smaller terminals shows accumulation of Dlg at these mutant terminals, so the underlying gene might be interacting with Dlg and regulating its expression or localisation at synapses. The mutant lines *0094-13* and *0066-40* show enlarged terminals with increased numbers of boutons and there might be an increase in the spacing of the boutons. Also the branching might be increased at these mutant terminals, but was not assessed in detail. Mutant line *0010-12* shows increased numbers of

***m1*** and ***m2*** are two separate recessive mutations that both result in the same **phenotype.**

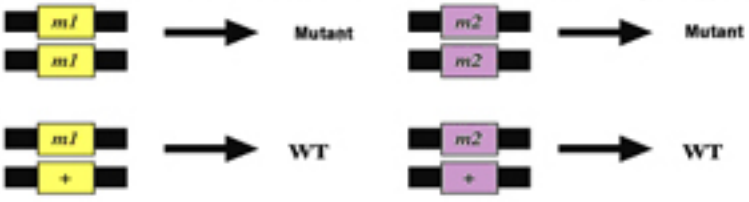


If both of these mutations are present in a *trans* configuration, and **phenotype is observed**

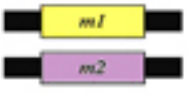


**Mutant** then these mutations DO NOT complement each other, **mutations are in the same gene**

But, if the *trans* configuration results in wild-type (WT)

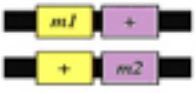


**WT** then these mutations DO complement each other, **mutations are in different genes.**

boutons and the boutons also look enlarged, but the phenotype is not highly significant. The growth phenotypes we recovered in the screen meets the expectation that NMJ growth is actively regulated, and therefore normal NMJ morphology is likely to be a dynamic balance between processes promoting growth, and processes inhibiting growth.

### *3.1.3 Selection of mutant strains for further investigation*

Taken together, we identified 8 mutant lines out of 14 with clear defects in the regulation of synaptic morphology, severe enough to be used as read out for subsequent analyses. Apart from the mutant line *1107-02*, which has fused or bigger boutons, all other mutant phenotypes can be broadly classified into two groups, namely overgrowth phenotypes (excessive boutons/or branches: *0066-40, 0094-13, 1227-10, 0151-02* and *0010-12*) and undergrowth phenotypes (reduced number of boutons/or branches: *0242-41* and *0287-07*; *0242-41* shows in addition accumulation of Dlg as well at mutant terminals).

**Fig. 3.1 Graphic representation of genetic complementation test.**

**Complementation is a specific genetic term that refers to the situation in which all the F1 progeny of two mutant parents with recessive mutation (double heterozygotes), do not show the mutant phenotype, and we can conclude that the mutations in the parents are in different genes, i.e. complement each other. On the other hand, if the F1 progeny exhibits the mutant phenotype, we can conclude that the mutations in the parents are in the same genes, i.e. fail to complement each other. Hence, non-complementation always would mean the mapping of a mutation, if the genetic identity of the other mutation is known.**

## 3.2. Complementation mapping of gene loci

### *3.2.1 The strategy*

The morphological analyses described in chapter 3.1.1. was carried out in homozygous mutant embryos. The P-element mobilisation that generated each of the P-element insertion lines may have created multiple site mutations (Appendix 6.5) or other forms of spontaneous mutations may also have been stabilised and propagated in these lethal mutant and balanced stocks. Background mutations such as these could contribute to the phenotypes identified in the screen and generate false positive results or phenotypes may represent the summation of mutations in more than one gene locus. Hence, it is required to use independent mutations to confirm mutant phenotypes in trans-heterozygous condition. Furthermore, genetic complementation studies carried out previously in the group of Cahir O'Kane were using lethality in trans-heterozygous mutant animals as read-out. However, lethality may not necessarily be coupled to the morphological NMJ phenotype but due to a separate mutation. Hence, in order to improve on the existing molecular and genetic mapping data, it was imperative to carry out complementation tests (FIG. 3.1) using the mutant NMJ phenotypes obtained in chapter 3.1.2. as read-outs.

The complementation experiments were planned on the basis of the existing molecular and genetic mapping data obtained in Cahir O'Kane's group (Appendix 6.5). As illustrated in (FIG. 3.2 to 3.8), these data predicted single P-element insertion sites for mutations *0010-12, 0094-13, 1227-10,* 2 for *0242-41, 0287-07, 1107-02* and 3 potential P-element insertions for mutations *0066-40 and 0151-02*. I screened the FlyBase database (Drysdale and Crosby, 2005; Grumbling and Strelets, 2006) for deletions, P-element insertions or other mutations, uncovering genes in the area of all predicted insertion sites. If available, fly stocks carrying such mutations were obtained from different sources (detailed in Chapter 2.1.2) and their balancer chromosomes were exchanged for the *TM3,Kr::GFP* green balancer facilitating genotype selection (Halfon et al., 2002). As

detailed in (FIG. 3.2 to 3.8), flies from these mapped mutant stocks were crossed to flies from the 8 mutant fly stocks selected from my NMJ analyses. Embryos of their offspring were dissected and their NMJs analysed following the same strategies used before (Chapter 3.2.).

In essence, a complementation test (FIG. 3.1) is a very simple test and, as described below, successfully confirmed molecular mapping data of some of the P-element mutations. However, results can be misleading or difficult to interpret: First, the mutations can cause different homozygous phenotypes. Second, the trans-heterozygote can exhibit a more severe phenotype than either homozygote alone. Third, a mutation can affect more than one gene product in a complex locus. Hence, complementation mapping is only a first step towards the identification of a gene and its responsibility for a respective mutant NMJ phenotype.

### *3.2.2 Complementation mapping of mutant fly strain 0094-13, 1227-10, 0010-12, 0066-40, 0287-07 and 1151-12*

Complementation tests with these 6 P-element insertions were relatively straightforward and will be summarised here.

#### *3.2.2.1 Complementation mapping of insertion 0094-13 ($wah^{P1}$)*

Molecular data predicts a single predicted insertion site at map position 89A in mutant line *0094-13* (later named $wah^{P1}$) (FIG. 3.2, Appendix 6.5). A complementation test was carried out with the lethal P-element insertion allele *P{lacw}I(3)06536*$^{j2E5}$ (later named $wah^{P2}$) at map position 89A4-5 (Spradling et al., 1999). Like $wah^{P1}$ homozygous mutant embryos (Chapter 3.1.2), transheterozygous $wah^{P1}/wah^{P2}$ mutant embryos are early larval (L1/L2) lethal, fail to fill the trachea, and anti-Synapsin and anti-Bruchpilot/nc82 stainings reveal the characteristically overgrown NMJ phenotype (FIG. 3.2, Table. 3.1). Therefore, both mutations fail to complement and, *per* definition, represent mutant alleles of the same gene. This complementation analysis together with the molecular data indicates that the annotated gene *CG4699* of yet unknown function is responsible for the

phenotype. I named this gene *waharan* (*wah*) and carried out more detailed analyses of its molecular and cellular function (Chapter 3.5).

| genotype | Wt | 094-13 | Wt | 094-13 | Wt | 094-13 |
|---|---|---|---|---|---|---|
| muscle | VL1 | | VL2 | | VL3/4 | |
| NMJ length / muscle length [%] | 16.7±7(n=13) | 21±8(n=15) | 10.0±2(n=13) | 11±4 (n=15) | 33.5±5 (n=13) | 39±10 (n=15) |
| significance | 0.108 | | 0.09 | | 0.119 | |
| no. nc82-dots | 8.5±4 (n=9) | 9±3 (n=9) | 7±3 (n=9) | 8±3 (n=9) | 11±3 (n=9) | 17±5 (n=9) |
| significance | n.s | | n.s | | 0.001 | |
| no. bouton | fused | 7±2 (n=19) | fused | 4±2 (n=19) | 12±3 (n=7) | 15±6 (n=19) |
| significance | n.d. | | n.d. | | 0.002 | |
| bouton size [µm] | n.d | n.d | n.d | n.d | 0.91 to 2.0 | 0.91 to 2.2 |

| genotype | Wt | 094-06536 | Wt | 094-06536 | Wt | 094-06536 |
|---|---|---|---|---|---|---|
| muscle | VL1 | | VL2 | | VL3/4 | |
| no. nc82-dots | 13±3 (n=10) | 15±3(n=10) | 10±3 (n=10) | 14±4(n=10) | 19±4 (n=10) | 28±7 (n=10) |
| significance | 0.102 | | 0.018 | | 0.003 | |
| no. bouton | fused | 9±2 (n=10) | Fused | 6±2 (n=10) | 12±3 (n=10) | 15±4(n=10) |
| significance | n.d | | n.d | | 0,001 | |
| bouton size [µm] | n.d | 0.91 to 2.0 | n.d | 0.91 to 2.0 | 0.91 to 2.0 | 0.91 to 2.2 |

| Mutant allele | Mapping position | Complementation results: | Comment: |
|---|---|---|---|
| *P{lacw}I(3)06536$^{j2E5}$* | 89 A4-5 | Fails to complement the lethality and phenotype | Indicates *CG4699* to be the gene. |

**Table 3.1 Summary of *0094-13* phenotype.**

**Summary of the phenotype and complementation analysis of the mutant line 0094-13, Different parameters of the mutant synapses, like ratio of NMJ length to muscle length (synaptic span) [%], bouton count, (anti-Syn, anti-HRP, or anti-Dlg), active zone count (nc82, together with HRP), bouton sizes by taking the longest diameter in arbitrary angle [µm] (anti-Syn) were measured and compared to wildtype. Top table shows the comparison between wildtype and mutants and the middle one shows the comparison between wildtype and (*0094-13/I(3)06536*) NMJs. The parameters showing significant deviation are shaded in grey. Comments on complementaion analysis is presented in bottom table.**

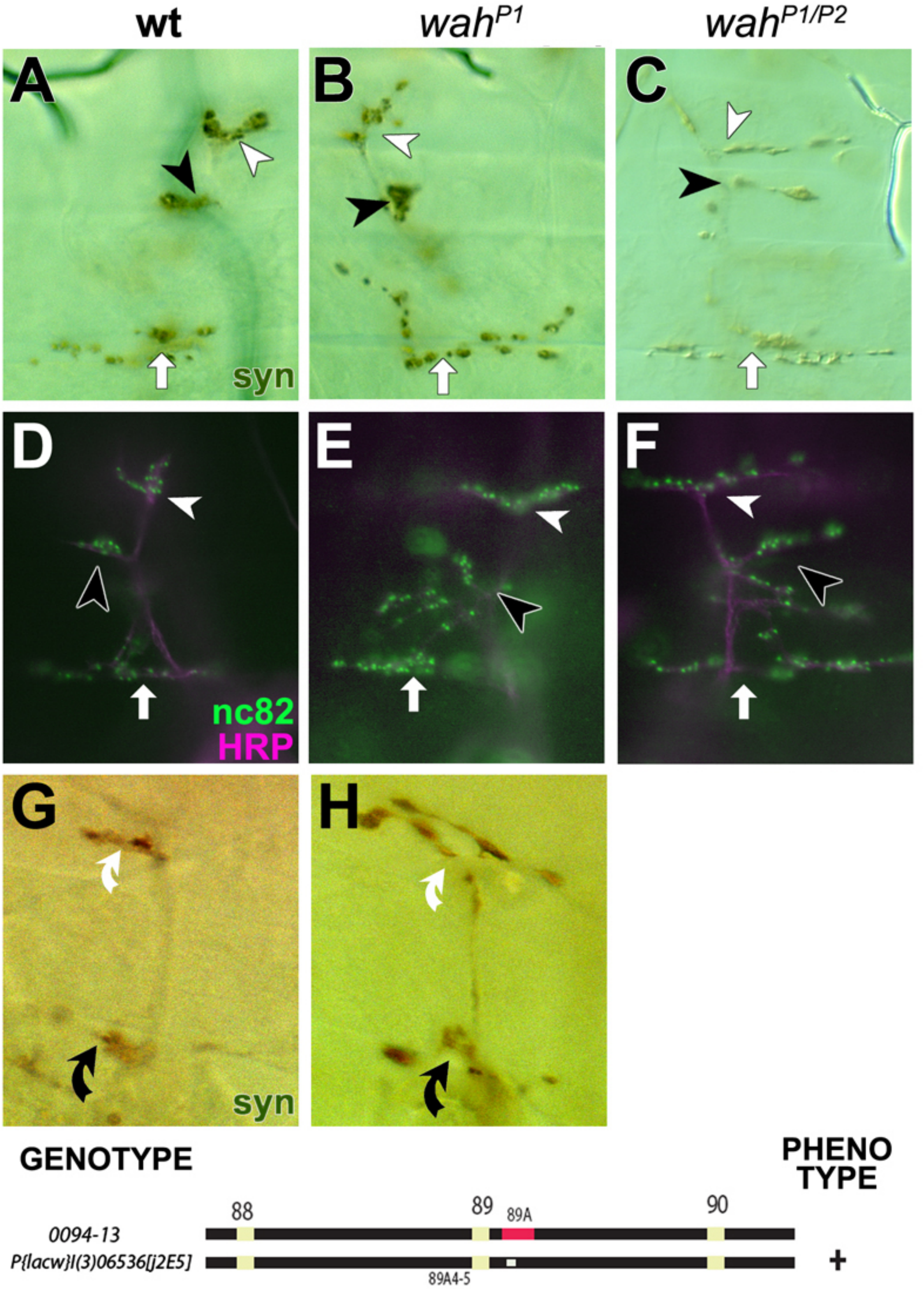
wt
wah^P1
wah^P1/P2
A
B
C
syn
D
E
F
nc82
HRP
G
H
syn


GENOTYPE
PHENO TYPE
88
89
89A
90
0094-13
P{lacw}l(3)06536[j2E5]
+
89A4-5

**Fig. 3.2 Over-grown NMJ phenotype and complementation analysis of mutant line 0094-13.**

**Light microscopic images of the mutant line 094-13 with different synaptic markers.**

**The mutant line 0094-13 (named as wah$^{P1}$) displays an interesting over-grown NMJ phenotype. Synapsin staining of the ventral muscle NMJs (synapses indicated by different symbols, VL1; white arrow head, VL2; black arrow head and VL3/4; white arrow) reveals over-grown NMJs with increased number of boutons (A vs. B). Active zones in these boutons are also increased as revealed by nc82 staining (compare D and E; labelled with anti-HRP, green and nc82, magenta). Synapsin staining of dorsal muscle NMJs (DO1; black arrow and DO2; black curved arrow) show a similar over-grown NMJ phenotype (G vs. H). Complementation analysis of the mutation reveals that another p-insertion *P{lacw}I(3)06536$^{j2E5}$* (named wah$^{P2}$), when heterozygous to Wah$^{P1}$ displays similar phenotype as shown by synapsin staining (A vs. C) and nc82 labelling (D vs. F). Graph represents the complementation analysis.**

*3.2.2.2 Complementation mapping of insertion 1227-10*

Molecular data predict a single predicted insertion site at map position 71E (FIG. 3.3, Appendix 6.5). A complementation test was carried out with deficiency *Df(3L)BK10* uncovering the region 71C3-71E5 (Rose et al., 1997). Upon complementation tests with the mutant *1227-10*, the deficiency *Df(3L)BK10* fails to complement lethality and the NMJ phenotype. Synapsin staining of *1227-10/Df(3L)BK10* embryos revealed a similar overgrown NMJ phenotype as observed for homozygous *1227-10* mutant embryos (FIG. 3.3, Table. 3.2).

Complementation analysis together with molecular data indicates that the gene *CG7372* is responsible for the phenotype. According to FlyBase, the gene encodes a protein with Myoneurin Zn-finger transcription factor activity (FBgn0036522)(Drysdale and Crosby, 2005).

| genotype | Wt | 1227-10 | Wt | 1227-10 | Wt | 1227-10 |
|---|---|---|---|---|---|---|
| muscle | VL1 | | VL2 | | VL3/4 | |
| NMJ length / muscle length [%] | 16.7±7(n=13) | 15±6(n=12) | 10.0±2(n=13) | 9±3 (n=12) | 33.5±5 (n=13) | 30±7(n=12) |
| Significance | 0.389 | | 0.661 | | 0.543 | |
| no. nc82-dots | 9±2(n=10) | 10±2(n=11) | 8±2 (n=10) | 9±3(n=11) | 12±3(n=12) | 14±2(n=12) |
| Significance: | 0.872 | | 0.908 | | 0.023 | |
| no. bouton | fused | n.d. | fused | n.d. | 12±3(n=14) | 18±5(n=18) |
| significance | n.d | | n.d | | 0,0010 | |
| bouton size [µm] | n.d. | n.d. | n.d. | n.d. | 0.91 to 1.82 | 0.45 to2.2 |

| genotype | Wt | 1227/BK10 | Wt | 1227/BK10 | Wt | 1227/BK10 |
|---|---|---|---|---|---|---|
| muscle | VL1 | | VL2 | | VL3/4 | |
| no. bouton | fused | 9±2 (n=10) | Fused | 6±2 (n=10) | 12±3(n=10) | 18±5(n=10) |
| significance | n.d. | | n.d. | | 0,0012 | |
| bouton size [µm] | n.d. | 0.91 to 2.0 | n.d. | 0.91 to 2.0 | 0.91 to 1.82 | 0.91 to2.2 |

| Mutant allele | Mapping position | Complementation results: | Comment: |
|---|---|---|---|
| ***Df(3l)BK10*** | 71C3-71E5 | Fails to complement the lethality and phenotype | indicates *CG7372* to be the gene |

**Table 3.2 Summary of *1227-10* phenotype.**

**The table summarises the phenotype and complementation analysis of mutant line 1227-10, Different parameters of the mutant synapses, like ratio of NMJ length to muscle length (synaptic span) [%], bouton count, (anti-Syn, anti-HRP, or anti-Dlg), active zone count (nc82, together with HRP), bouton sizes by taking the longest diameter in arbitrary angle [µm] (anti-Syn) were measured and compared to wildtype. Top table shows the comparison between wildtype and mutants and the middle one shows the comparison between wildtype and (*1227-10/Df(3L)BK10*) NMJs. All the measurements were carried out manually using a scale. Significance of data was tested with standard statistics procedures (t-test) (Chapter 2.1.12). The parameters showing significant deviation are shaded in grey.**

**Comments on complementaion analysis of the mutant is presented in bottom table**

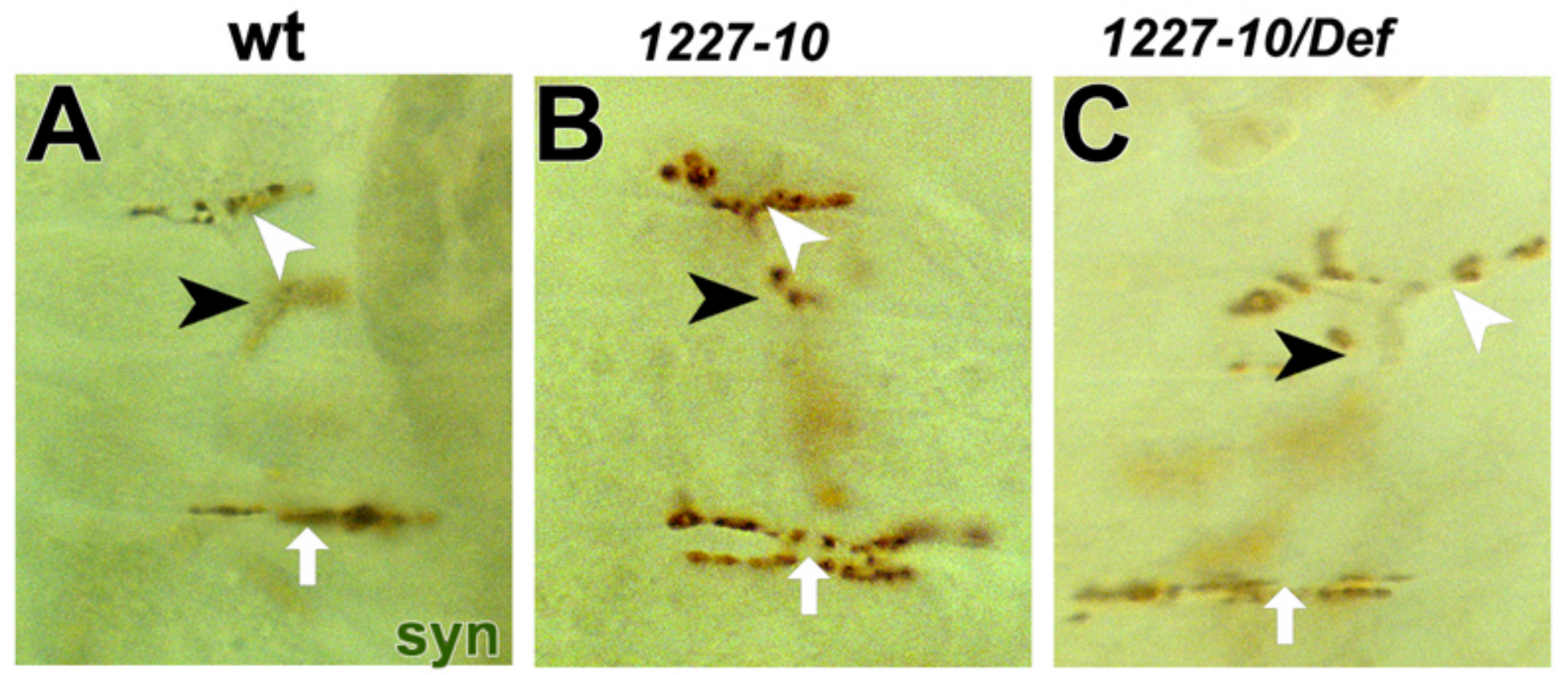
wt
1227-10
1227-10/Def
A
B
C
syn
D
E
Dlg
HRP
GENOTYPE
1227-10
Df(3L)BK10
71
71E
72
71C3-71E5
PHENOTYPE
+
wt
0010-12
0010-12/P
F
G
H
syn
I
J
K
nc82
HRP
GENOTYPE
0010-12
P{GT1}GB01673
89
89B
90
89B16
PHENOTYPE
+

**Fig. 3.3 Enlarged NMJ phenotypes and complementation analysis of mutant lines 1227-10 and 0010-12.**

**Light microscopic images of the mutant lines 1227-10 and 0010-12 NMJs with different synaptic markers.**

**Both the mutant lines 1227-10 and 0010-12 display enlarged NMJ phenotype (synapses analysed are indicated by different symbols, VL1; white arrow head, VL2; black arrow head and VL3/4; white arrow). Analysis of the mutation 1227-10 (A to E), synapsin staining reveals enlarged NMJs with more boutons (A vs. B) another synaptic marker Dlg confirms the phenotype (compare D and E; labelled with anti-HRP, green and Dlg, magenta). Complementation analysis of the mutation reveals that the deficiency *Df (3L)BK10,* when heterozygous to 1227-10 displays similar phenotype as shown by synapsin staining (A vs. C) (Chapter 3.2.2.2).**

**Analysis of 0010-12 (F to K), synapsin staining reveals more boutons in the mutant NMJ (F vs. G). Active zones in these boutons are also increased in number as revealed by nc82 staining (compare I and J; labelled with anti-HRP, green and nc82, magenta). Complementation analysis of the mutation reveals another p-insertion *P{GT1}BG01673* when heterozygous to 0010-12 displays similar phenotype as shown by synapsin staining (F vs. H) and nc82 labelling (I vs. K).**

*3.2.2.3 Complementation mapping of insertion 0010-12*

Molecular data predict a P-element insertion at map position 89B (FIG. 3.3, Appendix 6.5). A complementation test was carried out with the P-insertion *P{GT1}BG01673* at map position 89B16 (according to Flybase: FBrf0105495). The *0010-12* insertion fails to complement the *P{GT1}BG01673* mutation with respect to lethality and NMJ phenotype. Synapsin and nc82 staining of *0010-12 /P{GT1}BG01673* mutant embryos revealed a similar overgrown NMJ phenotype as the homozygous mutant embryos (FIG. 3.3, Table. 3.3).

Complementation analysis together with molecular data indicates that the *taranis* gene is responsible for the phenotype. Taranis is a Trithorax-group gene involved in chromatin-mediated regulation of gene transcription (FBgn0040071). Since the analysis of transcriptional regulation does not fall into the remit of my project (Chapter 4.1) I did not consider this gene for further analysis.

| genotype | Wt | 0010-12 | Wt | 0010-12 | Wt | 0010-12 |
|---|---|---|---|---|---|---|
| muscle | VL1 | | VL2 | | VL3/4 | |
| NMJ length / muscle length [%] | 16.7±7(n=13) | 21±8(n=13) | 10.0±2(n=13) | 11±4(n=13) | 33.5±5 (n=13) | 39±10(n=13) |
| significance | 0.108 | | 0.09 | | 0.119 | |
| no. nc82-dots | 13±4 (n=10) | 18±6(n=9) | 10±3 (n=10) | 14±4 (n=10) | 19±7 (n=10) | 20±6 (n=10) |
| significance | 0.032 | | 0.037 | | 0.515 | |
| no. bouton | fused | 6±2(n=10) | fused | 4±2(n=10) | 12±3(n=10) | 12±4(n=10) |
| significance | n.d. | | n.d. | | 0.745 | |
| Bouton size [µm] | n.d. | n.d. | n.d. | n.d. | 1.6 to 1.82 | 1.27 to 2.2 |
| Significance | n.d. | | n.d. | | 0.267 | |

| genotype | Wt | 0010-12 | Wt | 0010-12 | Wt | 0010-12 |
|---|---|---|---|---|---|---|
| muscle | VL1 | | VL2 | | VL3/4 | |
| NMJ length / muscle length [%] | 16.7±7(n=13) | 20±7(n=10) | 10±2(n=13) | 12±5(n=13) | 33±6 (n=13) | 38±11(n=12) |
| significance | 0.11 | | 0.08 | | 0.12 | |
| no. nc82-dots | 13±4 (n=10) | 18±6(n=9) | 10±4 (n=10) | 14±5 (n=10) | 19±8 (n=10) | 19±6 (n=10) |
| significance | 0.032 | | 0.037 | | 0.32 | |
| no. bouton | fused | 6±2(n=10) | fused | 4±2(n=10) | 12±4(n=10) | 11±5(n=10) |
| significance | n.d. | | n.d. | | 0.35 | |
| Bouton size [µm] | n.d. | n.d. | n.d. | n.d. | 1.6 to 1.82 | 1.27 to 2.2 |
| significance | n.d. | | n.d. | | 0.29 | |

| Mutant allele | Mapping position | Complementation results: | Comment: |
|---|---|---|---|
| *P{GT1}BG01673* | 89B14 | Fails to complement the lethalith and phenotype | Indicates taranis is responsible |

**Table 3.3 Summary of *0010-12* phenotype.**

**Summary of the phenotype and complementation analysis of mutant line 0010-12, Different parameters of the mutant synapses, like ratio of NMJ length to muscle length (synaptic span) [%], bouton count, (anti-Syn, anti-HRP, or anti-Dlg), active zone count (nc82, together with HRP), bouton sizes by taking the longest diameter in arbitrary angle [µm] (anti-Syn) were measured and compared to wildtype. Top table shows the comparison between wildtype and mutants and the middle one shows the comparison between wildtype and (*0010-12/P{GT1}BG01673*) embryo NMJs. All the measurements were carried out manually using a scale. Significance of data was**

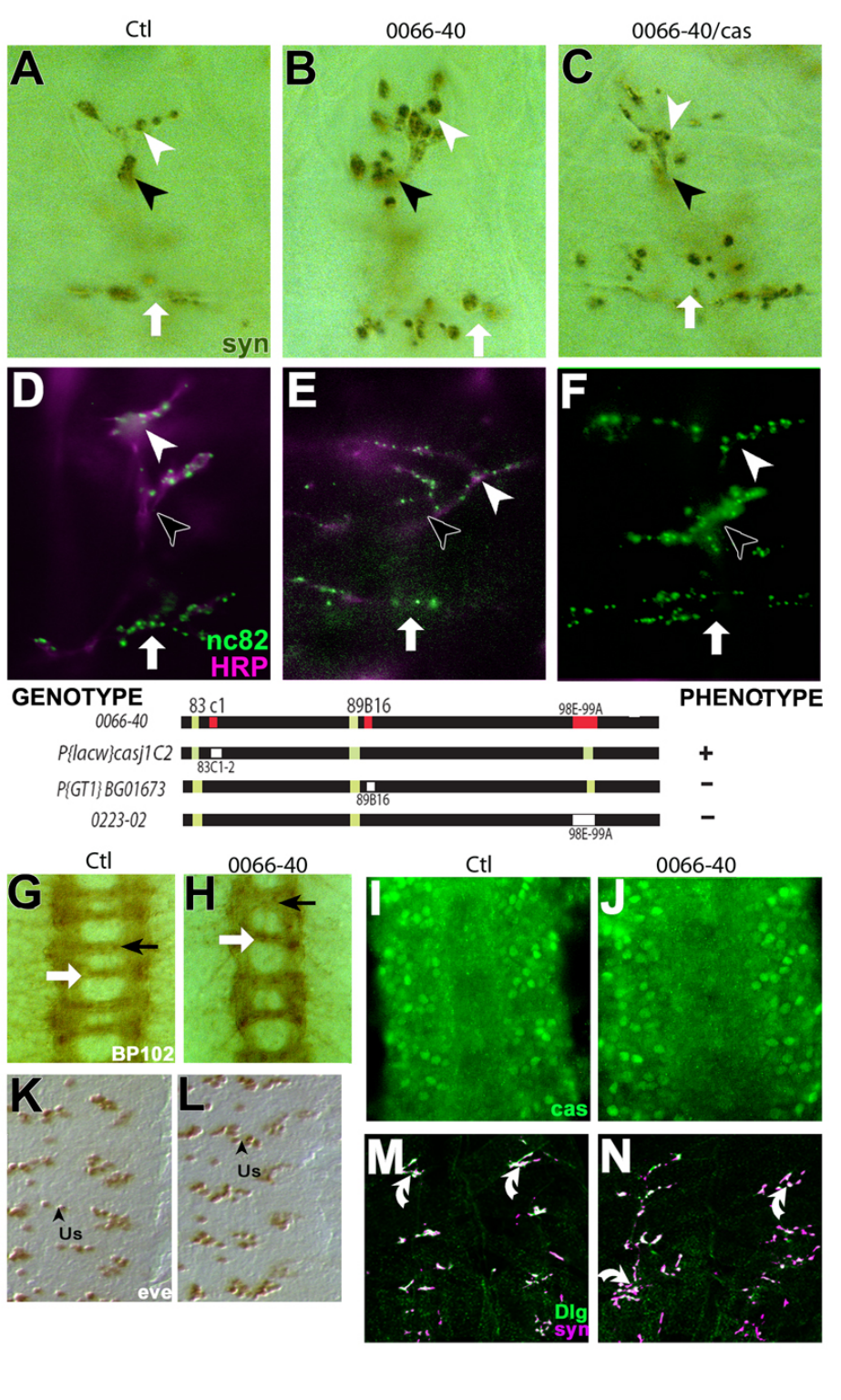
Ctl
0066-40
0066-40/cas
A
B
C
syn
D
E
F
nc82
HRP
GENOTYPE
PHENOTYPE
83 c1
89B16
98E-99A
0066-40
P{lacw}casj1C2
83C1-2
+
P{GT1}BG01673
89B16
-
0223-02
98E-99A
-
Ctl
0066-40
G
H
BP102
Ctl
0066-40
I
J
cas
K
L
Us
Us
eve
M
N
Dlg
syn

**tested with standard statistics procedures (t.test) (Chapter 2.1.12). Comments on complementaion analysis of the mutant are presented in bottom table.**

**Fig. 3.4 Mutant line 0066-40 shows known castor phenotypes and Over-grown presynaptic terminals partly attach to the muscles.**

**The mutant line 0066-40 displays an interesting over-grown NMJ phenotype. Synapsin staining of ventral muscle NMJs (synapses indicated by different symbols, VL1; white arrow head, VL2; black arrow head and VL3/4; white arrow) reveals over-grown NMJs with increased number of boutons (A vs. B). Active zones inside these boutons are also increased as revealed by nc82 staining (compare D and E; labelled with anti-HRP, green and nc82, magenta). Complementation analysis of the mutation reveals another p-insertion *P{lacw}cas*$^{j1C2}$, when heterozygous to 0066-40 displays similar phenotype as shown by synapsin (A vs. C) and nc82 labelling (D vs. F). The graph summarises the outcome of complementation tests, other two p-insertion stocks at 89B16 and 98E complement the phenotype (Chapter 3.2.2.4). Further analysis of 0066-40 (G toN), BP102 staining (G, H; black arrow, anterior commissure and white arrow, posterior commissure) reveals the posterior commissure of 0066-40 is thinner as compared to anterior one. Anti-castor immunostaining (labeled; green) reveals rather normal castor expression in the mutants (I vs. J). Anti-eve staining shows increased number of Q/U motor neurons (black arrowheads; Q/U motorneurons) in mutants compared to the wildtype (K vs. L). Double labeling with pre and post-synaptic markers reveals that over-grown presynaptic boutons partly attach to the postsynaptic muscles as shown (M and N, curved arrows) Dlg not completely colocalising with synapsin (green vs. magenta).**

*3.2.2.4 Complementation mapping of insertion 0066-40*

Molecular data predict P-element insertions at map position 83C1, 89B16 and 99 (FIG. 3.4, Appendix 6.5). Complementation tests of *0066-40* were carried out with 3 mutations mapped to these loci. First, the P-element insertion *P{GT1}BG01673* at map position 89B16 (FBrf0105495) complements lethality and the NMJ phenotype observed for *0066-40* (Chapter 3.3). Second, the P-element insertion *0223-02* (mapped to the chromosomal area 98E;99A through non-complemention with *Df(R)3450*; C. O'Kane, personal communication) fails to complement lethality but complements the NMJ phenotype. Third, the P-element insertion $P\{lacw\}cas^{j1C2}$ (Spradling et al., 1999) fails to complement lethality and NMJ phenotype (FIG. 3.4, Table. 3.4). Anti-Synapsin and anti-Bruchpilot/nc82 stainings of $0066\text{-}40/P\{lacw\}cas^{j1C2}$ mutant embryos revealed a similar overgrown NMJ phenotype as *0066-40* homozygous mutant embryos (FIG. 3.4).

Complementation analysis together with molecular data indicates that the gene *castor* is responsible for the phenotype. Castor is a neuronal transcription factor. Although studies of transcriptional control do not fall into the remit of this work (Chapter 4.1), some additional studies were carried out with *castor* mutant embryos (Chapter 3.3).

| genotype | Wt | 0066-40 | Wt | 0066-40 | Wt | 0066-40 |
|---|---|---|---|---|---|---|
| muscle | VL1 | | VL2 | | VL3/4 | |
| NMJ length / muscle length [%] | 16.7±7(n=13) | 32±9(n=15) | 10.0±2(n=13) | 17±6 (n=15) | 33.5±5 (n=13) | 48±13(n=15) |
| Significance | 0.001 | | 0.026 | | 0.004 | |
| no. nc82-dots | 14±2(n=10) | 18±6(n=10) | 8±3 (n=10) | 12±3(n=10) | 10±6(n=10) | 22±4(n=10) |
| Significance: | 0.100 | | 0.001 | | 0.001 | |
| no. bouton | fused | n.d. | fused | n.d. | 12±4(n=17) | 16± 4(n=17) |
| significance | n.d. | | n.d. | | 0.001 | |
| bouton size [µm] | n.d. | n.d. | n.d. | n.d. | 0.91 to 1.82 | 0.91 to2.2 |

| genotype | Wt | 066-pcas | Wt | 066-pcas | Wt | 066-pcas |
|---|---|---|---|---|---|---|
| muscle | VL1 | | VL2 | | VL3/4 | |
| NMJ length / muscle length [%] | 16.5±6(n=10) | 30±9(n=10) | 10.5±2(n=10) | 16±5 (n=10) | 30.7±10 (n=10) | 43±10 (n=10) |
| significance | 0.002 | | 0.042 | | 0.001 | |
| no. nc82-dots | 13±3 (n=10) | 15±5(n=10) | 10±3 (n=10) | 16±5 (n=10) | 19±4 (n=10) | 25±6 (n=10) |
| significance | 0.193 | | 0.005 | | 0.002 | |
| no. bouton | fused | 9±2 (n=10) | fused | 6±2 (n=10) | 12±3 (n=10) | 15±5(n=10) |
| significance | n.d | | n.d | | 0.006 | |
| bouton size [µm] | n.d | 0.91 to 2.0 | n.d | 0.91 to 2.0 | 0.91 to 1.82 | 0.91 to 2.2 |

| Mutant allele | Mapping position | Complementation results: | Comment: |
|---|---|---|---|
| *P{lacw}cas$^{j1C2}$* | 83C1 | Fails to complement the lethality and phenotype | indicates *castor* to be the gene |
| P{GT1}BG01673 | 89B16 | Complements both | P element insertion from bloomington. |
| *0223-02* | 98E-99A | Complements phenotype but not lethality. | another of the mutant P-element alleles from Cahir |

**Table 3.4 Summary of *0066-40/castor* phenotype.**

**Summary of the phenotypic and complementation analysis of mutant line 0066-40. Different parameters of the mutant synapses, like ratio of NMJ length to muscle length (synaptic span) [%], bouton count, (anti-Syn, anti-HRP, or anti-Dlg), active zone count (nc82, together with HRP), bouton sizes by taking the longest diameter in arbitrary angle [µm] (anti-Syn) were measured and compared to wildtype. Top table shows the comparison between wildtype and mutants and the middle one shows the comparison between wildtype and *(0066-40/P{lacw}cas$^{j1C2}$)* embryos. All the measurements were carried out manually using a scale. Significance of data was**

**tested with standard statistics procedures (t-test) (Chapter 2.1.12). The parameters showing significant deviation are shaded in grey. Comments on complementaion analysis of the mutant are presented in bottom table**

*3.2.2.5 Complementation mapping of insertion 0287-07*

Molecular data predict P-element insertions at map position 86F and 97C (FIG. 3.5, Appendix 6.5). The insertion at position 86F is predicted to affect two candidate loci, *LK6*, a protein kinase of the ras pathway which controls phosphorylation of eIF4E and promotes normal growth and development (Arquier et al., 2005) and/or the gene *CG31234* which was later on declared a prediction artefact (FBgn0051234). The insertion at 97C potentially affects the gene *CG5484*. Complementation tests of the line *0287-07* were attempted with 2 mutations mapped to these loci: the P-element insertion *I(3)10621* at 86F6-7 (Spradling et al., 1999) and *Df(3R)T1-X* uncovering the region 97B-97D (Anderson et al., 1985). Due to the fact that *0287-07* could not be kept over the green balancer used in my studies (*TM3,Sb,Kr::GFP*) the complementation crosses could unfortunately not be carried out in time. I later got a suitable GFP-labelled *TM6B* balancer which does not cause this lethality. However, respective complementation crosses were no longer of sufficient priority at that stage of my project and are still pending.

wt

0287-07

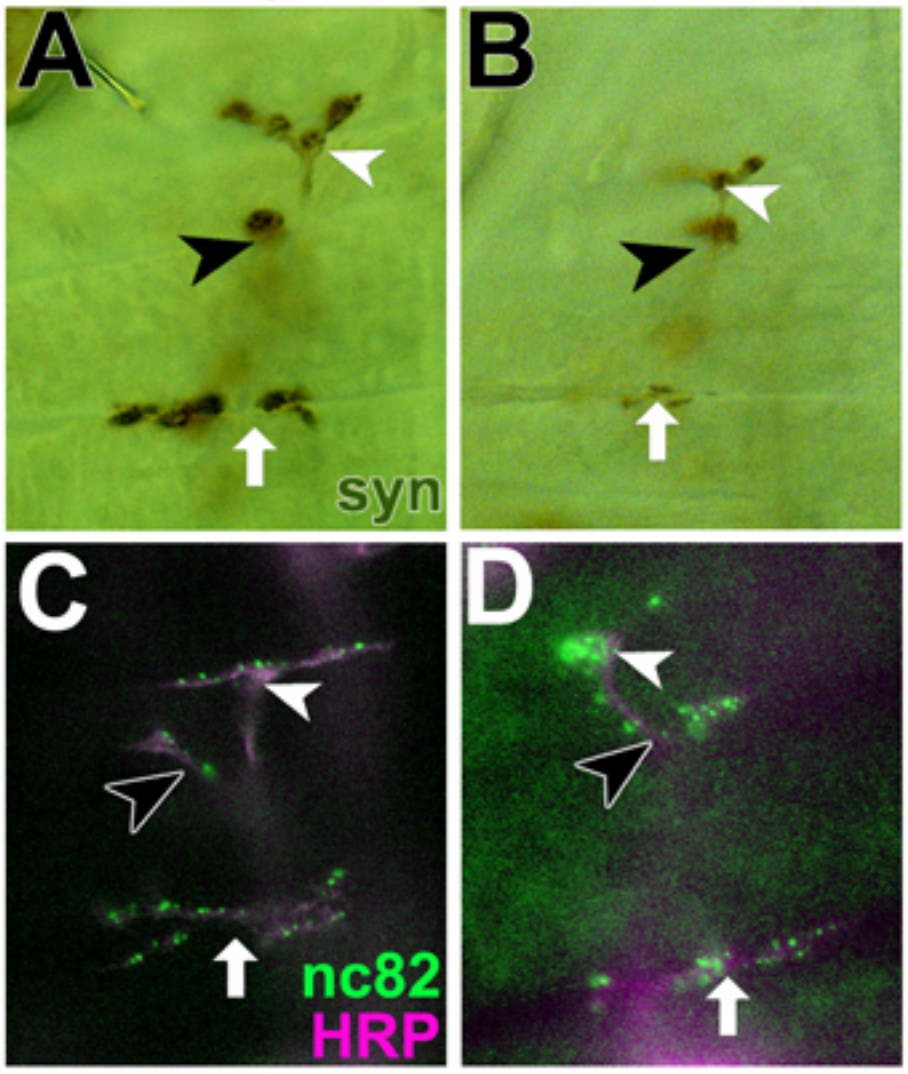


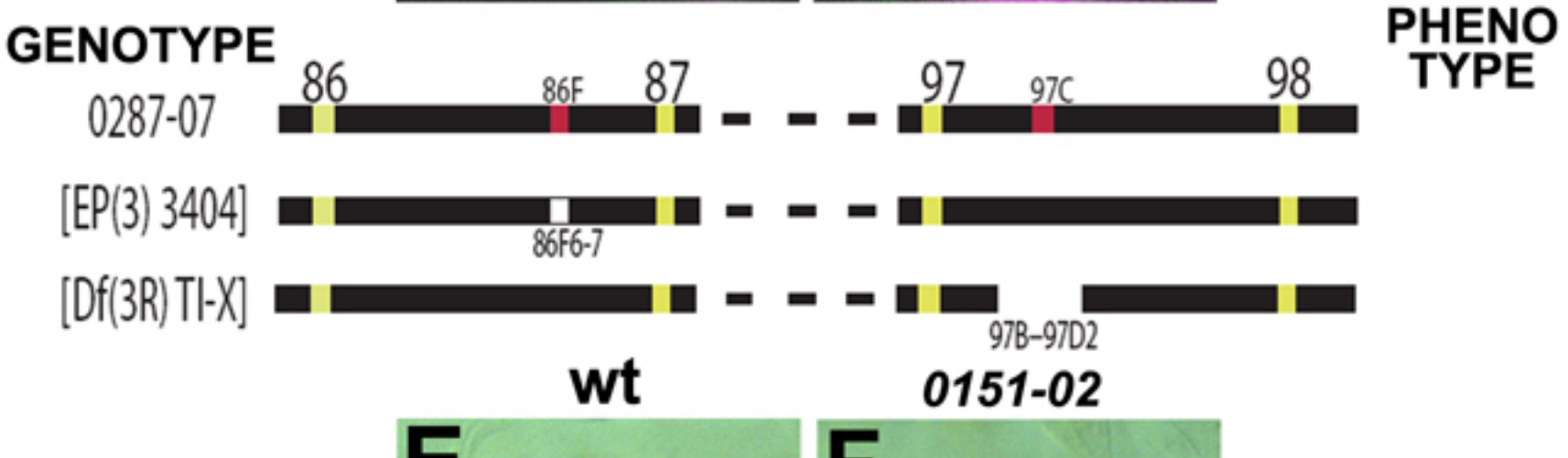


wt

0151-02

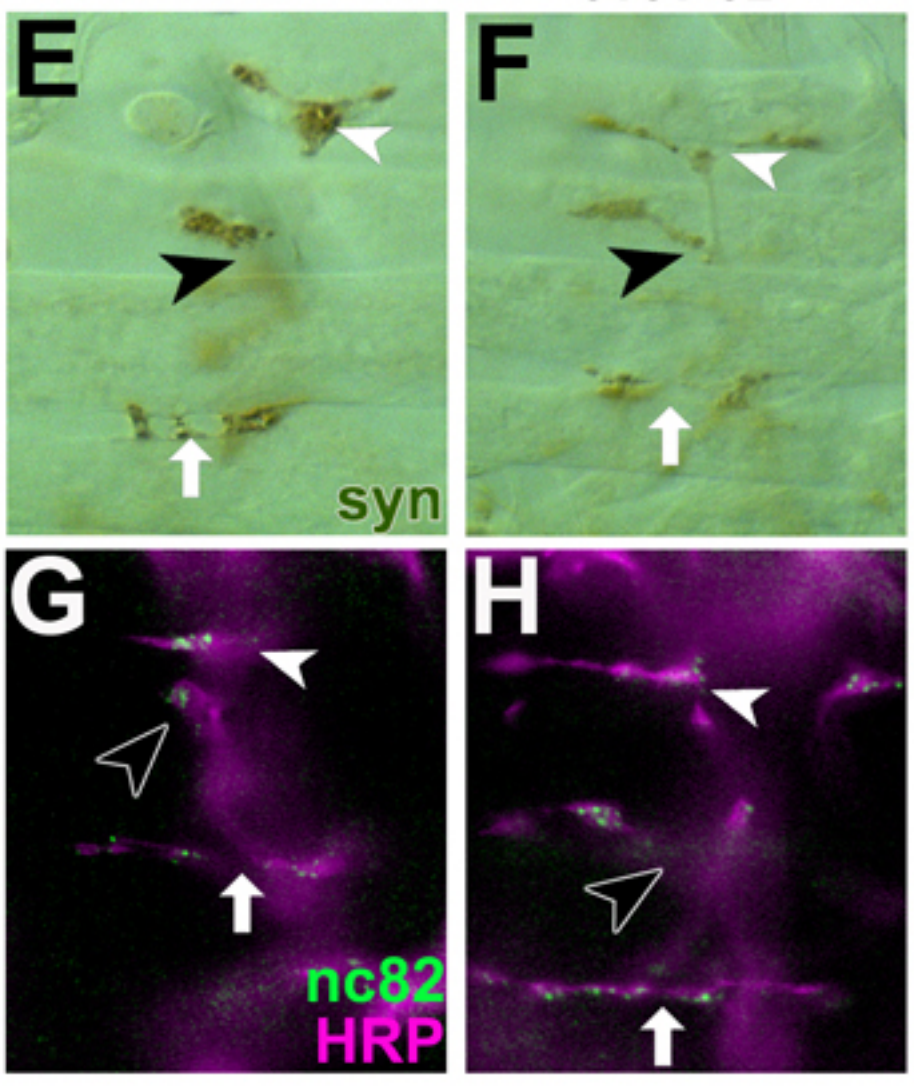


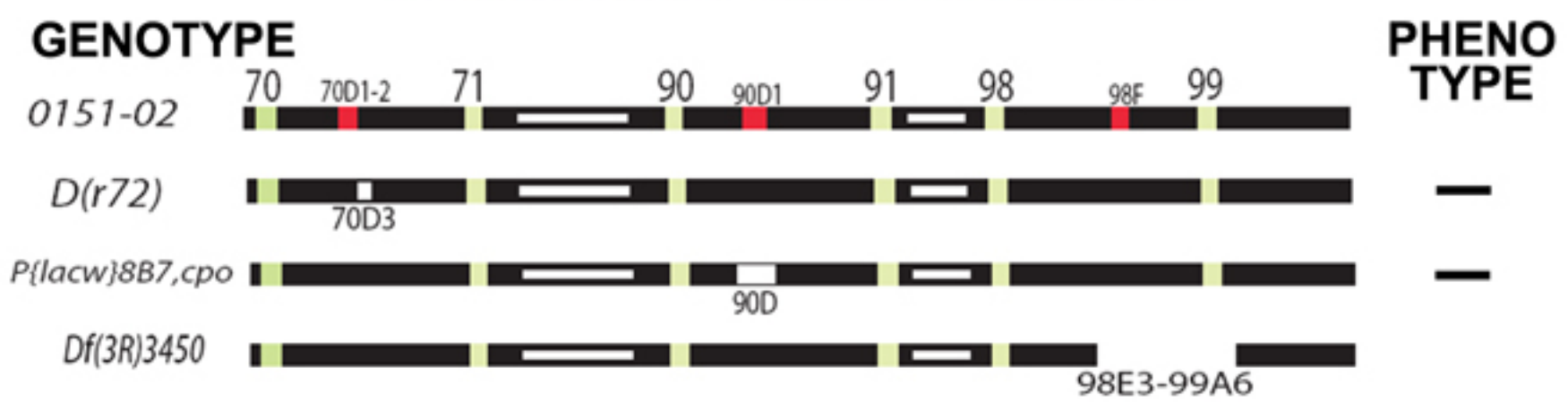

**Fig. 3.5 Mutant lines 0287-07 ans 1151-12 respectively displays under-grown and enlarged NMJ phenotypes.**

**Light microscopic images of the mutants with different synaptic markers. The two mutations display opposite phenotypes (synapses analysed are indicated by different symbols, VL1; white arrow head, VL2; black arrow head and VL3/4; white arrow). (A-D) show analysis of the mutation 0287-07. Synapsin staining reveals smaller NMJs with reduced number of boutons (A vs.B). Active zones in these boutons are also reduced as revealed by nc82 staining (compare C and D; labelled with anti-HRP, green and nc82, magenta). Complementation analysis for both the insertions is pending (Chapter 3.2.2.5).**

**0151-02 analysis (E-H), Synapsin staining reveals enlarged or expanded NMJs (E vs. F). Active zone number in these boutons remains unaffected as revealed by nc82 staining compare (G and H; labelled with anti-HRP, green and nc82, magenta). No clear data for complementation analysis of 1151-02 so far (Chapter 3.2.2.6).**

*3.2.2.6 Complementation mapping of insertion 1151-12*

Molecular data predict 3 P-element insertions at map positions70D, 90D and 98F (FIG. 3.5, Appendix 6.5). Complementation studies of *1151-12* with three different mutations mapped to these positions were carried out. First, complementation tests with the mutation *Dichaete*$^{r72}$ at map position 70D3 (FBrf0107195), were carried out, it fails to complement lethality and seems to fail to complement the elongated NMJ phenotype. Second, to my surprise, also the P-element insertion *P{lacw}8B7,cpo* at map position 90D (Bellen et al., 1992) fails to complement lethality and NMJ phenotype. Third, the deficiency *Df(3R)3450* at map position 98E-99A (Ahmad and Golic, 1998; Salzberg et al., 1997) complements both lethality and NMJ phenotype. Therefore, the genetics of the *1151-12* mutant strain look complicated and, at first hand, the results are not straightforward. However, it has to be mentioned, that these results are preliminary and need to be repeated for confirmation. Due to the mapping complications and time limitations, analyses of the *1151-12* mutant strain have not been followed up within the frame work of this project,

### *3.2.3. Complementation mapping of insertion 1107-02*

*3.2.3.1 Initial complementation mapping of insertion 1107-02*

Molecular data predict 2 P-element insertions at map position 75A and 76E (FIG. 3.6, Appendix 6.5). First, complementation tests were carried out with deficiency *Df(3L)XS-533* at map position 76 B4;77 B1 (FBrf0107806). *Df(3L)XS-533* fails to complement lethality but complements the NMJ phenotype. Thus, *1107-02/Df(3L)XS-533* embryos died at late embryonic stage17 or during the first larval instar, but anti-Synapsin staining revealed a normal bouton size. Second, complementation tests with the deficiency *Df(3L)W10* at map position 75A6-7;75C1-2 (Deak et al., 1997; Prout et al., 1997) complements lethality but fails to complement the fused bouton NMJ phenotype observed upon anti-Synapsin staining in *1107-02* homozygous mutant embryos (FIG. 3.6, Table 3.5). However, these results were hampered by the fact that *Df(3L)W10* could not be balanced over *TM3Sb,Kr-Gal4,UAS-GFP* (due to lethality of individuals balanced this

way) and my judgement relied on the finding that the predicted fraction of animals (according to Mendelian rules) showed the mutant NMJ phenotype. Third, the deficiency *Df(3L)ED4710* at map position 74D1;75B11 (FBab0035953) seems to fail to complements the NMJ phenotype. However, this stock could likewise not be balanced with *TM3Sb,Kr-Gal4,UAS-GFP*, it was very weak and died, eventually. However, analyses with both *Df(3L)W10* and *Df(3L)ED4710* suggest that the insertion at 75A potentially causes the phenotype and the other insertion at 76E alone or together with this insertion may be causing the lethality. In order to separate the effects caused by the two P-element insertions and to obtain further proof that the insertion at 75A causes the NMJ phenotype, I carried out chromosomal recombinations to separate the P-element insertions at 75A and 76E onto different chromosomes.

*3.2.3.2 Chromosomal separation of the P-insertion at 75A and 76E*

Following standard procedures of classical *Drosophila* genetics (Fly-Pushing) I carried out chromosomal recombinations making use of the dominant *white*$^{+}$ markers of the P-elements, the lethality potentially mapping to 76E and the NMJ phenotype potentially mapping to 75A. Due to the calculated expected recombination frequency of 2% I obtained only one recombinant fly line potentially carrying one isolated P-element insertion at 75A (*1107-02*$^{75A}$). To my surprise, the *1107-02*$^{75A}$ fly line is pupal lethal but does not show the fused bouton NMJ phenotype. Also analyses of NMJs at late larval stages (L3) did not reveal any obvious phenotype. This indicates that the recombination experiment was either not successful, or our interpretation of the initial complementation studies were not correct. Due to time limitations, molecular analyses of the *1107-02*$^{75A}$ mutant strain confirming the presence and position of the remaining P-element insertion were not carried out.

wt

1107-02

1107-02/P

A

B

C

syn

D

E

F

nc82
HRP

G

H

syn

GENOTYPE

PHENO TYPE

1107-02

75 75A 76 76E 77

PBac(W11)MED +

75A6-75C2

Df(3L)XS-533 -

76B4-77B

**Fig. 3.6 Fused bouton phenotype and complementation analysis of mutant line 1107-02.**

**The mutant line 1107-02 displays an interesting phenotype. Synapsin staining of ventral muscle NMJs (synapses indicated by different symbols, VL1; white arrow head, VL2; black arrow head and VL3/4; white arrow) reveals smaller NMJs with fused boutons (A vs.B). Active zones in these boutons also appear fused as revealed by nc82 staining (compare D and E; labelled with anti-HRP, green and nc82, magenta). Synapsin staining of dorsal muscle NMJs (DO1; black arrow and DO2; black curved arrow) shows a similar phenotype (G vs. H). Complementation analysis of the mutation reveals that another p-insertion *PBac{WH}MED19*$^{f07123}$, when heterozygous to 1107-02 displays a similar phenotype as shown by synapsin staining (A vs. C) and nc82 labelling (D vs. F). The graph summarises the outcome of complementation tests.**

*3.2.3.3 Precise mapping of insertion 1107-02*

The molecular data from Cahir O'Kane's laboratory suggest that the P-element at 75A is inserted into the gene *CG5567* (Appendix 6.5). The P-element is inserted into an exon at base pair 231 of the gene (about 2.010kb at genomic level). The gene is separated by just 260bps from the next downstream gene *CG5546*. Therefore, it is possible that the regulation of *CG5546* might be affected by the insertion and causing the observed phenotype. Recently, 4 newly generated P-element insertions in the 75A region became available: *PBac{WH}CG5567*$^{f05921}$ (lethal, unverified) and *PBac{WH}MED19*$^{f07123}$ (semi-lethal) represent P-element insertions into the gene *CG5567*, whereas *P{SUPor-P}CG5577*$^{KG00497}$ and *P{EPgy2}CG5577*$^{EY08509}$ are viable P-element insertion into the locus *CG5577*. No P-element insertion into the gene *CG5546* is available so far. My analyses of homozygously mutant embryos showed that the P-element insertions into gene *CG5577*, i.e. *P{SUPor-P}CG5577*$^{KG00497}$and *P{EPgy2}CG5577*$^{EY08509}$ do not show any obvious NMJ phenotypes, whereas at least one of the P-element insertion into *CG5567* (*PBac{WH}MED19*$^{f07123}$) displays a fused bouton NMJ phenotype similar to that of the mutant line *1107-02*. Preliminary analysis of the other P-element insertion *PBac{WH}CG5567*$^{f05921}$ suggests that this insertion might also cause the NMJ phenotype, but rebalancing of the stock with the *TM3Sb,Kr-Gal4,UAS-GFP* is required to confirm this statement. Taken together, all these above results demonstrate that the gene *CG5567* is responsible for the phenotype. According to FlyBase (FBgn0036760), *CG5567* codes for an enzyme with 4-Nitrophenylphosphatase activity. Unfortunately, the precise mapping of this phenotype occurred too late to trigger further functional and molecular analyses of this locus within the framework of this project.

| genotype | Wt | 1107-02 | Wt | 1107-02 | Wt | 1107-02 |
|---|---|---|---|---|---|---|
| muscle | VL1 | | VL2 | | VL3/4 | |
| NMJ length / muscle length [%] | 16±3(n=10) | 16±4(n=25) | 9±2(n=10) | 8.5±3(n=25) | 32±12 (n=10) | 27±10 (n=25) |
| significance | 0.731 | | 0.474 | | 0.088 | |
| no. nc82-dots | 8±3 (n=5) | 9±2 (n=10) | 6±1(n=5) | 6±3 (n=10) | 13±3 (n=5) | 13±3 (n=10) |
| no. bouton | fused | n.d | fused | n.d | 14±1 (n=10) | 13±4 (n=10) |
| bouton size [µm] | n.d. | n.d. | n.d. | n.d. | 0.91 to 1.82 1.36±.45 (n=14) | 1.27 to 2.7 2,18±.40 (n=22) |
| significance | n.d. | | n.d. | | 0.003 | |

| Mutant allele | Mapping position | Complementation results: | Comment: |
|---|---|---|---|
| Df(3L)XS533 | 76B4-77B1 | Complements phenotype but not lethality. | Deficiency from Bloomington. |
| Df(3L)ED4710 | 74D1-75B11 | Seems to complement the phenotype | Deficiency from Drosdel. |
| Df(3L)W10 | 75A6-75C2 | Fails to complement the lethality. | Deficiency from Bloomington. |
| PBac{WH}MED19$^{f07123}$ | 75A6 | Fails to complement phenotype | CG5567 is responsible for the phenotype |

**Table 3.5 Summary of *1107-02* phenotype.**

**Summary of the phenotype and complementation analysis of mutant line 1107-02, Different parameters of the mutant synapses, like ratio of NMJ length to muscle length (synaptic span) [%], bouton count, (anti-Syn, anti-HRP, or anti-Dlg), active zone count (nc82, together with HRP), bouton sizes by taking the longest diameter in arbitrary angle [µm] (anti-Syn) were measured and compared to wildtype.**

**All the measurements were carried out manually using a scale. Significance of data was tested with standard statistics procedures (t-test) (Chapter. 2.1.12). Only the parameters showing significant deviation are shaded in grey.**

**Comments on complementaion analysis of the mutant is presented in bottom table**

### *3.2.4 Complementation mapping of insertion 0242-41*

#### *3.2.4.1 Initial complementation mapping of insertion 0242-41*

Molecular data predict 2 P-element insertions at map position 84F11 and 87CD (FIG. 3.7, Appendix 6.5). Complementation tests of *0242-41* were carried out with deficiency *Df(3R)CA3* at map position 84F2-85A7 (Bender et al., 1987; Roseman et al., 1995) which fails to complement late embryonic lethality and the NMJ phenotype. Synapsin staining of *0242-41/Df(3R)CA3* mutant embryos revealed a similar undergrown NMJ phenotype as homozygous *0242-41* mutant embryos (FIG. 3.7, Table 3.6). Inverse-PCR data from the laboratory of C. O'Kane suggest that the other insertion at 87CD affects the gene locus at 87C6-7 which encodes Malic enzyme (FBgn0002719, Appendix 6.5). Unfortunately, no suitable independent mutations were available for this area so that complementation studies could not be carried out. However, later experiments confirmed my results with deficiency *Df(3R)CA3* and made complementation studies at 87CD obsolete.

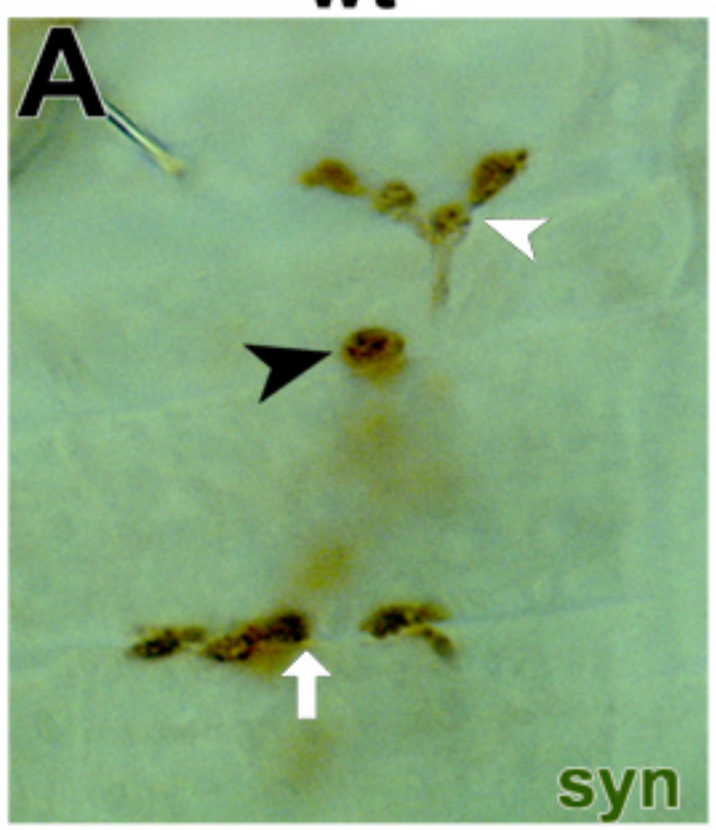
wt
A
syn

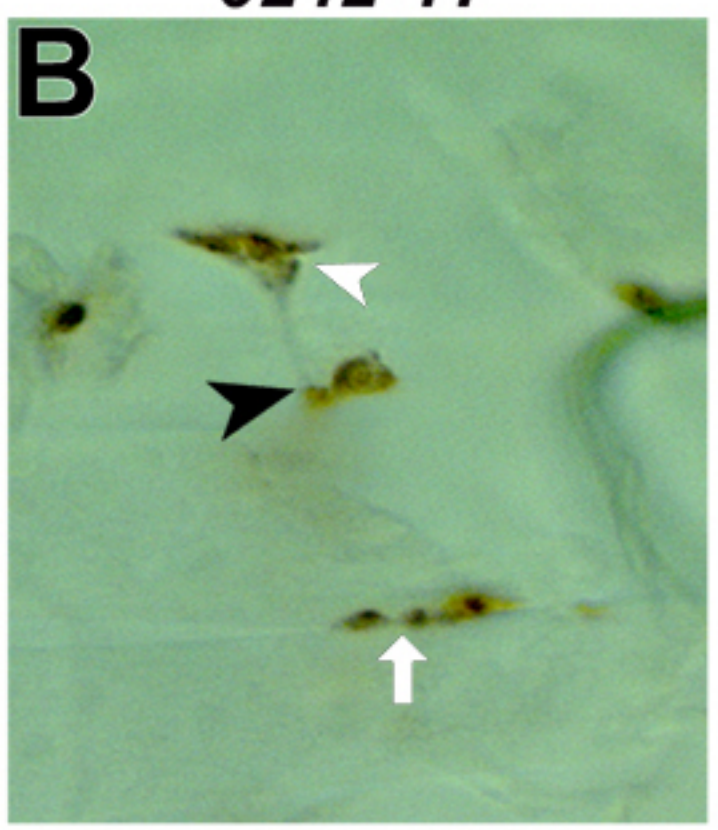
0242-41
B

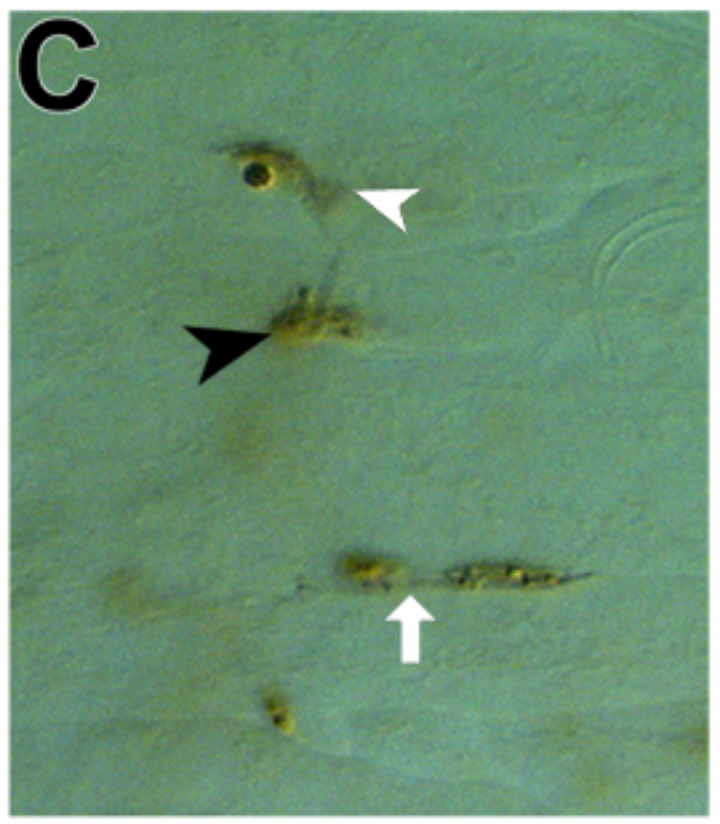
0242-41/def
C

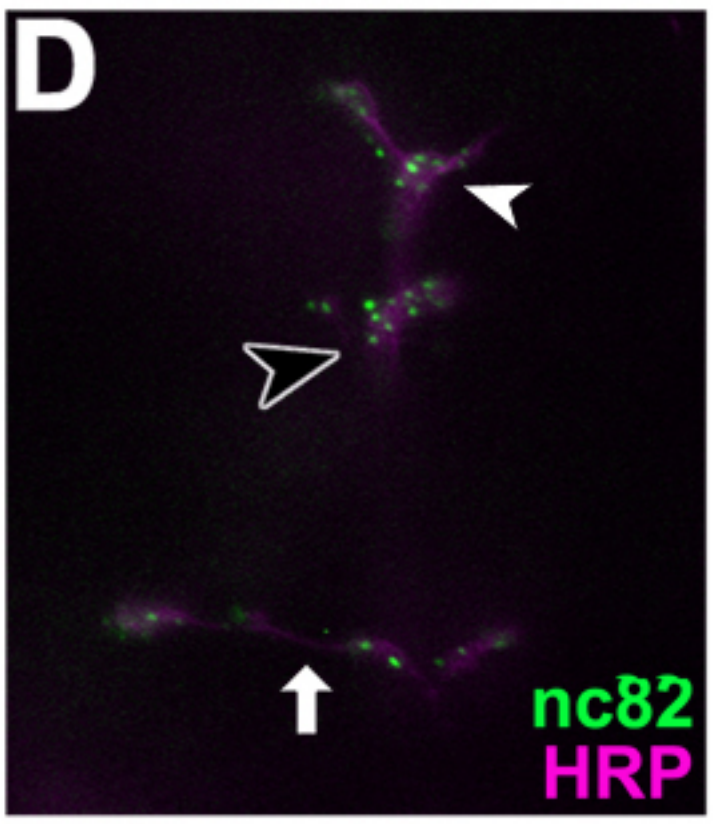
D
nc82
HRP

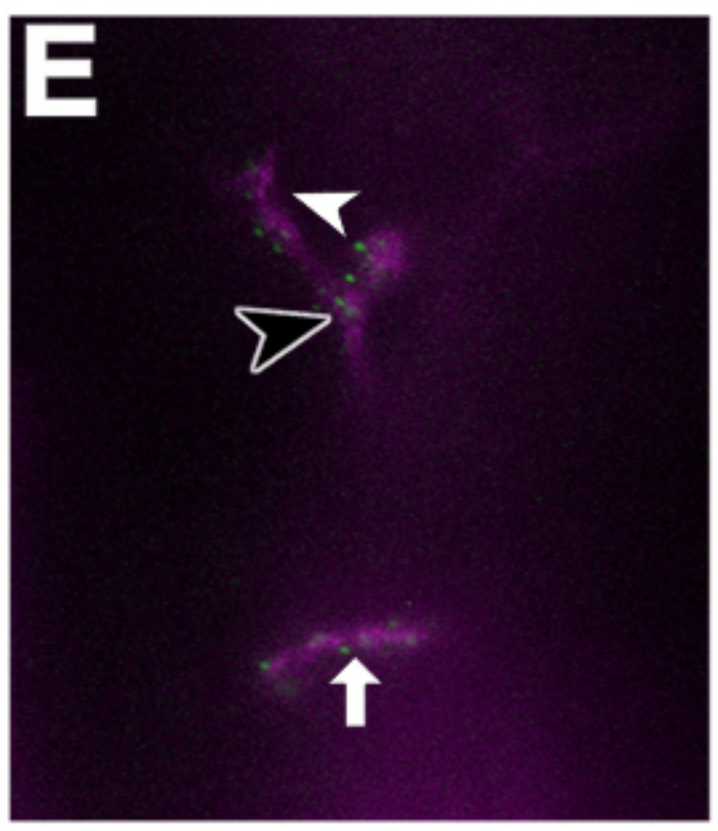
E

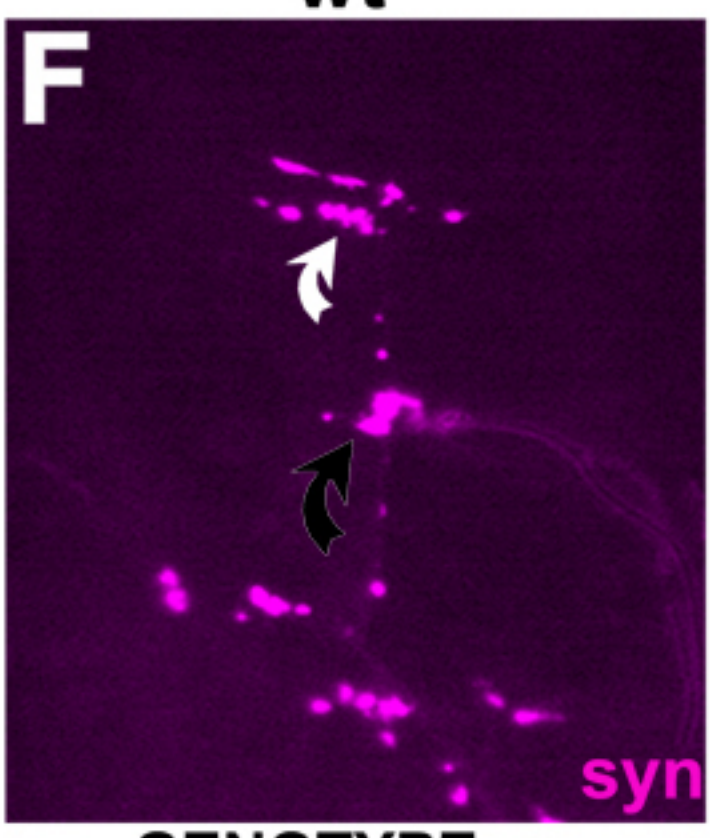
wt
F
syn

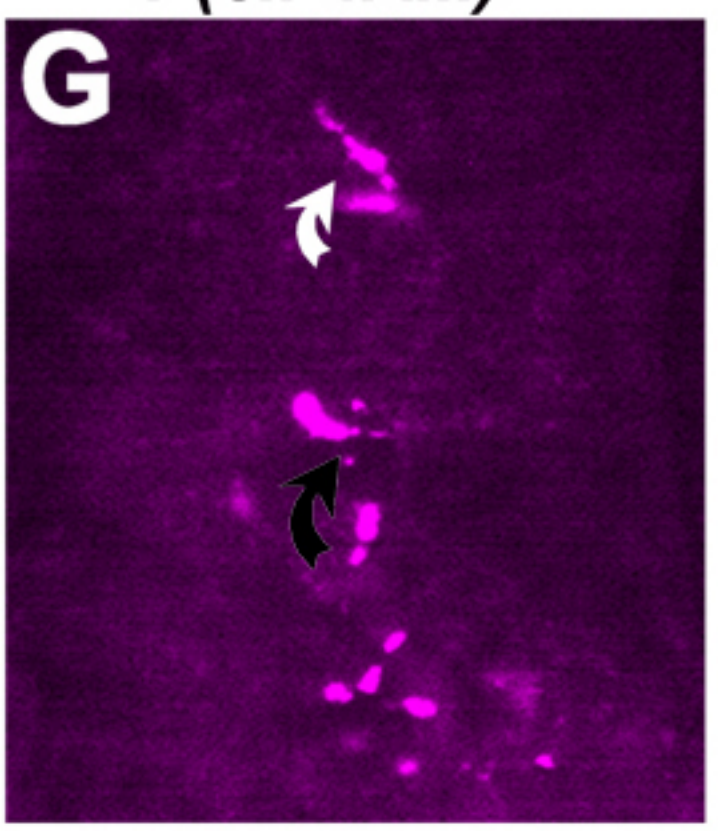
P(eIF4AIII)
G


GENOTYPE
PHENOTYPE
242-41
84
84F6
85
87
87CD
88
Df (3R) CA3
84
84F2-85A7
87
88
+
Df (3R)116
84
85
87
88
–
P{EPgy2}eIF4AIIIEY14207
84
84F6
85
87
87CD
88
+

**Fig. 3.7 Under-grown NMJ phenotype and complementation analysis of the mutant line 0242-41.**

**Light microscopic images of the mutant line 0242-41 with different synaptic markers.**

**The mutant line 0242-41 displays an interesting under-grown NMJ phenotype. Synapsin staining of ventral muscle NMJs (synapses indicated by different symbols, VL1; white arrow head, VL2; black arrow head and VL3/4; white arrow) reveals smaller NMJs with reduced number of boutons (A vs. B). Active zones in these NMJs are also reduced as revealed by nc82 staining (compare D and E; labelled with anti-HRP, green and nc82, magenta). Complementation analysis of the mutation reveals that the deficiency *Df (3R) CA3* when heterozygous to 0242-41 displays similar phenotypeas as shown by synapsin staining (A vs. C). Synapsin staining (F and G) of another p-insertion *P{EPgy2}eIF4AIII*$^{EY14207}$ affecting the same gene (*eIF4AIII*) as mutation 242-41 independently yields similar phenotype, synapsin staining of dorsal muscle NMJs ( DO1; black arrow and DO2; black curved arrow) reveals a similar under-grown NMJ phenotype (F vs. G). Graph summarises the outcome of complementation analysis (Chapter 3.2.4).**

*3.2.4.2 Precise mapping of 0242-41*

The molecular data from Cahir O'Kane's laboratory show that the P-element is inserted in the 3' region of the gene *CG7483/eIF4AIII*. The gene encodes a translation initiation factor (*eIF4AIII*; )(Lasko, 2000; Palacios and St Johnston, 2002). It is also close to or even in the 3' end of *CG9613* (polyprenyltransferase; Appendix 6.5). This raises the possibility that this locus might likewise be affected by the *0242-41* mutation and cause the NMJ phenotype. In order to assign the involvement in NMJ formation to either of these loci, further complementation studies were carried out.

The deficiency *Df(3R)116* deletes the gene *CG9613* without affecting *eIF4AIII* (Palacios and St Johnston, 2002), and it complements the NMJ phenotype as well as the lethality of *0242-41*, arguing against the involvement of *CG9613* in NMJ development. In order to confirm involvement of *eIF4AIII* in NMJ formation, complementation tests have been and are being carried out with known mutant allele of this locus. The mutant allele *l(3)84Fi* carries a point mutation in *eIF4AIII* causing a single serine to glycine exchange in a conserved DEAD-Box domain (Palacios and St Johnston, 2002). The mutation causes pupal lethality in homozygous condition, but homozygous mutant embryos and larvae do not show any synaptic phenotype. 0*242-41*/*l(3)84Fi* transheterozygous mutant animals likewise lack embryonic or larval NMJ phenotypes. However, they display semi-lethality (about 50% die at early pupal stage). Thus, lethality seems to be partially rescued in this constellation. However, eclosed female flies are sterile. This sterility may indicate a failure of both mutations to complement each other, since *eIF4AIII* has a proposed role during oogenesis. This possibility is presently being tested in collaboration with I. Palacios (Cambridge, UK). Since the complementation experiments with 0*242-41*/*l(3)84Fi* transheterozygous mutant animals delivered unclear results, I made use of two more P-element insertions in the *eIF4AIII* gene which have become available since then. Transheterozygous animals carrying the *0242-41* mutation over the *P{EPgy2}eIF4AIII*$^{EY14207}$ (inserted in the 5' UTR of *eIF4AIII*; FBti0057889), are larval lethal and cause the undergrown NMJ phenotype. The other, non-lethal P-element

insertion *P{GT1}eIF4AIII*$^{GT\text{-}000230}$ (inserted in the 5' UTR of *eIF4AIII*; FBti0058520) has yet to be tested.

Taken together, my complementation studies strongly suggest that the *eIF4AIII* gene is required for size regulation at the newly established embryonic NMJ. This notion is supported by at least two independent lethal P-element insertions which show the same phenotype and fail to complement each other, and by the fact that the adjacent *CG9613* locus could be excluded successfully.

| **genotype** | **Wt** | **242-41** | **Wt** | **242-41** | **Wt** | **242-41** |
|---|---|---|---|---|---|---|
| **muscle** | VL1 | | VL2 | | VL3/4 | |
| **NMJ length / muscle length [%]** | 16±7(n=13) | 13±4(n=13) | 10.0±2(n=13) | 7±3 (n=13) | 33.5±5 (n=13) | 27±5(n=13) |
| **significance** | 0.063 | | 0.002 | | 0.014 | |
| **no. nc82-dots** | 8.5±4 (n=10) | 7±2 (n=9) | 7±3 (n=9) | 4±1 (n=9) | 11±3 (n=9) | 8±3 (n=9) |
| **significance** | 0.329 | | 0.502 | | 0.165 | |
| **no. bouton** | fused | n.d. | fused | n.d. | 12±3 (n=7) | 6±4 (n=10) |
| **significance** | n.d. | | n.d. | | 0.0010 | |
| **Bouton size [μm]** | n.d. | n.d. | n.d. | n.d. | 1.6 to 1.82 | .91 to 2.2 |
| **significance** | n.d. | | n.d. | | 0.267 | |

| **genotype** | **Wt** | **242/CA3** | **Wt** | **242/CA3** | **Wt** | **242/CA3** |
|---|---|---|---|---|---|---|
| **muscle** | VL1 | | VL2 | | VL3/4 | |
| **NMJ length / muscle length [%]** | 16±8(n=10) | 12±5(n=10) | 10±3(n=10) | 6.5±3 (n=10) | 33±5 (n=10) | 26.5±5(n=10) |
| **significance** | 0.052 | | 0.002 | | 0.019 | |
| **no. bouton** | fused | 9±2 (n=10) | fused | 6±2 (n=10) | 12±3 (n=10) | 7±4 (n=10) |
| **significance** | n.d. | | n.d. | | 0.0012 | |
| **Bouton size [μm]** | n.d. | 0.91 to 2.0 | n.d. | 0.91 to 2.0 | 1.6 to 1.82 | .91 to 2.2 |

| **Mutant allele** | **Mapping position** | **Complementation results:** | **Comment:** |
|---|---|---|---|
| *Df(3R)CA3* | 84F2-85A7 | Fails to complement the lethality and phenotype | indicates *CG7483* to be the gene |
| | 87CD | Not done | (Malic enzyme) Non-essential. |

**Table 3.6 Summary of 242-41/eIF4AIII phenotype.**

**Summary of the phenotype and complementation analysis of mutant line 0242-41, Different parameters of the mutant synapses, like ratio of NMJ length to muscle length (synaptic span) [%], bouton count, (anti-Syn, anti-HRP, or anti-Dlg), active zone count (nc82, together with HRP), bouton sizes by taking the longest diameter in**

**arbitrary angle [µm] (anti-Syn) were measured and compared to wildtype. Top table shows the comparison between wildtype and mutants and the middle one shows the comparison between wildtype and *(242-41/Df(3R) CA3)* NMJs. All the measurements were carried out manually using a scale. Significance of data was tested with standard statistics procedures (t-test) (Chapter 2.1.12). The parameters showing significant deviation are shaded in grey.**
**Comments on complementaion analysis of the mutant is presented in bottom table**

### *3.2.5 Selection of mutant fly strains for further investigation*

Out of the 8 mutations, 6 were precisely mapped and 4 selected for further genetic and molecular investigations, which include 2 known genes Castor and Eukaryotic translation initiation factor eIF4AIII and 2 novel genes CG4699 (named Waharan) and CG5567 (4-nitrophenylphosphatase) see Discussion (Chapter 4).

## 3.3 Analysis of *0066-40*/*castor*

### *3.3.1 Confirmation of castor as the gene affected by the 0066-40 insertion*

The complementation mapping studies of *0066-40* revealed that the mutation affects the gene *castor* (Chapter. 3.2.2.4) as it fails to complement the P-insertion line *P{lacw}cas*$^{j1C2}$. The result strongly suggests that *castor* is required for growth regulation at NMJs. Taking the advantage of the vast literature and available tools and antibodies I tried to explore the role of *castor* in this novel overgrown NMJ phenotype and performed further genetic analysis.

First, I performed anti-*castor* staining on stage 16 embryos. Anti-castor immuno-staining (Kambadur et al., 1998) revealed rather normal expression in the mutant demonstrating that *0064-40* is not a protein null allele of *castor*. Therefore, I tested the potential involvement of *castor* in other ways by using aspects of *castor* mutant phenotypes mentioned in the literature. Castor is a neuronal zinc finger transcription factor containing a novel zinc-binding domain and multiple transcriptional activation domains. At larval and pupal stages, it is expressed in brain cell clusters where it interacts genetically with *lio* participating in the elaboration of adult structures (Hitier et al., 2001). In the embryo, *castor* is expressed in a subset of CNS neuronal precursor cell, i.e. a subset of delaminated CNS neuroblasts and ventral midline glial precursor cells. Its function is required for the normal development of a subset of neuronal precursors (Mellerick et al., 1992) and loss of *castor* function results in reproducible alterations of CNS gene expression (e.g. of engrailed), defects in axogenesis and embryonic lethality. *Castor* embryos have been shown to diplay subtle but clear defects in the pattern of CNS axons (Cui and Doe, 1992). The wild type CNS has two longitudinal connectives and a segmentally repeated pair of commissures (anterior and posterior), which can be detected with *BP102* monoclonal antibody (Klambt et al., 1991). All *castor* alleles show reduction in the width of the posterior commissures. I wondered whether the *0066-40* allele also shows this phenotype. To this end, I performed anti-*BP102* staining of *0066-40* mutant embryos. Like other *castor* alleles, anti-*BP102* staining of *0066-40* mutant line revealed

reduction in the width of posterior commissures but not the anterior ones (FIG. 3.4). These results further demonstrate that mutant line *0066-40* is a *castor* mutant allele.

### *3.3.2. 0066-40 displays increased number of Q/ motorneurons*

My analyses suggest that *castor* function is required for the quantitative aspects at developing NMJs. According to published data, *castor* mutant embryos display a significantly increased numbers of Q motor-neurons in the NB4-2 lineage, at the expense of inter-neurons (Schmid and Doe, 1998). In order to find out whether the *0066-40* mutation also has an increased number of motor-neurons, I performed anti-*eve* staining of the mutant embryos. Anti-*eve* labels a sub-fraction of motorneurons including that of the NB4-2 and NB1-1 lineages. Anti-*eve* stainings confirmed increased numbers of Q motor-neurons (but possibly not the aCC motorneuron) also in the mutant line *0066-40* (FIG. 3.4). Therefore, the increase of bouton numbers at *066-40* mutant NMJs could well be a result of increased numbers of motor-neurons causing more axons emerging out of the CNS and innervating the muscles. However, Q neurons innervate dorsolateral to dorsal muscles only, whereas the increased NMJ phenotype is displayed by all the terminals, including ventral NMJs. Therefore, I used a general motorneuronal marker pSmad to check if there is an overall increase in numbers of motorneurons. Anti-pSmad staining may show any obvious increase in number of motoneurons. Furthermore, I carried out anti-Fasciclin2 stainings as a motoraxonal marker. Since increased number of motorneurons is expected to lead to increased number of motoraxons, we expected a thicker motornerve leaving the CNS. However, my Fasciclin2 stainings in stage 16 embryos revealed normal motornerves when compared to wildtypic animals. Thus, my analysis does not reveal any increase in the density of axon fascicle leaving the CNS.

### *3.3.3. Increased pre-synaptic area is not well compensated by the post-synaptic muscles*

The NMJ phenotype with an increased number of boutons and active zones displayed by the mutant line *0066-40* reflects that there is increased pre-synaptic area. Is this increase matched by postsynaptic specialisations of the muscle? Two possibilities arise, either the

synapses would spread over other parts of the muscles and form additional synapses in areas which are otherwise devoid of synapses, or presynaptic specialisations remain partly unattached to muscles as has been described previously for *mbc* or *mef2* mutant embryos (Prokop et al., 1996). In order to distinguish between these possibilities, I did double-labelling experiments using a pre-synaptic and a post-synaptic marker to see how far they co-localize. I used synapsin as pre-synaptic and Discs large as post-synaptic marker. The double stainings in *0066-40* mutant embryos usually show overlap of both markers, as in the wild type (FIG. 3.4). However, in the mutants there are Synapsin spots non-matched by post-synaptic Dlg, suggesting some of the pre-synaptic boutons fail to attach to post-synaptic muscle partners. Ultrastructural analysis of the mutant embryos is underway.

wt

242

A

Fas2

B

RND ;; uas-CD8-GFP

RND ;; Uas-CD8-GFP ;; 242

C

GFP

D

wt

242-42

E

HRP

F

Mj94 ;; Uas-CD8

Mj94 ;; Uas-CD8:: 242

G

CD8

H

**Fig. 3.8 0242-42 specifically cause NMJ undergrowth.**

**Confocal images showing different aspects of development of embryonic nervous system of 0242-41 mutants.**

**The CNS of 0242-41 mutants and wildtype control (labeled with anti-Fas2, magenta), nerve pattern is unaffected in the mutants (B) and is comparable to wildtype control (A). Dendrites and dendritic arborisations analysed (C, D: labeled with anti-GFP, green indicated by curved white arrows), by driving *Uas-CD8-GFP* with *RND-Gal4* in mutant background (D) revealed that these structures are unaffected in the mutants and appeared normal and comparable to *RN2D ;;Uas-CD8-GFP* dendrites (C). Sensory, chordotonal organs (E,F: labeled with anti-HRP, green) also look comparable to wildtype (E vs. F).**

**Another sensory tissue, mutidendritic organs analysed (G, H: labeled with anti-CD8, green) by driving *Uas-CD8* with *MJ94* in mutant background (H) revealed they are unaffected and appear normal and comparable to *MJ94 ;;Uas-CD8* multidendritic organs (G).**

## 3.4 Analysis of *0242-41*/*eIF4AIII*

I obtained clear results for the complementation mapping of the mutation *0242-41* from the failure to complement P-element insertion *P{EPgy2}eIF4AIII*$^{EY14207}$ (Chapter. 3.2.4) strongly suggesting that the gene encoding *eIF4AIII* is required for normal growth of NMJs. As detailed in the Discussion, eIF4AIII is a eukariotic translational initiation factor most likely of inhibitory nature (Chapter. 4.3.2). As described in the following, my analyses suggest that *eIF4AIII* may be regulating synaptic growth by inhibiting the local translation of Dlg in NMJ.

### *3.4.1. The phenotype is specific to Neuromuscular terminals*

Defects of translational control are likely to have a global effect on embryos. To check whether the undergrown NMJ phenotype of *0242-41*/*eIF4AIII* mutant embryos is specific, I analysed mutant embryos in greater detail. My analyses with anti-Dlg (labelling NMJs strongly but also whole muscles at lower intensity) suggest that the muscle pattern looks more or less normal (FIG. 3.8). Stainings with anti-Fasciclin2 revealed no obvious defects in the nerve pattern in mutant embryos (FIG. 3.8). Sensory chordotonal organs in the mutants (labelled with anti-HRP) appeared likewise normal. Also arborisations of a subset of motorneuronal dendrites in the CNS of the mutant embryos appeared normal as revealed by GFP staining of *RN2D+O;0242*/*Uas-CD8-GFP;0242* embryos. Finally I analysed multi-dendritic neurons in the mutant embryos by staining *MJ94-Gal4;Uas-CD8;0242/0242* embryos against *CD8*, and found no phenotype. Taken together, these results demonstrate that reduced NMJ size phenotype is a specific effect caused by the mutation in the gene eIF4AIII.

### *3.4.2. Dlg accumulates in mutant NMJs*

Various synaptic markers used for the analysis of the mutant phenotype like synapsin, nc82/Bruchpilot and the neuronal surface markers *HRP* and Fascilin2 are normally expressed and localised at *0242* mutant terminals (FIG. 3.9). The membrane-associated

PDZ domain protein *Dlg* is accumulated on the postsynaptic side of NMJs in the wildtype (FIG. 3.9). When comparing mutant and wildtype NMJs of specimens dissected and stained in parallel on the same slide, Dlg had a clear tendency to accumulate stronger at the mutant NMJ in mutant NMJs. We speculated that the reduced terminal may have an impact on the appearance of Dlg localisation and tested therefore another independent mutation, short stop, in which terminals are likewise reduced. However, the expression of Dlg in *shortstop* mutant embryos did not show an obvious enhancement. We therefore assume that Dlg staining is genuinely enhanced at *0242* mutant terminals.

Like other MAGUK proteins such as PSD-95 (Sheng and Pak, 1999; Sheng and Pak, 2000), Dlg is involved in the recruitment and/or stabilization of a variety of synaptic proteins, as has been shown for Fasciclin2 and B-type *Drosophila* glutamate receptors (DGluRIIB; )(Chen and Featherstone, 2005; Thomas et al., 1997; Zito et al., 1997). I therefore wanted to test whether any of these target proteins would be altered, too. Such a finding would open up avenues for further research, since Fascilin2 as well as DGluRIIB have been involved in size regulation at NMJs previously (DiAntonio et al., 1999; Schuster et al., 1996). I did not manage yet to carry out anti-DGluRIIB stainings, but tested my hypothesis with anti-Fasciclin2 stainings. Surprisingly, my analysis revealed that Fas2 expression and localisation remains unaffected in these terminals. Taken together, my results tempt to speculate that eIF4AIII might be negatively regulating NMJ size through local translation of Dlg at the terminals, but so far we have no evidence that localisation of other synaptic proteins known to be localised by Dlg are affected in the mutant terminals.

### *3.4.3. Pre- or postsynaptic overexpression of Dlg causes no obvious NMJ phenotype*

If the reduced terminal phenotype observed in *eIF4AIII* mutant embryos is due to enrichment of Dlg at the terminals, its over-expression in muscles should yield *0242/eIF4AIII*-like reduced NMJ phenotypes. I tested this possibility by over-expressing *Dlg-S97N-EGFP* (Bachmann et al., 2004) in muscles, using the mesoderm specific Gal4-driver line *24B*-Gal4 (Kidd et al., 1999). These animals are viable and do not show any obvious undergrown NMJ phenotype. Thus, post-synaptic over-expression of Dlg did not

cause any phenotype. I also tested whether I can phenocopy the reduced NMJ phenotype by over-expressing *Dlg* in the presynaptic motorneurons. In order to do this, I used the neuron-specific Gal4–driver line *RN2D+O*. Again I did not find any obvious NMJ phenotype (FIG. 3.9).

Taken together, we could not phenocopy the reduced terminal phenotype by over-expressing *dlg* in muscles or neurons. It seems therefore, that Dlg is not sufficient to induce *eIF4AIII*-like mutant phenotypes.

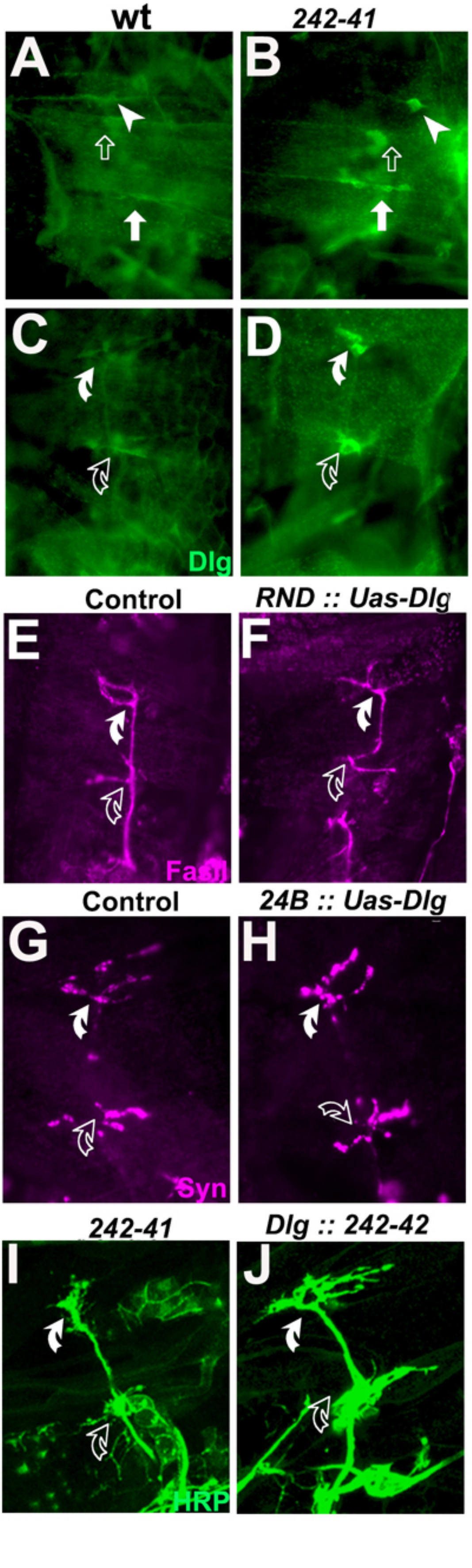
wt
242-41
A
B
C
D
Dlg
Control
RND :: Uas-Dlg
E
F
FasII
Control
24B :: Uas-Dlg
G
H
Syn
242-41
Dlg :: 242-42
I
J
HRP

**Fig. 3.9 Dlg accumulates in 0242-41 mutant under-grown NMJs, and the phenotype is suppressed in Dlg mutant background.**

**Light microscopic and confocal images of the different staining of embryonic NMJs (A and B ventral muscle and C to J dorsal muscle NMJs)**
**0242-41 and wildtype embryonic NMJs (labelled with anti-Dlg, green), show Dlg is accumulated in mutant NMJs compared to wildtype (B, D ventral vs. A, C dorsal muscle NMJs, synapses indicated by different symbols). Dlg overexpression experiments (E,F,G and H) reveal that Dlg (Uas-*Dlg-S97N-EGFP*) over expression either in motorneurons by *RN2* (E, F labelled with anti-fas2, magenta) or in mesoderm by *24B-Gal4* (G, H labelled with anti-synapsin, magenta) does not cause under-grown NMJ phenotype. (I, J) Under-grown NMJ phenotypes caused by the mutation 0242-42, is suppressed by Dlg mutation as double mutants of Dlg (*$Dlg^{PG100}$* ; 0242-41) (I and J, anti-HRP green) have normal NMJs compared to the mutant (I vs. J).**

### *3.4.4 Synaptic phenotype of eIF4AIII is suppressed in dlg mutant background*

Even if mimicking Dlg overexpression of *eIF4AIII* mutations via the Gal4/UAS system is not sufficient to cause reduced NMJ phenotypes, this does not exclude an involvement of Dlg. I therefore addressed, whether Dlg is required for the *eIF4AIII*-induced mutant phenotype. To this end, I tested whether taking out *dlg* in *eIF4AIII* mutant embryos would rescue the undergrown NMJ phenotype. To perform this experiment, I generated a double mutant stock using the $dlg^{PG100}$ mutant allele in combination with the *0242* allele and examined the phenotype to ascertain the relationship between the two genes. Double mutants do not show the reduced terminal phenotype as displayed by the *eIF4AIII* mutant alone but appear indistinguishable from control terminals (FIG. 3.9). Therefore, taking out *dlg* in the *eIF4AIII* mutant background rescues the undergrown NMJ phenotype indicating that there may be a genetic link between the two. One possible scenario in agreement with our findings is that eIF4AIII upregulates DGluRIIB and Dlg expression, of which DGluRIIB is the essential factor influencing NMJ size (for details see Discussion 4.3.2).

## 3.5 Analysis of *cG4699/waharan*

One of the mutations which obtained clear results from the complementation mapping experiments was the *0094-13* P-element insertion which could be mapped to the *CG4699* gene locus and confirmed by a second non-complementing P-element insertion (Chapter 3.2.2.1). The complementation data strongly suggests that the assigned gene locus *CG4699* is required for growth regulation of NMJs. I named this gene *waharan* (*wah*), which is the Kashmiri word for "to expand". As described in the following, various lines of investigation were used to confirm the identity and phenotypic involvement of *wah* and to gain insights into the molecular nature of its function.

# wah homology with Rad23 and KiAA1267

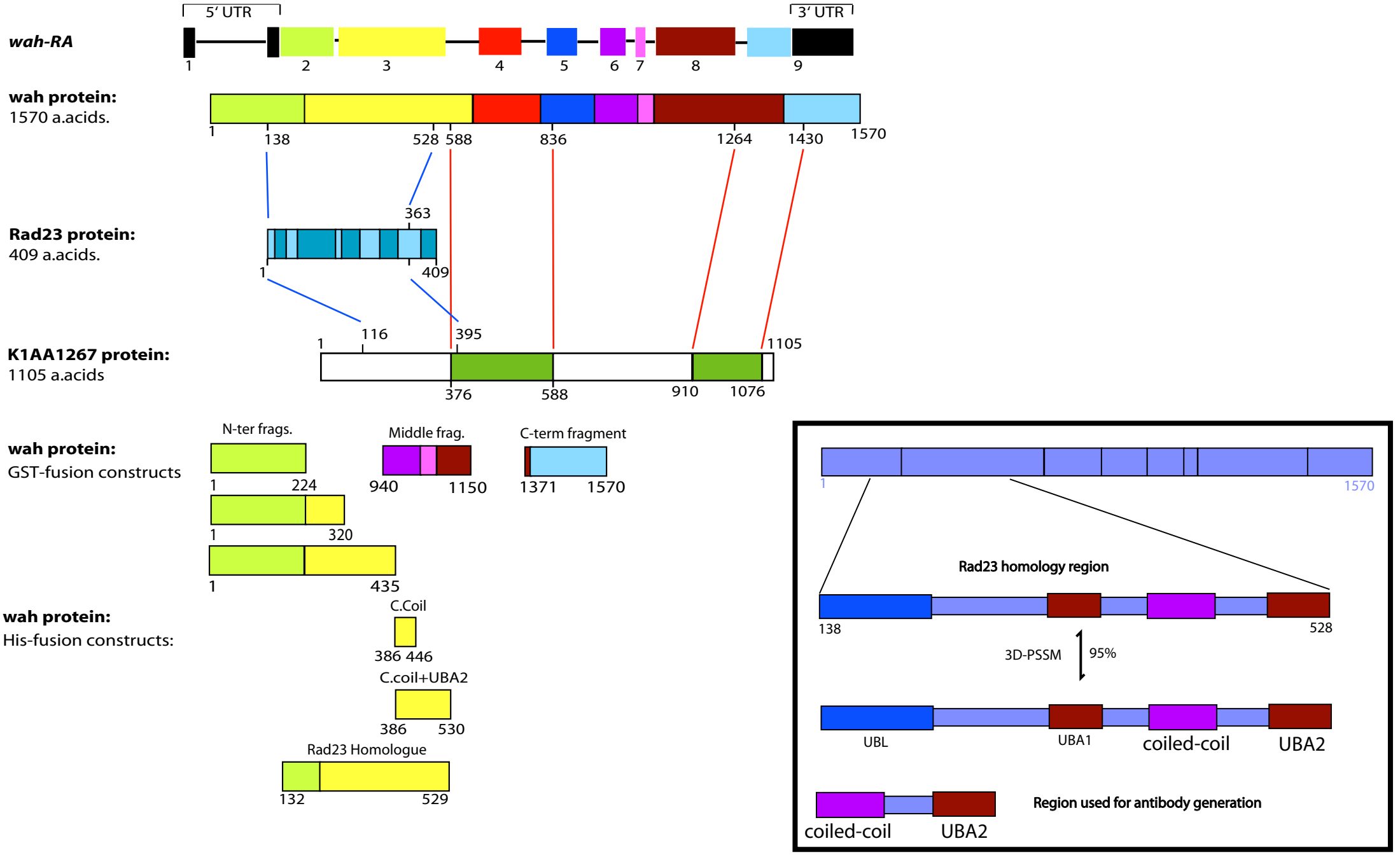

**<u>Fig. 3.10 3D-PSSM predicts 95% confident structural homology of wah with Rad23</u>.**
**A) Graphic representation of the structural homology of wah and its human ortholog (*KIAA1267*) with Rad23. Sequence homology of wah with *KIAA1267* and different portions of the wah protein that were attempted to express as GST and/or His-tag fusion products.**
**Wah gene with 9 exons (each color represents an exon) encodes the protein of 1570 a.acids. Rad23 has 10 exons (alternate light and dark blue colors) and encodes the protein 409a.acids and *KIAA1267* with 15 exons (separate exons not depicted here) encodes a protein of 1105a.acids.**
**N-terminal region of wah, 138-528a.acids is homologous to 1-363a.acid region of Rad23, similarly the region 116-395a.acids of *KIAA1267* shows homology to the same region (1-363) of Rad23 as shown by the blue lines, though this homology is weaker compared to wah. Since this is a structural homology so there is no one to one a.acid ratio.**
**Wah shares sequence homology with *KIAA1267* in two different regions (wah 588-836a.a; *KI* 376-588a.a and 1264- 1430a.a; 910-1076 are homologous) as shown by red lines.**
**In total 5 GST fusion products were tried for expression:**
**3 N-terminal: 1) 1-124a.acids. 2) 1-320a.acids. 3) 1-435a.acids**
**Middle fragment (211a.acids): 940-1150a .acids**
**C-terminal fragment (200a.acids): 1371-1570a.acids.**
**And 3 His-tag constructs tried for expression:**
**1) Coiled-coil (61a.acids): 386-446 a.acids,**
**2) Coiled-coil + UBA2 (145a.acids): 386-530 a.acids**
**3) Rad23 Homologue (399a.acids): 132- 529.**
**Coiled-ciol + UBA (145a.acids) product was used to generate anti-body.**
**B) Detailed illustration of Rad23 domains and wah homology, Rad23 has 4 domains 1 N-terminal UBL domain, 2 UBA domains, and one coiled-coil domain in between two UBA domains.**

### *3.5.1. In silico analyses*

The gene *CG4699* is 8.150 kb long at the genomic level. It has three different predicted transcripts (*FBtr0083175:* CG4699-PA, *FBtr0083176:* CG4699-PB and *FBtr0083177:* CG4699-PC; numbers refer to FlyBase database)[1] but they give rise to only one genuine translation initiation site and isoform. Instead, these three heterogeneous transcripts differ in the 5'UTR region and might therefore have impact on the spatial or temporal regulation of *wah* translation. The mature full length cDNA is about 4713 bp in length and encodes a protein of 1570 amino acids[2]. The predicted molecular weight is 170kDa. According to the novel Ensemble prediction, based on reciprocal BLAST analysis, the *wah* gene is a putative ortholog and shares a decent sequence homology with *K1AA1267*[3] (FIG. 3.10). *KIAA1267* is one of the genes selected from two sets of size-fractionated human adult and fetal brain cDNA libraries (Nagase et al., 1999; Poorkaj et al., 2001; Strausberg et al., 2002). The gene is expressed in human brain and encodes a bigger protein, but its function has not yet been explored. The gene *KIAA1267* has got orthologues across many animal species comprising invertebrates and vertebrates[4]

According to the Yale Developmental Expression database[5] *wah* is expressed in *Drosophila* embryos, and our own *in-situ* hybridisation data confirm this notion (Chapter 3.5.2). According to the GEO database for larval tissue expression, *wah* is also expressed in larval CNS and wing imaginal discs[6]. As described later (Chapters 3.5.3.2, 3.5.3.3), I could confirm this information experimentally.

---

[1] http://flybase.bio.indiana.edu/cgi-bin/getseq.html?source=dmel&id=FBgn0038364&chr=3R&dump=PrecompiledFasta&targetset=transcript

[2] source: RefSeq_peptide NP_732070; http://srs.sanger.ac.uk/srsbin/cgi-bin/wgetz?-e+%5BREFSEQPROTEIN-alltext:NP_732070%5D)

[3] http://www.ensembl.org/Homo_sapiens/alignview?class=Homology;gene=ENSG00000120071;g1=CG4699

[4] http://www.ensembl.org/Homo_sapiens/geneview?gene=ENSG00000120071

[5] http://genome.med.yale.edu/Lifecycle/query_gen.php?input1=FBgn0038364

[6] http://www.ncbi.nlm.nih.gov/projects/geo/gds/gdsGraph.cgi?&dataset=JQQMHFcckHGAybz&dataset=6gg-70ors77Twqr$&labels=4490p1p1p16p7p5p4p6p4p7p6p5p7p5p4&group=4490p1p1:4508p7p5:4524p6p4:4541p6p5:4559p5p4&grouplabel=tissue&gmax=1.97397&gmin=-0.0827133&title=GDS444+/+17735%20/%20CG4699:CG4699-PB,%20isoform%20B

Data mining in a number of data bases was carried out, but the only strong prediction for the Wah protein was made by the PSORT programme[7] which highlights a number of nuclear targeting sequences and predicts an overall chance of 82.6% for Wah to be targeted to the nucleus (FIG. 3.11). Other data bases queried comprised PROSITE (on the EXPASY server)[8], and a number of programmes provided by the Baylor link (BCM search launcher)[9]. Only few domain predictions were made by these programmes, but all of them are rather vague, as explained in the following. First, a SMART plot (BCM) predicts a coiled-coil domain at aa395-423. This is also predicted by the COILS programme (BCM) which also highlights a couple of potential coiled-coil domains of even lower probability at different positions of the molecule and the transmembrane prediction (TMpred; BCM) predicts one possible transmembrane domain (aa193-212), which is not predicted by the SMART plot (Appendix 6.4, FIG. 6.3). According to the fly-GRID interaction data link of FlyBase (based on yeast two-hybrid interactions)[10], *wah* interacts with the gene products of three genes: *CG30115*, *sec6* and *TSG101*. *CG30115* encodes a protein having predicted guanyl-nucleotide exchange factor activity, inferred from sequence similarity with human Trio protein (AF091395) according to FlyBase[11]. Sec6 is a member of a protein complex abundant in *Drosophila* NMJs required for regulation of synaptic microtubule formation, synaptic growth and glutamate receptor trafficking (Liebl et al., 2005). The tumor suppressor protein 101 (TSG101) plays a potential role in ubiquitin-dependent regulation of proteins and growth regulation[12]. Since predictions on the basis of sequence homology did not yield satisfactory results, I used the 3D-PSSM programme[13] which analyses potential similarities at the level of predicted protein structure. 3D-PSSM predicts a 95% confident structural homology of Wah with Rad23 (FIG. 3.10), although the sequence homology is very weak. Interestingly, the same program also predicts a structural homology of Rad23 to the human big brain protein

[7] http://psort.nibb.ac.jp/form2.html
[8] http://www.expasy.org/cgi-bin/prosite/ScanView.cgi?scanfile=42151676377.scan.gz
[9] http://searchlauncher.bcm.tmc.edu/seq-search/struc-predict.html; used programmes: *Coils* : prediction of coiled coil regions (ISREC), *TMpred* : transmembrane region and orientation prediction (ISREC), *SOPM*: self optimized prediction method (IBCP-CNRS)
[10] http://flight.licr.org/search/return_gene_results.jsp?history=N&gene_id=FBgn0038364&taxid=7227&return=8
[11] http://flybase.bio.indiana.edu/.bin/fbidq.html?FBgn0050115&content=full-report
[12] http://flybase.bio.indiana.edu/.bin/fbidq.html?FBgn0036666&content=full-report
[13] http://www.sbg.bio.ic.ac.uk/~3dpssm/index2.html

*KIAA126*, the mammalian orthologue of *wah* (FIG. 3.10). Rad23 is highly conserved from yeast to humans and has a potential role of targeting poly-ubiquitinated proteins to the proteasome in the final process of ubiquitin-mediated protein degradation (Glickman and Ciechanover, 2002; Walters et al., 2003). This functional prediction for *wah* proved very helpful for my further investigations of *wah*, helping me to formulate working hypotheses which I could prove experimentally (Chapter 3.5.4). It needs to be mentioned here that the newer version of 3D-PSSM (Phyre)[14] no longer shows the structural homology with Rad23, although Rad23 is still contained as a data set. Similarly, biochemically confirmed ubiquitin-associated domains of other proteins were predicted only by the old but not new version of 3D-PSSM (Richard Kammerer, personal communication), strongly suggesting that the algorithm of the new program might be unfavorable for this kind of structure.

```
NUCDISC: discrimination of nuclear localization signals
pat4: KRPR (4) at 532
pat4: RPRK (4) at 533
pat4: RKRK (5) at 731
pat4: KRPK (4) at 1226
pat7: PMKRPRK (4) at 530
pat7: PLPKRPK (3) at 1223
pat7: PKRPKLE (5) at 1225
bipartite: RRSGDAAKRRYIRRKER at 858
content of basic residues: 11.4%
NLS Score: 2.28
Results of the k-NN Prediction
k = 9/23
82.6 %: nuclear
8.7 %: cytoskeletal
4.3 %: plasma membrane
4.3 %: vesicles of secretory system
>> prediction for QUERY is nuclear (k=23)
```

**Fig. 3.11 Nuclear localisation signals of Wah and its likelihood of nuclear targeting as predicted by the PSORT database (http://psort.nibb.ac.jp/form2.html).**

[14] http://www.sbg.bio.ic.ac.uk/~phyre/

### *3.5.2. Gene expression analysis via in situ RNA hybridisation*

If *wah* is the gene responsible for the NMJ phenotype, we would expect expression of *wah* in either neurons or muscles. Therefore, I decided to carry out *in situ* hybridisation analyses to investigate the spatial and temporal transcription pattern of *wah*. Attempts to use a 925bp long DNA or RNA probe for the longest exon 8 failed to reveal any results (Appendix 6.1). Therefore, I synthesised an about 3440bp long Digoxignin-labelled probe (covering two thirds of the C-terminal portion of the *wah* gene; FIG. 3.12) by *in vitro* transcription using the 4.249kb long cDNA clone *LP09056* as template. Eventually, I got satisfactory signal with this *wah* RNA probe at 45°C hybridisation temperature.

The *wah* probe revealed a hybridisation pattern which appeared rather ubiquitous at stage 11/12 but showed accumulation in the CNS towards later stages 15/16 (FIG. 3.12). The experiment was repeated about 4 times with consistent results suggesting that the gene is expressed in the *Drosophila* CNS starting from mid embryonic stages into, at least, the mature embryo. These data would be consistent with the late embryonic *wah* mutant NMJ phenotype and suggest that *wah* is required presynaptically.

However, to strengthen the above observations, I had to demonstrate specificity of the used *wah* probe. To this end, I capitalised on the two mutant alleles $wah^{P1}$ and $wah^{P2}$, both of which carry P-element insertions in the 5'UTR of *wah* (FIG. 3.13), potentially affecting its transcription and/or translation. Clean and un-biased *in situ* hybridisation experiments were performed, in which stage 11/12 old mutant embryos and stage 15/16 old wild type embryos were pre-selected (and *vice versa*) and then stained together in the same tube. Most wild type embryos (identifiable by their stage) showed the staining patterns described above. The $wah^{P2}$ mutant embryos showed a similar expression pattern although it appeared clearly weaker than in wild type. In contrast, $wah^{P1}$ mutant embryos did never show any staining (FIG. 3.12)

A number of conclusions can be drawn from these final *in situ* hybridisation experiments: First, the *wah* probe used in our experiments is clearly highly specific. Second, even light staining in the periphery (muscles and/or epidermis) of older wild type embryos (FIG. 3.12) does reflect true low level expression of *wah*, suggesting that Wah

might play a postsynaptic role. Third, the $wah^{P1}$ allele represents a transcriptional null allele, whereas $wah^{P2}$ might affect transcriptional efficiency. This nature of the $wah^{P1}$ allele is strong confirmation for the hypothesis that the *wah* locus is responsible for the NMJ phenotype.


wah P1
wah P2
3.5kb DIG-labeled RNA probe
1
2
3
4
5
6
7
8
9

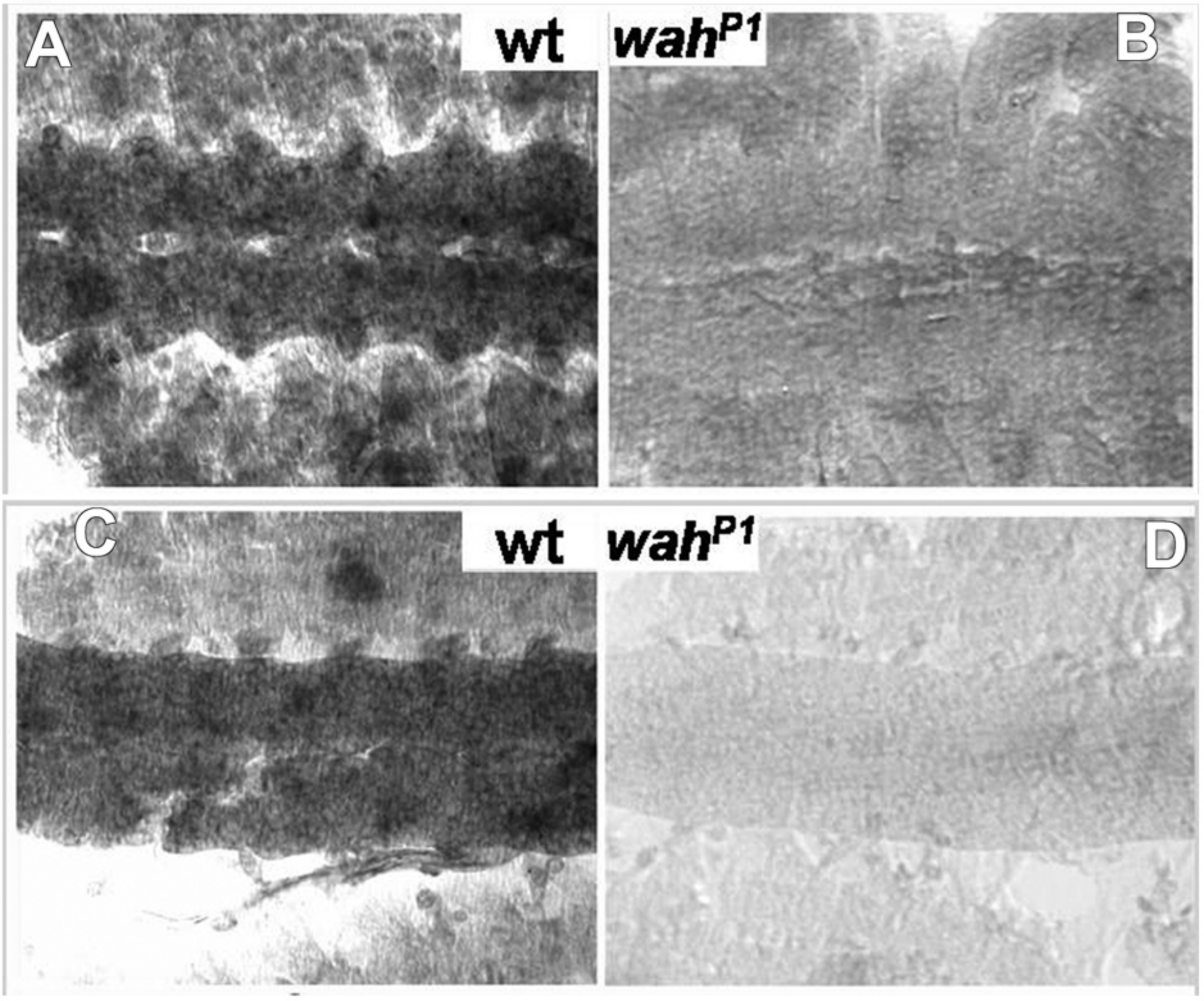
A
wt
wahP1
B
Stage 12-13
C
wt
wahP1
D
Stage 15-16

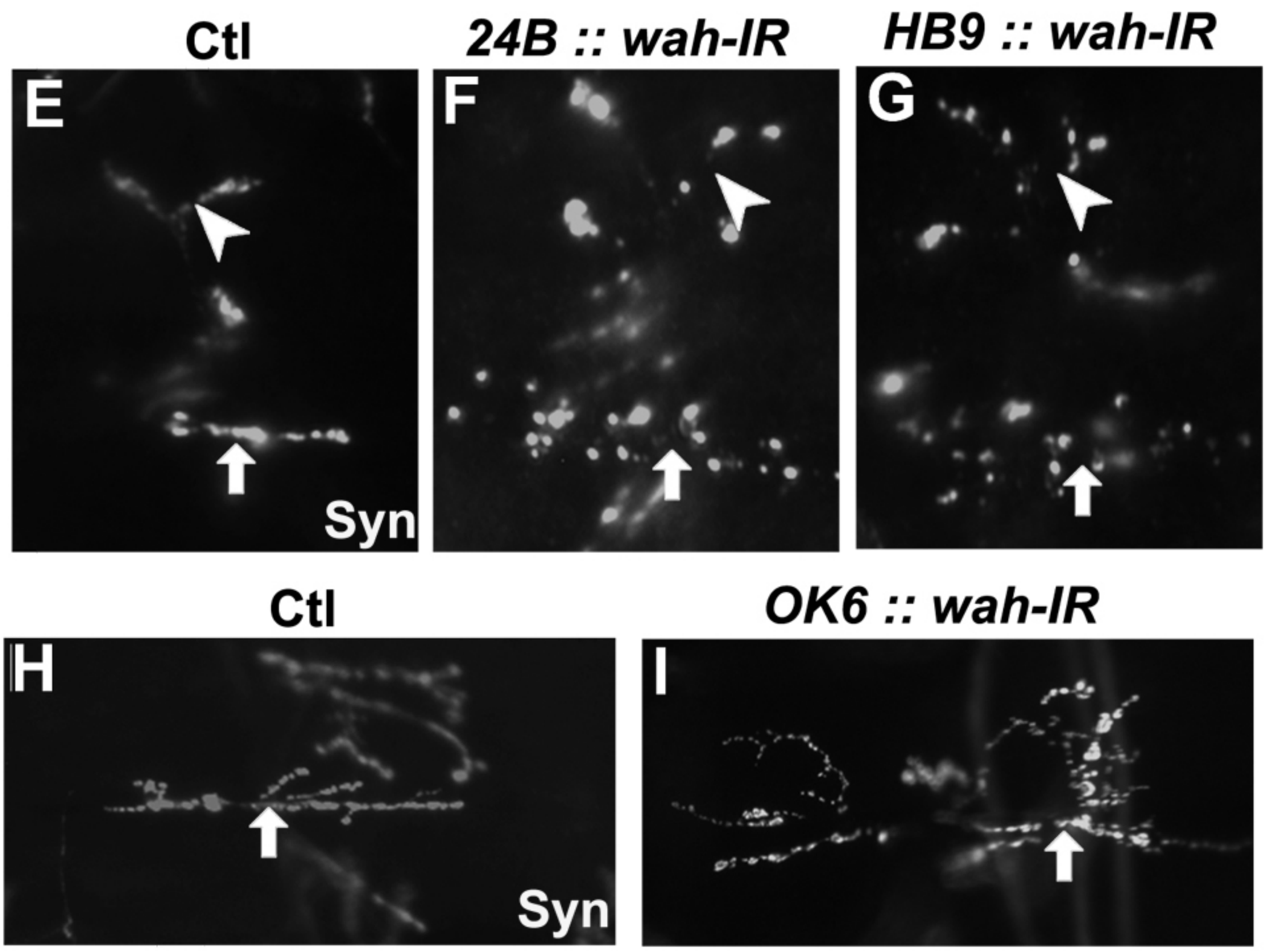
Ctl
24B :: wah-IR
HB9 :: wah-IR
E
F
G
Syn
Ctl
OK6 :: wah-IR
H
I
Syn

**Fig. 3.12 Wah is required both pre and postsynaptically to regulate synaptic growth in both embryo and larvae.**

**Light microscopic images of wah transcript expression and phenotypes caused by wah knockdown.**

**In-situ hybridization using 3.5 Kb DIG-labeled RNA probe (Chapter 6.1) reveals that wah transcripts are expressed early on from stage 12-13 and are detectable until late stage 15-16 embryos (A, C). Wah transcripts express in both CNS and the mesoderm (though the expression in mesodem is weaker) in contrast $Wah^{P1}$ does not show any expression of the transcript (compare B, D to A, C), demonstrating that the mutation is transcriptional null (Chapter 3.5.2).**

**Consistent with this, phenotype can be induced upon knock down of wah in embryos either in muscles via *24B-Gal4* or in neurons via *Hb9-Gal4* driven *Uas-wah-IR* (F and G) and in larvae via *OK6-Gal4* driven *UAS-wah-IR* (I) as revealed by anti-synapsin staining (overgrown terminals indicated by arrows and arrow heads).**

### *3.5.3. Analysis with specific RNA interference*

A quick strategy to gain further support for the involvement of *wah* in NMJ development and determine its temporal and spatial requirements was to make use of already existing UAS-coupled double-stranded RNA constructs. Thus, it is well established that double-stranded RNA (dsRNA) raised against a specific gene, silences expression of this gene post-transcriptionally by rapidly degrading its mRNA, a phenomenon commonly referred to as RNA interference (Hammond et al., 2001). In *Drosophila*, RNAi can be induced by injecting dsRNA into the embryo, introducing it with a "gene gun", or via targeted expression of dsRNA constructs using the Gal4/UAS system.

To carry out RNAi experiments, I used *UAS-wah-RNAi* transgenic flies (*4699 R2-III*) designed to knock down *CG4699* gene function. These constructs were raised by Prof. Ryu Ueda (NIG, Japan) in a genome wide RNAi project and kindly provided to us. Principal activity of the *UAS-wah-RNAi* transgenic fly strain was suggested by first experiments in which strong ubiquitous expression with the *tubulin*-Gal4 driver line (Lee and Luo, 1999) caused embryonic lethality, as is the case in $wah^{P1}$ and $wah^{P2}$ mutant embryos (Chapter 3.2.2.1). The *UAS-wah-RNAi* construct is inserted into the 3rd chromosome and causes female but not male sterility. Therefore, I used homozygous *UAS-wah-RNAi* males for all my experiments, distributing the RNAi construct to all F1 individuals used for my analyses.

#### *3.5.3.1. Pre- and postsynaptic requirement of wah*

Our *in situ* hybridisation data suggest that the *wah* gene is expressed strongly in the nervous system, but also in the periphery (Chapter 3.5.3). Therefore, the gene might be required pre- and/or postsynaptically for NMJ development. To clarify the spatial requirement of wah, I used various Gal4-driver lines. Using the pan-neuronal Gal4 driver *elav*-Gal4 (Lin and Goodman, 1994; Luo et al., 1994) to target wah-RNAi expression to all neurons caused early larval lethality. Since *wah* mutant embryos display more obvious phenotypes in ventral NMJs compared to NMJs on dorsal muscles, I used specific Gal4

driver lines such as *HB9-Gal4* and *ftz-Gal4* both expressing in SNb and SNd (Broihier and Skeath, 2002; Thor et al., 1999) to target *wah-RNAi* expression to ventral neuromuscular terminals. These animals are viable and display enlarged NMJ phenotype as observed in *wah* mutant animals (FIG. 3.12), the NMJ phenotype is stronger in *HB9-Gal4* than in *ftz-Gal4* embryos. These results reveal that the *wah* gene is required pre-synaptically for the formation of NMJs. However, when targeting wah-RNAi expression in muscles using *24B-Gal4*, which is expressed in mesoderm (Kidd et al., 1999), the animals are early larval (L1/L2) lethal and display an enlarged NMJ phenotype comparable to *wah* mutant embryos (FIG. 3.12).

Taken together, these results demonstrate that the *wah* gene is required both pre- and post-synaptically for the formation of NMJs in Drosophila. To confirm these different tissue requirements of *wah*, I will complement my RNA-interference data by performing rescue experiments with *UAS-wah* constructs (Chapter 3.5.5).

# Wah transcripts and different ESTs used for cloning

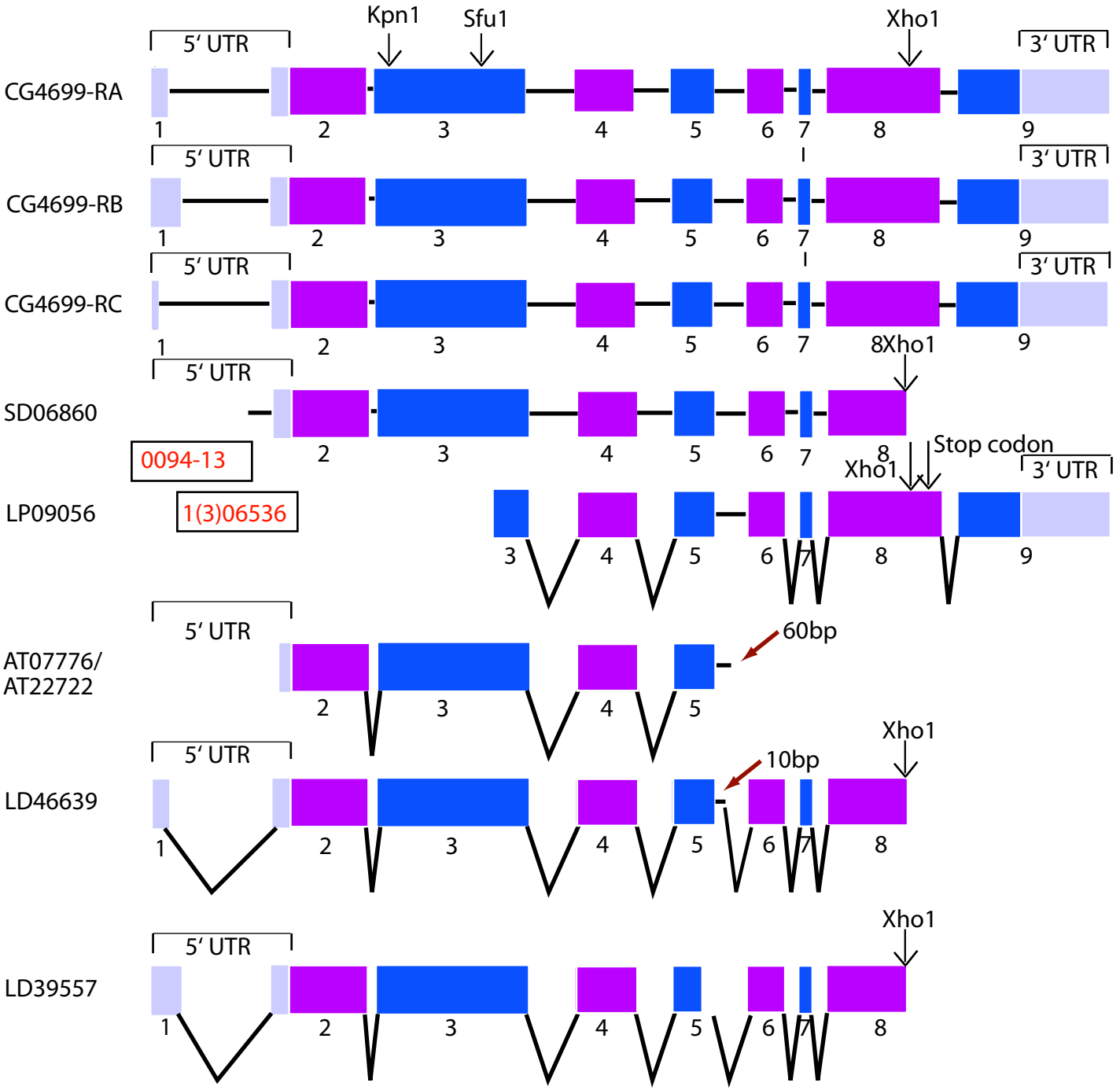

**Fig. 3.13 Different ESTs used to clone the wah gene.**

**Graphic representation of wah transcripts, two wah p-insertions and the ESTs that were used to clone the full length wah constructs.**

**Wah has 3 isoforms (CG4699-RA, CG4699-RB and CG4699-RC) which differ in 5' UTR region, have only one translation initiation site and encode a protein of 4.7kb length. Both the p-insertions $wah^{P1}$ and $wah^{p2}$ are in 5'UTR of the gene.**

**Different ESTs obtained for cloning the full length wah gene were sequenced, none of these represents a full length cDNA, Individual ESTs are described here (also see Table 3.7):**

***SD06860*: This cDNA clone has got 80bp from the first intron, part of 5'UTR and rest of the introns in full and terminates at Xho1 site at 3838bp.**

***LP09056*: This cDNA clone represents 2/3rd C-terminal of the gene. It starts at 1639 bp and covers rest of the coding sequence and 3'UTR. It has complete intron 5-6 sequence and also a premature stop codon at 3859bp.**

***AT07776/AT22722*: This cDNA clone has got 50bp from the 5'UTR and covers 5 exons before terminating into the intron 5-6. It has about 60bp from the intron 5-6 followed by poly A tail.**

***LD46639*: This cDNA clone represents isoform A. It has complete 5'UTR and terminates at Xho1 site at 3838bps. This clone has got no introns except 10bps from intron 5-6.**

***LD39557*: This cDNA clone represents isoform B. It has got complete 5'UTR and terminates at Xho1 site at 3838bps. This clone has got no introns but it lacks about 63bp of exon 5.**

*3.5.3.2. Requirement of wah in larval neurons*

Since the *wah* mutation is embryonic lethal, so far the analysis was carried out on embryonic NMJs. But according to GEO (Gene Expression Omnibus) database link of FlyBase[15] *wah* is also expressed in the larval CNS (Chapter 3.5.1). In order to test the potential function of *wah* in NMJs of larvae, I used the *Ok6-Gal4* driver line specific to larval motorneurons to target the expression of *wah-RNAi* to larval NMJs. This treatment did not cause lethality but caused slow development of the animals. Late larval NMJs were clearly enlarged and, like in *wah* mutant embryos, terminals in dorsal areas appeared less affected than ventral ones. When looking at NMJs on the ventral muscles VL3 and VL4 nomenclature according to (Bate and Martínez-Arias, 1993), I observed a significant increase in the number of synaptic boutons and an increase in synaptic span (the extent of muscle covered by the synapse, measurements to be done) (FIG. 3.12, 3.15). These results demonstrate that, like in embryos, the *wah* gene is also required in the larval nervous system to control the size of NMJs. The fact that NMJ phenotypes are more severe in ventral than dorsal NMJs, in embryos and larvae alike, could either mean that *wah* requirement is specific to ventral motorneurons, or that loss of *wah* function causes an imbalance in growth regulation which is more obvious in ventral muscles than dorsally. I favour the second option as will be explained later (Discussion 4.4.3).

As explained before, pre- or postsynaptic loss of *wah* function can cause overgrowth at the late embryonic NMJ (Chapter 3.5.3). The larval NMJ is more complex than the embryonic NMJ providing more detailed structural parameters for analysis (Prokop and Meinertzhagen, 2006). Therefore, it would be desirable to test for effects of postsynaptic loss of *wah* function in larvae and ask to which degree potential NMJ

15 http://www.ncbi.nlm.nih.gov/projects/geo/gds/gdsGraph.cgi?&dataset=JQQMHFcckHGAybz&dataset=6gg-70ors77Twqr$&labels=4490p1p1p16p7p5p4p6p4p7p6p5p7p5p4&group=4490p1p1:4508p7p5:4524p6p4:4541p6p5:4559p5p4&grouplabel=tissue&gmax=1.97397&gmin=-0.0827133&title=GDS444+/+17735%20/%20CG4699:CG4699-PB,%20isoform%20B

phenotypes resemble those caused by presynaptic knock-down of *wah*. This would tell us whether *wah* is likely to affect very different mechanisms in neurons and muscles, or whether it affects different components of the same pathways mediating cross-talk between muscles and motorneurons (for details see Discussion 4.4.3). As explained in (Chapter 3.5.3.1), the *24B-Gal4* driver used to targeted expression of *wah-RNAi* to muscles causes embryonic lethality, making larval analysis impossible. I have now obtained a muscular Gal4 driver (*Mhc-Gal4)* (Schuster et al., 1996) which turns on Gal4 expression only at larval stages. I hope that this driver will allow me to carry out the desired larval analyses.

*3.5.3.3. Requirement of wah in wing imaginal discs*

Apart from larval expression of Wah in the nervous system (as confirmed by my RNAi experiments), the GEO data base indicates high levels of *wah* transcripts also in late larval wing imaginal discs, the larval anlagen of fly wings and thoracic parts of the body wall. In order to test for potential function of *wah* in wing imaginal discs, I used various wing disc-specific Gal4 driver lines to target *wah-RNAi* to this tissue. First, I used *dpp-Gal4* which expresses along the A/P-border of the wing disc throughout larval life (Klein and Arias, 1998; Wilder and Perrimon, 1995), corresponding to the area between the L3 and L4 veins in adult wings (Raftery et al., 1991)(FIG. 3.14). Expression of *wah-RNAi* with *dpp-Gal4* at 25°C causes lethality at late pupal stages and only few flies are able to eclose. Only 3 flies eclosed, all showing a comparable reduction of the wing blade area between the L3 and L4 veins with occasional cross-veins forming between them (FIG. 3.14). At lower temperature (18°C), flies eclose and show a milder phenotype, whereas at higher temperatures (29°C) all animals are pupal lethal. The second wing-specific driver line I used was *vg-Gal4* which shows different region-specific levels of expression in the wing disc with maximal levels in a stripe of cells along the length of the future wing margin (Williams et al., 1993). The use of *vg-Gal4* to target the expression of *wah-RNAi* at 25°C causes notches at the margin of the adult wing (FIG. 3.14), the area where *vg-Gal4* is expressed at highest levels. The phenotype is highly penetrant, with all flies showing this phenotype. When the same flies were grown at 18°C, phenotype becomes a

little milder. At 29°C, it causes pupal lethality. Both these results demonstrate that *wah* is required in wing imaginal discs. The third wing disc-specific Gal4-driver line, *MS1096-Gal4*, is expressed at modest levels in the ventral half of the prospective wing blade and parts of the notum (prospective dorsal body surface), and at high levels in the area of the prospective dorsal wing blade (Capdevila et al., 1994; Neumann and Cohen, 1996). When expressing RNAi-*wah* with *MS1096-Gal4*, hatching flies display wings dramatically reduced to haltere-like shape and their notum is also deformed. A very similar phenotype was observed with the fourth Gal4-driver, *ptc-Gal4*, which is expressed in a stripe along the anteroposterior parasegmental boundary from late larval stages onwards with highest levels of Gal4 expression in a sharp stripe at the posterior border and gradually lower levels towards the more irregular anterior border (Johnson et al., 1995; Speicher et al., 1994). I obtained interesting phenotypes like deformed notum and reduced bristle number with another Gal4-driver line, *sca-Gal4*. Importantly, these phenotypes are reminiscent to those of expression of dominant-negative proteasome (DTS5 and DTS7) with the same *Gal4* driver line (Schweisguth, 1999). *Sca-Gal4* is expressed in proneural clusters and in sense organ cells in third-instar larvae and early pupae (Mlodzik et al., 1990).

Taken together, these results clearly demonstrate that *wah* is required in the wing discs. I hoped to find phenotypes which would be reminiscent of known phenotypes obtained by activation or loss-of-function of genes, such as *dpp*, *Notch* or *hedgehog* (Schweisguth, 1999; Tanimoto et al., 2000). However, talking to experts in the field (A. Martinez-Arias, M. Baron, K. Brennan, S. Bray), I had to accept that the observed *wah-RNAi*-induced phenotypes are very complex, displaying traits of various regulatory pathways. Probably, *wah* is involved in the regulation of several molecular pathways of wing development in parallel, ruling out the use of wings as a system in which to study genetic interactions of *wah*.

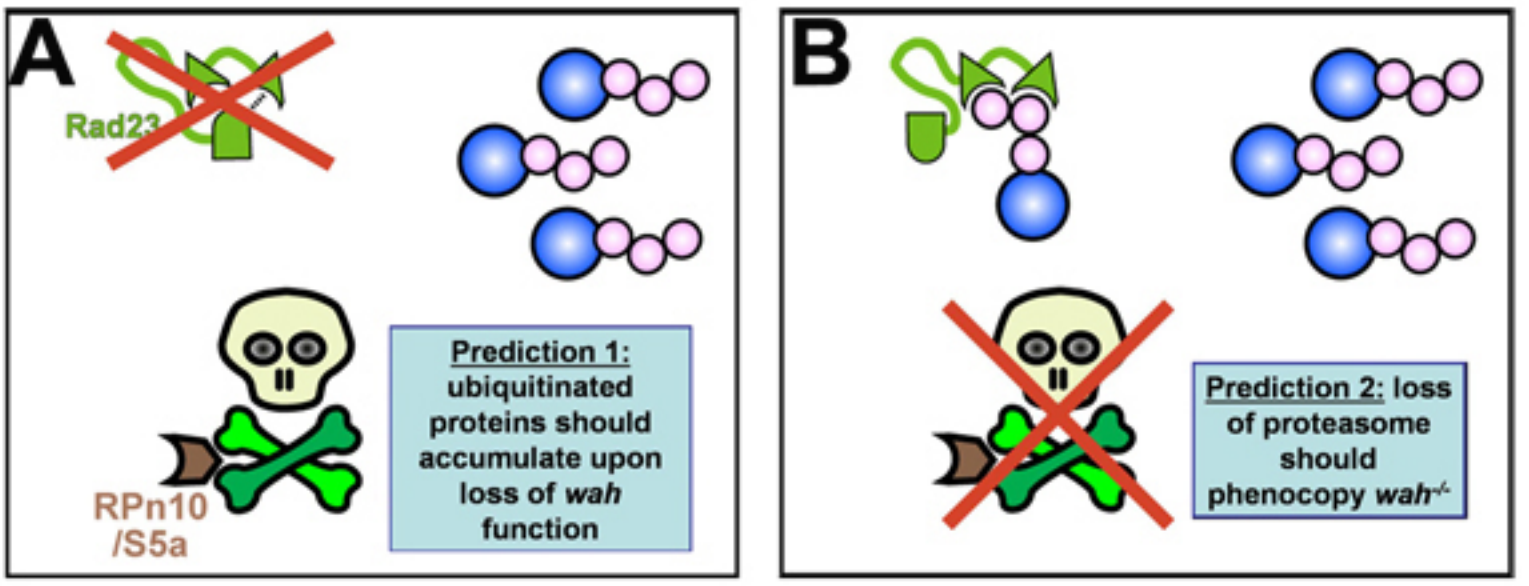
A
Rad23
RPn10
/S5a
Prediction 1:
ubiquitinated
proteins should
accumulate upon
loss of wah
function
B
Prediction 2: loss
of proteasome
should
phenocopy wah-/-

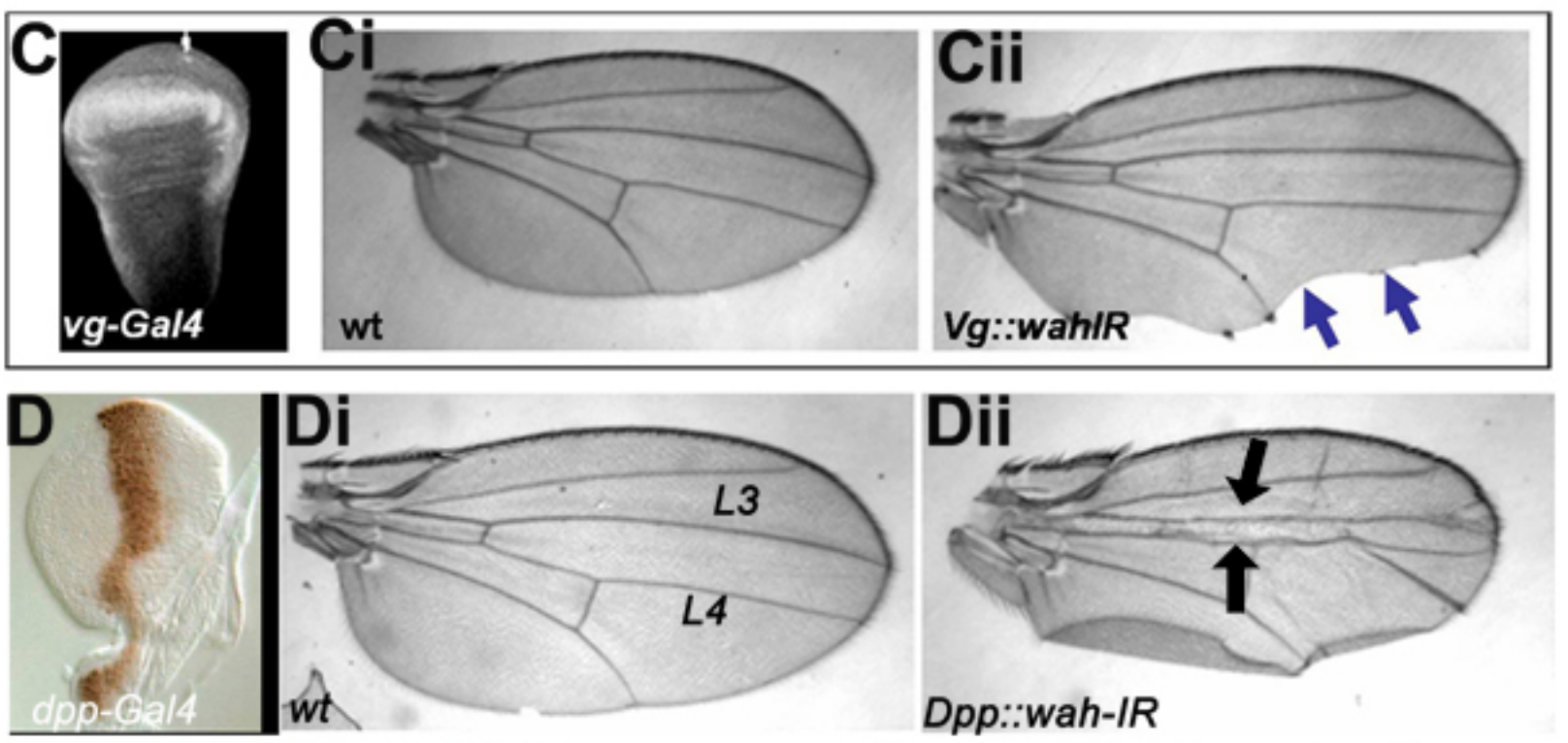
C
vg-Gal4
Ci
wt
Cii
Vg::wahIR
D
dpp-Gal4
Di
L3
L4
wt
Dii
Dpp::wah-IR

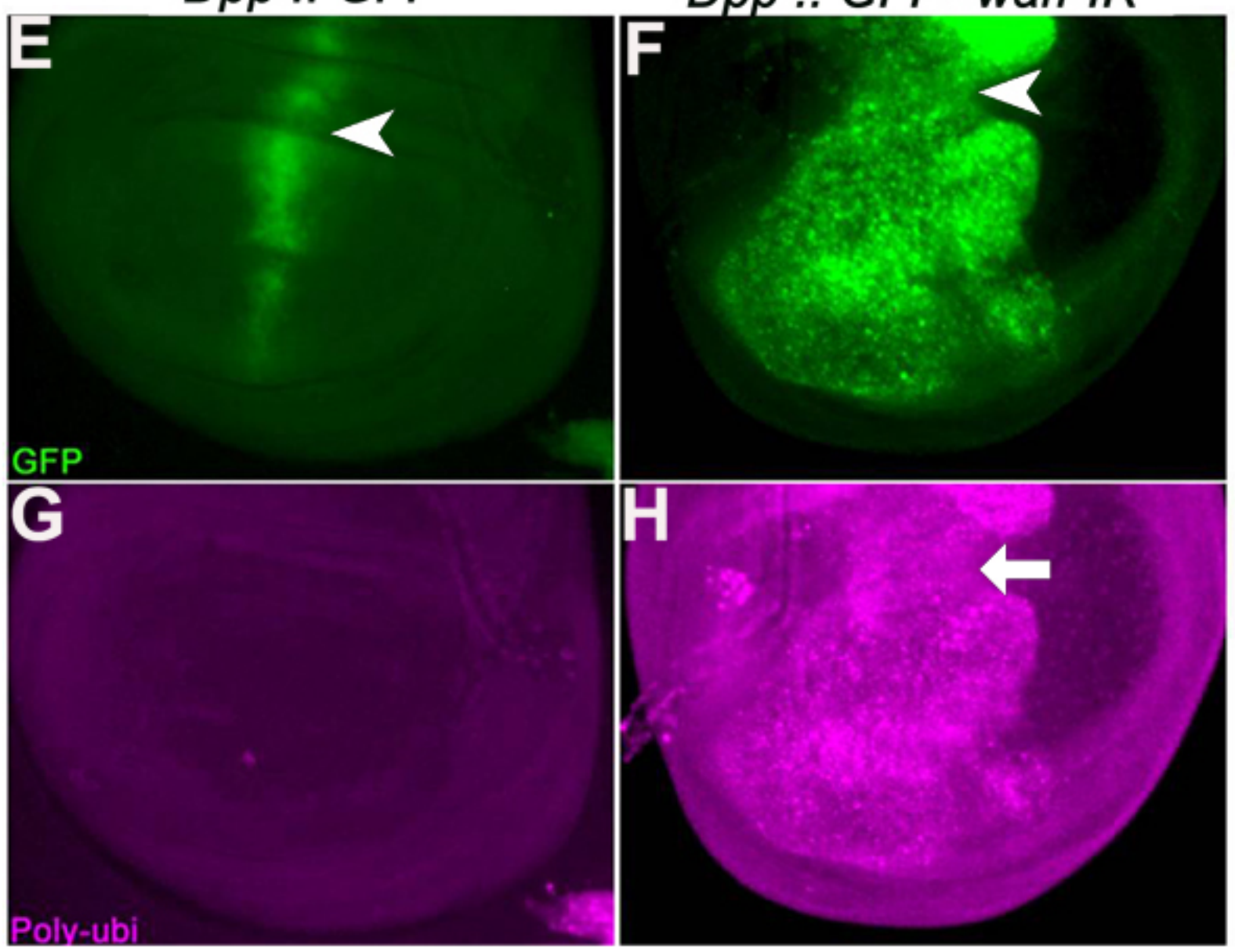
Dpp :: GFP
Dpp :: GFP- wah-IR
E
GFP
F
G
Poly-ubi
H

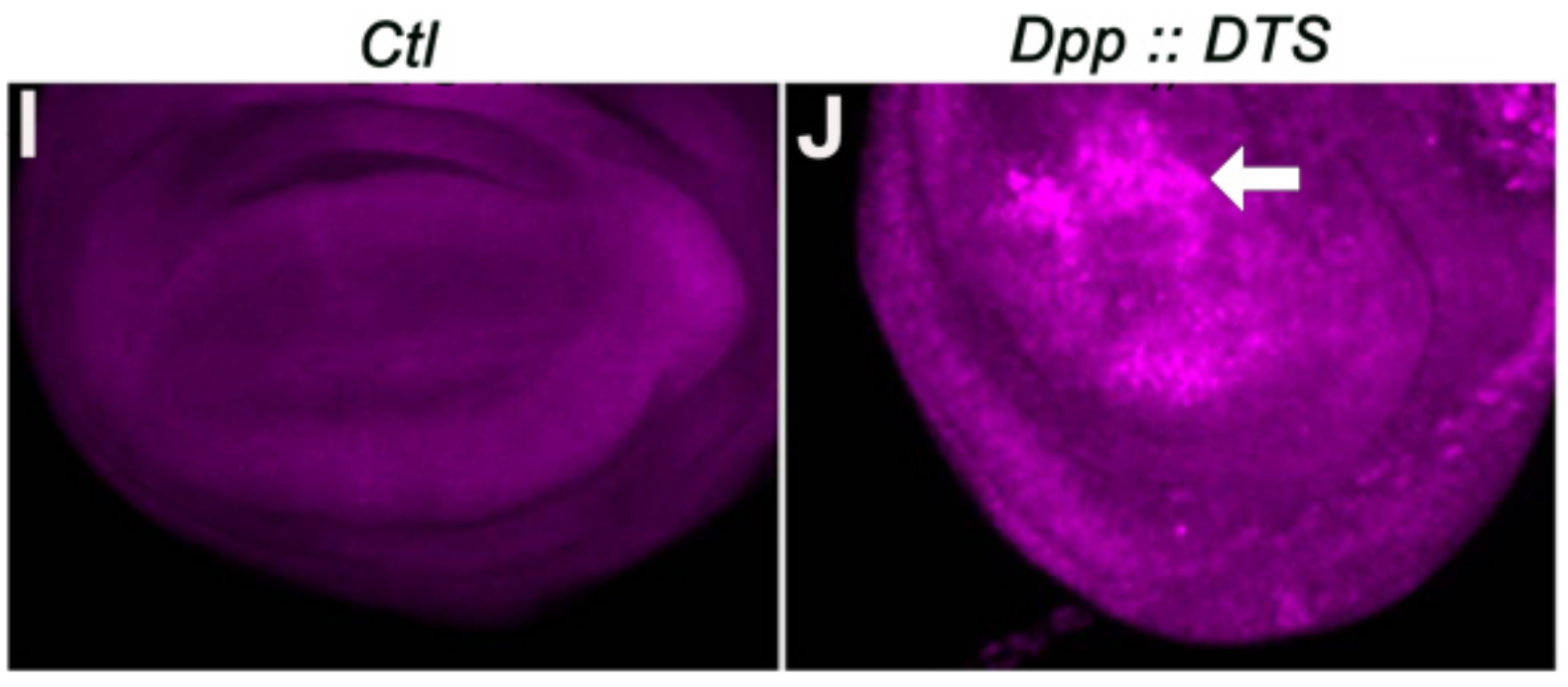
Ctl
Dpp :: DTS
I
J

**Fig. 3.14 Wah has a role in patterening during wing development potentially involving ubiquitin mediated protein degradation.**

**Light microscopic images of affected wings and anti-polyubiquitin stainings (magenta) in these wing imaginal discs.Knocking down wah should cause accumulation of polyubiquitinated proteins (A) and the proteasome should phenocopy the same (B). Upon wah knockdown via wing specific *vg* (C) and *dpp-Gal4* (D) driven *UAS-wah-IR,* specific effects are caused in adult wings. Notches are formed in the areas of *vg* expression in wing margin when driven *wah-IR* with *vg* (Ci, Cii) and the area of *dpp* expression (between veins L3 and L4) is reduced in wings when *wah-IR* is driven by *dpp-Gal4* (Di, Dii). Phenotypes in wing discs are shown (E to J). *Dpp* expression pattern is disturbed in wah knockdown background visualised by copmarision of GFP expression in *dpp ;; Uas-GFP* and *dpp ;; Uas-GFP ;; wah-IR* wing discs (E vs. F) and in (G, H) poly-ubiquitinated proteins accumulate in the areas of wah-IR expression. (I) and (J) show the similar but slightly milder accumulation phenotype caused when dominant temperature sensitive proteasome (*Uas-DTS5-Prot*.) is driven in wing discs with the same *dpp-Gal4* driver line (Chapter 3.5.4).**

### *3.5.4. Addressing the molecular function of Wah*

As described above I was able to demonstrate a number of phenotypes at embryonic and larval NMJs, in wing discs and fly wings. So far I have used them to determine spatial and temporal requirements of Wah. In the following I used these phenotypes to address the potential molecular function of Wah. These experiments were based on the prediction obtained from the 3D-PSSM data base (Chapter 3.5.1.) that *wah* shares structural similarity with Rad23 (2 UBA and 1 UBL domain; FIG. 3.10), a protein potentially involved in catalysing the transfer of ubiquitinated proteins to the proteasome. This potential molecular link was even more attractive, since recent studies have demonstrated that ubiquitination is a potent regulatory mechanism involved in NMJ growth. Thus, mutations of the E3 ubiquitin ligase Highwire or of the APC complex member Morula cause NMJ overgrowth (Chang and Balice-Gordon, 2000; DiAntonio et al., 2001; Marques et al., 2002; McCabe et al., 2004; van Roessel et al., 2004), potentially reminscent of the phenotype I observed for loss of function of *wah* (FIG. 3.15). Therefore, based on the phenotypes and the structural prediction for Wah, I hypothesised that Wah may be involved in the final step of the ubiquitin-mediated protein degradation pathway (Glickman and Ciechanover, 2002; Walters et al., 2003). In order to test this hypothesis, I made predictions which could be tested experimentally.

#### *3.5.4.1. Loss of wah function induces accumulation of polyubiquitinated proteins*

The first prediction I made was that loss of *wah* function should lead to an accumulation of poly-ubiquitinated proteins (FIG. 3.14). In order to test this hypothesis, I used antibodies raised against polyubiquitin and expressed wah-RNAi in larval motorneurons using *Ok6-Gal4*. I have already shown that these larvae display enlarged neuromuscular terminals at 29ºC (FIG. 3.15). Therefore I analysed *OK6::wah-RNAi* and control larvae in order to test for potential accumulation of polyubiquitin using commercial anti-polyubiquitin antibodies. In wild type larvae, polyubiquitin accumulation at NMJ terminals was modest and mainly homogeneous. In contrast, terminals with knock-down

of *wah* displayed irregularly distributed, focal, mostly vesicular accumulations of polyubiquitin (FIG. 3.16). Hence, it seems that, in the absence of Wah, polyubiquitinated protein accumulate in the terminal, as was predicted by my working hypothesis. Due to time restrictions, double stainings with markers for intracellular vesicular compartments to determine the subcellular localisation of polyubiquitin were no longer possible, but will be carried out in the nearer future.

Given the wing phenotypes generated upon targeting of *wah-RNAi* to wing discs (Chapter 3.5.3.3), I also looked at potential accumulation of polyubiquitin in these tissues. As explained before, *dpp-Gal4* is expressed in a stripe along the anteroposterior compartment border of the wing disc, and I expected accumulation of polyubiquitin in this area when expressing *wah-RNAi* with this driver. When staining these wing discs with anti-polyubiquitin antibody I found irregular accumulations of polyubiquitin (not visible in control discs), but the staining pattern did not at all restrict to the *dpp-Gal4* expression area but expanded mostly into the anterior area of the prospective wing blade. Puzzled by this result, I asked whether Gal4 expression might have extended into these ectopic areas by co-expressing a celluler marker mCD8-GFP (FIG. 3.14). Targeting mCD8-GFP alone via *dpp-Gal4*, reveals the expected stripe of GFP expression along the anteroposterior compartment border. Driving mCD8-GFP together with *wah-RNAi*, generated wing discs in which the pattern of GFP was greatly enhanced in levels and extended into areas outside the usual stripe. Double-labelling experiments demonstrated that anti-polyubiquitin accumulation occurred in precisely the area covered by ectopic mCD8-GFP expression (FIG. 3.14). Interestingly, this enhanced wing disc phenotype was temperature-dependent, consistent with the well known fact that Gal4 activity is enhanced at higher temperatures. Thus, ectopic mCD8-GFP expression and accumulation of polyubiquitin occurred consistently in all discs at 29°C (animals shifted to higher temperature at mid larval stages), whereas at 25°C only a fraction of discs expressed this phenotype and the others looked wildtype with respect to both stainings.

These results with wing discs do not only provide further support for the prediction that Wah is involved in ubiquitin-mediated protein degradation, they also allow to draw further conclusions. Thus, an expansion of the dpp-Gal4 expression area seems to be a very unusual phenotype distinct from any known wing disc phenotype reported in the

literature. This is consistent with my findings that wing phenotypes induced by *wah-RNAi* are extraordinary (Chapter 3.5.3.3), suggesting that wah-RNAi might affect several parallel genetic pathways in wing discs. For example, Wah might disturb *hedgehog* signalling at the anteroposterior compartment border, which in turn regulates *dpp* signalling (Tanimoto et al., 2000), which is itself regulated via ubiquitination at the level of the Smad complex (Attisano and Wrana, 2002; Moustakas et al., 2001; Shi and Massague, 2003). In addition, Notch, another important regulator at the anteroposterior compartment border, is regulated via ubiquitination (Schweisguth, 1999). Interference with various of these pathways at the same time is likely to generate an integrated output which is no longer interpretable.

So far, my data with polyubiquitin accumulation depend on artificial RNAi interference. In order to confirm my findings in the absence of the endogenous gene, I analysed $wah^{P1}$ mutant embryos. My data with *wah-RNAi* in embryos (Chapter 3.5.3.1) had suggested that Wah is required in both the nervous system and musculature, consistent with the data from *in situ* hybridisation experiments (Chapter 3.5.2). This notion was confirmed when staining wild type and *wah* mutant embryos with anti-polyubiquitin, which demonstrated *wah* mutant effects in both tissues (FIG. 3.16). Wildtype embryos showed a more or less homogeneous distribution of anti-polyubiquitin staining. In contrast, *wah* mutant embryos displayed a far more irregular staining pattern with random accumulations of polyubiquitin in different tissues including NMJs, supporting my data obtained with *wah-RNAi* expression. Furthermore, whereas polyubiquitin staining was found in nuclei of most tissues in wild type embryos, there was a clear reduction of anti-polyubiquitin staining in muscular and neuronal nuclei of $wah^{P1}$ mutant embryos. This may be a key observation for our further analyses, since the loss of nuclear polyubiquitin is in agreement with the predicted nuclear targeting of Wah (FIG. 3.11) and with the fact that Wah-HA localises to nuclei (as explained later; Chapter 3.5.5.1).

Taken together, these results clearly confirm the prediction that Wah is involved in ubiquitin-mediated protein regulation with clear relevance for developmental processes. The accumulation of polyubiquitin in the cytoplasm or in endosomal compartments may hint at blockage of the proteasome-dependent protein degradation pathway. Reduced

nuclear staining of polyubiquitin might hint at an involvement of Wah in nuclear import or stabilisation of ubiquitinated proteins. Such a role would not be surprising given the ever more complex view of the role of ubiquitin in the regulation of intracellular trafficking (Chen and Madura, 2002; Rao and Sastry, 2002). In fact, the phenotypes caused by loss of Wah function may be an overlap of both these functions (Discussion 4.4.3).

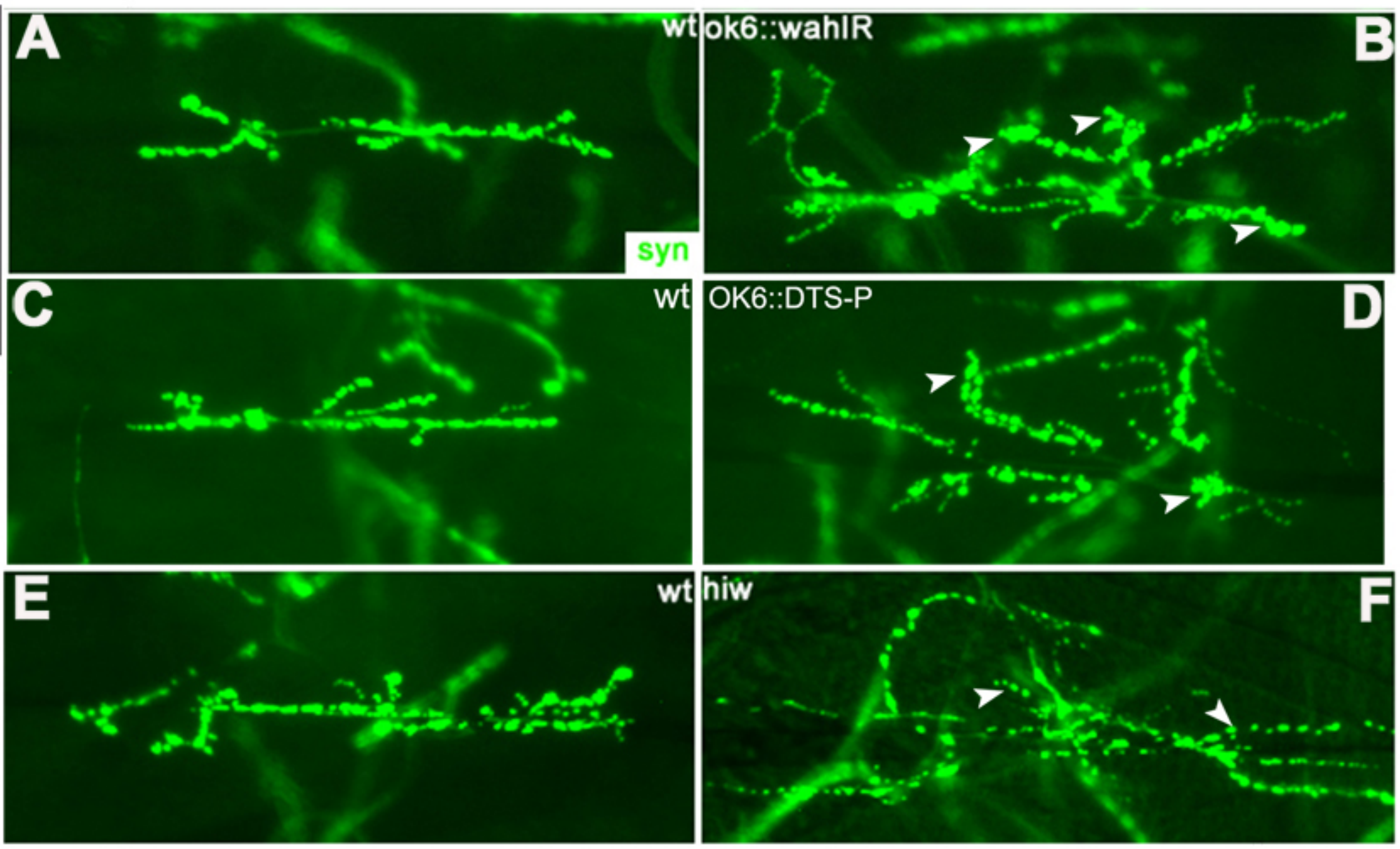


| Phenotype | hiw | wah | DTS-Prot |
|---|---|---|---|
| terminals enlarged | +++ | + | + |
| boutons elongsted | + | - | - |
| Reduced levels of synaptic markers | + | - | - |

**Fig. 3.15 Wah and hiw have obvious phenotypic differences.**

**Light microscopic images of anti-synapsin stainings of larval NMJs.**

**In larval NMJs (labeled with anti-synapsin green), overgrown phenotype can be induced upon knock-down of wah via *OK6-Gal4* driven *UAS-wah-IR* (B) and the similar phenotype was induced upon expression of (*DTS5*) via *OK6-Gal4* driven *UAS-DTS5* in the motorneurons as shown in (D). Hiw mutant displays the overgrown NMJ phenotype as shown in (F). Comparison of two phenotypes (B vs. D and F) reveals crucial phenotypic differences between the two (hiw: far more enlarged terminals, boutons stretched indicated by arrowheads, reduced synaptic staining).**

### *3.5.4.2. wah mutant phenotypes can be phenocopied via knock-down of proteasome function*

In order to determine a potential role of Wah in catalysis of proteasome-mediated protein degradation, I made a second prediction that proteasome knock-down should phenocopy the *wah* mutant phenotypes (FIG. 3.14). In order to test this hypothesis, I capitalised on a dominant-negative temperature-sensitive proteasome subunit DTS5 which is supposed to affect the β6 gene of 20S core proteasome core subunit, (Schweisguth, 1999). Interestingly, published experiments using sca-Gal4 to drive these constructs revealed scutellar bristle phenotypes similar to the ones I observed upon driving wah-RNAi with this driver line, providing a first example of similarity. To extend on this finding, I used the *OK6-Gal4* line and asked whether expression of DTS5 would phenocopy the enlarged NMJ phenotype observed upon targeted expression of *wah-RNAi* (FIG. 3.15). *OK6::DTS5* larvae were kept at the permissive temperature of 25°C until the late embryonic or early larval L1 stage and then shifted to the restrictive temperature of 29°C supposed to knock down proteasome function in motorneurons throughout larval development. These animals develop slowly, as similarly observed upon *wah-RNAi* expression. In addition, these *OK6::DTS5* larvae displayed an enlarged NMJ phenotype very similar to the one observed upon *wah-RNAi* expression but slightly weaker. Thus, these NMJs displayed a significant increase in the number of synaptic boutons and in synaptic span (the extent of muscle covered by the synapse, measurements to be done) (FIG. 3.15). Interestingly, the phenotype is more severe in ventral NMJs compared to dorsal ones, as is the case for loss of Wah function (Chapter 3.5.3.2).

Next I tested for similarities in wing imaginal discs employing a similar temperature regime as with *OK6-Gal4*, but using *dpp-Gal4* as driver line instead. In these experiments, accumulation of polyubiquitin was observed in a similar extended pattern as observed upon *dpp-Gal4* mediated knock-down of *wah,* but the accumulation was slightly weaker (FIG. 3.14). These animals also die at late pupal stages.

Taken together, these results confirm the prediction and strongly suggest that Wah has the predicted function of targeting poly-ubiquitinated proteins to the proteasome for degradation. However, this does not exclude its potential involvement in nuclear targeting/stabilisation of polyubiquitinated proteins.

Wt

OK6 :: Wah-IR

A

Dlg
Ubi

B

Wt

WahP1

C

HRP
Ubi

D

E

Ubi

F

G

Ubi

H

**Fig. 3.16 Wah is likely to be involves in trafficking of polyubiquitinated proteins.**

**Confocal images of anti-polyubiquitin stainings (magenta) in different tissues in normal and *wah* mutant background.**

**In larval NMJs (labelled with anti-Dlg, green), polyubiquitin protein (magenta and white in insets) is accumulated to a far lesser extent in the wildtype (A) than upon knock-down of wah via *OK6-Gal4* driven *UAS-wah-IR* (B). Comparisons of late embryonic tissues of wildtype (C,E,G) to $wah^{P1}$ mutant embryos (D,F,H) reveal similar accumulation of polyubiquitin in mutant NMJs (C vs. D). (C; labelled with anti-HRP, green; boutons indicated with white arrows) and dotty extra-nuclear accumulation in the cytoplasm of neuronal somata (small arrows) in the mutant CNS (D). In contrast, nuclei have a higher content in the wildtype (arrow heads) than in $wah^{P1}$ mutant embryos, as shown for CNS (E vs. F) and the muscles (G vs. H)**

*3.5.4.3. Attempts to link Wah function to ubiquitin-regulated signalling pathways involved in NMJ growth regulation*

One of the signaling pathways with the largest effects on synaptic size at the *Drosophila* NMJ is the BMP pathway (Aberle et al., 2002; Marques et al., 2002; Marques et al., 2003; McCabe et al., 2004; McCabe et al., 2003), which stimulates synaptic growth. This pathway is regulated by highwire (*hiw*), an E3 ubiquitin ligase supposed to target Medea a member of the Smad complex required to pass on BMP signals to the nucleus (McCabe et al., 2004). *Hiw* mutant larvae show an enlarged NMJ phenotype. Based on our findings so far, we hypothesised that Wah might be acting downstream of *hiw* to regulate terminal growth, by targeting ubiquitinated Medea to the proteosome. However, when analysing *hiw* mutant NMJs in detail (FIG. 3.15)(Wan et al., 2000), there are crucial phenotypic differences. *Hiw* mutant NMJs are far more dramatically enlarged, their synaptic boutons appear stretched and reduced in size, and synaptic stainings with various synaptic markers are reduced in level. In contrast, NMJs of *OK6:: wah-RNAi* larvae are normal in morphology and with respect to marker expression, apart from the fact that they are overgrown. This difference in phenotypes is a clear indication that the *wah* mutant NMJ phenotype is not simply explainable by assigning it to the Hiw pathway. To further test this notion, I studied genetic interactions with another component of this pathway. Thus, it has been shown that overexpression of a constitutively active version of the BMP receptor Thick vein (*UAS-Act-Tkv*), enhances NMJ expansion in *hiw* mutants (McCabe et al., 2004). We tested whether in *wah* knockdown, activated *Tkv* causes a similar overexpansion phenotype. This was done by expressing *UAS-Act-Tkv* and *wah-RNAi* together in larval motorneurons using *Ok6-Gal4*. My preliminary results suggest that this constellation does not cause overexpansion of NMJ.

So far, my results demonstrate that *wah* is not simply acting downstream of *hiw* to regulate synaptic growth. This does not exclude an involvement in this pathway, but it appears more likely that other ubiquitin-regulated pathways are affected alike by loss of Wah function, as has been suggested from the wing disc experiments. In this scenario, affected pathways with opposite phenotypes might cancel each other out, which might

explain the milder NMJ phenotype (as compared to *hiw* mutant NMJ) and perhaps also the dorsoventral gradient of the *wah* mutant NMJ phenotype. This interpretation is vastly supported by my observation that proteasome knock-down causes a *wah*-like mutant phenotype (and for the proteasome one would not expect selective interference with ubiquitin-mediated degradation).

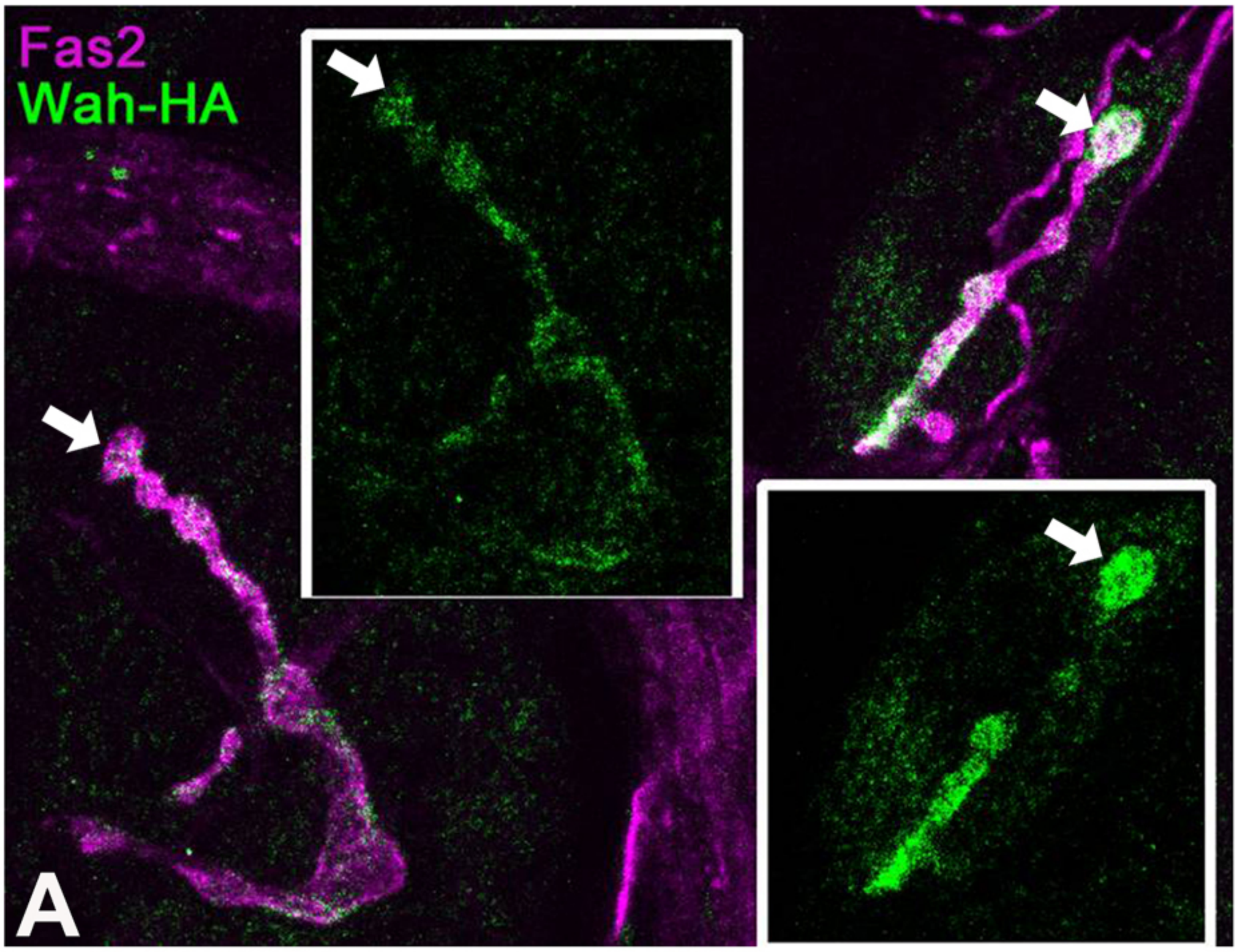
Fas2
Wah-HA
A

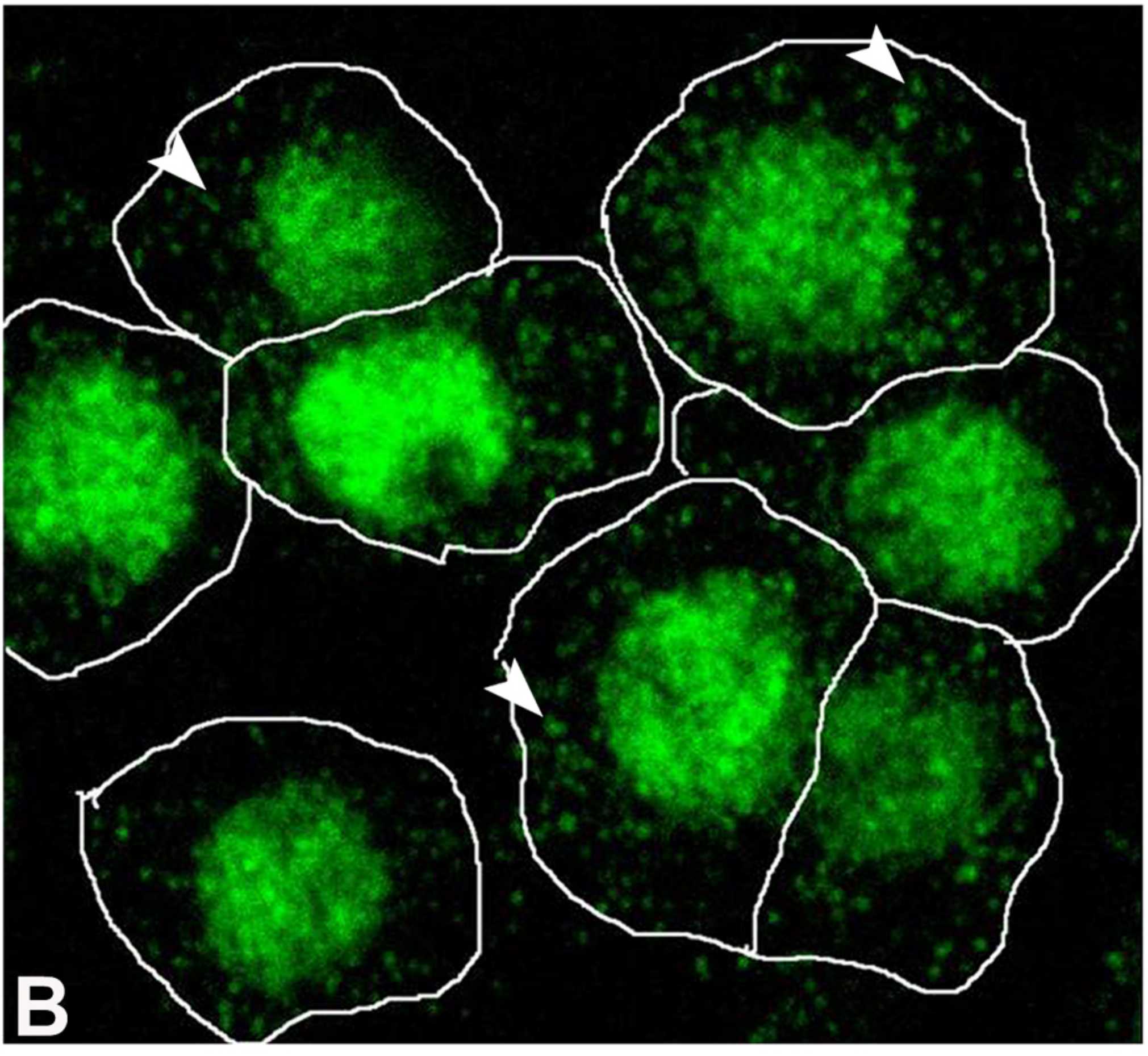
B

**Fig. 3.17 HA-wah localises in neuronal cell body, somata and the boutons.**

**HA-wah overexpression in larval motorneurons was analysed, driving *UAS-HA-wah* by *OK6-Gal4* as shown by the representative confocal image (A) NMJ co-stained with anti-Fas2 (magenta), HA-wah (green) is expressed in synaptic boutons (arrow heads and the insets). (B) In the CNS HA-wah can be visualised in the cell body nucleus and appears as puncta in the soma also.**

### *3.5.5. Generation of transgenic fly strains for the targeted expression of wah*

In *Drosophila*, the Gal4/UAS system for targeted gene expression in a temporal and spatial fashion has proven to be one of the most powerful strategies for addressing gene function *in vivo* (Duffy, 2002). I have used this strategy successfully in the context of this work by expressing *wah-RNAi* or DTS5 (Chapters 3.5.3). To enable Gal4 induced expression, the gene of choice has to be cloned into the expression vector pUAST, downstream of the UAS sequence (upstream activator sequence; responsive element for Gal4; (Fischer et al., 1988), which consists of five tandemly arrayed and optimised GAL4 binding sites. In order to complement studies described so far, I cloned the *wah* gene into the pUAST vector to generate *UAS-wah* transgenic animals to be used for experiments with Gal4-induced targeted expression.

As explained before, there is only one predicted protein isoform of Wah (Chapter 3.5.1). About 30 different ESTs are listed for the *wah* gene in the BDGP database[16]. EST *LP09056* was already used by me as template to synthesise probe for RNA *in situ* hybridisation (Chapter. 3.5.2). This cDNA clone does not cover the full length coding sequence, instead lacks about 1638bp from the 5' end. Furthermore, it contains the intron 5-6, a stop codon at 3859bp, and about 920bp of 3'UTR, including polyA sequence (FIG. 3.13, Table 3.7). To amend these irregularities and complete the sequence, I analysed the remaining 29 ESTs *in silico*. 5 clones (*AT07776, AT22722, SD06860, LD39557* and *LD46639*) were selected for further analysis. Two of these cDNAs, *LD39557* and *LD46639*, were the only ones with both 5' and 3' sequence available, and they cover most of the 5' part of gene, up to 3843bp (the Xho1 site; FIG. 3.13), i.e. they both seemed to overlap with *LP09056* suitable to generate a full length cDNA of *wah.* The cDNA clones associated with these ESTs were obtained from the *Drosophila* Genome Research Center (DGRC; inserted into POT2 vector at EcoR1-Xho1 restriction sites) and transformed into *DHSα E. coli* strains for gel and sequence analysis. My sequencing data confirmed that both cDNAs covered the complete sequence from translation start up to the Xho1 restriction site, however, there were irregularities in the area of intron 5-6 (in *LD46639,*

[16] http://flybase.bio.indiana.edu/cgi-bin/fbidq.html?FBan0004699

10 base pairs of the intron were present; in *LD39557,* 63 base pairs of exon 5 adjacent to the splice site were missing). In order to resolve the irregularities with intron 5-6 shown by all three cDNAs analysed by me so far, I ordered and sequenced 3 further cDNAs for which 5' EST sequences were available (*AT07776, AT22722, SD06860*). I hoped that at least one of these would extend beyond the Xho1 restriction site and potentially cover the full coding region or atleast show no irregularities in intron 5-6. None of these three cDNAs fulfilled the criteria. *SD06860* turned out to be much bigger than the full gene sequence of *wah* (5.3kb compared to 4.7kb full cDNA sequence) because it contained all introns (FIG. 3.13, Table. 3.7). The other two cDNAs, *AT07776* and *AT22722*, turned out to be identical clones, both of them terminating within the intron 5-6 directly fused to a polyA tail (FIG. 3.13, Table. 3.7)

Taken together, none of the sequenced cDNAs represents the full length cDNA and almost all maintain or display irregularities in or around intron 5-6. Therefore, I decided to keep this intron in my final constructs, since I could not rule out the possibilitiy that the gene may terminate in this intron *in situ*. A further problem was posed by the finding that the *LP09056* cDNA (the only one covering the 3' region of the gene) contained a stop codon in position 3859bp. I sequenced genomic DNA from OregonR wildtype flies (obtained from the Institute of Genetics in Mainz, Germany) and from CantonS wildtype flies (obtained from Hilary lab in Manchester, UK). Of these, the OregonR DNA contained the same stop codon as found in the cDNAs, whereas the CantonS DNA did not show it. Although we can not exclude that some naturally occurring regulatory mechanism (such as RNA editing) may be associated with this codon, we decided to eliminate the stop codon in our full length constructs.

After careful consideration, I decided to build two constructs (Appendix 6.2, 6.3 for details of construction). First, I built a non-tagged construct containing intron 5-6. This construct should avoid potential splice regulation, thus allowing for strong expression of the gene. Second, I generated an HA-tagged *wah* construct containing all the introns. Leaving all the introns should allow posttranscriptional regulation, which might be important for proper function of wah and thus improve the outcome of rescue experiments. The HA-tag should enable me to carry out localisation studies *in vivo* in a mosaic fashion, thus complementing and/or substituting studies with anti-Wah antibodies

generated in parallel (Chapter 3.5.6). Moreover the tagged protein should be extractable from flies and be useful for interaction and binding assays. Both the constructs were generated and successfully sub-cloned into pUAST and transgenic flies were generated (details in Appendix 6.2, 6.3).

| cDNA | Source | Length | Region | Isoform | 5'UTR | 3'UTR | Introns in | Flaws in or around intron 5-6 | Stop codon |
|---|---|---|---|---|---|---|---|---|---|
| **LP09056** | Larval and pupal tissue | 4249bp | 1640-- | X | X | all | 5-6 | complete intron | at 3859 |
| **SD06860*** | Schnieder Cells | 5340bp | 1-3843 | X | X | X | All introns. | complete intron | No |
| **AT07776 or AT22722** | Adult testes | 2950bp | 1-2797 | X | 50bp | X | 5-6 | 60bp of intron followed by poly A tail. | No |
| **LD46639** | 0-22hr embryos | 4070bp | 1-3843 | A | full | X | part of 5-6 | 10bp of intron | No |
| **LD39557** | 0-22hr embryos | 4270bp | 1-3843 | B | full | X | none | lacks 63bp of exon5. | No |

* SD06860 has got 80bp region of first intron.

**Table 3.7 Summary of 6 different ESTs that were obtained and sequenced in order to clone full length wah gene. These clones either belong to different tissue or are recovered from different stages of Drosophila life cycle (see source). All of these clones except (LP09056) start from within the 5'UTR and cover most of the N-terminal region of the gene where as LP09056 starts at 1640bp and covers rest of the gene sequence, including 3'UTR and has polyA sequence in the end, but this clone has a pre-mature stop codon at 3859bp. 3 of the rest terminate at Xho1 site (3843bp). All these have irregularities in or around intron 5-6, with either complete intron in there (LP09056 and SD06860), a part of it (AT07776/AT22722, LD46639). (LD39557) has part of exon 5 missing (also see FIG. 3.13)**

*3.5.5.1. HA-wah localises in neuronal cell body, somata and the boutons*

To facilitate studies of *wah* localization, I used *UAS-HA-wah* transgenic flies. In an effort to determine the actual localization of wah, I analyzed the localization of the full length, HA-tagged *UAS-HA-wah* transgene in larvae. When expressed by a pan-neuronal larval Gal4 driver *OK6-Gal4*, this over-expressed transgene localizes not only in the nuclei of cell bodies but also in the somata and at synapses it localizes in the boutons (FIG 3.17). Similar localisation experiments of wah in the embryos are under way. Although these experiments give us first indication about the localization of wah, I am generating antibody against wah (Chapter 3.5.6) to complement these localization studies and to clearly show the localization of wah. Moreover I did not observe any dominant NMJ phenotype associated with this over-expressed construct.

Same transgenic construct lines were mapped to respective chromosomes in order to use them for rescue experiments. The genetic crosses to generate the required fly stocks for rescue experiments are being done.

### *3.5.6. Protein purification for antibody production and biochemical assays*

*3.5.6.1. General considerations*

In order to complement the localisation studies of Wah-HA with stainings against the endogenous proteins and to prepare biochemical studies (such as binding studies of wah with ubiquitin), it was necessary to raise appropriate amounts of (preferably soluable) protein. Antibodies specific to a protein of interest can be generated by immunising animals using the entire protein, a larger fraction of it or a small oligo peptide. Oligo-peptides are mainly produced by chemical peptide synthesis, a straightforward and rapid procedure. However, better antigenicity is often achieved with larger protein fragments of several hundred amino acids length. Such protein fragments can be produced as fusion

products in bacterial cells using specific expression vectors and tend to induce better antibody titers than oligopeptides, especially when raising polyclonal antibodies.

The choice of suitable protein fragments of Wah for antibody production or biochemical analyses was not straightforward due to the rather vague domain predictions obtained from *in silico* analyses (Chapter 3.5.1). In order to choose soluble and/or highly antigenic regions of the protein, the sequence was analysed on different programmes provided by the BCM search launcher[17], such as *Protein Hydrophilicity / Hydrophobicity Search* or *SOPM* (*s*elf-optimized prediction method; IBCP-CNRS). The hydrophilicity plot from the first programme shows a couple of slightly hyrdophobic regions, but none as strong as the potential transmembrane domain predicted by TMpred programme mentioned above (aa193-212; Chapter 3.5.1). The SOPM server predicts a protein that is mainly unstructured. Therefore it is difficult to make predictions for proteins soluble in *E. coli*.

On the basis of this information, I decided to start with the regions of the protein that do not contain coiled-coil domains. Thus, I chose an N-terminal region comprising the first complete exon (1-224aa), although it contains the hydrophobic region weakly predicted as a transmembrane domain (aa193-212). I learned from discussions with Richard Kammerer that usually one exon forms one complete domain. Therefore, cleaving off the exon at aa192 is more likely to disrupt the integrity of such a potential but yet unknow domain and lead to insolubility or instability of the expressed product, whereas the hydrophobic area (i.e. predicted transmembrane domain) is more likely to help its folding.

The other two regions, a middle fragment (940-1150aa) and a C-terminal fragment (1371-1570aa; FIG. 3.10), were chosen because these regions do not contain the coiled-coil domains and are relatively more hydrophilic, therefore likely to be more antigenic. Uniqueness of the sequences was ascertained by BLAST before starting with the cloning of these fragments.

[17] http://searchlauncher.bcm.tmc.edu/seq-search/struc-predict.html

*3.5.6.2. GST-fusion constructs*

First trials were carried out before I learned about the potential structural similarity to Rad23 (Chapter 3.5.1). I decided to generate GST fusion constructs to be purified on sepharose columns and started with these three regions of Wah: an N-terminal fragment (1-224aa) comprising the complete first exon, a middle fragment (940-1150aa), and a C-terminal fragment (1371-1570aa; FIG. 3.10). These three peptides were amplified via PCR from different cDNA clones and then sub-cloned into the GST-fusion vector pGEX-4T1 (using EcoR1 and Xho1 restriction sites), and transformed into *E.coli* expression strains BL21 (Table 3.8 and Materials and Methods 2.3.1).

Out of the three fusion constructs, only the N-terminal construct got expressed at 37°C but the peptide was mainly insoluble, being trapped in inclusion bodies. One of the possible reasons for forming inclusion bodies can be that the protein is expressed at higher rate and does not fold properly. To reduce expression levels I lowered the temperature to 30°C which allowed me to yield the protein in soluble form. However, this peptide started degrading before eluting it off the sepharose column (used to purify GST fusion proteins) in the presence of protease inhibitor cocktail (Amersham; containing a mixture of both competitive and non-competitive protease inhibitors that inhibit serine, cysteine, and calpain proteases) and at low temperature (4°C). However, further degradation was not seen during period the protein solution was frozen at -20°C. This degradation problem rendered the protein unsuitable for antibody production.

From discussion with structural Biologists (J. Bella, R. Kammerer, Manchester) I learned that the N-terminal fragment I used has only a brief helical portion of about 20 amino-acids (153-175aa), which can fold and attain some secondary structure. But this structure is possibly de-stablised by a long unstructured N-terminal portion. This constellation could explain why the protein attains some structure but degrades instantly or over some period of time. Therefore, I built two longer N-terminal constructs (1-320 aa and 1-435aa) hoping that the additional fragments might help the protein to stabilize. The first construct did not express at all, whereas the long construct (containing the coiled-coil region at 395-423aa; FIG. 3.10) got expressed but was mainly insoluble. Details of

cloning and expression of all these constructs can be found in Materials and Methods (Chapter 2.3.1).

GST-Fusion products

| Construct name | Length | Region | Template | Primers | Comments |
|---|---|---|---|---|---|
| **N-terminal 224** | 224aa | 1-224 | LD46639 | F1 and F2 | Soluble but unstable |
| **N-terminal 320** | 320aa | 1-320 | LD46639 | F1 and F7 | Failed to express |
| **N-terminal 435** | 435aa | 1-435 | LD46639 | F1and F8 | Expressed but Insoluble |
| **Middle** | 211aa. | 940-1150 | LP09056 | F3 and F4 | Failed to express |
| **C-terminal** | 200aa | 1371-1570 | LP09056 | F5 and F6 | Failed to express |

**Table 3.8 GST-fusion constructs generated and tested for expression.**

**In all, 5 constructs were tested for expression. These include 3 N-terminal constructs of different lengths (224, 320 and 435a.acids), synthesized from template LD46639. One middle (940-1150a.acids) and one C-terminal (1371-1570a.acids), synthesized from the template LP09056. These constructs were cloned into the pGEX-4TI (Materials and Methods 2.3.1) and tried for expression. Three constructs (N-ter 320, Middle and C-ter) did not express at all. N-ter 224 got expressed as soluble protein but was highly unstable (Chapter 3.5.6.2, FIG.3.10) and N-ter 435 expressed but was mainly insoluble, forming inclusion bodies**.

*3.5.6.3. His-tag Fusion constructs*

One of the reasons for insolubility and/or failure to fold properly could be the vector itself, because GST forms homo-dimers that affects folding of the protein and facilitates aggregation (Murray et al., 1995). Thus, I used another vector, pHis-Trx (Kammerer et al., 1998), which fuses the protein fragments to His-tag (does not mediate dimerisation) and thyroidoxine (increases solubility). In addition, I had learned meanwhile about the prediction made by the 3D-PSSM programme (Chapter 3.5.1)[18].and decided to capitalise on the structural homology of Wah with Rad23. According to this prediction, Wah

[18] http://www.sbg.bio.ic.ac.uk/~3dpssm/index2.html

contains one N-terminal UBL, two UBA and a potential coiled-coil domain (FIG. 3.10, Table 3.9). I decided to clone a 183kb fragment (386-446aa) comprising the coiled-coil domain and a second 435kb fragment (386-530aa) comprising the coiled-coil domain together with the second UBA domain. The second fusion construct would also provide the possibility that it could be used for ubiquitin binding assays. Upon transformation into the *E. coli* strain BL21 the products of both fusion proteins were again mainly in-soluble and aggregated in inclusion bodies. I tried to recover the protein from inclusion bodies with 8M urea in binding buffer (to denature and solubilise the protein) and subsequent refolding via 5 subsequent rounds of dialysis at 4ºC. This protocol allowed me to recover reasonable amounts of soluble proteins, but subsequent thrombin digestion to remove the thyroidoxine (Materials and Methods 2.3.4) did not work for unknown reasons rendering these fusion proteins unsuitable for antibody production (due to the high antigenicity of thyroidoxine). To overcome this problem the same constructs were sub-cloned into a different His-Tag vector, pHis, without thyridoxine (designed by Richard Kammerer)(Kammerer et al., 1998). Again both the products got expressed but were mainly insoluble. Only the bigger product (coiled coil+UBA domains) was extracted and re-folded as explained above. Coomassie stained gels revealed one very heavily stained band of 17kD and a number of weaker higher running bands (FIG. 3.18) likely to represent either bacterial products or protein aggregates, even after stringent washings using the non-ionic detergent Triton-X 100 which destabilises protein complexes through solubilisation. Even narrow fragmentation of the eluate from the 1ml His-column did not help to separate the 17kD band from the higher running ones suggesting that the other bands might represent oligo- or multimeres. Mass spectrometry analysis using MALDI technology at the proteomics core unit at the Faculty of Life Sciences in Manchester confirmed that the strongly staining 17kD band represents the expressed His-fusion protein fragment, and tests of some of the larger bands suggested (though at lower prediction level) that they represent oligo- or multimeres of the expressed protein. About 8mg of protein could be purified in 15ml volume, but turned out to degrade over time, though far slower than the initial fragments described above. Therefore, this fragment was not suitable for biochemistry but was used for antibody production. To this end, about 800µg were loaded on a Poly-acrylamide gel, the 17kD band was cut out and sent for

injection into rabbits for antibody production (carried out at Eurogentec[19]). Using gel slices has the advantage that the antigen is released slowly over time providing a constant source of antigen. The disadvantage is that antibodies are raised against denatured protein. I have already got the third and final anti-serum against wah and will be tested soon.

In order to obtain protein for biochemical studies, I expressed one more 44kb fragment covering the full Rad23 homology region (132-529aa), using the same strategy as for other two constructs. This product again got expressed but was mainly insoluble. In collaboration with R. Kammerer (Manchester, UK) I will attempt now to express the full length gene in *Drosophila* S2 cells, and the cloning into suitable vectors has been started. If this protein is soluble we will carry out enzymatic proteolytic digests to fragment the protein for biochemical analyses.

His-tag fusion products

| Construct name | Length | Region | Template | Primers | Comments |
|---|---|---|---|---|---|
| **Coiled-coil** | 61aa | 386-446aa | LD46639 | F9 and F10 | Expressed but Insoluble |
| **Coiled-coil+UBA2** | 145aa | 386-530aa | LD46639 | F9 and F11 | Expressed but Insoluble |
| **Rad23 homologue** | 399aa | 132-529aa | LD46639 | F12 and F13 | Expressed but Insoluble |

**Table 3.9 His-tag Fusion constructs generated and tested for expression.**

**3 constructs were tried for expression. First one 61a.aicd long comprised of predicted coiled-coil region of the protein (384-446 a.acids), second one 145a.acid long comprised of coile-coil and UBA domain (386-530a.acids) and the third 399a.acids long complete Rad23 homologous region (132-529a.acids). These products were synthesized form the template LD46639, cloned into the pHis/pHis-Trx vectors (Materials and Methods 2.3.2) and tried for expression. All the three constructs got expressed but were insoluble forming inclusion bodies (Chapter 3.5.6.3, Table 3.10).**

[19] http://www.eurogentec.com/carte/carte.asp

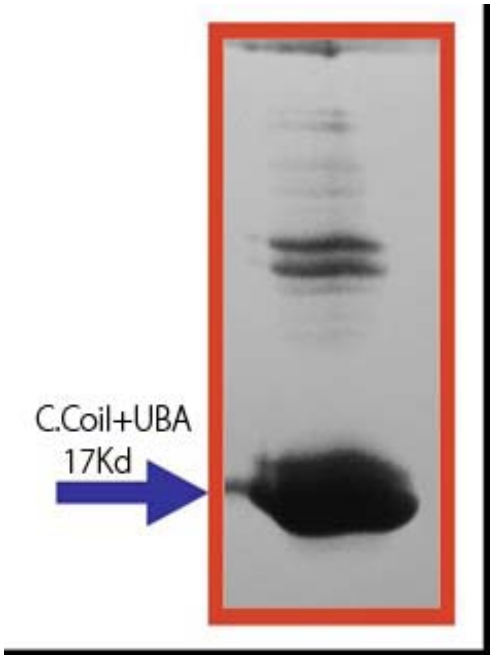


**Fig. 3.18 band of 17kD and a number of weaker higher running bands**

**Gel showing 17Kd band of the product (C.coil+UBA) with contaminations. Cut gel slice was used to inject and generate anti-serum against wah (Chapter 3.5.6.3).**

# 4. DISCUSSION

## 4.1. Some novel genes involved in Drosophila NMJ formation were discovered in this screen

The goal of this screen was to identify genes with immediate requirement at the forming NMJ, i.e. coding for gene products such as cell adhesion molecules, cytoskeletal molecules, or contributors to local signalling or assembly events. For me the prospect of this screen was highly attractive, because only 14 mutants with potential defects in NMJs were preselected in Cahir O'Kane's laboratory from a large collection of about 2460 mutant lines (Salzberg et al., 1997) and the insertion for each mutant was already identified via inverse PCR and plasmid rescue. However, due to the extremely difficult preparation techniques required, their phenotypic descriptions were rather superficial and, as I could later show, not reliable. For the same reason, also the molecular mapping was not validated by genetic complementation analysis.

My own phenotypic analyses revealed various NMJ aberrations. As detailed below, the most prominent phenotypes found are increased or reduced NMJs, enlarged or increased numbers of boutons, and altered amounts or arrangements of active zones. Only two mutant stocks, *0242-41* and *1107-02*, showed qualitative defects potentially reflecting structural changes. Thus, mutant line *1107-02* has bigger or fused boutons and nc82 staining reveals enlarged almost continuous active zones (most likely due to their fusion), suggesting that the mutation causes structural aberrations at synapses (for details see Chapter 4.2). The mutant line *0242-41* which displays smaller terminals shows accumulation of Dlg at these mutant terminals, and Dlg has been shown to be required to establish a proper architecture and molecular composition of NMJs (Budnik et al., 1996; Tejedor et al., 1997; Thomas et al., 1997).

All other mutant phenotypes represent quantitative defects. The mutant lines *0094-13* and *0066-40* show enlarged terminals with increased numbers of boutons and there might be an increase in the spacing between boutons. Also the branching might be increased at these mutant terminals, but was not assessed in detail. Mutant line *0010-12* shows increased numbers of boutons and the boutons also look enlarged, but the

phenotype is not highly significant. These growth phenotypes meet the expectation that NMJ growth has to be actively regulated during embryonic development and, therefore, normal NMJ morphology is likely to be a dynamic balance between processes promoting and inhibiting growth. Hence, a promising number of relevant mutations was uncovered in this screen.

Complementation analysis to map the mutations was time consuming and less straight-forward as expected. Only three of the selected stocks (*0010-12, 0094-13, 1227-10*) carried just one P-element insertion and were mapped first. For all other stocks existing molecular data suggested that there are either 2 or 3 P-element insertions, demonstrating that the quality of the original screen carried out in Hungary (Salzberg et al., 1997) was not satisfactory and complicating the mapping procedure enormously. For these stocks with multiple insertions, complementation tests were carried out one by one with all the deficiencies or P-element insertions described to affect the respective regions or genes. For mutant line *1151-02*, which carries 3 insertions, complementation tests with two different P-element insertions were carried out, but both failed to complement the phenotype. One possible explanation could be that the two P-element insertions show genetic interaction, making it difficult to pinpoint the responsible gene. Furthermore, the phenotype (elongated terminals without any increase in active zone numbers) is unlikely to represent a structural aberration and, hence, of less interest to us. For two other mutant lines *1107-02* and *242-41*, precise mapping of the mutation was further delayed because of the late availability of suitable P-element insertions in the potentially affected genes. This problem delayed their mapping and further investigations enormously. Furthermore, mutant line *0287-07* could not be mapped so far due to the fact that the available GFP-labelled balancer chromosome interfered genetically with the mutant chromosome, and experiments with other now available balancers are underway.

In spite of all these problems, this screen successfully identified genes with diverse functions. Three of the genes are potentially involved in transcriptional control. Thus, the *1227-10* insertion affects *CG7372* (a potential Myoneurin Zn-finger transcription factor), *0066-40* turned out to be an allele of *castor* (a neuronal transcription factor), and the *0010-12* mutation seems to affect *taranis* (involved in chromatin-mediated transcription control). The processes of transcription would be expected to be an essential process

regulating the timing and quantity of the provision of cell adhesion proteins, cytoskeletal molecules, functional components and signalling molecules during NMJ formation. Their analysis would therefore provide good opportunities to advance our understanding of synaptogenesis. However, the understanding of transcriptional control does not fall into the area of my interest. These 3 genes were therefore excluded from further analyses, although some aspects of *castor* function were investigated because crucial literature and genetic tools were available and antibodies made it easy to analyse the phenotype in some detail. My genetic analysis as described (Chapter 3.3) suggests that the overgrown NMJ phenotype might be a secondary effect of an increased number of motor neurons caused by the mutation.

Of interest in the remit of this project were 3 mutations: First, the mutation *1107-02* affects the *CG5567* locus coding for an enzyme with 4-Nitrophenylphosphatase activity. The phenotype of line *1107-02* is extremely interesting since it displays bigger or fused boutons and active zones appear to be enlarged or fused, suggesting that this is the only mutation causing ultrastructural aberrations. Unfortunately, mapping of this gene occurred too late to be considered for further analysis in the framework of this project. Second, the line *242-41* was chosen for further analysis since it shows a significantly reduced NMJ phenotype and affects the *eIF4-AIII* gene encoding a eukaryotic initiation factor (discussed 4.3). Finally, the mutant line *0094-13* shows a statistically significant NMJ overgrowth phenotype (discussed 4.4) and codes for Wah, a protein potentially involved in the regulation ubiquitin-mediated protein trafficking at the NMJ.

Taken together, the following principal conclusions can be drawn from this screen. First out of 14 pre-selected mutant lines only 8 (57%) show NMJ phenotypes. Therefore, the output was far lower than expected. Second, the screen aimed at the discovery of genes with potential roles in qualitative aspects of NMJ formation, but there seems only one mutant line *1107-02* which shows potential structural aberrations. All other mutations display mere quantitative growth defects, i.e. increase or decrease of NMJs. Third, gene mapping was far more laborious than expected, primarily because of multiple P-element insertions. Fourth, I discovered many genes, with transcriptional and translational role, but only three genes which fall potentially into our remit.

## 4.2. Is CG5567/4-Nitrophenylphosphatase a good candidate gene for further investigation?

The *1107* mutation turned out to be a mutation of *CG5567*, showing a vague similarity to a potassium-dependent 4-nitrophenylphosphatase ($K^+$-pNPPase). $K^+$-pNPPase forms part of the $Na^+K^+$-ATPase complex, which is believed to maintain $Na^+$ and $K^+$ gradients (Schneider and Kraig, 1990). The enzyme ($K^+$-pNPPase) was found to be localized on the surface of synaptic vesicles, the pre- and post-synaptic membranes and on the post-synaptic density in adult mouse cerebral cortex (Vorbrodt et al., 1982), rat hippocampal formation and in adult guinea pig sympathetic ganglia (Anderson et al., 1985). It seems to be involved in neurotransmitter uptake (Nagafuji et al., 1992), in cellular homeostasis at synapses (Andersson Forsman and Elfvin, 1986; Wood et al., 1977), and also in the differentiation of the nervous system, potentially by modifying the influence of nerve growth factor on nerve cells (Rodriguez de Lores Arnaiz, 1992). In general, cation homeostasis seems to have differentiational potential, as demonstrated by work on other cation pumps (Messenger and Warner, 2000). Therefore, CG5567 might indeed play a role in such a pathway, but this thought is highly speculative. The only other functional link of CG5567 is its reported upregulation upon knock-down of the cell cycle regulatory gene SIN3 (Neufeld et al., 1998; Pile et al., 2002; Pile et al., 2003), but next to nothing can be said about this link and potentially learned lessons at this stage.

## 4.3. Translational regulation of size at the newly forming embryonic NMJ

### *4.3.1. Nature of the gene*

One of the genes discovered in my screen was uncovered by the *0242-41* mutation and encodes the eukaryotic initiation factor eIF4AIII. Failure to complement the lethality with another P-element insertion in the same gene showing the same undergrown NMJ phenotype, confirmed the involvement of eIF4AIII in the mutant phenotype suggesting this factor to regulate the size of NMJs in *Drosophila* embryo. This undergrown NMJ phenotype caused by the mutation is specific, as all other aspects of nervous system and

muscle development remain unaffected in the mutant (Chapter 3.4.1). However, further proof for the involvement of eIF4AIII is required. RNAi interference, *in situ* hybridisation and/or genomic rescue experiments are required to prove and demonstrate the involvement of eIF4AIII. To this end, genomic rescue experiments are being planned, and I have obtained a wildtype cDNA construct (kindly provided by Isabela Palacios, Cambridge, UK).

The eukaryotic translation initiation factor complex 4F (eIF4F) is composed of eIF4E, eIF4A and eIF4G. It is involved in the recognition of the mRNA cap and the ATP-dependent unwinding of the 5'-terminal secondary structure and recruitment of the mRNA to the ribosome. eIF4A is one of the components of the complex and has three isoforms. Two of these eIF4A isoforms, eIF4AI and eIF4AII, which are encoded by two different genes, are functionally indistinguishable. A third member of the eIF4A family eIF4AIII which shares 82% identity with *Xenopus* eIF4AIII (Li et al., 1999; Weinstein et al., 1997), and is 66% identical to eIF4AI. eIF4AIII contains approximately nine short conserved sequences which are not present in eIF4AI and eIF4AII. These sequences are dispersed across the entire length of the molecule among the conserved domains of the DEAD box family (Li et al., 1999). The eIF4AIII protein contains domains such as ATP-dependent helicase, a DEAD box and DEAD/DEAH box helicase.

Although it is assumed that eIF4AIII functions in translation, it is possible that eIF4AIII has a function also in some other mechanistic contexts. The RNA helicases of the DEAD-box protein family could play key roles in different aspects of RNA metabolism, including pre-mRNA splicing, rRNA processing, mRNA turnover, mRNA transport, and ribosome assembly (Luking et al., 1998). eIF4AIII has been demonstrated to play roles in many cellular processes, such as oogenesis, spermatogenesis, cell growth, and division. Thus, it has been shown that an eIF4AIII-containing complex is required for mRNA localisation in *Drosophila* oocytes and nonsense-mediated mRNA decay in mammalian cells where eIF4AIII constitutes at least part of the platform anchoring other exon junction complex proteins to spliced mRNAs (Ferraiuolo et al., 2004; Palacios et al., 2004; Shibuya et al., 2004). In *Xenopus* cells, cultured in the presence of the epidermis inducer BMP-4, eIF4AIII transcripts are elevated and are also elevated in the ventral ectoderm. Overexpression of eIF4AIII inhibits neuralisation and induces epidermis

instead (Weinstein et al., 1997). It remains to be determined which mRNAs are translationally affected by eIF4AIII in this context.

Biochemical characterisation of eIF4AIII reveals that, unlike the other two isoforms, eIF4AI and eIF4AII, it inhibits translation in a reticulocyte lysate system. Thus, it is suggested that eIF4AIII might play an inhibitory role in translation under physiological conditions (Li et al., 1999).

### *4.3.2. Potential mechanism of eIF4AIII at the developing NMJ*

Local translation at NMJs has been shown to be involved in plastic growth regulation during larval life (Sigrist et al., 2000), but there have so far not been any reports linking it to size regulation during *de novo* formation. This statement is not self-evident, since developmental processes at the embryonic and larval NMJ are distinct. Thus, embryonic NMJs form through break-down of a large growth cone covering the future NMJ field (Yoshihara et al., 1997), whereas larval growth occurs through budding or splitting of larval boutons and their subsequent enlargement (Zito et al., 1999). Rapid growth in larvae, when they begin to move vigorously, is accompanied by local increase in postsynaptic proteins. In few hours aggregates of eIF4E and polyA binding protein (PABP) appear at these NMJs, and both are involved in translational control. Glutamate receptors (DGluRII) are synthesised locally, targeted to their postsynaptic receptor fields, additional active zones are recruited to these sites and, finally, new boutons are added to the NMJ (Sigrist et al., 2003; Sigrist et al., 2000).

Similarly, *eIF4AIII* may potentially be required post-synaptically at NMJs, as the antiserum labels muscle nuclei (personal communication, I. Palacios) and I saw effects on the expression level of the predominantly postsynaptic factor Dlg. Accumulation of Dlg at the NMJ could therefore be the consequence of translational de-inhibition through loss of eIF4AIII, consistent with the functional role described for its mammalian orthologue (previous Chapter). Dlg is a membrane associated PDZ domain protein involved in clustering of synaptic components at NMJs (e.g. ) (Tejedor et al., 1997; Thomas et al., 1997). Furthermore, *dlg* regulates the amount of postsynaptic infoldings at larval NMJs called SSR (subsynaptic reticulum; )(Budnik et al., 1996). It also plays crucial roles for

the organisation of epidermal adhesion junctions and signalling processes associated with them (Caruana, 2002). Thus, Dlg was a good candidate for a mediator of eIF4AIII regulatory influences on NMJ growth. However, I could not pheno-copy the undergrown NMJ phenotype by either over-expressing Dlg in mesoderm (*24B-Gal4* driven Dlg-S97N-EGFP) or in neurons (*RN2D+O*), in agreement with the fact that there is so far no report of Dlg mutants or its over-expression causing any growth phenotype in embryonic or larval NMJs. Interestingly, the undergrown NMJ phenotype in the mutants was rescued when Dlg was removed together with eIF4AIII function. This indicates that there may be some genetic link between Dlg and the translation initiation factor eIF4AIII. One possible scenario in agreement with these findings is that mutations of *eIF4AIII* up-regulate DGluRIIB together with Dlg expression, of which DGluRIIB is the essential factor influencing NMJ size. Consistent with this idea, it has been shown that absence of DGluRIIB enhances NMJ growth, whereas DGluRIIB overexpression tends to suppress enhanced NMJ growth induced by independent means, such as elevation of GluRIIA (Sigrist et al., 2002). Since Dlg is required for DGluRIIB localisation (Chen and Featherstone, 2005), enhanced Dlg levels (caused by absence of eIF4AIII) might further increase the effects of DGluRIIB over-expression by overcoming rate-limiting aspects of the postsynaptic localisation of this receptor. This hypothesis would also explain why absence of Dlg suppresses the *eIF4AIII*: it simply prevents growth-regulatory effects of up-regulated DGlurIIB levels by preventing their synaptic localisation. It is now required to test this hypothesis with anti-DGluRIIB antibodies, mutations and UAS-constructs.

## 4.4. Waharan represents a novel gene potentially involved in ubiquitin-mediated protein trafficking.

The *CG4699*/*waharan* locus represents an annotated sequence without known function. My work has now shed light on this gene with potential impact for its orthologue KIAA1267 the function of which is likewise unknown. To investigate the role of *wah* I carried out genetic and molecular analyses of the mutant and found that *wah* regulates the synaptic growth in *Drosophila* embryos and potentially in larvae and plays a role in wing development. I found *wah* to be expressed in CNS and weakly in mesoderm from early embryonic stages. My further analysis revealed that *wah* is required both pre- and postsynaptically to regulate NMJ size. Although, I can not show the endogenous localization pattern of *wah* yet (antibodies have just been generated), my HA-tagged constructs (*UAS-HA-wah* transgenic flies) reveal localisation to motorneuronal nuclei and NMJs. My results suggest that Wah's molecular function is to regulate intracellular trafficking/processing of ubiquitinated proteins, as supported by my studies with anti-polyubiquitin antisera and knock-down of proteasome function.

### *4.4.1. Is wah the gene in question?*

To confirm that loss of *wah* function causes the NMJ phenotype of *0094-13* mutant embryos, several experimental approaches were used. First, the molecular mapping of the P-element insertion $wah^{P1}$ (i.e. our original mutation *0094-13*) using inverse-PCR methodology mapped it to 5' UTR region of the *wah* gene just few bases before the first codon. Second, the outcome of genetic complementation tests clearly supports the involvement of *wah*. One more P-element insertion in the gene $P\{lacw\}I(3)06536^{j2E5}$ which we named $wah^{P2}$ also maps to the 5'UTR of the gene and fails to complement the early larval (L1) lethality and the overgrown NMJ phenotype of $wah^{P1}$. Third, my *in situ* hybridisation analyses revealed that *wah* transcripts are expressed rather ubiquitous at stage 11/12 but showed accumulation in the CNS towards later stages 15/16 and mild expression in muscles, i.e. in both tissues involved in NMJ formation. Fourth, the same probe failed to detect any expression in $wah^{P1}$ mutant embryos and showed weaker

expression in $wah^{P2}$ confirming specificity of the RNA probe and, at the same time, confirming that the two P-element mutations causing the NMJ phenotype clearly affect the *wah* locus. Fifth, my RNA interference experiments phenocopied the $wah^{P1}$ and $wah^{P2}$ mutant phenotype. They also indicate pre- and postsynaptic requirements for Wah during NMJ growth, since knocking down *wah* expression by in either neurons or muscle causes the overgrown NMJ phenotype.

Taken together, we have almost unequivocal proof for the role of *wah* in the NMJ phenotype. However, genomic rescue experiments to support and strengthen our argumentation are under way and would further strengthen our argument.

### *4.4.2. Spatio-temporal requirement of wah during development.*

Spatially, the *wah* transcript is abundant in nervous system and to some extent in muscles, as revealed by my *in situ* hybridisation data. This is in agreement with pre- and postsynaptic requirements revealed by my RNAi experiments at embryonic stages. RNAi experiments furthermore support statements from the GEO database suggesting expression of *wah* in the larval nervous system and wing discs. Thus, I found that expression of *wah-RNAi* at larval stages in all motorneurons leads to increase in synapse growth indicating that *wah* not only acts in the embryo but can function throughout the larval growth period to control synaptic growth. To support this argumentation I also found that *HA-wah* localizes at synaptic boutons in larvae apart from the cell body. The experiments to show whether I can rescue the overgrown NMJ phenotype caused by the mutation in embryo and the larvae with *UAS-wah* constructs are in progress. At the moment my data clearly indicate that *wah* is involved in embryonic and larval phases of NMJ development.

It would now be important to determine the localisation of endogenous Wah. To this end, I generated antisera which are only now available. This unfortunate delay was due to the complications with the choice of suitable protein fragments of Wah due to the rather vague domain predictions obtained from *in silico* analyses (Chapter 3.5.1) resulting in fusion products which were either not express, insoluble or unstable. Only when choosing the His-tag and the 435kb *wah* fragment (386-530aa) comprising the coiled-coil domain

together with the second UBA domain, I was eventually able to send gel slices with sufficient protein to Eurogentec for antibody production (Chapter 3.5.6). The antiserum has been obtained and will be tested soon. Therefore, the only localisation data I have at present are derived from the HA-tagged *wah* construct (*UAS-HA-wah*; raised in parallel to non-tagged *UAS-wah*). The localisation of Wah-HA has not been tested in embryos so far, but I could show that it localises to larval NMJs, although its co-localisation with other synaptic proteins has to be checked. The transgenic protein does appear to be enriched at the terminal and is barely detectable along the axon. However, this overexpressed protein is also visible in punctuate patterns in the somatic cytoplasm and in the nucleus of the larval motorneurons.

### *4.4.3. The molecular mechanism of Wah function.*

The localisation of Wah at synapses is conceivable as involvement in the regulation of preatosome-mediated degradation, especially since an involvement of this regulation in the formation and maintenance of synapses and synaptic plasticity is well documented (Cline, 2003; DiAntonio et al., 2001). The assumption that Wah catalyses degradation of ubiquitinated proteins is in line with the prediction of a Rad23-like structure, the fact that polyubiquitin proteins accumulate at synapses in *wah* mutant background, and that proteasome knock-down phenocopies knock-down of *wah*. Rad23 is highly conserved from yeast to humans and has a potential role of targeting poly-ubiquitinated proteins to the proteasome in the final process of ubiquitin-mediated protein degradation (Glickman and Ciechanover, 2002; Walters et al., 2003).

Futhermore, my analysis reveals that there is reduced polyubiquitin staining in nuclei of *wah* mutant muscles and CNS compared to wild type embryos, indicating that Wah may be involved in nuclear import of ubiquitinated proteins as well. This finding is in agreement with a highly predicted nuclear targeting of Wah (FIG. 3.11). Furthermore, also Rad23 has been shown to localise in the nucleus as well as in cytoplasm (Katiyar and Lennarz, 2005). Given the increasing complexity of ubiquitination pathways (Ciechanover, 1994), such a function would no longer be surprising, but such a role of Wah would open up a new avenue of research.

Localisation of Wah to the nucleus is also in accord with the fact that nuclear proteins are reported to be degraded through ubiquitin- and proteasome-mediated degradation mechanisms. For example, SnoN, a negative regulator of the TGFβ signaling pathway, and p53 are degraded by ubiquitin-mediated proteasomal degradation (Bonni et al., 2001). p53 degradation involves ubiquitin-mediated proteasomal degradation wherein hHR23, the human homologue of Rad23, is intrinsically involved as a bridging factor between ubiquitinylated p53 and the 26S proteasome (Glockzin et al., 2003). Such events could happen in the nucleus, since it has been reported that the proteasome is found in the nucleus and cytoplasm (Kirschner, 1999), and most likely also ubiquitination can be carried out directly in the nucleus. However, if Wah would carry out a similar function in the nucleus as it seems to do in the cytplams (where polyubiquitinated proteins accumulate in the absence of Wah; FIG. 3.16), we would expect polyubiquitin aggregates to increase in nuclei in *wah* mutant cells. This is not the case, but rather the contrary. Therefore, I postulate that either Wah facilitates nuclear import, or that it prevents ubiquitination to occur in the nucleus. The latter is harder to imagine given the stuctural insight we have into Wah at present, so that import of ubiquitinated proteins is the more likely function. For example, Notch activation has been shown to depend on ubiquitination (Hori et al., 2004), and experiments addressing potential involvement of Wah in Notch function and import are planned at the moment. Such experiments seem not unreasonable given the notched wing phenotype we observe upon wah RNAi knock-down with the *vestigial-Gal4* driver line (FIG. 3.14)

### *4.4.4. Potential genetic interactions of wah.*

The *wah* gene negatively regulates growth at NMJs whereas their initial formation on appropriate muscles and synaptic markers localisation is normal, indicating that the integrity of synapses is intact and the phenotype merely quantitative. Three mutations in components of pathways involving ubiquitination have been described so far leading to increased NMJs when deleted: mutations of *spinster*, the APC/C complex and of *highwire*. All of them will be discussed below and potential interactions assessed.

A well studied signalling pathways with the largest effects on synaptic size at the *Drosophila* NMJ is the TGF-β/BMP pathway (Aberle et al., 2002; Marques et al., 2002; Marques et al., 2003; McCabe et al., 2004; McCabe et al., 2003), which stimulates synaptic growth, induced by the TGF-β homologue Glass bottom boat (Gbb). The TGF-β and closely associated BMP pathways are tightly regulated by ubiquitin-mediated proteasome degradation at different molecular levels. For example, at the level of transcriptional control, this pathway is regulated by highwire (*hiw*), an E3 ubiquitin ligase supposed to ubiquitinate Medea, a member of the Smad complex required to pass on BMP signals to the nucleus (McCabe et al., 2004). Therefore, the synaptic overgrowth phenotype of *hiw* mutant embryos is believed to be caused by enhanced BMP/TGF-β signalling. However, *hiw* mutant larvae show an enlarged NMJ phenotype which is distinct from the *wah* mutant phenotype. This difference in phenotype is a clear indication that the *wah* mutant NMJ phenotype is not simply explainable by assigning it to the Hiw pathway. Furthermore, I could not link activated thick vein (an essential receptor in this BMP pathway) genetically to *wah*, in contrast to similar experiment with *hiw* which revealed such interaction with activated thick vein (McCabe et al., 2004). Further ubiquitin-mediated regulation of BMP/TGF-β signalling at the transcriptional level is implemented by the E3-ubiquitin ligase Smurf2. Smurf2 can fulfil temporally distinct functions in TGF-β signalling with opposite effect, dependent on its partnership with different classes of Smad proteins. In the context of the initiation of BMP/TGF-β signaling, Smurf2 is thought to bind to Smad2 to facilitate activation of the pathway by degrading transcription inhibitors such as SnoN, thus initiating TGF-β signalling (Bonni et al., 2001). As a result of continued BMP/TGF-ß signalling, Smad2 (and sometimes Smad3) can also associate with the anaphase promoting complex (APC/C) and recruit it to SnoN (Wan et al., 2001). The APC/C has likewise E3 ubiquitinase activity mediating ubiquitination of SnoN and its subsequent proteasomal degradation.

Smurf2 is also involved in regulation of the BMP/TGF-β signalling pathway at the level of receptor molecules. Thus, Smurf2 partners with inhibitory Smad (Smad7), the levels of which increase as a result of active TGF-β signalling. The Smurf2/Smad7 complex is targeted to TGF-β receptors for degradation, thereby shutting down the signalling pathway. This degradation of the BMP/TGF-β receptor complex occurs either

directly via the proteasome (Bonifacino and Weissman, 1998) or via sorting processes in the late endosome (Izzi and Attisano, 2004; Strous and van Kerkhof, 2002). The latter regulation involves Spinster, which is an integral protein of the late endosomal compartment, and loss of *spinster* function causes NMJ overgrowth (Sweeney and Davis, 2002. This effect is proposed to be caused by malfunctioning in the endosomal sorting process causing BMP receptors (which fail to degrade) to continue to activate the TGF-ß pathway, thus causing excessive growth at the NMJ. Interestingly, the expanded wah mutant NMJ phenotype resembles that of spinster mutants {Sweeney, 2002 #363), though the phenotype in *wah* is slightly weaker (but it should be noted that we compare a RNAi interference phenotype of *wah* to mutant phenotypes of *spinster*). Like Wah, Spinster is expressed both pre- and postsynaptically at NMJs. Since Wah has a comparable phenotype, and a ubiquitin-mediated trafficking or degradation function, it can have a role in this sorting process. Therefore, it will be pivotal to test for potential colocalisation of Wah with Rab5 (early endosomal) and Spinster (late endosomal) proteins to check whether Wah may have a specific role in this pathway. To this end, my UAS-HA-wah transgenic flies can be used already, and anti-Wah antisera are ready to be tested.

As briefly mentioned above, another ubiquitination-mediated pathway potentially interacting with *wah* is the anaphase promoting complex APC/C which has E3 ubiquitin ligase activity in other contexts than the BMP/TGF-β signalling pathway. APC/C is localized not only in neuronal and muscle nuclei but also both pre- and postsynaptically at NMJs. It has been shown to regulate local proteasome-mediated protein degradation at synapses and the mutation in the *morula* gene (one of its components) causes an overgrown NMJ phenotype (van Roessel et al., 2004). In neurons APC/C might ubiquitinate Liprin-α thus constraining the number of boutons, and in muscles it upregulates the levels of postsynaptic glutamate receptor DGluRIIA, potentially through Liprin-α independent mechanisms. GluR *C. elegans*, glutamate receptor GLR-1 is ubiquitinated and mutations that disrupt ubiquitination cause accumulation of GLR-1 (Burbea et al., 2002). The same might be true for DGluRIIA. Since *wah* is expressed both pre and post-synaptically and has a comparable phenotype to APC/C, *wah* may be involved in the APC/C pathway to regulate synapse growth. Potential accumulation of Liprin-α in *wah* mutant NMJs would be a good candidate to check presynaptically.

Postsynaptically, potential accumulation of GluRIIA at *wah* mutant NMJs could be checked. Interestingly, as discussed above in the context of eIF4AIII (Chapter 4.3.2), DGluRIIA accumulation has been shown to cause enlarged terminals in *Drosophila* larvae (Chen et al., 2005; Sigrist et al., 2002).

Taken together, my results demonstrate that *wah* is not simply acting downstream of *hiw* to regulate synaptic growth. This does not exclude an involvement in this pathway, but it appears more likely that Wah is involved in regulating further ubiquitinated proteins than the Hiw target Medea, potentially affecting various ubiquitin-regulated pathways in parallel, as has been suggested from the wing disc experiments. This interpretation is further supported by my observation that proteasome knock-down causes a *wah*-like mutant phenotype and for the proteasome one would not expect selective interference with ubiquitin-mediated degradation. In this scenario, affected pathways with opposite phenotypes at the NMJ might cancel each other out, which might explain the milder NMJ phenotype compared to *hiw* mutant NMJs and perhaps also the dorsoventral gradient of the *wah* mutant NMJ phenotype. As has become clear from the above discussion, a number of potential target molecules can now be tested, including Medea, Spinster, Liprin-α and DGluRIIA.

## 5. SUMMARY

The establishment of appropriate synapses between neurons and their target cells is an essential requirement for the formation of functional neuronal circuits. However, there is very little insight into the mechanisms underlying *de novo* formation of synapses and synaptic terminals. To identify novel genes involved in signalling or structural aspects of these processes I capitalised on possibilities provided by the model organism *Drosophila*. Thus, I contributed to a screen of a collection of third chromosomal mutations (Salzberg et al., 1997, Genetics 147, 1723ff.) selecting those mutant strains displaying structural defects of *Drosophila* neuromuscular junctions (NMJ). Carrying out genetic mapping experiments, I could assign 7 genes to interesting candidate mutations.

All 7 mutations selected in this process cause size alterations of the embryonic NMJ, and one shows additional disturbances in the distribution of synaptic markers. 4 of these turned out to be transcription factors, not falling into the remit of this project. Only for one of these, the neuronal transcription factor Castor, I could show that its overgrown mutant NMJ phenotype is due to an increase in the number of motorneurons. The remaining genes encode a potential nitrophenylphosphatase, the translation initiation factor eIF4AIII, and a novel protein Waharan.

Unfortunately, the nitophenylphosphatase gene was identified too late to carry out functional studies in the context of this project, but potential roles are discussed. eIF4AIII promotes NMJ size tempting to speculate that local translation at the NMJ is affected. I found that the synaptic scaffolding molecule Discs large (Dlg; orthologue of PSD95) is upregulated at *eIF4AIII* mutant NMJs. Targeted upregulation of Dlg can not mimic the *eIF4AIII* mutant phenotype, but *dlg* mutations suppress it. Therefore, Dlg function is required but not sufficient in this context. My findings are discussed in detail, pointing out future directions.

The main focus of this work is the completely novel gene *waharan* (*wah*), an orthologue of the human gene *KIAA1267* encoding a big brain protein of likewise unknown structure and function. My studies show that mutations or RNAi knock-down of *wah* cause NMJ overgrowth and reveal additional crucial roles in the patterning of wing imginal discs. RNAi studies suggest Wah to be required pre- and postsynaptically at NMJs and, consistently, *wah* is transcribed in the nervous system and muscles. Anti-Wah antisera were produced but could no longer be tested here, but preliminary studies with newly generated HA-targeted constructs suggest that Wah localises at NMJs and in neuronal nuclei. *In silico* analyses predict Wah to be structurally related to the Rad23-family of proteins, likely to target ubiquitinated proteins to the proteasome for degradation (Chen et al., 2002, Mol Cell Biol 22, 4902ff.) . In agreement with this prediction, poly-ubiquitinated proteins were found to accumulate in the absence of *wah* function, and *wah*-like mutant phenotypes were induced in NMJs and wing discs by knocking down proteasome function. My analysis further revealed that poly-ubiquitinated proteins are reduced in nuclei of *wah* mutant neurons and muscles, suggesting that Wah may play additional roles in ubiquitin-mediated nuclear import.

Taken together, this study has uncovered a number of interesting candidate genes required for the *de novo* formation of *Drosophila* NMJs. 3 of these genes fell into the focus of this project. As discussed in detail, discovery of these genes and insights gained into their function have high potential to be translatable into vertebrate systems.

# 6. APPENDIX I

## 6.1 Different strategies to generate probes for *in situ* hybridisation analyses of *wah*

The simplest way to perform *in situ* hybridisation is to use labelled DNA probes, as these probes are usually sensitive enough and easy to work with as compared to RNA probes. Therefore, I started my investigations with DNA whole mount *in situ* hybridisation. To this end, we chose the longest exon 8 to create an about 925bp long DNA probe. Using the cDNA clone *LP09056* (Chapter 3.5.5) as template in combination with the primers P1 and P2 (Appendix 7.9), a Digoxigenin-labelled DNA probe was synthesized via PCR and confirmed by gel electrophoresis (based on overall length). Unfortunately, no positive stainings were obtained via whole mount *in situ* hybridisations using this probe (Materials and Methods 2.2.18). Therefore, I tried RNA *in situ* hybridisation instead, which tends to be more sensitive (Lehmann and Tautz, 1994). Thus, RNA-RNA hybrids are more stable than RNA-DNA hybrids so that elevated hybridisation temperatures can be employed, usually resulting in higher specificity and less background.

To perform the RNA *in situ* hybridisation, I sub-cloned the same PCR product (925bp) into the TOPO-vector to synthesise RNA probe. The TOPO-vector was digested with Not1 restriction enzyme to linearise the DNA, and SP6 RNA polymerase was used for *in vitro* transcription to generate a Digoxigenin-labelled RNA probe (Materials and Methods. 2.2.19). The probe was successfully transcribed and confirmed by obtaining positive signal on the dot blot. Again, the *in situ* hybridisation was performed but did not work. I speculated that either the probe degraded or that the size of the probe (925bp) was too small. To synthesise a longer probe, the same 4.249kb long cDNA clone *LP09056* (inserted in POT2 vector) covering two thirds of the C-terminal portion of the *wah* gene (FIG. 13) was used as template. After digesting it with Bgl1 at 824bp to linearise the template DNA, I synthesised an about 3440bp long Digoxignin-labelled probe by *in vitro* transcription using T7 RNA polymerase. This new probe covers 2262bp of the coding sequence, 253 bp of intron (5-6) and 925bp of the 3' UTR). A positive control probe

(clone name 13B20, kindly provided by B. Altenhein) was synthesised in parallel. The two probes were run on a RNA gel delivering a very weak signal for the control and even weaker signal for the experimental probe. *In situ* hybridisation was performed using this Digoxigenin-labelled probe. Using the conventional 65°C annealing temperature did not work for the *wah* probe, though it worked fine for the control. I therefore tested 50°C and 45°C as alternative annealing temperatures and got a satisfactory signal for the *wah* and control probe at 45°C (Chapter. 3.5.3.).

# Cloning of p{UAST}-wah

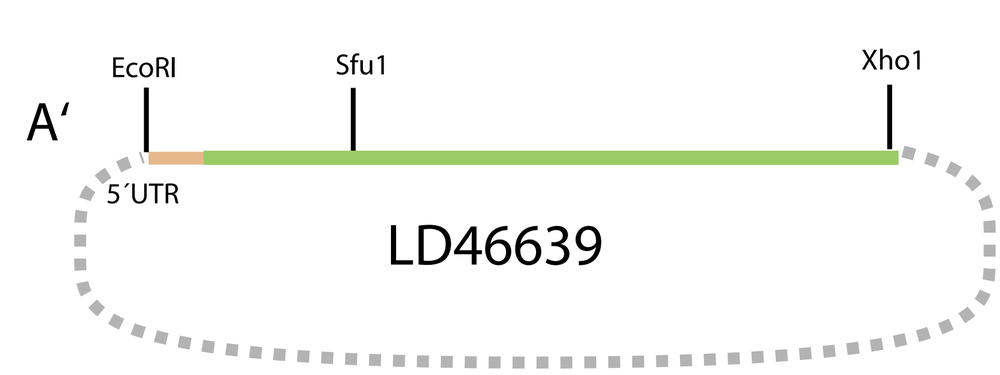


Sfu1, Xho1 digested, dephos-phorylated and gel extracted

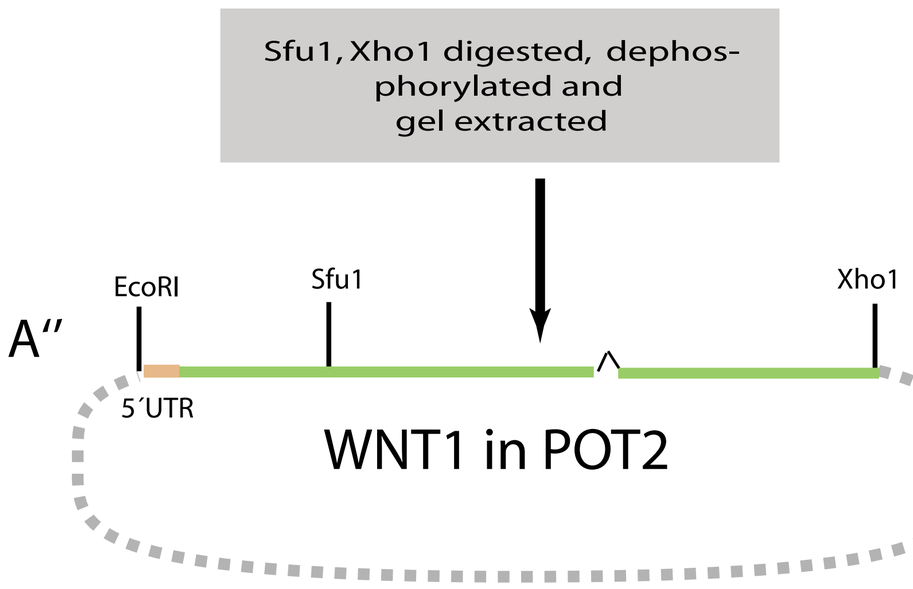


EcoR1, Xho1 digested and gel extracted



Sfu1, Xho1 digested and gel extracted


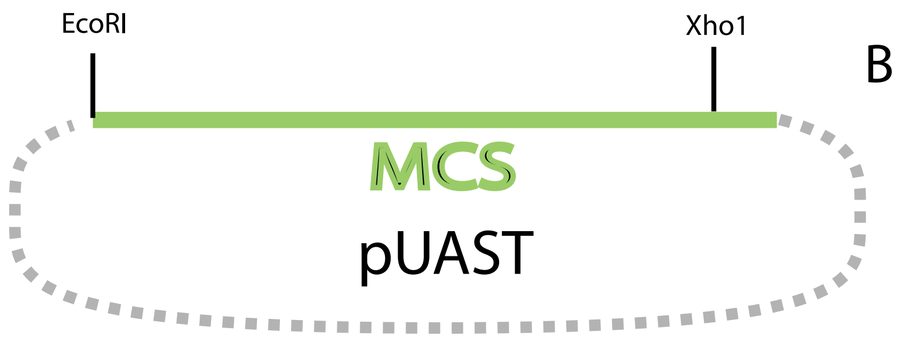


EcoR1,Xho1 digested and de-phosphorylated




PCR amplified Xho1, Xho1digested C-terminal feag-ment

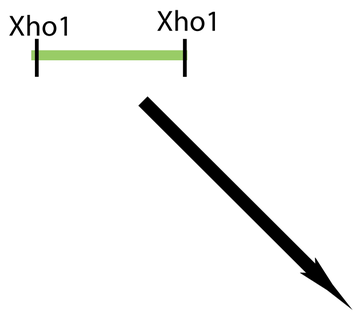


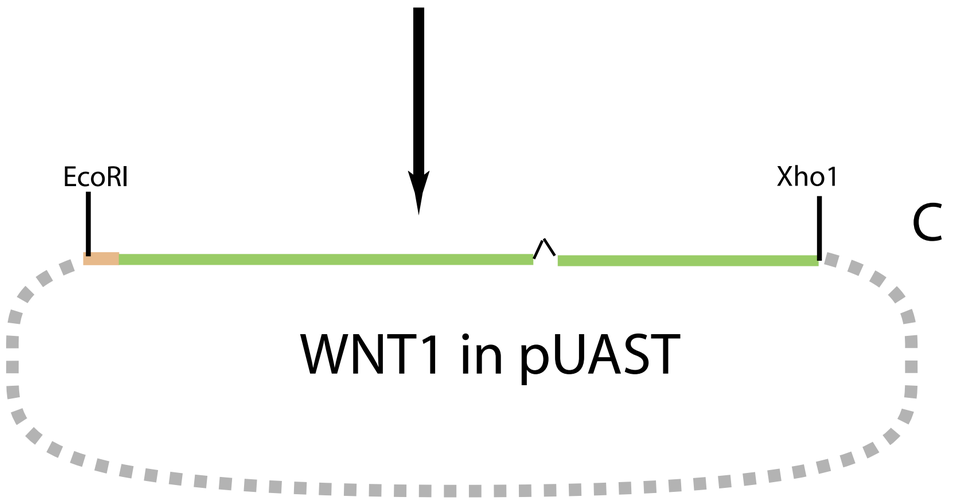


Xho1digested, dephosphory-lated

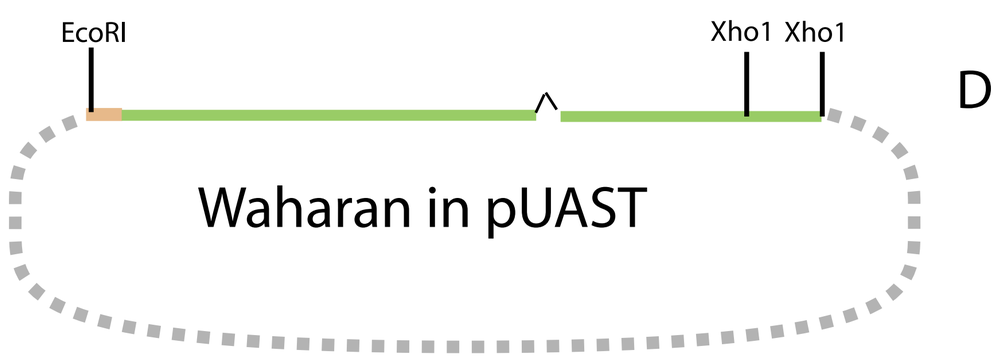

**Fig. 6.1 Summary of wah cloning.**

**Wah gene into pUAST was cloned using two cDNA clones *LD46639* and *LP09056* (Chapter 3.5.5) with partial overlapping sequences. *LD46639* covers 1 to 3843bp, it has got 10bps of intron 5-6. and *LP09056* covers the region from 1639 to the end of the gene with 3'UTR. *LP09056* has got intron 5-6 and a premature stop codon. It was decided to keep full intron 5-6 in to final construct.**

**For cloning, LP09056 was cut with Sfu1, Xho1 enzymes (A), and this fragment (1714-3843bp) with intron 5-6, was used to replace the portion of *LD46639* to get the intermediate construct (WNT1 in POT2) (A'') . The gene product in the vector was excised and cloned into pUAST (WNT1 in pUAST) using EcoR1, Xho1 restriction enzymes (C). Rest of 3'region (3843-4710) was PCR amplified from cDNA clone LP09056 (A''') using a modified sense primer to remove the premature stop codon at position (3859bp). This fragment was introduced in to rest of the construct using Xho1 restriction sites to get the final construct (D) (wah in pUAST).**

## 6.2 Cloning of non-tagged construct in to the expression vector pUAST

As mentioned above, all the cDNA clones sequenced have some kind of flaw in or around the intron 5-6 (FIG. 3.13, Table 3.7). Keeping this in mind, I decided to clone full length cDNA including the intron 5-6 into the pUAST vector. Even if this intron is not coded for, we expect the fly to splice it out.

To generate this construct, I used two cDNA clones, *LD46639* and *LP09056*. The 4.07kb cDNA clone *LD46639* covers a portion of the 5'UTR (253bp) and goes up to 3843bp of the annotated gene sequence. This has got none of the introns, except 10bps of the beginning of intron 5-6. The 4.246kb cNDA clone *LP09056*, lacks the N-terminal 1639 bps, this cDNA contains complete intron of about 253bp. This cDNA also has a premature stop codon (TAG) at 3859bp. These two ESTs (*LD46639* and *LP09056*) containing an overlapping sequence were used to generate 1-3838 bp of a full length wild-type cDNA. The rest of the gene sequence (3838-4710) was PCR-amplified from *LP09056* using a modified sense primer to eliminate the stop codon present in the clone at 3859bp and then subcloned into the pUAST vector (FIG. 6.1).

*LP09056* was cut out of POT2 vector with Sfu1 (1714bp) and Xho1 (3838bp) and the fragment (2382bp, including intron 5-6) was gel extracted and ligated into pre-digested (Sfu1 and Xho1), de-phosphorylated and gel extracted *LD46639* in POT2 vector. The successful ligation was judged by PCR screening of single colonies, using primers sense1659bp (S5) and asense2264bp (S6). Positive colonies were cultured overnight and, on the next morning, the DNA was extracted and sequenced from one of the colonies to confirm its correctness around the insertion sites using primers sense1401bp (S22), and sense 3600bp (S19). The obtained DNA (an 4330bp insert in vector POT2; WNT1 in POT2) was excised by digesting with EcoR1 and Xho1, gel extracted and sub-cloned into EcoR1-Xho1 digested, de-phosphorylated pUAST vector. Again the successful ligation was judged by PCR screening of single colonies, using Sense3600bp (S19) and 3' pUAST primers (3’pUAST). Positive colonies were cultured overnight and DNA representing the intermediate construct (WNT1 in pUAST) from one of the colonies was isolated and sequenced using primers 5'pUAST (5’pUAST) and 3'pUAST (3’pUAST) to make sure the

sequences around the insertion site are correct. Meanwhile the C-terminal 870bp fragment was PCR amplified from template *LP09056* using modified sense primer (senseXho1; inserts a Xho1 restriction site and eliminates the stop codon at 3859bp) and anti-sense primer (AsenseXho1; inserting a Xho1 restriction site and a stop codon). The introduced Xho1 restriction sites were used to insert this fragment into the rest of the construct in pUAST (Xho1 digested and de-phosphorylated) . Again, positive ligation was judged by PCR screening of single colonies using Sense3600bp (S19) and Asense4400bp (S20) primers. Positive colonies were cultured overnight and DNA was isolated and sequenced using primers sense3600bp (S19), asense 4400bp (S20) and sense 4250bp (S21) The final construct (wah in pUAST) was injected and transgenic fly lines were generated through the service of Bestgene[20]

[20] http://www.thebestgene.com/

# Cloning of p{UAST}-HA-wah

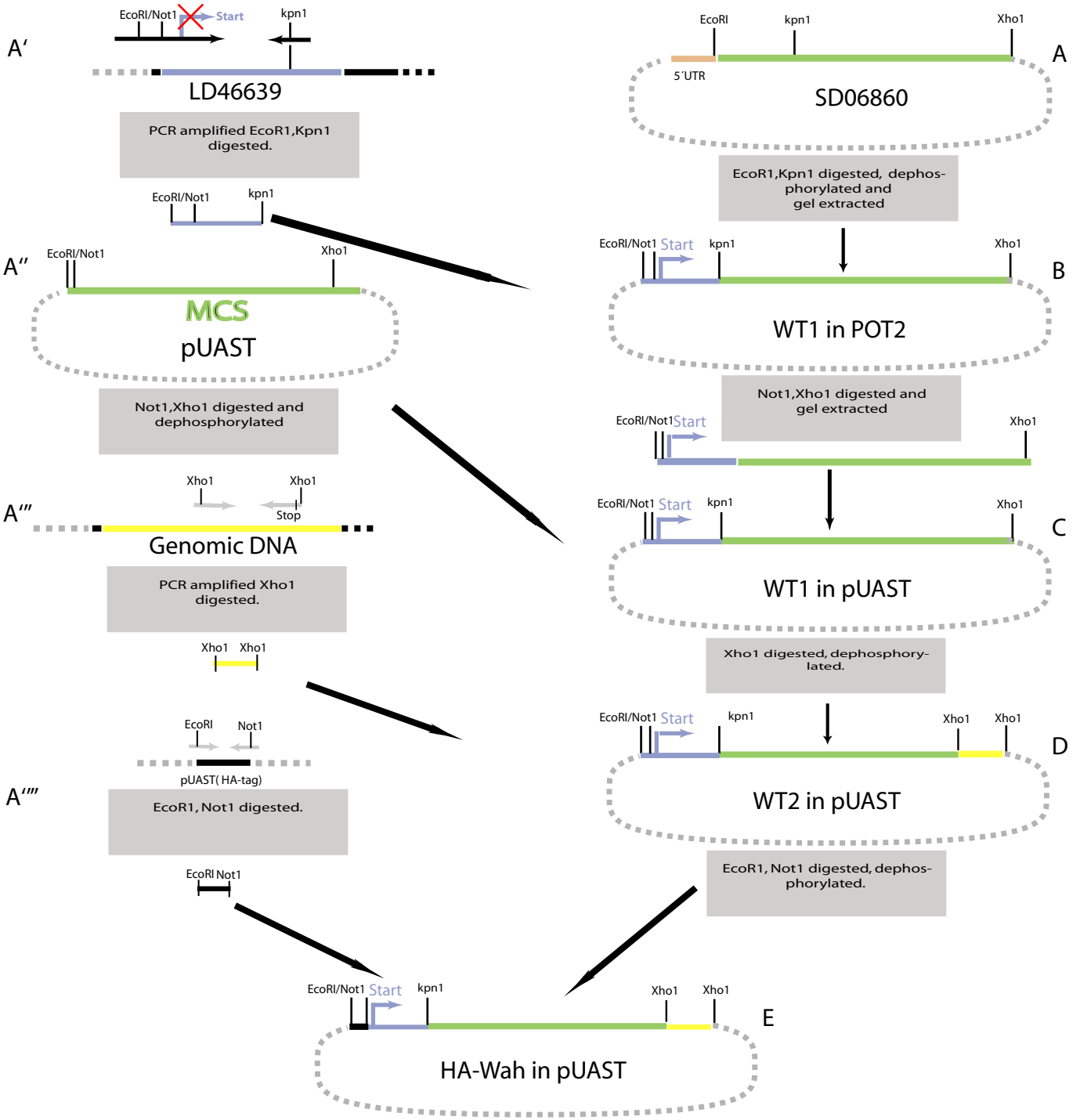

**Fig. 6.2 Summary of HA-tag wah cloning.**

**HA-wah ( with all the introns) was cloned from cDNA clone *SD06860* which covers 5' 3843bp of the(4710bp) gene, rest of the 3' portion (1030bps)was synthesised from genomic DNA. The introns are not shown in the graphs. (A) *SD06860* has also got a portion of the 5'UTR. To remove the 5' UTR portion in order to introduce HA-tag just before the initiation start site, 748bp fragment was synthesized from LD46639 using EcoR1, Kpn1 restriction sites. (A') and was used to replace the part of *SD06860* (B), to get an intermediate product (WT1 in POT2). (C) The gene product in the vector was excised and cloned into pUAST (WT1 in pUAST) using Not1, Xho1 restriction enzymes. (A''') C-terminal 1030bp portion was PCR amplified from genomic DNA and introduced into rest of the construct in pUAST using Xho1 restriction sites to get (WT2 in pUAST) (D). Finally the HA-tag was synthesised from another construct (EB1aff-2HA in pUAST) (A'''') and introduced in the 5'end of the construct using EcoR1, Not1 restriction enzymes to get the final construct (E) HA-was in pUAST**

## 6.3 Cloning of HA-tagged construct in to expression vector pUAST

Whereas the non-tagged *wah* construct lacks all but one intron, HA-wah contains all the introns to allow maximal post-transcriptional regulation. Tagging at the C-terminus has the advantage that a successful detection of the tag via antibody stainings indicates that the full length gene gets expressed. However, in case of the *wah* gene, we have some indications that the gene might have splice variants, because all the annotated cDNA clones have irregularities around intron 5-6, most alarmingly, *AT07776* terminates with a polyA tail inside the intron, and *LP09056* has a premature stop codon at 3859bp. Interestingly, when this portion was PCR amplified using wild type genomic DNA template, we found the stop codon in the genomic DNA as well. However, to confirm our findings, when a different source of wild-type DNA was used as template, the stop-codon was not there. Due to the unpredictable C-terminus the HA-tag was added at the N-terminus. Furthermore, this tag would allow me to distinguish potential isoforms created via alternative splicing in Western blot analyses. We used HA-tag, due to good experiences with it at synapses and the existence of excellent commercial anti-HA antibodies.

To generate a full length HA-tagged construct (FIG. 6.2), I used the cDNA clone *SD06860*, containing all the introns (FIG. 3.13, Table 3.7). *SD06860* covers most of the N-terminal part of *wah*, including a portion of the 5'UTR and goes upto 3843bps. First, an N-terminal fragment was synthesised from template *LD46639.* In order to remove the part of 5'UTR present in the clone SD06860 and start with the first codon ATG, so that tag will be then put just upstream and in-frame with the coding sequence. I used modified sense primer with restriction sites EcoR1-Not1 (C1; Not1 restriction used in the primer will be used in subsequent steps of cloning) and anti-sense primer kpn1 (C2; inserting a kpn1 restriction site). The successful ligation was judged PCR screening of single colonies using primers sense 527bp (S1) and asense1081bp (S2). To generate the construct, *SD06860* was cut out of POT2 with EcoR1 and Kpn1, de-phosphorylated and gel extracted and the N-terminal part was replaced by the EcoR1-Kpn1 digested and cleaned 748bp fragment generated in the first step, resulting in the first intermediate construct (WT1 in POT2). Positive colonies were cultured overnight and DNA

representing the intermediate WT1 construct was isolated from one the colonies and sequenced to make sure the sequences are correct in and around the insertion sites using primers T7 of POT2 (**T7 primer**), and sense527bp (S1). The full insert of about 5054bp of the WT1 construct (in POT2) was then excised with Not1 and Xho1, gel extracted and sub-cloned in to Not1-Xho1 digested, de-phosphorylated pUAST vector. Again, the successful ligation was judged by single colony screening PCR, using Sense 3600bp (S19) and 3' pUAST (**3'pUAST**) primers. Positive colonies were cultured overnight DNA isolated and sequenced from one of the colonies using primers 5'pUAST (**5'pUAST**) and 3'pUAST (**3'pUAST**) to make sure the sequences around the insertion site are correct. This DNA represents the intermediate construct WT1 in pUAST. Meanwhile the C-terminal 870bp fragment was PCR amplified from genomic DNA using modified sense primer senseXho1 (C3) and asenseXho1 (C4) both inserting Xho1 restriction sites. AsenseXho1 has in addition a stop codon, just after the last codon of the gene before the Xho1 site. The insertion sites were introduced in order to make it possible to insert this fragment into the WT1 construct in pUAST. This fragment was then Xho1-digested and ligated to Xho1-digested, de-phosphorylated pUAST vector containing WT1. Again, the positive ligation was judged by PCR screening of single colonies using Sense (3600bp) and Asense (4400) primers. Positive colonies were cultured, DNA isolated and sequenced using primers sense3600bp (S19), asense 4400bp (S20) and sense4250bp (S21). This DNA represents the intermediate construct (WT2 in pUAST). To introduce the N-terminal tag, HA-tag was synthesized from another HA-tag construct in the lab using senseEcoR1-tag (**C5**) and asenseNot1-tag (**C6**) primers. The construct was digested with EcoR1 and Not1, dephosphorylated and this fragment was ligated into the construct after digesting it with EcoR1 and Not1, to get the final HA-tagged construct (*HA-wah* in pUAST). Again, the successful ligation was judged by PCR screening of single colonies using primers 5'pUAST (**5'pUAST**) and asense Not1-tag (C6). DNA was isolated from overnight cultures and sequenced to confirm the final construct. The final *HA-wah* construct in pUAST was sent to TheBestGene for the generation of transgenic flies.

## 6.4 Domain prediction for wah

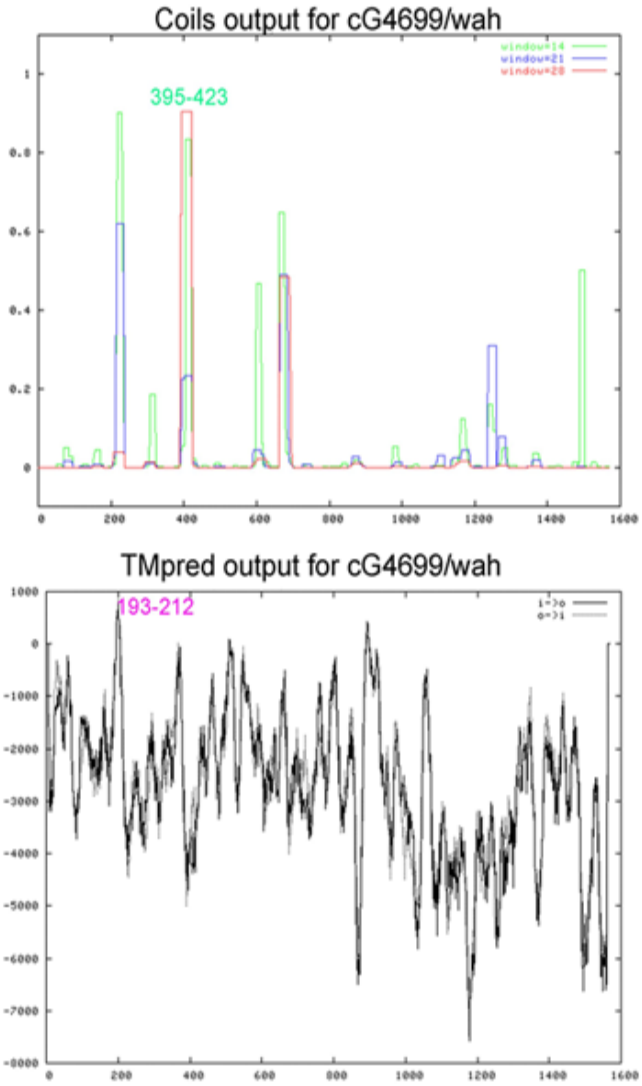


**Fig. 6.3 Domain prediction for wah.**

**Coiled-coiled programme predicts one coiled-coil domain for wah protein. The region of protein (395-423a.acids) as highlighted by green colour is predicted to be a coiled-coil domain. 3D-PSSM (Chapter 3.5.1) also gives same prediction.**

**TMpred programme predicts a transmembrane domain in the region (193-212 a.acids) highlighted by magenta, though this is not predicted by SMART**

## 6.5 Molecular mapping data for the selected mutants.

**Mutant line: 0010/12** (5')
GCCCCAACCAACAAAGACTCCACTCCACATCCCATGCCTACATATGTATGTATGTACATCCACAGCTACATCCAATGTTGCTGACTCGA
CTCACCGCATACATACAGACGCTCCGTTCGTATATATGTAAAAACATGTACAAGCGAACGAGCCGAACGACCGACACACGAAGTACAGT
CGCACAGTTAAAAATAAAGTATGGGCCGCTGCAACGCAGAGGGGTAAAGGGAGATGACACGAGAGAGAAGGAAGGCAAAGAGAAGAAGA
AGAGAGCGAGCGAGGGCAAAACAACAAAGCGAATGCTGGTAAATAATGATGATGGAACCAGTGTGCTGTATATGTATGTAGGCATGTGT
TCGTATGCGTGTGTGTGTATACTGCACAGTAAAATTTCATGTATTAAAATCGCTTGTTCGTGTATATGCACTGTACAGGGTAAGAGCTG
CCATCGCTGNGCTGTTGATAGCGAGGGACGTAATATCGCAACTTTTGCCGNTCCAAAAGCACGGAGCCAAGCGAACGTTCGTTCGTCGT
TCGCTGGTCGTTCGAGTTTAATTTTGNAGGTACGTANCANGAAAAAAANGAAACGACGAAAAAATAAATGATGGCGGNAACAACAACGA
CNACAACNGCGA

>gadfly|SEG:AE003712|gb|AE003712|Drosophila melanogaster genomic scaffold
142000013386035 section 37 of 105, complete sequence.|AE003712.1
GI:7300108
Length = 226,200
Query: 37 GCATGGGATGTGGAGTGGAGTCTTTGTTGGTTGGGGC 1
||||||||||||||||||||||||||||||||||||
Sbjct: 134443 GCATGGGATGTGGAGTGGAGTCTTTGTTGGTTGGGGC 134479

**0010/12** (3')
Flanking:
GACTG
From P element:
CCGATCCGTCGAGCGTATAACCATCTGTACAAAAAAGGATTTCCTTTGCCCAGTCGTACGACTTTGTACAGATGGTTATCAGATGTGGA
CATAAAAAGAGGATGTTTGGATGTGGTCATAGACCTAATGGACAGTGATGGAGTTGATGACGCCGCCA

**Mutant Line: 0066/40** (3')
CACTTGGGCATGGATTTGCGCAATTTTTGCTATATTAGCCGGAGGCCGCGGAAGAGTTGAAGCAGTTTGAGCCTCGCAGCCGAACTTTG
AG

```
>gadfly|SEG:AE003602|gb|AE003602|Drosophila melanogaster genomic scaffold
            142000013386043 section 3 of 8, complete sequence.|AE003602.1
            GI:7296683
            Length = 297,266
Query:     1 CACTTGGGCATGGATTTGCGCAATTTTTGCTATATTAGCCGGAGGCCGCGGAAGAGTTGA 60
             ||||||||||||||||||||||||||||||||||||||||||||||||||||||||||||
Sbjct: 21591 CACTTGGGCATGGATTTGCGCAATTTTTGCTATATTAGCCGGAGGCCGCGGAAGAGTTGA 21650

>gb|L04487|DROCASTR Fruitfly castor mRNA sequence.
            Length = 3676
Query:     1 CACTTGGGCATGGATTTGCGCAATTTTTGCTATATTAGCCGGAGGCCGCGGAAGAGTTGA 60
             ||||||||||||||||||||||||||||||||||||||||||||||||||||||||||||
Sbjct:   437 CACTTGGGCATGGATTTGCGCAATTTTTGCTATATTAGCCGGAGGCCGCGGAAGAGTTGA 496
Query:    61 AGCAGTTTGAGCCTCGCAGCCGAACTTTGAG 91
             |||||||||||||||||||||||||||||||
Sbjct:   497 AGCAGTTTGAGCCTCGCAGCCGAACTTTGAG 527
>CG2102|FBgn0004878|CT6850|FBan0002102 last_updated:000321
            Length = 3679
Query:     1 CACTTGGGCATGGATTTGCGCAATTTTTGCTATATTAGCCGGAGGCCGCGGAAGAGTTGA 60
             ||||||||||||||||||||||||||||||||||||||||||||||||||||||||||||
Sbjct:   438 CACTTGGGCATGGATTTGCGCAATTTTTGCTATATTAGCCGGAGGCCGCGGAAGAGTTGA 497
Query:    61 AGCAGTTTGAGCCTCGCAGCCGAACTTTGAG 91
             |||||||||||||||||||||||||||||||
Sbjct:   498 AGCAGTTTGAGCCTCGCAGCCGAACTTTGAG 528
```

**Mutant Line: 0094/13** Sau3A1 iPCR

GTCTAAGCGATGAAANAANTAAANGAGGAAAANAGTCCGNGAAGCGAAAACCGTAGTTCCTACAGTGCGAGTNGCGCCATTGTGTTTGC
AAAAAATATTNGCCAATTGTGCTACGGGCAATTTTTCGGAACGGCCGAATTGTGCGTATAATGAAAAAAAATACTACTTAATTTTTAAG
CAATTTACAAATTCTTGCGTGCTGCCTGCCTGCTGTCGGTGTGTTCTTGCTTGCATGTGTTAGTGAGTACGATTACTTTCGCGCTGAAA
ACCTTTTTCCACTGCCCTTTCGCTGGAATCTGGGCGAATATAGATAGGACACANAGCACATATAACTGATTTTTACTGCAGAATTGATC
G

>gadfly|SEG:AE003710|gb|AE003710|arm:3R [11413871,11638809]
estimated-cyto:89A2-89A11 gadfly-seqname:AE003710.2
Length = 224,939

Plus Strand HSPs:

Score = 1655 (254.4 bits), Expect = 6.0e-68, P = 6.0e-68
Identities = 339/357 (94%), Positives = 339/357 (94%), Strand = Plus / Plus

```
Query:      1 GTCTAAGCGATGAAANAANTAAANGAGGAAAANAGTCCGNGAAGCGAAAACCGTAGTTCC 60
              ||||||||||||||| || |||| |||||||| |||||| |||||||||||||| ||||
Sbjct: 139101 GTCTAAGCGATGAAAAAAATAAATGAGGAAAAAAGTCCGTGAAGCGAAAACCGTAATTCC 139160

Query:     61 TACAGTGCGAGTNGCGCCATTGTGTTTGCAAAAAATATTNGCCAATTGTGCTACGGGCAA 120
              ||||||||||||  |||||||||||||||||||||||| ||||||||||||||||||||
Sbjct: 139161 TACAGTGCGAGTCACGCCATTGTGTTTGCAAAAAATATTTGCCAATTGTGCTACGGGCAA 139220

Query:    121 TTTTTCGGAACGGCCGAATTGTGCGTATAATGNNNNNNNNTACTACTTAATTTTTAAGCA 180
              ||||||||||||||||||||||||||||||||         ||||||||||||||||||||
Sbjct: 139221 TTTTTCGGAACGGCCGAATTGTGCGTATAATGAAAAAAAATACTACTTAATTTTTAAGCA 139280

Query:    181 ATTTACAAATTCTTGCGTGCTGCCTGCCTGCTGTCGGTGTGTTCTTGCTTGCATGTGTTA 240
              ||||||||||||||||||||||||||||||||||||||||||||||||||||||||||||
Sbjct: 139281 ATTTACAAATTCTTGCGTGCTGCCTGCCTGCTGTCGGTGTGTTCTTGCTTGCATGTGTTA 139340

Query:    241 GTGAGTACGATTACTTTCGCGCTGAAAACCTTTTTCCACTGCCCTTTCGCTGGAATCTGG 300
              ||||||||||||||||||||||||||||||||||||||||||||||||||||||||||||
Sbjct: 139341 GTGAGTACGATTACTTTCGCGCTGAAAACCTTTTTCCACTGCCCTTTCGCTGGAATCTGG 139400

Query:    301 GCGAATATAGATAGGACACANAGCACATATAACTGATTTTTACTGCAGAATTGATCG 357
              ||||||||||||||||||| ||||||||||||||||||||||||||||||||||||
Sbjct: 139401 GCGAATATAGATAGGACACAAAGCACATATAACTGATTTTTACTGCAGAATTGATCG 139457
```

**Mutant Line: 0151/12** (band 1, 5')
GTTTNTACTTTANNGTCCGACAGGTTTTCGGGGNCTGGANTANGANGGNNAAGANGGCGCCNGAAGCGATAGAGAACCNNACGAGCTAC
TGAAACTCGAGGATTAAAATNGCCAACTGGATCTCTTCNCNNTGTAAACGATCAATANAGGANANNNTGCANCAGGACATGCTGGTGAT
GGTNCGGGGTCAACAGATGGCGCCNGCAAAACGAN

```
>gadfly|SEG:AE003747|gb|AE003747|Drosophila melanogaster genomic scaffold
           142000013386035 section 72 of 105, complete sequence.|AE003747.1
           GI:7301134
           Length = 204,469
Query:   202 GGC-GCCATCTG-TTGACCCCGNACCATCACCAGCATGTCCTGNTGCANNNTNTCCTNTA 145
             ||| | || ||  |||||| |   |||| ||||||||||||||  ||||   | |||  ||
Sbjct: 83670 GGCTGTCAACTCCTTGACCACTC-CCATGACCAGCATGTCCTCCTGCAGCGTGTCC-ATA 83727
Query:   144 TTGATCGTTTACANNGNGAAGAGATCCAGTTGGCNATTTTAATCCTCGAGTTTCAGTAGC 85
             |||| ||||| |   | ||||   |||||||||| |||||  |||||| ||||| |||||
Sbjct: 83728 TTGAGCGTTTCCGCGGAGAAGGCCTCCAGTTGGCCATTTTGTTCCTCG-GTTTC-GTAGC 83785
Query:    84 TCGTNNGGTTCTCTATCGCTTCNGGCGCCNTCTTNNCCNTCNTANTCCAGNCCCCGAAAA 25
             ||    |||||||| |  |||  |||||| ||||  || || |   | || | |||||||
Sbjct: 83786 TCAGAAGGTTCTCTTTTACTTTCGGCGCCTTCTTCACCTTCTTCTGCGAGGCACCGAAAA 83845
Query:    24 CCTGTCGGACNNTAAAGTA 6
             ||||| ||||   ||||||
Sbjct: 83846 CCTGTGGGACAGAAAAGTA 83864

>CG5728|FBgn0039182|CT18011|FBan0005728 last_updated:000321
           Length = 4542
Query:    24 GTTTTCGGGGNCTGGANTANGANGGNNAAGANGGCGCCNGAAGCGATAGAGAACCNNACG 83
             |||||||| | || |   | || ||  |||| ||||||  |||  | ||||||||    |
Sbjct:   150 GTTTTCGGTGCCTCGCAGAAGAAGGTGAAGAAGGCGCCGAAAGTAAAAGAGAACCTTCTG 209
Query:    84 AGCTACTGAAACTCGAGGATTAAAATNGCCAACTGGATCTCTTCNCNNTGTAAACGATCA 143
             |||||| ||||| ||||||  ||||| |||||||||    |||| |   | ||||| |||
Sbjct:   210 AGCTAC-GAAAC-CGAGGAACAAAATGGCCAACTGGAGGCCTTCTCCGCGGAAACGCTCA 267
```

**0151/02** (band 2, 5')
GTNCNTACTTNNNTGGCNNACAGGNTTTCGGGGNCTGGNNTANNANGGTNNNGANGGCGCCNGAAGNAATAGAGAACCTTNCGAGCTAC
TGAAACTCGAGNCATCAAATTGNCCAACTGNAGGTCTTCTCNNTGTAATCGATCAATATAGGANANTCTTGTAGCTAGGACATGCTTGG
TGATTGGTNGGCGGTCAANGATGGCNCAGCAANACGANTGGAGANCGCANGAGCTANCTNCACAGTGNNTCNNNGNGGNCNNNGGGGGT
ANTACNCCAGGNGGNNAAA

**0151/12** (3')
GNNNAGGCNATTNGGATTCGGATCCGTNGAGCGTNTAACCATNTGTACANAAAAGGATTNCCTTTGCCCAGTCGTACGACTTTGTACAG
ATGGNTATNANATGNGGACATAAAAAGAGGATGTTTGGATGAGGTCATAGACCTAATGGACAGTGATGGAGNTGATGACGCCGACAA
BLAST - P element

**Mutant Line: 0242/41 – 2 PCR bands**

**1, 0242/41 5'iPCR - Msp1 top band**

GCNGNACATNCNTNCCCCNAGCCCACACATCGNTGGNGATGAGCNCTNGCNACTGGCCGG
AAACCACGNNANGCGCCNTTCNCCATTCNNGCTGCNCAACTGNNGNGANGGGCNANCGNTGCGGGNCTNTTCNCTATTACGCCAGCTGG
CGAANGGGGGATGCGCTGCANGGCGANTANGGTGGGTNNCGCCNNGNGTTNCCCNNNCNCNACNNTGTNAAACNACGGNCAGCGCCAAG
CTCTGCTGNTNTAANCGACGCATTTCGCCTCCAAAGGGCNNNTTCNNTCCCTCAAGCTCTTATTTTCATTAAACAATGAACAGGACCTA
ACGCACAG

| Sequences producing High-scoring Segment Pairs: | | High Score | Sum Probability P(N) | N |
|---|---|---|---|---|
| gb\|X01803\|ATPG418 | Transposable P vector conferring G41... | 549 | 1.6e-18 | 1 |
| gb\|X06590\|DMKP | Drosophila KP element DNA (P factor ... | 373 | 8.0e-11 | 1 |
| gb\|AF377341\|AF377341 | Drosophila melanogaster transposon P... | 373 | 1.2e-10 | 1 |
| emb\|X06779\|PPI251 | Complete sequence of transformation ... | 373 | 1.4e-10 | 1 |
| l(3)neo8 | AQ026353 inserted at base 122 5' end... | 364 | 2.3e-10 | 1 |
| BACN02D09-SP6 | (STS) made from BACN02D09 | 290 | 4.6e-07 | 1 |

(NGCNGNACATNCNTNCCCCNAGCCCACACATCGNTGGNGATGAGCNCTNGCNACTGGCCGG - highlighted in sequence above; BLAST alignment below shows complementary strand)

- The insertion is inserted in the 3’ region of CG7483 – EIF4AIII
- It is also close to (in?) the 3’ end of CG9613 (polyprenyltransferase)
- It’s also upstream of a 3’ EST, GM14810. The rest of the cDNA clone doesn’t appear to have been mapped, but could potentially lie to the right of the 242-41 insertion.

**BLASTN On 28/11/01:**

```
>gadfly|SEG:AE003678|gb|AE003678|arm:3R [4010676,4244813]
           Length = 234,138

  Minus Strand HSPs:

 Score = 214 (38.2 bits), Expect = 0.0069, P = 0.0069
 Identities = 48/60 (80%), Positives = 48/60 (80%), Strand = Minus / Plus

Query:     60 CCGGCCAGTNGCNAGNGCTCATCNCCANCGATGTGTGGGCTNGGGGNANGNATGTNCNGCN 1
              ||||||||| || || ||||||| ||| |||||||||||||| |||| |   |||| | ||
Sbjct: 114863 CCGGCCAGTCGCGAGTGCTCATCACCACCGATGTGTGGGCTCGGGGTATCGATGTACAGC 114922
```

The rest may be P sequence from the recircularised iPCR product.

**Insertion site is 114916-114923 of AE003678.**
AE003678 lies at 4024906-4269662 of the 3R scaffold, at 84F11 (coordinates on 28 Sept 2004)
Therefore the insertion site lies at 4139821-4139828 of the 3R scaffold.

**2, 0242/41 5' iPCR - Msp1 bottom band**

GGTGGGATATACCGGAAACCAGGCAAAGCGCCATTCGCCATTCAGGCTGCGCAACTGTTGGGAAGGGCGATCGGTGCGGGCCTCTTCGC
TATTACGCCAGCTGGCGAAAGGGGGATGTTGCAAGGCGATTAAGTTGGGTAACGCCAGGGTTTTCCCAGTCACGACGTTGTAAAACGAC
GGCCAGTGCCAAGCTCTGCTGCTCTAAACGACGCATTTCGTACTCCAAAGTACGAATTTTTTCCCTCAAGCTCTTATTTTCATTAAACA
ATGAACAGGACCTAACGCACAGTAGC

| | | | | | |
|---|---|---|---|---|---|
| gb\|X01803\|ATPG418 | Transposable P vector conferring G41... | 838 | 1.3e-31 | 1 |
| gb\|X06590\|DMKP | Drosophila KP element DNA (P factor ... | 485 | 4.4e-16 | 1 |

(query GGTGGGATATACCGG - highlighted in SeqEd file; the rest may be P sequence from recircularised iPCR product)

**Pattern search results: Show sequence containing pattern**
AF187998 Drosophila melanogaster malic enzyme (Men) mRNA, complete cds. CDS:217..2508.

283-298

AGGCGGTTCGGAGTTGCTAAGTCAAGCGCAATAGCTCAAAATACACTTTT
TTTAATTTTTGTTAATAACTGTTTTTAATAATTCCGGTGAAACATCGCGT
GGTCAAGCGAACTGAGTTAATTTTCGCGTTAGAAAAGTTCACAAGTTTTG
CGTTTACCAAATAATTAACTATAACTATTTAACTGGAGCTAATTTAACTG
AAATTTAGAACCCAAAATGGGTAATTCCAGTTCCATTTGCGCCGATCGCA
ATGTCATAACAAATTTCGATGAAAATGGCACGCCGGTATATCCCACCGCC
AACAATTCGCAGAGTCCTTCCTCATATAGTCGCGGCAAAGAGCGCGAGCT
CGGCTGTTACACGAAGAGAAACAGCAACAGCAACAACAACAATAGCCATG
AGAGAGAGAGTCAGAGCTGTTGTAGTAGTCGTGTGTGTAAAAATCATACG

**Mutant Line: 0287-07** *[CG5484]*, 97C3. GH16644.5prime AI386534
GGTGATGTNTTAAAAAGCGAAATTTTGAATACAATTTACT

```
>CG5484|FBgn0039450|CT17398|FBan0005484 last_updated:000321
           Length = 1480
Query:     1 GGTGATGTNTTAAAAAGCGAAATTTTGAATACAATTTACT 40
             |||||||| ||||||||||||||||||||||||||||||||
Sbjct:    29 GGTGATGTGTTAAAAAGCGAAATTTTGAATACAATTTACT 68

>gadfly|SEG:AE003757|gb|AE003757|Drosophila melanogaster genomic scaffold
           142000013386035 section 82 of 105, complete sequence.|AE003757.1
           GI:7301475
           Length = 191,851
Query:      1 GGTGATGTNTTAAAAAGCGAAATTTTGAATACAATTTACT 40
              |||||||| ||||||||||||||||||||||||||||||||
Sbjct: 121714 GGTGATGTGTTAAAAAGCGAAATTTTGAATACAATTTACT 121753
```

**Mutant Line: 1107/02** (higher band 1), CG5567 (enzyme)75A4, gadfly|SEG:AE003522,
GTCGNTAGCCTGCTNTCCACTCGGTCACCTTGGCGGAGGATAATTCCAGGAGATTGGTGCACGACTGCTTGTACATGTTGATAGCTGCC
TGTCGCGAAAATCTGGCGAAGTTACAACTCATCTATGGCTTTGCAGCGACGACTATCTTATACACATCACTTTTAATTTATTAATTGAC
TCTCGATTGCGAGAAACTCCCTGAGAATTAAAGCAGCTGTTGGCGCCTGTTAAGGCTATGTTACTATCTGTCAGATTTCAGCGTAGCTG
TTAATGCGCCATGTTAAAGTCAACAGAGTGCTAACAAGTGTTTGGCGCCAAATTTGAATTTAAGGGCTCCTTGGAAGCAGAACTTCTGT
GCAACAAATGCTTATATTCGAAAAATGAACTAAGCTCCCCAAACTATTGTAAACACACACTTT

```
>gadfly|SEG:AE003522|gb|AE003522|Drosophila melanogaster genomic scaffold
            142000013386050 section 9 of 54, complete sequence.|AE003522.1
            GI:7293918
            Length = 290,837
Query:     59 CACCAATCTCCTGGAATTATCCTCCGCCAAGGTGACCGAGTGGANAGCAGGCTANCGAC 1
              ||||||||||||||||||||||||||||||||||||||||||  ||||||||  ||||
Sbjct: 225143 CACCAATCTCCTGGAATTATCCTCCGCCAAGGTGACCGAGTGGCTAGCAGGCT-TCGAC 225200

>CG5567|FBgn0036760|CT17604|FBan0005567 last_updated:000321
            Length = 1231
Query:    67 CAGTCGTGCACCAATCTCCTGGAATTATCCTCCGCCAAGGTGACCGAGTGGANAGCAGGCTANCGAC 1
             ||||||||||||||||||||||||||||||||||||||||||||||||||  ||||||||  ||||
Sbjct:   121 CAGTCGTGCACCAATCTCCTGGAATTATCCTCCGCCAAGGTGACCGAGTGGCTAGCAGGCT-TCGAC
```

**1107/02** (lower band 2) CG14184, 76E4, gadfly|SEG:AE003515
GACCCGGTGAACCATAGTCCTGCCCTTCGACGGAGCAACTCCGATGGCCTCAGCACCGACTACGCCCACTCCCTTCCCAAGAAGGAC

```
>gadfly|SEG:AE003515|gb|AE003515|Drosophila melanogaster genomic scaffold
            142000013386050 section 2 of 54, complete sequence.|AE003515.1
            GI:7293706
            Length = 273,521
Query:     1 GACCCGGTGAACCATAGTCCTGCCCTTCGACGGAGCAACTCCGATGGCCTCAGCACCGAC 60
             ||||||||||||||||||||||||||||||||||||||||||||||||||||||||||||
Sbjct: 22791 GACCCGGTGAACCATAGTCCTGCCCTTCGACGGAGCAACTCCGATGGCCTCAGCACCGAC 22850

>CG14184|FBgn0036932|CT33793|FBan0014184 last_updated:000321
            Length = 543
Query:     1 GACCCGGTGAACCATAGTCCTGCCCTTCGACGGAGCAACTCCGATGGCCTCAGCACCGAC 60
             ||||||||||||||||||||||||||||||||||||||||||||||||||||||||||||
Sbjct:   118 GACCCGGTGAACCATAGTCCTGCCCTTCGACGGAGCAACTCCGATGGCCTCAGCACCGAC 177
```

**Mutant Line**: **1227/10** Msp1.Seq
NTTTNNAGGCACACTGCACTGAATTTAAGTGTATACTTCGGTAAGCTTCGGCTATCGACGGGACCACCTTATGT**TATTTCATCATG**
TTCTGAACGCTGCGCCGCAGTTTTTGCCGATTTGTTAAAAGAAAAGCAAGCGTTTCGTGTCTGACATGCTGAAAATGGCAATGGCAAAT
GGTGCAAATCCGCTGCAAACAATGAAGAAAGCAAACGGCGACGAGGAGTCCGATGAGTCCGATATGGAAGAAGAGGAGGAGGATGAGGA
AGACGAGGAGGAGGACGATCNGNNCGNNNCNANGCGNNNTTNCNNNAGCNNNTNAAGGNGGGNTNCNGTNGAGAGNGNCNAANGNGGCN
NNCCTCNNGGCTATTACANCNNCTANNGNNTGGNNNANNTGCNGNAGNNNNACTNNGTTGNNCTANNCCANGNNTTTCCNACTCCNNAN
GTCGAAATTNNACCNTCAAGCTCNNATTTTGTNNATCTAATNAACAGGACCTANCTNCAANNNNCNAANNNTTTCCTNAAGCTNTTATT
NNNATTAANCANTGANCAGGACCTACGNNNNNNNNNNNNNNNNNNNNNNNNNNNNNNNNNNNNNNNNNNNNNNNNNNNNNNNNNNNN
NNNNNNNNNNNNNNNNNNNNNNNNNNNNNNNNNNNNN

>gadfly|SEG:AE003530|gb|AE003530|arm:3L [15387945,15667019]
estimated-cyto:71C4-71F3 gadfly-seqname:AE003530.2
Length = 279,075

Plus Strand HSPs:

Score = 990 (154.6 bits), Expect = 6.5e-38, P = 6.5e-38
Identities = 198/198 (100%), Positives = 198/198 (100%), Strand = Plus / Plus

```
Query:      1 TTCTGAACGCTGCGCCGCAGTTTTTGCCGATTTGTTAAAAGAAAAGCAAGCGTTTCGTGT 60
              ||||||||||||||||||||||||||||||||||||||||||||||||||||||||||||
Sbjct: 130685 TTCTGAACGCTGCGCCGCAGTTTTTGCCGATTTGTTAAAAGAAAAGCAAGCGTTTCGTGT 130744

Query:     61 CTGACATGCTGAAAATGGCAATGGCAAATGGTGCAAATCCGCTGCAAACAATGAAGAAAG 120
              ||||||||||||||||||||||||||||||||||||||||||||||||||||||||||||
Sbjct: 130745 CTGACATGCTGAAAATGGCAATGGCAAATGGTGCAAATCCGCTGCAAACAATGAAGAAAG 130804

Query:    121 CAAACGGCGACGAGGAGTCCGATGAGTCCGATATGGAAGAAGAGGAGGAGGATGAGGAAG 180
              ||||||||||||||||||||||||||||||||||||||||||||||||||||||||||||
Sbjct: 130805 CAAACGGCGACGAGGAGTCCGATGAGTCCGATATGGAAGAAGAGGAGGAGGATGAGGAAG 130864

Query:    181 ACGAGGAGGAGGACGATC 198
              ||||||||||||||||||
Sbjct: 130865 ACGAGGAGGAGGACGATC 130882
```

**1227/10** Sau3A1.Seq
P element
AGGCAAACTTGCACTGAATTAAGTGTATACTTCGGTAAGCTTCGGCTATCGACGGGACCACCTTATGTTATTTCATCATG
**Flanking**

***GCCGAAACGANACAGGAAGACCGACCGG***

More P element
AAACCAGGCAAAGCGCCATTCGCCATTCAGGCTGCGCAACTGTTGGGAAGGGCGATCGGTGCGGGCCTCTTCGCTATTACGCCAGCTGG
CGAAAGGGGGATGTGCTGCAAGGCGATTAAGTTGGGTAACGCCAGGGTTTTCCCAGTCACGACGTTGTAAAACGACGGCCAGTGCCAAG
CTCTGCTGCTCTAAACGACGCATTTCGTACTCCAAAGTACGAATTTTTTCCCTCAAGCTCTTATTTTCATTAAACAATGAACAGGACCT
AACGCCNNGNANNNNNNNNNNNNNNNNNNNNNNNNNNNNNNN

>gi|55380551|gb|AE003694.4| Drosophila melanogaster chromosome 3R, section 32 of 118 of
the
complete sequence
Length=226075

Features flanking this part of subject sequence:
2157 bp at 5' side: CG3132-PA
2872 bp at 3' side: CG3571-PB, isoform B

Score = 42.1 bits (21), Expect = 0.001
Identities = 26/28 (92%), Gaps = 0/28 (0%)
Strand=Plus/Plus

```
Query  1      GCCGAAACGANACAGGAAGACCGACCGG  28
              |||||||||| |||||||| ||||||||
Sbjct  27689  GCCGAAACGAAACAGGAAGCCCGACCGG  27716
```

# 7. APPENDIX II

## 7.1 Chemicals

If not stated differently, chemicals used in the course of this work were purchased from Roth, Karlsruhe, Germany. Chemicals not mentioned elsewhere are: Acetone (VWR, Darmstadt, Germany), Acid-washed glass beads (425-600µm; Sigma, Osterode, Germany), Agarose (GENterprise, Mainz, Germany), Glycerol (50% and 70% in autoclaved PBS or H2O; Sigma, Osterode, Germany), nail polish, Vectashield Mounting Medium H-1000 (Vectashield, Vector Laboratories, Burlingame, USA). Protease inhibitor cocktail (Amersham Pharmacia biotech). Tryptone, yeast extract and agar bacteriological were from OXOID Ltd. (Hampshire, UK). Acrylamide/Bisacrylamide was from National Diagonastics (UK). Imidazole and Sodium phosphate were from USB corporation (USA)

## 7.2 Kit-systems

GenElute Plasmid **Midiprep** Kit (Sigma, Osterode, Germany)
QIAquick **Gel extraction** Kit (Qiagen, Hilden, Germany)
QIAprep Spin **mini prep** Kit (Qiagen, Hilden, Germany)
**TOPO TA Cloning** Kit (Invitrogen, Carlsbad, USA)
TripleMaster **PCR** System (Eppendorf, Hamburg, Germany)

## 7.3 Enzymes and buffers

### *7.3.1 Restriction Enzymes*

Restriction Enzymes: Restriction Enzyme Buffer
BamH1 (Roche Biochemicals)
BglII (MBI Fermentas, St. Leon-Rot, Germany) Y+Tango buffer
EcoRI (MBI Fermentas) EcoRI or 2x Y+Tango buffer
EcoRV (MBI Fermentas) R+Tango buffer
Kpn1 (Roche Biochemicals)
Not1 (Roche Biochemicals)
Sfu1 (Roche Biochemicals)
XhoI (MBI Fermentas) O+Tango or 2x Y+Tango buffer

### *7.3.2 Other Enzymes*

PCRs were run with TripleMaster Enzyme Mix containing 5U/µl *Taq* **Polymerase** (Eppendorf,
Hamburg, Germany). Buffer used was 10x High Fidelity Buffer with Mg2+ (Eppendorf, Hamburg,
Germany)
1mg/ml RNase (Boehringer, Ingelheim, Germany) was used to prevent contamination of the
DNA plasmid preparations with RNAs

## 7.4 Equipment

Accurate scale Mettler PM4600 Delta Range (Mettler Instruments, Giessen, Germany)
Agarose Gel Unit Hoefer HE33 (VWR, Darmstadt, Germany)
CCD video camera Sony 3 CCD colour (Olympus, Hamburg, Germany)
Centrifuge Eppendorf 5417R (Eppendorf, Hamburg, Germany)
Centrifuge Eppendorf 5410 (Eppendorf, Hamburg, Germany)
Centrifuge Sigma 3K20 (Sigma, Osterode, Germany)
Camera Zeiss AxioCam (Zeiss, Jena, Germany)
Confocal Microscope Leica TCS (Leica, Bensheim, Germany)
Dissecting Microscope Leica MZ FLIII (Leica, Bensheim, Germany)
Dissecting Microscope Olympus SZX-ZB12 (Olympus, Hamburg, Germany)
EasyjecT Prima Electroporator (peqlab, Erlangen, Germany)
Heat plate and stirrer MB 3001 (Heidolph, Germany)
Incubator WTB Binder (VWR, Darmstadt, Germany)
Light Source ebq100 (LFS Leistungselektronik, Jena, Germany)
Light Source Olympus U-RFL-T-200 (Olympus, Hamburg, Germany)
Light Source Zeiss KL1500LCD (Schott, Mainz, Germany)
Microscope Zeiss Axiophot (Zeiss, Jena, Germany)
Microscope Olympus BX50WI (Olympus, Hamburg, Germany)
Monitor Monacor B+W video monitor (Intermercador GmbH+co, Bremen, Germany)
Phillips Digital Quartz Tuner (Saturn, Mainz, Germany)
pH-meter CG840 (Schott, Mainz, Germany)
Photometer Eppendorf Biophotometer RS232C (Eppendorf, Hamburg, Germany)
Power supply Biometra Power Pack P25 (Biotron, Göttingen, Germany)
Power supply Gene GPS200/400 (Pharmacia, Sweden)
Printer DPU-414 Seico Thermal printer (Eppendorf, Hamburg, Germany)
Printer Mitsubishi p91 video copy processor (VWR, Darmstadt, Germany)
Puller P-97 Sutter micropipette puller (Science Product GmbH, Hofheim, Germany)
Pump ILMVAC LVS301 (Ilmvac, Ilmenau, Germany)
Semidry-blotter Biometra Fast-Blot B34 (Biotron, Göttingen, Germany)
Shaker GFL3015 (Gesellschaft für Labortechnik, Burgwedel, Germany)
Shaker IKA VIBRAX-VXR (IKA-Werk, Staufen, Germany)
Speedvac Savant (Thermo Life Sciences, Egelsbach, Germany)
Sterile banch Steril-VBH (Mahl Labortechnik, Kaarst. Germany)
Thermoblock Biometra TB1 (Biotron, Göttingen, Germany)
Thermocycler Biometra T-Gradient (Biotron, Göttingen, Germany)
Transilluminator MS Laborgeräte (Benda, Wiesloch, Germany)
Vortex Vibrofix VF1 Janke + Kunkel (IKA-Werk, Staufen, Germany)
Waterbath Certomat WR (Braun Biotech, Melsungen, Germany)
Waterbath GFL1002 (Gesellschaft für Labortechnik, Burgwedel, Germany)
Macintosh Powermac G-4 (Apple)
PC

## 7.5 Buffers, Solutions and Media

***A&B phosphate Buffer*:**

Solution A: 28.39g Na2HPO4 in 1L H2O
Solution B: 27.6g NaH2PO4 in 1L H2O
A mixture of 36ml solution A and 14 ml solution B is filled up to 100ml with H2O. The resulting buffer is set to pH 7.2

***Alkaline phosphatase (AP) detection buffer*:** 10ml 5M NaCl, 25ml 1M MgCl2, 50ml 1M Tris (pH9.5), 0.5ml Tween20, 412ml H2O, pH set to 9.5

***Anode buffer I*:** 0.3 M Tris, 10% methanol, pH 10.4

***Anode Buffer II*:** 25mM Tris, 10% methanol, pH10.4

***Apple-agar* :** 27-28g of agar are dissolved in 1L commercially available apple juice. Mixture is poured into petridishes, which are stored upside down at 4°C

***Binding buffer (8X)*** 40mM Imidazole, 4M Nacl, 160mM Tris, pH 7.9

***Broadie and Bate buffer*:** 135mM NaCl, 5mM KCl, 4mM MgCl2, 0.5mM CaCl2, 5mM TES – N-tris[Hydroxymethyl]methyl-2-aminoethansulfonic acid, 36mM sucrose, pH is set with NaOH to 7.15

***5-Bromo-4-chloro-3-indolyl phosphate (BCIP)*:** solution for AP-staining (Chapter 2.1.8.3.): 50mg/ml BCIP in 100% N,N-Dimethylformamide

***Cathode buffer*:** 25mM Tris base, 40mM 6-amino-n-caproic acid, 10% methanol, pH 9.4

***Charge buffer (8X):*** 400mM Nickel sulphate

***Coomassie staining solution*:** 0.25% (w/v) Comassie brilliant blue, 7.5% (v/v) Acetic acid, 50% (v/v) Methanol, 42.2% (v/v) water.

***Coomassie destaining solution*:** 45% (v/v) Methanol, 50% (v/v) water, 5% (v/v) Acetic acid.

***DAB-Solution*:** 10mg 3,3'-Diaminobenzidine Tetrahydrochloride are dissolved in 30ml PBT and subsequently aliquoted in volumes of 1ml and stored at -20°C.

***Elute Buffer (4X):*** 4M imidazole, 2M NaCl, 80mM Tris-HCl, pH 7.9

***LB agar:*** 0.17M NaCl, 1.0% (w/v) Tryptone, 0.5% (w/v) Yeast extract, 2.0% (w/v) Agar

***LB Broth*:** 0.17M NaCl, 0.8% (w/v)Tryptone, 1.0% (w/v) Yeast extract

***LB agar and ampicillin plates*:** add 15g/L agar to freshly prepared LB broth (see below), autoclave and cool to 50°C, add ampicillin to 100µg/ml, pour plates and store at 4°C

***LB agar and chloramphenicol plates:*** add 15g/L agar to freshly prepared LB broth, autoclave and cool down to 50°C, add chloramphenicol 30µg/ml. pour plates and store at 4°C.

***Lysis buffer*** for DNA Miniplasmid preparation: 4.3ml ddH2O, 0.5ml 10% SDS, 0.2ml 5N NaOH. Make fresh before any usage with sterile solutions.

***MOPS buffer:*** 23.1gMOPS, 3.4g sod.acetate, 0.93g EDTA in 500ml, pH 7.0

***Nitro-blue-tetrazolium (NBT*):** 50mg/ml NBT in 70% N,NDimethylformamide

***Neutralisation buffer*** for DNA Miniplasmid preparation: 4.3ml ddH2O, 0.5ml 10% SDS, 0.2ml 5N NaOH.

***PBS with Tween detergent (PBT)*:** 0.3% Tween-20 in PBS

***Phenol-Chloroform-Isoamyl alcohol*:** Phenol, chloroform and isoamyl alcohol are added together in a ratio of 25:24:1 (v/v)

***Phosphate-buffered saline (PBS)*:** 137mM NaCl, 2.7mM KCl, 4.3mM Na2HPO4 .7H2O, 1.4mM KH2PO4, pH 7.3; autoclaved

***SDS-PAGE resolving gel (15% w/v)*:** 15% (v/v) Acrylamide/bisacrylamide, 0.375M Tris-HCl pH 8.8, 0.1% (w/v) SDS, 0.05% (w/v) Ammonium sulphate, 0.05% (v/v) TEMED.

***SDS-PAGE stacking gel (15% w/v)*:** 4% (v/v) Acrylamide/bisacrylamide, 0.125M Tris-HCl pH 6.8, 0.1% (w/v) SDS, 0.05% (w/v) Ammonium sulphate, 0.1% (v/v) TEMED.

***SDS-PAGE running buffer (5X):*** 125mM Tris, 0.96M Glysine, 0.5%SDS pH 8.3

***SDS-PAGE sample buffer (5X):*** 15% Glycerol, 2.0% SDS, 0.001% Bromophenol blue, 62.5mM Tris, 100mM Mercapto ethanol (for reducing buffer) pH 6.8

***Strip Buffer (4x):*** 400mM EDTA, 2M NaCl, 80mM Tris-HCl pH 7.9

***Resuspension buffer for DNA Miniplasmid preparation***: 50mM Glucose, 10mM EDTA (pH8.0), 25mM Tris (pH 8.0), autoclaved, stored at 4°C

***Tris-Acetate buffer (50x)*:** 2M Tris Base, 1M Glacial acetic acid, 0.5M EDTA pH8.0

***Tris-EDTA (TE)-buffer*** (pH 7.4): 10mM Tris-HCL (pH 7.4), 1mM EDTA (pH 8.0)

***Tris buffered saline (TBS)*:** 37.5ml 2M Tris-HCl (pH9.5), 2.9g NaCl, 25ml 1M MgCl2 in a total volume of 500ml

***Wash Buffer (8x):*** 480mM Imidazole, 4M NaCl, 160mM Tris-HCl pH 7.9

***X-Gal (5-bromo-4-chloro-3-indolyl-b-D-galactopyranoside)* stock solution**: X-Gal was dissolved in N,N-Dimethylformamide at a concentration of 20mg/ml and stored in the dark at -20°C

***Z-buffer/X-Gal solution*:** 100ml Z-buffer, 0.27ml b-mercaptoethanol, 1.67ml X-Gal stock solution

## 7.6 Fixative Solutions

***4% paraform aldehyde***: 4% paraform aldehyde is dissolved in A&B
phosphate buffer. The solution was stored at -20°C. Before using, the solution is thawed at room temperature.

***Bouin's fixative solution*** *(Featherstone et al., 2002)*: 7.5ml saturated picrinic acid, 2.5ml formaldehyde (37%), 0.5ml glacial acetic acid.

## 7.7 Dissection Tools

### *7.7.1 Sharpened tungsten wires*

Tungsten needles (0.005x3 inch, TW5-3, Science Products, Hofheim, Germany) were sharpened at one end and used to cut open the embryos. One terminal of a MTR27 power supply (Leitz, Wetzlar, Germany) was connected to a carbon electrode and the other terminal to the tungsten needle. The needle was sharpened by dipping it repeatedly in a KOH/NaNO2 solution (34g/71g in 100 ml of dH2O) until the end gets sharp.

### *7.7.2 Sylgard*

Dissections of stage 17 embryos and third instar larvae (Chapter 2.1.5.) were carried out on Sylgard coated coverslips and petridishes, respectively. Sylgard was produced by mixing 7 volumes of Sylgard 184 silicone elastomer base with 3 volume Sylgard 184 curing agent (both from Dow Corning, Wiesbaden, Germany). After thorough mixing at room temperature for about 20 minutes the Sylgard was stored at -20°C. After casting the sylgard over coverslips and petridishes, they were kept at 68°C overnight for polymerization.

### *7.7.3 Dissection glass needles*

Dissection glass needles were produced using Vitrex capillary tubes (0.780-1-00x80mm, GB100T8P, Science Products, Hofheim, Germany) and a P-97 micropipette horizontal puller (Sutter Instruments, Science Products, Hofheim, Germany). Parameters???

*Forceps* Dumont INOX Nr.5 (neolab, Heidelberg, Germany)

*Microscissors* 15004-08 (Fine Science Tools GmbH, Heidelberg, Germany)

## 7.8 Vectors

pGEX-4T1 vector.
http://www.addgene.org/pgvec1?f=d&cmd=genvecmap&vectorid=5108&format=html&mtime=1143219887

pOT2 vector.
http://www.fruitfly.org/about/methods/pOT2vector.html

pUAST.
http://www.gurdon.cam.ac.uk/~brandlab/reagents/pUAST.html

TOPO vector.
http://ymbc.ym.edu.tw/est/pcriitopo_map.pdfv

pHis vector.

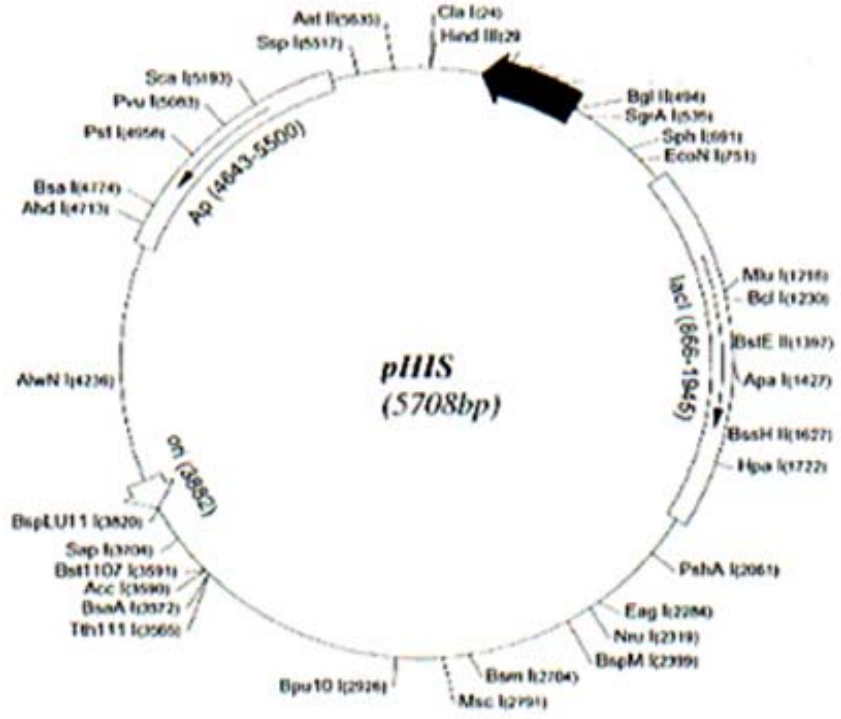


pHis consists of 6 His coding sequence downstream of promoter site, internal lac Iq gene and Thrombin cleavage site for cleaving the desired protein off the tag . Multiple cloning site with Bst B1, BamH1, EcoRI, Sma1, Sal1, Xho1, NotI, Eag1 and Aat1 restriction sites

followed by stop codon in all three frames. This vector is used for efficient expression and rapid purification of proteins.

## 7.9 Oligonucleotides

| **Sequencing primers(**number refers to the No. of bp of mature wah cDNA**)** |
|---|
| S1, **Sense1_527bp**<br>AAAACCCTACCCGATGTGAGTCTGG |
| S2, **Asense1_1081bp**<br>CCGGCACATCCACCACATTT |
| S3, **Sense2_1057bp**<br>CCCGAAAATGTGGTGGATGTG |
| S4, **Asense2_1686bp**<br>TGCCTGTCTAGATGTTACCGCTCCT |
| S5, **Sence3_1659bp**<br>GCCAGGAGCGGTAACATCTAGACA |
| S6, **Asense3_2264bp**<br>TTAATGTTGCTGGGGCGTGC |
| S7, **Sense4_2235bp**<br>CAAGAAAGCCGCACGCCCCA |
| S8, **Asense4_2834bp**<br>GTTGGGTGTTGTGGTTGCCG |
| S9, **Sense5_2811bp**<br>CAAGCGGCAACCACAACACC |
| S10, **Asense5_3439bp**<br>TGTGCTTGACTGCTTGATTTTCCTT |
| S11, **Sense6_3413bp**<br>TAAAGGAAAATCAAGCAGTCAAGC |
| S12, **Asense6_3870bp**<br>AAGGAAAGTCTCGAAGCGGC |
| S13, **Sense7_2120bp**<br>ATGGCATTAAGGAGGAGCCCGG |
| S14, **Asense7_2551bp**<br>CTGCCACCTTGTCCGCCGAC |
| S15, **Sense8_2658bp**<br>TAAAGCTGCTGCTGTCG |
| S16, Asense8_2947bp<br>CTGTTGGTTGCGGATTTGCG |
| S17, **Sense9_3250bp**<br>GATAACGATAAGGGAAAACA |
| S18, **Asense9_3580bp**<br>AAGTTTCCGTTGAGCTTGGG |
| S19, **Sense_3600bp**<br>ATAAAGAATCCGATTGA |
| S20, **Asense_4400bp**<br>CCATTGAGCTGGCCAT |
| S21, **Sense_4250bp**<br>CAGGTCAATGACCGTC |
| S22**, Sense-Seq_1401bp**<br>GCGTCCGAGCTCAACCTT |

| |
|---|
| S23**, Sense-seq_2001b**<br>CGATTTGGAGATGAAGAT |
| S24**, Sense-seq_2651b**<br>GCGGAGCTAAAGCTGCTG |
| **Wah Cloning Primers:** |
| C1, **Sense_EcoR1_Not1**<br>TAATATA GAATTC GCGGCCGC ATGGCCCCAGCGCTCACAGC<br>--EcoR1-- ----Not1---- |
| C2**, Asense_Kpn1**<br>CCTGCACG GGTACC GGAACA<br>--Kpn1-- |
| C3**, Sense_Xho1**<br>AGCTCTT CTCGAG GAGCGACGCCGCTTCGAGACTTTCCTTAAGTTC<br>--Xho1-- |
| C4, **Asense_Xho1**<br>TAATATA CTCGAG TTA GATGCGTCTGCTGCGAA<br>--Xho1-- stop |
| C5**, Sense_EcoR1 tag**<br>TCGCGGG GAATTC CACCGACGGAGAAGCATGGGC<br>-EcoR1- |
| C6, **Asense_Not1 tag**<br>TAATATA GCGGCCGC TATAGTTCTAGAGGCTCGAGAGGCCTTGA<br>----Not1---- |
| **General sequencing primers:** |
| 1**, T7 primer**<br>AATACGACTCACTATAGG |
| 2**, PM001**<br>CGTTAGAACGCGGCTACAAT |
| 3**, 5'pUAST**<br>AACTACTGAAATCTGCCAAG |
| 4**, 3'pUAST**<br>GTCACACCACAGAAGTAAGG |
| **Primers for generating fusion products:** |
| **Primers for GST-fusion products:** |
| F1**, Sense_EcoR1 (N-terminal)**<br>ATTCTAAGAATTCATGGCCCCAGCGCTCACAGC |
| F2**, Asense Xho1 (N-terminal)**<br>ACGGTCCACTCGAGGGTACTGTTGCTGTCGTTAT |
| F3**, Sense EcoR1 (C-terminal)**<br>ATTCTAAGAATTCAAGGATCAGCTGGAACGGCG |
| F4**, Asense Xho1 (C-terminal)**<br>CATAATACTCGAGGATGCGTCTGCTGCGAACAC |
| F5**, Sense EcoR1 (Middle)**<br>ATTCTAAGAATTCCAACCACAACACCCAACTGG |
| F6**, Asense Xho1 (middle)**<br>CGTCCGACTCGAGATTATTGTTATTGTGCTTGA |
| F7**, Asense Xho1 (960bp)**<br>CGGTCCACTCGAGTGTTTTGAGCGCTTTAAGCA |

| |
|---|
| F8**, Asense Xho1 (1305bp)**<br>ACGGTCCACTCGAGCATGATACCAACCACCTCC |
| **Primers for HIS-tag fusion products:** |
| F9**, Sense BamH1 (c.coil)**<br>CTATTCGGATCCGAGCAGCGGCCCTGG |
| F10**, Asense EcoR1 (c.coil)**<br>CTCGTCGAATTCTTATTATGGAGCCTTATGGG |
| F11**, Asense EcoR1 (c.coil+UBA)**<br>CTCGTCGAATTCTTATTACGGCAGCGCAGAGCTG |
| F12**, Sense BamH1 (Rad23)**<br>CTATTCGGATCCAGCAACAGTACCTCCGCC |
| F13**, Asense EcoR1 (Rad23)**<br>CTCGTCGAATTCTTATTACAGCGCAGAGCTGTTGC |
| **Cloning primers for insitu-hybridisation:** |
| P1**, Sense_3241bp**<br>GTGGCGCATTGTAGACAG |
| P2**, Asense_4155bp**<br>CTCCCGCAGATCGGGCGT |

## 7.10 DNA/protein markers and quantifying standards

λDNA HindIII digest DNA marker (MBI Fermentas)
DNA Molecular weight Marker II, 0.12-23.1 kbp (Roche)
.0
.0-
DNA Molecular weight Marker XVI, 250bp ladder (Roche)
GeneRulerTM 100 bp Ladder Plus DNA marker (MBI Fermentas)
HyperLadder IV, 100bp Quantitative DNA ladder (Bioline).
Low Molecular Weight Calibration Kit for SDS-electrophoresis (Amersham Biosciences)
High Molecular Weight Calibration Kit for SDS-electrophoresis (Amersham Biosciences)

# 8. REFERENCES

**Aberle, H., Haghighi, A. P., Fetter, R. D., McCabe, B. D., Magalhaes, T. R. and Goodman, C. S.** (2002). wishful thinking encodes a BMP type II receptor that regulates synaptic growth in Drosophila. *Neuron* **33**, 545-58.

**Adams, M. D. Celniker, S. E. Holt, R. A. Evans, C. A. Gocayne, J. D. Amanatides, P. G. Scherer, S. E. Li, P. W. Hoskins, R. A. Galle, R. F. et al.** (2000). The genome sequence of *Drosophila melanogaster*. *Science* **287**, 2185-95.

**Ahmad, K. and Golic, K. G.** (1998). The transmission of fragmented chromosomes in Drosophila melanogaster. *Genetics* **148**, 775-92.

**Albright, T. D., Jessell, T. M., Kandel, E. R. and Posner, M. I.** (2000). Neural science: a century of progress and the mysteries that remain. *Cell* **100 Suppl**, S1-55.

**Anderson, K. V., Jurgens, G. and Nusslein-Volhard, C.** (1985). Establishment of dorsal-ventral polarity in the Drosophila embryo: genetic studies on the role of the Toll gene product. *Cell* **42**, 779-89.

**Andersson Forsman, C. and Elfvin, L. G.** (1986). Cytochemical localization of ouabain-sensitive, K+-dependent para-nitrophenylphosphatase (transport ATPase) in the guinea pig sympathetic ganglia. *J Submicrosc Cytol* **18**, 711-5.

**Aravamudan, B., Fergestad, T., Davis, W. S., Rodesch, C. K. and Broadie, K.** (1999). Drosophila UNC-13 is essential for synaptic transmission. *Nat Neurosci* **2**, 965-71.

**Arquier, N., Bourouis, M., Colombani, J. and Leopold, P.** (2005). Drosophila Lk6 kinase controls phosphorylation of eukaryotic translation initiation factor 4E and promotes normal growth and development. *Curr Biol* **15**, 19-23.

**Attisano, L. and Wrana, J. L.** (2002). Signal transduction by the TGF-beta superfamily. *Science* **296**, 1646-7.

**Atwood, H. L., Govind, C. K. and Wu, C. F.** (1993). Differential ultrastructure of synaptic terminals on ventral longitudinal abdominal muscles in Drosophila larvae. *J Neurobiol* **24**, 1008-24.

**Bachmann, A., Timmer, M., Sierralta, J., Pietrini, G., Gundelfinger, E. D., Knust, E. and Thomas, U.** (2004). Cell type-specific recruitment of Drosophila Lin-7 to distinct MAGUK-based protein complexes defines novel roles for Sdt and Dlg-S97. *J Cell Sci* **117**, 1899-909.

**Bate, M. and Martínez-Arias, A.** (1993). The development of *Drosophila melanogaster* (2 Vol.). Cold Spring Harbor, New York: Cold Spring Harbor Laboratory Press.

**Baylies, M. K., Bate, M. and Ruiz Gomez, M.** (1998). Myogenesis: a view from Drosophila. *Cell* **93**, 921-7.

**Bellen, H. J., O'Kane, C. J., Wilson, C., Grossniklaus, U., Pearson, R. K. and Gehring, W. J.** (1989). P-element-mediated enhancer detection: a versatile method to study development in Drosophila. *Genes Dev* **3**, 1288-300.

**Bellen, H. J., Vaessin, H., Bier, E., Kolodkin, A., D'Evelyn, D., Kooyer, S. and Jan, Y. N.** (1992). The Drosophila couch potato gene: an essential gene required for normal adult behavior. *Genetics* **131**, 365-75.

**Bender, M., Turner, F. R. and Kaufman, T. C.** (1987). A development genetic analysis of the gene regulator of postbithorax in Drosophila melanogaster. *Dev Biol* **119**, 418-32.

**Bier, E., Vaessin, H., Shepherd, S., Lee, K., McCall, K., Barbel, S., Ackerman, L., Carretto, R., Uemura, T., Grell, E. et al.** (1989). Searching for pattern and mutation in the Drosophila genome with a P-lacZ vector. *Genes Dev* **3**, 1273-87.

**Bonifacino, J. S. and Weissman, A. M.** (1998). Ubiquitin and the control of protein fate in the secretory and endocytic pathways. *Annu Rev Cell Dev Biol* **14**, 19-57.

**Bonni, S., Wang, H. R., Causing, C. G., Kavsak, P., Stroschein, S. L., Luo, K. and Wrana, J. L.** (2001). TGF-beta induces assembly of a Smad2-Smurf2 ubiquitin ligase complex that targets SnoN for degradation. *Nat Cell Biol* **3**, 587-95.

**Brand, A. H. and Perrimon, N.** (1993). Targeted gene expression as a means of altering cell fates and generating dominant phenotypes. *Development* **118**, 401-15.

**Broadie, K. and Bate, M.** (1993a). Activity-dependent development of the neuromuscular synapse during Drosophila embryogenesis. *Neuron* **11**, 607-19.

**Broadie, K. and Bate, M.** (1993b). Innervation directs receptor synthesis and localization in Drosophila embryo synaptogenesis. *Nature* **361**, 350-3.

**Broadie, K., Prokop, A., Bellen, H. J., O'Kane, C. J., Schulze, K. L. and Sweeney, S. T.** (1995). Syntaxin and synaptobrevin function downstream of vesicle docking in Drosophila. *Neuron* **15**, 663-73.

**Broadie, K., Sink, H., Van Vactor, D., Fambrough, D., Whitington, P. M., Bate, M. and Goodman, C. S.** (1993). From growth cone to synapse: the life history of the RP3 motor neuron. *Development* **(Suppl.)**, 227-238.

**Broihier, H. T. and Skeath, J. B.** (2002). Drosophila homeodomain protein dHb9 directs neuronal fate via crossrepressive and cell-nonautonomous mechanisms. *Neuron* **35**, 39-50.

**Budnik, V. and Gramates, L. S.** (1999). Neuromuscular junctions in *Drosophila*. San Diego London Boston NewYork Sydney Tokyo Toronto: Academic Press.

**Budnik, V., Koh, Y. H., Guan, B., Hartmann, B., Hough, C., Woods, D. and Gorczyca, M.** (1996). Regulation of synapse structure and function by the Drosophila tumor suppressor gene dlg. *Neuron* **17**, 627-40.

**Budnik, V., Zhong, Y. and Wu, C. F.** (1990). Morphological plasticity of motor axons in Drosophila mutants with altered excitability. *J Neurosci* **10**, 3754-68.

**Burbea, M., Dreier, L., Dittman, J. S., Grunwald, M. E. and Kaplan, J. M.** (2002). Ubiquitin and AP180 regulate the abundance of GLR-1 glutamate receptors at postsynaptic elements in C. elegans. *Neuron* **35**, 107-20.

**Campos-Ortega, J. A. and Hartenstein, V.** (1997). The embryonic development of *Drosophila melanogaster*. Berlin: Springer Verlag.

**Capdevila, J., Estrada, M. P., Sanchez-Herrero, E. and Guerrero, I.** (1994). The Drosophila segment polarity gene patched interacts with decapentaplegic in wing development. *Embo J* **13**, 71-82.

**Caruana, G.** (2002). Genetic studies define MAGUK proteins as regulators of epithelial cell polarity. *Int J Dev Biol* **46**, 511-8.

**Chang, Q. and Balice-Gordon, R. J.** (2000). Highwire, rpm-1, and futsch: balancing synaptic growth and stability. *Neuron* **26**, 287-90.

**Chen, K. and Featherstone, D. E.** (2005). Discs-large (DLG) is clustered by presynaptic innervation and regulates postsynaptic glutamate receptor subunit composition in Drosophila. *BMC Biol* **3**, 1.

**Chen, K., Merino, C., Sigrist, S. J. and Featherstone, D. E.** (2005). The 4.1 protein coracle mediates subunit-selective anchoring of Drosophila glutamate receptors to the postsynaptic actin cytoskeleton. *J Neurosci* **25**, 6667-75.

**Chen, L. and Madura, K.** (2002). Rad23 promotes the targeting of proteolytic substrates to the proteasome. *Mol Cell Biol* **22**, 4902-13.

**Ciechanover, A.** (1994). The ubiquitin-proteasome proteolytic pathway. *Cell* **79**, 13-21.

**Cline, H.** (2003). Synaptic plasticity: importance of proteasome-mediated protein turnover. *Curr Biol* **13**, R514-6.

**Cooley, L., Kelley, R. and Spradling, A.** (1988). Insertional mutagenesis of the Drosophila genome with single P elements. *Science* **239**, 1121-8.

**Cui, X. and Doe, C. Q.** (1992). ming is expressed in neuroblast sublineages and regulates gene expression in the *Drosophila* central nervous system. *Development* **116**, 943-52.

**Dalby, B., Pereira, A. J. and Goldstein, L. S.** (1995). An inverse PCR screen for the detection of P element insertions in cloned genomic intervals in Drosophila melanogaster. *Genetics* **139**, 757-66.

**Davis, G. W., DiAntonio, A., Petersen, S. A. and Goodman, C. S.** (1998). Postsynaptic PKA controls quantal size and reveals a retrograde signal that regulates presynaptic transmitter release in Drosophila. *Neuron* **20**, 305-15.

**Davis, G. W. and Goodman, C. S.** (1998). Synapse-specific control of synaptic efficacy at the terminals of a single neuron. *Nature* **392**, 82-6.

**Deak, P., Omar, M. M., Saunders, R. D., Pal, M., Komonyi, O., Szidonya, J., Maroy, P., Zhang, Y., Ashburner, M., Benos, P. et al.** (1997). P-element insertion alleles of essential genes on the third chromosome of Drosophila melanogaster: correlation of physical and cytogenetic maps in chromosomal region 86E-87F. *Genetics* **147**, 1697-722.

**DiAntonio, A., Haghighi, A. P., Portman, S. L., Lee, J. D., Amaranto, A. M. and Goodman, C. S.** (2001). Ubiquitination-dependent mechanisms regulate synaptic growth and function. *Nature* **412**, 449-52.

**DiAntonio, A., Petersen, S. A., Heckmann, M. and Goodman, C. S.** (1999). Glutamate receptor expression regulates quantal size and quantal content at the Drosophila neuromuscular junction. *J Neurosci* **19**, 3023-32.

**DrosDel.** An isogenic deficiency kit for Drosophila melanogaster, (ed.

**Drysdale, R. A. and Crosby, M. A.** (2005). FlyBase: genes and gene models. *Nucleic Acids Res* **33**, D390-5.

**Duffy, J. B.** (2002). GAL4 system in *Drosophila*: a fly geneticist's Swiss army knife. *Genesis* **34**, 1-15.

**Entchev, E. V., Schwabedissen, A. and Gonzalez-Gaitan, M.** (2000). Gradient formation of the TGF-beta homolog Dpp. *Cell* **103**, 981-91.

**Fabini, G., Freilinger, A., Altmann, F. and Wilson, I. B.** (2001). Identification of core alpha 1,3-fucosylated glycans and cloning of the requisite fucosyltransferase cDNA from

Drosophila melanogaster. Potential basis of the neural anti-horseadish peroxidase epitope. *J Biol Chem* **276**, 28058-67.

**Featherstone, D. E. and Broadie, K.** (2000). Surprises from Drosophila: genetic mechanisms of synaptic development and plasticity. *Brain Res Bull* **53**, 501-11.

**Ferraiuolo, M. A., Lee, C. S., Ler, L. W., Hsu, J. L., Costa-Mattioli, M., Luo, M. J., Reed, R. and Sonenberg, N.** (2004). A nuclear translation-like factor eIF4AIII is recruited to the mRNA during splicing and functions in nonsense-mediated decay. *Proc Natl Acad Sci U S A* **101**, 4118-23.

**Fischer, J. A., Giniger, E., Maniatis, T. and Ptashne, M.** (1988). GAL4 activates transcription in Drosophila. *Nature* **332**, 853-6.

**FlyBase.** (1999). The FlyBase database of the *Drosophila* genome projects and community literature. *Nucleic Acids Res.* **27**, 85-88; http://flybase.bio.indiana.edu/.

**FlyMove.** (ed.

**Fly-Pushing.** Fly Pushing : The Theory and Practice of Drosophila Genetics; Ralph Greenspan.

**Glickman, M. H. and Ciechanover, A.** (2002). The ubiquitin-proteasome proteolytic pathway: destruction for the sake of construction. *Physiol Rev* **82**, 373-428.

**Glockzin, S., Ogi, F. X., Hengstermann, A., Scheffner, M. and Blattner, C.** (2003). Involvement of the DNA repair protein hHR23 in p53 degradation. *Mol Cell Biol* **23**, 8960-9.

**Gloor, G. B., Preston, C. R., Johnson-Schlitz, D. M., Nassif, N. A., Phillis, R. W., Benz, W. K., Robertson, H. M. and Engels, W. R.** (1993). Type I repressors of P element mobility. *Genetics* **135**, 81-95.

**Goda, Y. and Davis, G. W.** (2003). Mechanisms of synapse assembly and disassembly. *Neuron* **40**, 243-64.

**Gomperts, S. N.** (1996). Clustering membrane proteins: It's all coming together with the PSD-95/SAP90 protein family. *Cell* **84**, 659-62.

**Gramates, L. S. and Budnik, V.** (1999). Assembly and maturation of the Drosophila larval neuromuscular junction. *Int Rev Neurobiol* **43**, 93-117.

**Grumbling, G. and Strelets, V.** (2006). FlyBase: anatomical data, images and queries. *Nucleic Acids Res* **34**, D484-8.

**Guan, B., Hartmann, B., Kho, Y. H., Gorczyca, M. and Budnik, V.** (1996). The Drosophila tumor suppressor gene, dlg, is involved in structural plasticity at a glutamatergic synapse. *Curr Biol* **6**, 695-706.

**Halfon, M. S., Gisselbrecht, S., Lu, J., Estrada, B., Keshishian, H. and Michelson, A. M.** (2002). New fluorescent protein reporters for use with the Drosophila Gal4 expression system and for vital detection of balancer chromosomes. *Genesis* **34**, 135-8.

**Hamilton, B. A., Palazzolo, M. J., Chang, J. H., VijayRaghavan, K., Mayeda, C. A., Whitney, M. A. and Meyerowitz, E. M.** (1991). Large scale screen for transposon insertions into cloned genes. *Proc Natl Acad Sci U S A* **88**, 2731-5.

**Hammond, S. M., Caudy, A. A. and Hannon, G. J.** (2001). Post-transcriptional gene silencing by double-stranded RNA. *Nat Rev Genet* **2**, 110-9.

**Handler, A. M., Gomez, S. P. and O'Brochta, D. A.** (1993). Negative regulation of P element excision by the somatic product and terminal sequences of P in Drosophila melanogaster. *Mol Gen Genet* **237**, 145-51.

**Hitier, R., Chaminade, M. and Preat, T.** (2001). The Drosophila castor gene is involved in postembryonic brain development. *Mech Dev* **103**, 3-11.

**Hori, K., Fostier, M., Ito, M., Fuwa, T. J., Go, M. J., Okano, H., Baron, M. and Matsuno, K.** (2004). Drosophila deltex mediates suppressor of Hairless-independent and late-endosomal activation of Notch signaling. *Development* **131**, 5527-37.

**Izzi, L. and Attisano, L.** (2004). Regulation of the TGFbeta signalling pathway by ubiquitin-mediated degradation. *Oncogene* **23**, 2071-8.

**Jan, L. Y. and Jan, Y. N.** (1976). L-glutamate as an excitatory transmitter at the Drosophila larval neuromuscular junction. *J Physiol* **262**, 215-36.

**Jan, Y.-N. and Jan, L.-L.** (1982). Antibodies to horseradish peroxidase as specific neuronal markers in *Drosophila* and grasshopper embryos. *Proc. Natl. Acad. Sci. USA* **79**, 2700-2704.

**Jin, Y.** (2002). Synaptogenesis: insights from worm and fly. *Curr Opin Neurobiol* **12**, 71-9.

**Johansen, J., Halpern, M. E., Johansen, K. M. and Keshishian, H.** (1989). Stereotypic morphology of glutamatergic synapses on identified muscle cells of Drosophila larvae. *J Neurosci* **9**, 710-25.

**Johnson, R. L., Grenier, J. K. and Scott, M. P.** (1995). patched overexpression alters wing disc size and pattern: transcriptional and post-transcriptional effects on hedgehog targets. *Development* **121**, 4161-70.

**Kambadur, R., Koizumi, K., Stivers, C., Nagle, J., Poole, S. J. and Odenwald, W. F.** (1998). Regulation of POU genes by *castor* and *hunchback* establishes layered compartments in the *Drosophila* CNS. *Genes Dev* **12**, 246-60.

**Kammerer, R. A., Schulthess, T., Landwehr, R., Lustig, A., Fischer, D. and Engel, J.** (1998). Tenascin-C hexabrachion assembly is a sequential two-step process initiated by coiled-coil alpha-helices. *J Biol Chem* **273**, 10602-8.

**Katiyar, S. and Lennarz, W. J.** (2005). Studies on the intracellular localization of hHR23B. *Biochem Biophys Res Commun* **337**, 1296-300.

**Kawasaki, F., Zou, B., Xu, X. and Ordway, R. W.** (2004). Active zone localization of presynaptic calcium channels encoded by the cacophony locus of Drosophila. *J Neurosci* **24**, 282-5.

**Keshishian, H., Broadie, K., Chiba, A. and Bate, M.** (1996). The drosophila neuromuscular junction: a model system for studying synaptic development and function. *Annu Rev Neurosci* **19**, 545-75.

**Kidd, T., Bland, K. S. and Goodman, C. S.** (1999). Slit is the midline repellent for the robo receptor in Drosophila. *Cell* **96**, 785-94.

**Kirschner, M.** (1999). Intracellular proteolysis. *Trends Cell Biol* **9**, M42-5.

**Klagges, B. R. E., Heimbeck, G., Godenschwege, T. A., Hofbauer, A., Pflugfelder, G. O., Reifegerste, R., Reisch, D., Schaupp, M., Buchner, S. and Buchner, E.** (1996). Invertebrate Synapsins: a single gene codes for several isoforms in *Drosophila*. *J. Neurosci.* **16**, 3154-3165.

**Klambt, C., Jacobs, J. R. and Goodman, C. S.** (1991). The midline of the Drosophila central nervous system: a model for the genetic analysis of cell fate, cell migration, and growth cone guidance. *Cell* **64**, 801-15.

**Klein, T. and Arias, A. M.** (1998). Interactions among Delta, Serrate and Fringe modulate Notch activity during Drosophila wing development. *Development* **125**, 2951-62.

**Koh, Y. H., Gramates, L. S. and Budnik, V.** (2000). Drosophila larval neuromuscular junction: molecular components and mechanisms underlying synaptic plasticity. *Microsc Res Tech* **49**, 14-25.

**Koh, Y. H., Popova, E., Thomas, U., Griffith, L. C. and Budnik, V.** (1999). Regulation of DLG localization at synapses by CaMKII-dependent phosphorylation. *Cell* **98**, 353-63.

**Kolodziej, P. A., Jan, L. Y. and Jan, Y. N.** (1995). Mutations that affect the length, fasciculation, or ventral orientation of specific sensory axons in the Drosophila embryo. *Neuron* **15**, 273-86.

**Landgraf, M., Bossing, T., Technau, G. M. and Bate, M.** (1997). The origin, location, and projections of the embryonic abdominal motorneurons of Drosophila. *J Neurosci* **17**, 9642-55.

**Landgraf, M., Jeffrey, V., Fujioka, M., Jaynes, J. B. and Bate, M.** (2003). Embryonic origins of a motor system: motor dendrites form a myotopic map in *Drosophila*. *PLoS Biol.* **1**, 221-230.

**Lasko, P.** (2000). The drosophila melanogaster genome: translation factors and RNA binding proteins. *J Cell Biol* **150**, F51-6.

**Lee, T. and Luo, L.** (1999). Mosaic analysis with a repressible neurotechnique cell marker for studies of gene function in neuronal morphogenesis. *Neuron* **22**, 451-461.

**Lehmann, R. and Tautz, D.** (1994). In situ hybridization to RNA. *Methods Cell Biol* **44**, 575-98.

**Li, Q., Imataka, H., Morino, S., Rogers, G. W., Jr., Richter-Cook, N. J., Merrick, W. C. and Sonenberg, N.** (1999). Eukaryotic translation initiation factor 4AIII (eIF4AIII) is functionally distinct from eIF4AI and eIF4AII. *Mol Cell Biol* **19**, 7336-46.

**Liebl, F. L., Chen, K., Karr, J., Sheng, Q. and Featherstone, D. E.** (2005). Increased synaptic microtubules and altered synapse development in Drosophila sec8 mutants. *BMC Biol* **3**, 27.

**Lin, D. M. and Goodman, C. S.** (1994). Ectopic and increased expression of Fasciclin II alters motoneuron growth cone guidance. *Neuron* **13**, 507-23.

**Luking, A., Stahl, U. and Schmidt, U.** (1998). The protein family of RNA helicases. *Crit Rev Biochem Mol Biol* **33**, 259-96.

**Luo, L., Liao, Y. J., Jan, L. Y. and Jan, Y. N.** (1994). Distinct morphogenetic functions of similar small GTPases: *Drosophila* Drac1 is involved in axonal outgrowth and myoblast fusion. *Genes Dev.* **8**, 1787-1802.

**Marques, G., Bao, H., Haerry, T. E., Shimell, M. J., Duchek, P., Zhang, B. and O'Connor, M. B.** (2002). The Drosophila BMP type II receptor Wishful Thinking regulates neuromuscular synapse morphology and function. *Neuron* **33**, 529-43.

**Marques, G., Haerry, T. E., Crotty, M. L., Xue, M., Zhang, B. and O'Connor, M. B.** (2003). Retrograde Gbb signaling through the Bmp type 2 receptor wishful thinking regulates systemic FMRFa expression in Drosophila. *Development* **130**, 5457-70.

**Martin, K. A., Poeck, B., Roth, H., Ebens, A. J., Ballard, L. C. and Zipursky, S. L.** (1995). Mutations disrupting neuronal connectivity in the Drosophila visual system. *Neuron* **14**, 229-40.

**Matthews, K. A., Kaufman, T. C. and Gelbart, W. M.** (2005). Research resources for Drosophila: the expanding universe. *Nat Rev Genet* **6**, 179-93.

**McCabe, B. D., Hom, S., Aberle, H., Fetter, R. D., Marques, G., Haerry, T. E., Wan, H., O'Connor, M. B., Goodman, C. S. and Haghighi, A. P.** (2004). Highwire regulates presynaptic BMP signaling essential for synaptic growth. *Neuron* **41**, 891-905.

**McCabe, B. D., Marques, G., Haghighi, A. P., Fetter, R. D., Crotty, M. L., Haerry, T. E., Goodman, C. S. and O'Connor, M. B.** (2003). The BMP homolog Gbb provides a retrograde signal that regulates synaptic growth at the Drosophila neuromuscular junction. *Neuron* **39**, 241-54.

**Mellerick, D. M., Kassis, J. A., Zhang, S. D. and Odenwald, W. F.** (1992). castor encodes a novel zinc finger protein required for the development of a subset of CNS neurons in Drosophila. *Neuron* **9**, 789-803.

**Messenger, N. J. and Warner, A. E.** (2000). Primary neuronal differentiation in Xenopus embryos is linked to the beta(3) subunit of the sodium pump. *Dev Biol* **220**, 168-82.

**Misra, S., Buratowski, R. M., Ohkawa, T. and Rio, D. C.** (1993). Cytotype control of Drosophila melanogaster P element transposition: genomic position determines maternal repression. *Genetics* **135**, 785-800.

**Mlodzik, M., Baker, N. E. and Rubin, G. M.** (1990). Isolation and expression of scabrous, a gene regulating neurogenesis in Drosophila. *Genes Dev* **4**, 1848-61.

**Moustakas, A., Souchelnytskyi, S. and Heldin, C. H.** (2001). Smad regulation in TGF-beta signal transduction. *J Cell Sci* **114**, 4359-69.

**Murray, A. J., Lewis, S. J., Barclay, A. N. and Brady, R. L.** (1995). One sequence, two folds: a metastable structure of CD2. *Proc Natl Acad Sci U S A* **92**, 7337-41.

**Nagafuji, T., Koide, T., Miyauchi, T. and Takato, M.** (1992). An activation of synaptosomal Na+,K(+)-ATPase by a novel dibenzoxazepine derivative (BY-1949) in the rat brain: its functional role in the neurotransmitter uptake systems. *J Neurochem* **58**, 362-8.

**Nagase, T., Ishikawa, K., Kikuno, R., Hirosawa, M., Nomura, N. and Ohara, O.** (1999). Prediction of the coding sequences of unidentified human genes. XV. The

complete sequences of 100 new cDNA clones from brain which code for large proteins in vitro. *DNA Res* **6**, 337-45.

**Neufeld, T. P., Tang, A. H. and Rubin, G. M.** (1998). A genetic screen to identify components of the sina signaling pathway in Drosophila eye development. *Genetics* **148**, 277-86.

**Neumann, C. J. and Cohen, S. M.** (1996). A hierarchy of cross-regulation involving Notch, wingless, vestigial and cut organizes the dorsal/ventral axis of the Drosophila wing. *Development* **122**, 3477-85.

**O'Hare, K. and Rubin, G. M.** (1983). Structures of P transposable elements and their sites of insertion and excision in the Drosophila melanogaster genome. *Cell* **34**, 25-35.

**Palacios, I. M., Gatfield, D., St Johnston, D. and Izaurralde, E.** (2004). An eIF4AIII-containing complex required for mRNA localization and nonsense-mediated mRNA decay. *Nature* **427**, 753-7.

**Palacios, I. M. and St Johnston, D.** (2002). Kinesin light chain-independent function of the Kinesin heavy chain in cytoplasmic streaming and posterior localisation in the Drosophila oocyte. *Development* **129**, 5473-85.

**Parnas, D., Haghighi, A. P., Fetter, R. D., Kim, S. W. and Goodman, C. S.** (2001). Regulation of postsynaptic structure and protein localization by the Rho-type guanine nucleotide exchange factor dPix. *Neuron* **32**, 415-24.

**Petersen, S. A., Fetter, R. D., Noordermeer, J. N., Goodman, C. S. and DiAntonio, A.** (1997). Genetic analysis of glutamate receptors in Drosophila reveals a retrograde signal regulating presynaptic transmitter release. *Neuron* **19**, 1237-48.

**Pile, L. A., Schlag, E. M. and Wassarman, D. A.** (2002). The SIN3/RPD3 deacetylase complex is essential for G(2) phase cell cycle progression and regulation of SMRTER corepressor levels. *Mol Cell Biol* **22**, 4965-76.

**Pile, L. A., Spellman, P. T., Katzenberger, R. J. and Wassarman, D. A.** (2003). The SIN3 deacetylase complex represses genes encoding mitochondrial proteins: implications for the regulation of energy metabolism. *J Biol Chem* **278**, 37840-8.

**Poorkaj, P., Kas, A., D'Souza, I., Zhou, Y., Pham, Q., Stone, M., Olson, M. V. and Schellenberg, G. D.** (2001). A genomic sequence analysis of the mouse and human microtubule-associated protein tau. *Mamm Genome* **12**, 700-12.

**Prokop, A.** (1999). Integrating bits and pieces: synapse structure and formation in Drosophila embryos. *Cell Tissue Res* **297**, 169-86.

**Prokop, A., Landgraf, M., Rushton, E., Broadie, K. and Bate, M.** (1996). Presynaptic development at the Drosophila neuromuscular junction: assembly and localization of presynaptic active zones. *Neuron* **17**, 617-26.

**Prokop, A. and Meinertzhagen, I. A.** (2006). Development and structure of synaptic contacts in Drosophila. *Semin Cell Dev Biol* **17**, 20-30.

**Prout, M., Damania, Z., Soong, J., Fristrom, D. and Fristrom, J. W.** (1997). Autosomal mutations affecting adhesion between wing surfaces in Drosophila melanogaster. *Genetics* **146**, 275-85.

**Raftery, L. A., Sanicola, M., Blackman, R. K. and Gelbart, W. M.** (1991). The relationship of decapentaplegic and engrailed expression in Drosophila imaginal disks: do these genes mark the anterior-posterior compartment boundary? *Development* **113**, 27-33.

**Rao, H. and Sastry, A.** (2002). Recognition of specific ubiquitin conjugates is important for the proteolytic functions of the ubiquitin-associated domain proteins Dsk2 and Rad23. *J Biol Chem* **277**, 11691-5.

**Rheuben, M. B., Yoshihara, M. and Kidokoro, Y.** (1999). Ultrastructural correlates of neuromuscular junction development. *Int Rev Neurobiol* **43**, 69-92.

**Rio, D. C., Laski, F. A. and Rubin, G. M.** (1986). Identification and immunochemical analysis of biologically active Drosophila P element transposase. *Cell* **44**, 21-32.

**Robertson, H. M., Preston, C. R., Phillis, R. W., Johnson-Schlitz, D. M., Benz, W. K. and Engels, W. R.** (1988). A stable genomic source of P element transposase in Drosophila melanogaster. *Genetics* **118**, 461-70.

**Rodriguez de Lores Arnaiz, G.** (1992). In search of synaptosomal Na+,K(+)-ATPase regulators. *Mol Neurobiol* **6**, 359-75.

**Rose, D. and Chiba, A.** (1999). A single growth cone is capable of integrating simultaneously presented and functionally distinct molecular cues during target recognition. *J Neurosci* **19**, 4899-906.

**Rose, R. E., Gallaher, N. M., Andrew, D. J., Goodman, R. H. and Smolik, S. M.** (1997). The CRE-binding protein dCREB-A is required for Drosophila embryonic development. *Genetics* **146**, 595-606.

**Roseman, R. R., Johnson, E. A., Rodesch, C. K., Bjerke, M., Nagoshi, R. N. and Geyer, P. K.** (1995). A P element containing suppressor of hairy-wing binding regions has novel properties for mutagenesis in Drosophila melanogaster. *Genetics* **141**, 1061-74.

**Saitoe, M., Tanaka, S., Takata, K. and Kidokoro, Y.** (1997). Neural activity affects distribution of glutamate receptors during neuromuscular junction formation in Drosophila embryos. *Dev Biol* **184**, 48-60.

**Salzberg, A., Prokopenko, S. N., He, Y., Tsai, P., Pal, M., Maroy, P., Glover, D. M., Deak, P. and Bellen, H. J.** (1997). P-element insertion alleles of essential genes on the third chromosome of Drosophila melanogaster: mutations affecting embryonic PNS development. *Genetics* **147**, 1723-41.

**Sanchez-Soriano, N. and Prokop, A.** (2005). The influence of pioneer neurons on a growing motor nerve in Drosophila requires the neural cell adhesion molecule homolog FasciclinII. *J Neurosci* **25**, 78-87.

**Schmid, A. and Doe, C. Q.** (1998). DiI labeling reveals CNS defects in mutant backgrounds. In *A. Dros. Res. Conf.*, vol. 39 (ed., pp. 519A.

**Schneider, B. G. and Kraig, E.** (1990). Na+, K(+)-ATPase of the photoreceptor: selective expression of alpha 3 and beta 2 isoforms. *Exp Eye Res* **51**, 553-64.

**Schuster, C. M., Davis, G. W., Fetter, R. D. and Goodman, C. S.** (1996). Genetic dissection of structural and functional components of synaptic plasticity. I. Fasciclin II controls synaptic stabilization and growth. *Neuron* **17**, 641-54.

**Schweisguth, F.** (1999). Dominant-negative mutation in the beta2 and beta6 proteasome subunit genes affect alternative cell fate decisions in the Drosophila sense organ lineage. *Proc Natl Acad Sci U S A* **96**, 11382-6.

**Searles, L. L., Jokerst, R. S., Bingham, P. M., Voelker, R. A. and Greenleaf, A. L.** (1982). Molecular cloning of sequences from a Drosophila RNA polymerase II locus by P element transposon tagging. *Cell* **31**, 585-92.

**Seeger, M., Tear, G., Ferres-Marco, D. and Goodman, C. S.** (1993). Mutations affecting growth cone guidance in Drosophila: genes necessary for guidance toward or away from the midline. *Neuron* **10**, 409-26.

**Sentry, J. W. and Kaiser, K.** (1994). Application of inverse PCR to site-selected mutagenesis of Drosophila. *Nucleic Acids Res* **22**, 3429-30.

**Sheng, M. and Pak, D. T.** (1999). Glutamate receptor anchoring proteins and the molecular organization of excitatory synapses. *Ann N Y Acad Sci* **868**, 483-93.

**Sheng, M. and Pak, D. T.** (2000). Ligand-gated ion channel interactions with cytoskeletal and signaling proteins. *Annu Rev Physiol* **62**, 755-78.

**Shi, Y. and Massague, J.** (2003). Mechanisms of TGF-beta signaling from cell membrane to the nucleus. *Cell* **113**, 685-700.

**Shibuya, T., Tange, T. O., Sonenberg, N. and Moore, M. J.** (2004). eIF4AIII binds spliced mRNA in the exon junction complex and is essential for nonsense-mediated decay. *Nat Struct Mol Biol* **11**, 346-51.

**Sigrist, S. J.** (2006). Neurobiology tools: flashdancing worms. *Curr Biol* **16**, R100-2.

**Sigrist, S. J., Reiff, D. F., Thiel, P. R., Steinert, J. R. and Schuster, C. M.** (2003). Experience-dependent strengthening of Drosophila neuromuscular junctions. *J Neurosci* **23**, 6546-56.

**Sigrist, S. J., Thiel, P. R., Reiff, D. F., Lachance, P. E., Lasko, P. and Schuster, C. M.** (2000). Postsynaptic translation affects the efficacy and morphology of neuromuscular junctions. *Nature* **405**, 1062-5.

**Sigrist, S. J., Thiel, P. R., Reiff, D. F. and Schuster, C. M.** (2002). The postsynaptic glutamate receptor subunit DGluR-IIA mediates long-term plasticity in Drosophila. *J Neurosci* **22**, 7362-72.

**Speicher, S. A., Thomas, U., Hinz, U. and Knust, E.** (1994). The Serrate locus of Drosophila and its role in morphogenesis of the wing imaginal discs: control of cell proliferation. *Development* **120**, 535-44.

**Spradling, A. C., Stern, D., Beaton, A., Rhem, E. J., Laverty, T., Mozden, N., Misra, S. and Rubin, G. M.** (1999). The Berkeley Drosophila genome project gene disruption project. Single P-element insertions mutating 25% of vital *Drosophila* genes. *Genetics* **153**, 135-177.

**Spradling, A. C., Stern, D. M., Kiss, I., Roote, J., Laverty, T. and Rubin, G. M.** (1995). Gene disruptions using P transposable elements: an integral component of the Drosophila genome project. *Proc Natl Acad Sci U S A* **92**, 10824-30.

**St Johnston, D.** (2002). The art and design of genetic screens: Drosophila melanogaster. *Nat Rev Genet* **3**, 176-88.

**Stewart, B. A., Schuster, C. M., Goodman, C. S. and Atwood, H. L.** (1996). Homeostasis of synaptic transmission in Drosophila with genetically altered nerve terminal morphology. *J Neurosci* **16**, 3877-86.

**Strausberg, R. L., Feingold, E. A., Grouse, L. H., Derge, J. G., Klausner, R. D., Collins, F. S., Wagner, L., Shenmen, C. M., Schuler, G. D., Altschul, S. F. et al.** (2002). Generation and initial analysis of more than 15,000 full-length human and mouse cDNA sequences. *Proc Natl Acad Sci U S A* **99**, 16899-903.

**Strous, G. J. and van Kerkhof, P.** (2002). The ubiquitin-proteasome pathway and the regulation of growth hormone receptor availability. *Mol Cell Endocrinol* **197**, 143-51.

**Suzuki, E., Rose, D. and Chiba, A.** (2000). The ultrastructural interactions of identified pre- and postsynaptic cells during synaptic target recognition in Drosophila embryos. *J Neurobiol* **42**, 448-59.

**Sweeney, S. T., Broadie, K., Keane, J., Niemann, H. and O'Kane, C. J.** (1995). Targeted expression of tetanus toxin light chain in Drosophila specifically eliminates synaptic transmission and causes behavioral defects. *Neuron* **14**, 341-51.

**Sweeney, S. T. and Davis, G. W.** (2002). Unrestricted synaptic growth in spinster-a late endosomal protein implicated in TGF-beta-mediated synaptic growth regulation. *Neuron* **36**, 403-16.

**Tanimoto, H., Itoh, S., ten Dijke, P. and Tabata, T.** (2000). Hedgehog creates a gradient of DPP activity in Drosophila wing imaginal discs. *Mol Cell* **5**, 59-71.

**Tejedor, F. J., Bokhari, A., Rogero, O., Gorczyca, M., Zhang, J., Kim, E., Sheng, M. and Budnik, V.** (1997). Essential role for dlg in synaptic clustering of Shaker K+ channels in vivo. *J Neurosci* **17**, 152-9.

**Thomas, U., Kim, E., Kuhlendahl, S., Koh, Y. H., Gundelfinger, E. D., Sheng, M., Garner, C. C. and Budnik, V.** (1997). Synaptic clustering of the cell adhesion molecule fasciclin II by discs-large and its role in the regulation of presynaptic structure. *Neuron* **19**, 787-99.

**Thor, S., Andersson, S. G., Tomlinson, A. and Thomas, J. B.** (1999). A LIM-homeodomain combinatorial code for motor-neuron pathway selection. *Nature* **397**, 76-80.

**Vactor, D. V., Sink, H., Fambrough, D., Tsoo, R. and Goodman, C. S.** (1993). Genes that control neuromuscular specificity in Drosophila. *Cell* **73**, 1137-53.

**van Roessel, P., Elliott, D. A., Robinson, I. M., Prokop, A. and Brand, A. H.** (2004). Independent regulation of synaptic size and activity by the anaphase-promoting complex. *Cell* **119**, 707-18.

**Vorbrodt, A. W., Lossinsky, A. S. and Wisniewski, H. M.** (1982). Cytochemical localization of ouabain-sensitive, K+-dependent p-nitro-phenylphosphatase (transport ATPase) in the mouse central and peripheral nervous systems. *Brain Res* **243**, 225-34.

**Wagh, D. A., Rasse, T. M., Asan, E., Hofbauer, A., Schwenkert, I., Durrbeck, H., Buchner, S., Dabauvalle, M. C., Schmidt, M., Qin, G. et al.** (2006). Bruchpilot, a protein with homology to ELKS/CAST, is required for structural integrity and function of synaptic active zones in Drosophila. *Neuron* **49**, 833-44.

**Waites, C. L., Craig, A. M. and Garner, C. C.** (2005). Mechanisms of vertebrate synaptogenesis. *Annu Rev Neurosci* **28**, 251-74.

**Walters, K. J., Lech, P. J., Goh, A. M., Wang, Q. and Howley, P. M.** (2003). DNA-repair protein hHR23a alters its protein structure upon binding proteasomal subunit S5a. *Proc Natl Acad Sci U S A* **100**, 12694-9.

**Wan, H. I., DiAntonio, A., Fetter, R. D., Bergstrom, K., Strauss, R. and Goodman, C. S.** (2000). Highwire regulates synaptic growth in Drosophila. *Neuron* **26**, 313-29.

**Wan, Y., Liu, X. and Kirschner, M. W.** (2001). The anaphase-promoting complex mediates TGF-beta signaling by targeting SnoN for destruction. *Mol Cell* **8**, 1027-39.

**Wang, J., Renger, J. J., Griffith, L. C., Greenspan, R. J. and Wu, C. F.** (1994). Concomitant alterations of physiological and developmental plasticity in Drosophila CaM kinase II-inhibited synapses. *Neuron* **13**, 1373-84.

**Weigmann, K., Klapper, R., Strasser, T., Rickert, C., Technau, G., Jackle, H., Janning, W. and Klambt, C.** (2003). FlyMove--a new way to look at development of Drosophila. *Trends Genet* **19**, 310-1.

**Weinstein, D. C., Honore, E. and Hemmati-Brivanlou, A.** (1997). Epidermal induction and inhibition of neural fate by translation initiation factor 4AIII. *Development* **124**, 4235-42.

**Wilder, E. L. and Perrimon, N.** (1995). Dual functions of wingless in the Drosophila leg imaginal disc. *Development* **121**, 477-88.

**Williams, J. A., Paddock, S. W. and Carroll, S. B.** (1993). Pattern formation in a secondary field: a hierarchy of regulatory genes subdivides the developing Drosophila wing disc into discrete subregions. *Development* **117**, 571-84.

**Wood, J. G., Jean, D. H., Whitaker, J. N., McLaughlin, B. J. and Albers, R. W.** (1977). Immunocytochemical localization of the sodium, potassium activated ATPase in knifefish brain. *J Neurocytol* **6**, 571-81.

**Yoshihara, M., Rheuben, M. B. and Kidokoro, Y.** (1997). Transition from growth cone to functional motor nerve terminal in Drosophila embryos. *J Neurosci* **17**, 8408-26.

**Zhai, R. G. and Bellen, H. J.** (2004). Hauling t-SNAREs on the microtubule highway. *Nat Cell Biol* **6**, 918-9.

**Zhong, Y., Budnik, V. and Wu, C. F.** (1992). Synaptic plasticity in Drosophila memory and hyperexcitable mutants: role of cAMP cascade. *J Neurosci* **12**, 644-51.

**Zhong, Y. and Shanley, J.** (1995). Altered nerve terminal arborization and synaptic transmission in Drosophila mutants of cell adhesion molecule fasciclin I. *J Neurosci* **15**, 6679-87.

**Zito, K., Fetter, R. D., Goodman, C. S. and Isacoff, E. Y.** (1997). Synaptic clustering of Fascilin II and Shaker: essential targeting sequences and role of Dlg. *Neuron* **19**, 1007-16.

**Zito, K., Parnas, D., Fetter, R. D., Isacoff, E. Y. and Goodman, C. S.** (1999). Watching a synapse grow: noninvasive confocal imaging of synaptic growth in Drosophila. *Neuron* **22**, 719-29.

# Versicherungsgemäß §11 Abs. 3d der Promotionsordnung vom 22.12.2002

1) Ich habe die jetzt als Dissertation vorgelegte Arbeit selbst angefertigt und alle benutzten Hilfsmittel (Literatur, Apparaturen, Material) in der Arbeit angegeben.

2) Ich habe und hatte die jetzt als Dissertation vorgelegte Arbeit nicht als Prüfungsarbeit für eine staatliche oder andere wissenschaftliche Prüfung eingereicht.

3) Ich hatte weder die jetzt als Dissertation vorgelegte Arbeit noch Teile einer Abhandlung davon bei einer anderen Fakultät bzw. einem anderen Fachbereich als Dissertation eingereicht.

| | ---------- |
|---|---|
| Mainz, den | (Mohiddin Lone) |

## **ABBREVIATIONS:**

| | |
|---|---|
| AEL | after egg laying |
| aCC | anterior corner cell |
| APC/C | Anaphase promoting complex |
| AP | alkaline phosphatase |
| B&B | Broadie and Bate buffer |
| BCIP | 5-bromo-4-chloro-3-indolyl phosphate |
| BMP | bone morphogenic protein |
| CaMKII | Calcium/calmodulin-dependent protein kinase II |
| *Cas* | castor |
| cAMP | cyclic adenosine monophosphatase |
| CIAP | calf intestine alkaline phosphatase |
| CNS | central nervous system |
| cDNA | complementary DNA |
| CSP | Cysteine string protein |
| DAB | diaminobenzidine |
| ddNTPs | dideoxynucleotides |
| *Df* | deficiency |
| DGRC | *Drosophila* genome research center |
| DLG | Disc large |
| DNA | deoxyribonucleotide acid |
| DO | dorsal oblique |
| Dpp | decapentaplegic |
| dsRNA | double stranded RNA |
| DTS | Dominat temperature sensitive |
| DTT | dithiothreitol |
| EMS | ethylmathylsulphonate |
| *eIF* | eukaryotic initiation factor |
| *elaV* | *embryonic lethal, abnormal vision* |
| *eve* | *even skipped* |
| FasII | Fasciclin II |
| Ftz | Fushi tarazu |
| Gbb | glass bottom boat |
| GluR | glutamate receptor |
| GFP | green fluorescent protein |
| Hiw | Highwire |
| HRP | horse radish peroxydase |
| IPTG | isopropyl-B-D-thiogalactoside |
| ISN | intersegmental nerve |
| JNK | c-Jun amino terminal Kinase |
| Kbp | Kilo base pairs |
| kDA | kilo Dalton |
| MAGUKs | membrane associated guanylate kinases |

| | |
|---|---|
| md | multiple dendrite |
| *mbc* | myoblastcity |
| *mef2* | *myocyte* |
| mRNA | messenger RNA |
| NB | neuroblast |
| NBT | nitro blue tetrazolium chloride |
| N-CAM | neural cell adhesion molecule |
| NMJ | neuromuscular junction |
| ORF | open reading frame |
| PAGE | polyacrylamide gel electrophoresis |
| PBS | phosphate buffered saline |
| PBT | PBS with Tween-20 |
| PCR | polymerase chain reaction |
| PDZ | acronym for PSD95, DLG, and ZO1 |
| PNS | peripheral nervous system |
| PSD95/SAP90 | post synaptic density 95/synapse associated protein 90 |
| RNA | ribonucleotide acid |
| RNAi | RNA interference |
| SDS | sodium dodecyl sulphate |
| Shot | short stop |
| SNa/b/c/d | segmental nerve a/b/c/d |
| Syn | synapsin |
| Syt | synaptotagmin |
| *Taq* | *Thermus aquaticus* |
| TBS | Tris buffered saline |
| TE | Tris-EDTA buffer |
| TAE | Tris-Acetate-EDTA buffer |
| TGF | transforming growth factor |
| Tkv | thickveins |
| Tris | Tris Hydroxymethylaminoethane |
| tub | tubulin |
| UAS | upstream activating site |
| *VUM* | *ventral unpaired median* |
| *Wah* | waharan |
| | |